The Functional Analysis and Characterization of the Liver-Specific MicroRNA miR-122 and of its Associated Target Genes

Inaugural-Dissertation

zur Erlangung des Doktorgrades
der Mathematisch-Naturwissenschaftlichen Fakultät
der Heinrich-Heine-Universität Düsseldorf

vorgelegt von

Martha Magdalene Paluschinski
aus Beuthen

Düsseldorf, Juli 2020

Aus der Klinik für Gastroenterologie, Hepatologie und Infektiologie
der Heinrich-Heine-Universität Düsseldorf

Gedruckt mit der Genehmigung der
Mathematisch-Naturwissenschaftlichen Fakultät
der Heinrich-Heine-Universität Düsseldorf

Berichterstatter:

1. Prof. Dr. Dieter Häussinger

2. Prof. Dr. Peter Westhoff

Tag der mündlichen Prüfung: 14. Dezember 2020

Parts of this thesis have been published as follows:

Manuscript in preparation:

The liver-specific microRNA-122 exerts its functions by antagonizing liver disease-associated transcription factors

Martha Paluschinski, Jessica Schira, Rossella Pellegrino, Thomas Longerich, Kai Stühler, Dieter Häussinger and Mirco Castoldi

Poster presentations:

The liver-specific microRNA-122 modulates hepatic response to infection and inflammation by antagonizing YY1, FOXP3, NRF1 and E2F4 molecular networks

Martha Paluschinski, Dieter Häussinger and Mirco Castoldi

32nd Annual Meeting of the German Association of the Study of the Liver (GASL), Düsseldorf, 22 – 23 January 2016.

The liver-specific microRNA-122 modulates hepatic response to infection and inflammation by antagonizing YY1, FOXP3, NRF1 and E2F4 molecular networks

Martha Paluschinski, Jessica Schira, Kai Stühler, Dieter Häussinger and Mirco Castoldi

Doctoral Symposium `deLIVER – Technology in Hepatology´, Düsseldorf, 28 – 29 September 2017.

The liver-specific microRNA-122 modulates hepatic response to infection and inflammation by antagonizing YY1, FOXP3, NRF1 and E2F4 molecular networks

Martha Paluschinski, Jessica Schira, Kai Stühler, Dieter Häussinger and Mirco Castoldi

34th Annual Meeting of the German Association of the Study of the Liver (GASL), Hamburg, 26 – 27 January 2018.

Oral presentations:

Functional analysis and characterization of the liver-specific microRNA miR-122 and of its associated targets

Martha Paluschinski

EMBO Practical Course: Analysis of small non-coding RNAs: *Per aspera ad astra*, Brno (Czech Republic), 25 – 31 July, 2015

Functional analysis and characterization of the liver-specific microRNA miR-122 and of its associated targets

Martha Paluschinski, Mirco Castoldi

EMBO Practical Course: Regulatory small and long ncRNAs: *Durat et lucet*, Povo-Trento (Italy), 11 – 17 June, 2016

Functional analysis and characterization of the liver-specific microRNA miR-122 and of its associated targets

Martha Paluschinski, Mirco Castoldi

EMBL Course: Analysis of non-coding RNAs: *Quaerite et invenietis*, Heidelberg (Germany), 9 – 15 September, 2017

The PhD student further contributed to the following studies:

Tauroursodeoxycholate protects from glycochenodeoxycholate-induced gene expression changes in perfused rat liver

Martha Paluschinski, Mirco Castoldi, David Schöler, Nils Bardeck, Jessica Oenarto, Boris Görg, Dieter Häussinger

Biological Chemistry (2019), Vol. 400, Issue 12, 1551 – 1565.

O-GlcNAcylation-dependent upregulation of HO1 triggers ammonia induced oxidative stress and senescence in HE

Boris Görg, Ayşe Karababa, Elina Schütz, Martha Paluschinski, Alina Schrimpf, Aygul Shafigullina, Mirco Castoldi, Hans J Bidmon, Dieter Häussinger

Journal of Hepatology (2019), Vol. 71, Issue 5, 930 – 941.

Hyperosmotic stress activates the expression of members of the miR-15/107 family and induces downregulation of anti-apoptotic genes in rat liver

David Santosa, Mirco Castoldi, Martha Paluschinski, Annika Sommerfeld and Dieter Häussinger

Scientific Reports (2015), Issue 5, article no. 12292.

Dedicated to my father Edward

We must have perseverance and above all confidence in ourselves. We must believe that we are gifted for something and that this thing must be attained.

– Maria Skłodowska-Curie

Dla mojego ojca, Edwarda

Trzeba mieć wytrwałość i wiarę w siebie. Trzeba wierzyć, że człowiek jest do czegoś zdolny i osiągnąć to za wszelką cenę.

– Maria Skłodowska-Curie

Table of contents

List of figures

List of tables

List of abbreviations

3´UTR	three prime untranslated region
5´UTR	five prime untranslated region
AGO	argonaute protein
ALD	alcoholic liver disease
ANOVA	one-way analysis of variance
BMP6	bone morphogenetic protein 6
CAT1	cationic amino acid transporter 1 (also known as SLC7A1)
C/EBPα	CCAAT enhancer binding protein alpha
CEP55	centrosomal protein 55
CHB	chronic hepatitis B
CHX	cycloheximide
CLIC1	chloride intracellular channel 1
c-Myc	MYC proto-oncogene, bHLH transcription factor
Cux1	Cut-like homeobox 1
DGCR8	DiGeorge syndrome critical region 8
E2F4	E2F transcription factor 4
E. coli	*Escherichia coli*
EGFR	epidermal growth factor receptor
EMT	epithelial-to-mesenchymal transition
EPS15L1	epidermal growth factor receptor pathway substrate 15 like 1
FC	fold change
FCS	fetal calf serum
FDR	false discovery rate
FOXP3	Forkhead box P3
G6PDH	glucose-6-phosphate dehydrogenase
GO	Gene Ontology enrichment
GTP	guanosine triphosphate
GW182	trinucleotide repeat-containing gene 6A protein

HBV	hepatitis B virus
HBx	hepatitis B viral X protein
HCC	hepatocellular carcinoma
HCV	hepatitis C virus
HNF1A/ HNF1α	hepatocyte nuclear factor 1A
HNF1B/ HNF1β	hepatocyte nuclear factor 1B
HO1	heme oxygenase-1
IFNβ	interferon beta
IL6	interleukin 6
IL10	interleukin 10
JARID2	Jumonji and AT-rich interaction domain containing 2
KIF11	kinesin family member 11
MCS	multiple cloning site
miR-122	mature microRNA-122
MIR122	miR-122 encoding gene
miRISC	microRNA-induced silencing complex
miRNA	microRNA
MRE	miRNA-responsive element (miRNA binding motif)
mRNA	messenger ribonucleic acid
NAFLD	non-alcoholic fatty liver disease
NANOG	Nanog homeobox
NASH	non-alcoholic steatohepatitis
ncRNAs	non-coding RNAs
NFκB	nuclear factor kappa B
NRF1	nuclear respiratory factor 1
p53	tumor protein P53
PACT	protein activator of PKR
PBC	primary biliary cholangitis
PDGF	platelet-derived growth factor

PDK1	pyruvate dehydrogenase kinase 1
piRNAs	PIWI-interacting RNAs
PKM2	pyruvate kinase M2
pre-miRNA	precursor microRNA
pri-miRNA	primary microRNA transcript
qPCR	quantitative *real-time* PCR
REST	RE1 silencing transcription factor
RISC	RNA-induced silencing complex
Rpm	revolutions per minute
rRNA	ribosomal RNA
RTase	reverse transcriptase
SEM	standard error of the mean
siRNAs	small-interfering RNAs
SLC1A5	solute carrier family 1 member 5
SLC7A1	solute carrier family 7 member 1
SMAD	sma- and mad-related protein
SOCS3	suppressor of cytokine signaling 3
SRF	serum response factor
STAT	signal transducers and activators of transcription
TGFβ1	transforming growth factor beta 1
THRA	thyroid hormone receptor alpha
TK1	thymidine kinase 1
TNFα	tumor necrosis factor alpha
TNRC6	trinucleotide repeat containing adaptor 6A
TRBP	TAR RNA binding protein
TSS	transcriptional starting site
WNT	wingless-type MMTV integration site family
XRN	5´ - 3´ exoribonuclease
YY1	Yin Yang 1 transcription factor

Summary

The liver-enriched microRNA miR-122 plays a central role in the maintenance of liver physiology. Aberrant levels of miR-122 are associated to the pathogenesis of liver diseases such as viral infections as well as cirrhosis and hepatocellular carcinoma. Despite the fact that numerous miR-122 targets have already been identified, the global effect of miR-122 on the cellular gene networks remains largely unknown.

To gain an insight into these genome-wide networks, two complementary approaches were used on Huh-7 cells: (I) Transcriptome analysis of polyribosome-bound RNAs revealed that miR-122 displays an antagonistic activity on the transcription factors Yin Yang 1 (YY1), Forkhead box P3 (FOXP3), E2F transcription factor 4 (E2F4), and nuclear respiratory factor 1 (NRF1). (II) By proteome analysis, several miR-122 target gene candidates were identified and validated, including genes upregulated in hepatocellular carcinoma (HCC), like glucose-6-phosphate dehydrogenase (G6PDH). Interestingly, an inverse correlation between miR-122 and *G6PDH* mRNA levels in the HCC tissue of patients suffering from chronic hepatitis B infection was determined, whereas no correlation was found in HCC patients without viral infection.

Furthermore, it was demonstrated that the biogenesis of miR-122 is modulated in response to cytokine and growth factor administration. While interleukin 6 (IL6), tumor necrosis factor α (TNFα), and to some extent bone morphogenetic protein 6 (BMP6) increased the promoter activity of the human *MIR122* gene, transforming growth factor β 1 (TGFβ1) significantly reduced the promoter activity and inhibited miR-122 *de novo* synthesis.

Taken together, the present study places miR-122 into a central position in the regulation and fine-tuning of liver homeostasis. It is proposed that alteration in the signaling pathways driven by cytokines or growth factors, which is frequently observed in chronic liver diseases, may be one of the factors contributing to miR-122 dysregulation. As a possible result, the decoupling of miR-122 from its regulatory networks, including those controlled by YY1, FOXP3, NRF1, and E2F4, may be one of the molecular mechanisms contributing to the complex cellular alterations that are involved in the pathogenesis of liver diseases.

Zusammenfassung

Die leberspezifische microRNA miR-122 ist für die Physiologie der Leber von zentraler Bedeutung. Eine Fehlregulation der miR-122 ist assoziiert mit der Pathogenese unterschiedlicher Lebererkrankungen, wie entzündlichen Lebererkrankungen (NAFLD), viralen Hepatitis (Typ B und C), sowie der Leberzirrhose und dem Leberzellkarzinom. Obwohl zahlreiche Zielgene der miR-122 bereits identifiziert werden konnten, ist der genomweite Effekt der miR-122 auf die zelluläre Genexpression weitgehend unbekannt.

Mit dem Ziel die genetischen Netzwerke, die durch miR-122 moduliert werden, zu identifizieren, wurden zwei komplementäre Methoden verwendet: (I) Transkriptomanalysen von Polysom-gebundenen mRNAs in humanen Hepatomazellen (Huh-7) ergaben, dass miR-122 einen antagonistischen Effekt auf die Transkriptionsfaktoren Yin Yang 1 (YY1), Forkhead Box P3 (FOXP3), E2F Transkriptionsfaktor 4 (E2F4) und nukleärer respiratorischer Faktor 1 (NRF1) ausübt. (II) Mittels Proteomanalysen wurden zahlreiche potentielle Zielgene der miR-122 identifiziert und validiert. Diese umfassten insbesondere solche, die in Lebererkrankungen wie dem Leberzellkarzinom verstärkt exprimiert werden, wie beispielsweise die Glucose-6-phosphat-Dehydrogenase (G6PDH). Des Weiteren wurde gezeigt, dass die Level der *G6PDH* mRNA sowie die relative Expression der miR-122 im Tumorgewebe von Leberzellkarzinompatienten mit Hepatitis B Infektion invers korrelieren. Im Gegensatz hierzu konnte keine signifikante Korrelation zwischen *G6PDH* mRNA und miR-122 im Tumorgewebe von Kontrollpatienten (ohne virale Hepatitis) gefunden werden.

In einem weiteren Teil der Arbeit wurde der Einfluss von Zytokinen und Wachstumsfaktoren auf die Biogenese der miR-122 untersucht. Es wurde gezeigt, dass Interleukin 6 (IL6), Tumornekrosefaktor alpha (TNFα) sowie tendenziell das knochen-morphogenetische Protein 6 (BMP6) die Aktivität des human *MIR122* Promoters erhöhen, wohingegen der transformierende Wachstumfaktor β 1 (TGFβ1) die Promoteraktivität verringert und die miR-122 Neusynthese inhibiert.

Die vorgelegte Arbeit misst der microRNA miR-122 eine Schlüsselrolle bei der Aufrechterhaltung der Leberhomöostase bei. Die hier gezeigten Befunde legen die Vermutung nahe, dass Zytokin- und Wachstumsfaktor-vermittelte Änderungen der Signaltransduktions-wege, wie sie bei Lebererkrankungen beschrieben sind, einen Einfluss auf die Fehlregulation der miR-122 bei Lebererkrankungen haben. In Folge dessen, werden miR-122-vermittelte genetische Netzwerke aus dem Gleichgewicht gebracht, wie zum Beispiel solche, die durch die Transkriptionsfaktoren YY1, FOXP3, NRF1 und E2F4 reguliert werden. Dieses Ungleichgewicht wiederum könnte ein möglicher molekularer Mechanismus sein, der zur Pathogenese der Lebererkrankungen beiträgt.

1. Introduction

1.1 The rise of the non-coding transcriptome

The discovery of non-coding RNAs (ncRNAs) in the early 1990s has changed our understanding of the function of ribonucleic acids (RNA) and their involvement in cellular processes completely. For several decades it was believed that RNA solely served as template for the protein synthesis in the form of messenger RNA (mRNA) and as structural platform for the translational machinery in the form of ribosomal RNA (rRNA) and transfer RNA (tRNA) [*1*, *2*]. However, the classical view on RNA has changed drastically since microarrays and deep sequencing techniques became widely available. Due to these applications, several independent studies identified that a large portion of the transcriptome does not encode for functional proteins [*3–7*]. Recent studies from the *Encyclopedia of DNA Elements* (ENCODE) project revealed that 80% of the human genome is actively transcribed, although only 2.9% of the genome account for protein-coding genes [*8*, *9*]. The discovery of the non-coding transcriptome (i.e. the total amount of non-protein coding RNAs) raised the question of its function. Despite skeptical views believing that most of these ncRNAs might be `translational noise´ or `genomic junk´ [*10*], compelling evidence indicate that ncRNAs are involved in the regulation of nearly every aspect of gene expression [*11*]. Moreover, already in 1994 Mattick *et al.* hypothesized that the development of so-called regulatory RNAs was a prerequisite for the development of complex organisms [*1*, *12*]. In line with this hypothesis, the number of ncRNAs is rising with increasing complexity of the organism [*13*].

Although uniform criteria for their classification are still lacking, ncRNAs have been grouped based on their function or their length (Figure 1.1; [*14*, *15*]). The functional classification distinguishes between `structural ncRNAs´ such as the well-known ribosomal RNAs [*16*], transfer RNAs [*17*], small nuclear RNAs [*18*, *19*] or small nucleolar RNAs [*20*] on the one hand and the `regulatory ncRNAs´ on the other hand. The latter group includes the small non-coding RNAs (small ncRNAs) and the growing class of long non-coding RNAs (lncRNAs). The small ncRNAs (also referred to as `short ncRNAs´) comprises ncRNAs with a length typically below 200 nucleotides, like microRNAs (miRNAs), short-interfering RNAs (siRNAs), and PIWI-interacting RNAs (piRNAs). Long non-coding RNAs can reach up to several kilobase pairs in length. Thus far, lncRNAs are often discriminated according to their genomic origin in

intergenic lncRNAs, intronic lncRNAs and antisense lncRNAs, although several other classifications are likewise in use [*21*, *22*].

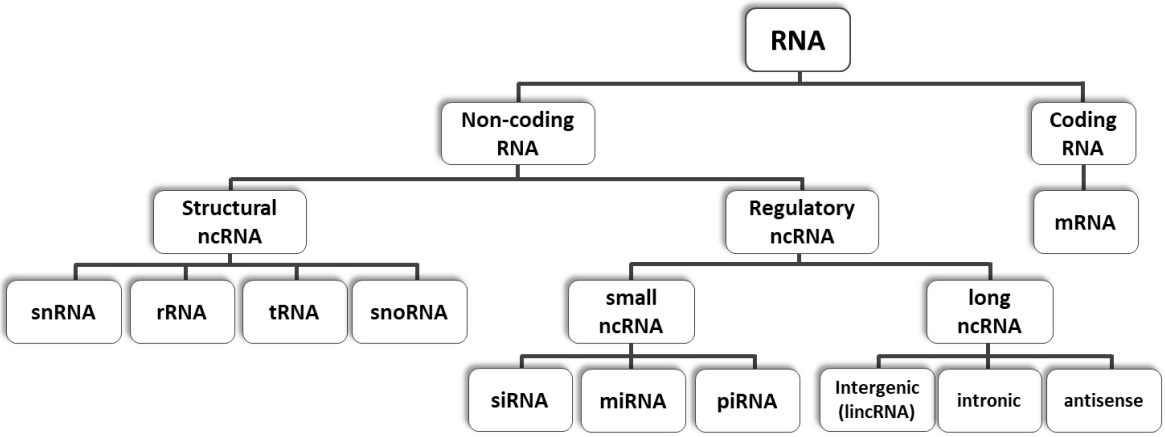

Figure 1.1: Classification of RNA subtypes in coding and non-coding RNAs. A proposed classification of RNA types in coding and non-coding RNAs (ncRNAs) as well as sub-classification of non-coding RNAs in `structural ncRNAs´ (also referred to as `housekeeping ncRNAs´ [*23*]) and `regulatory ncRNAs´. Findings were combined from [*14*, *15*] and illustrated herein. Abbreviations: miRNA: microRNA, piRNA: PIWI-interacting RNAs, rRNA: ribosomal RNA, siRNA: small-interfering RNAs, snRNA: small nuclear RNAs, snoRNA: small nucleolar RNA, tRNA: transfer RNA.

Since the research on regulatory ncRNAs is still in its infancy, it becomes apparent that their classification will become more complex and might change due to the identification of new subclasses or novel functions of ncRNAs.

The discovery of ncRNA opened up a new research field with major emphasis on the functional involvement of ncRNAs in cellular processes. Nowadays, it is known that regulatory ncRNAs participate in a variety of process including epigenetic mechanisms such as DNA and histone modifications as well as the regulation of gene expression at the transcriptional and the post-transcriptional level. In this way, ncRNAs not only play important roles in the maintenance of the cellular integrity and the response to environmental influences, but also in differentiation processes and development.

1.1.1 The discovery of microRNAs

The first founding member of miRNA family (lin-4) was discovered as regulator of *C. elegans* larval development in the laboratories of Ambos and Ruvkun in 1993 [*24*, *25*]. In these early works it was demonstrated that lin-4 controls temporal development by targeting the 3´-untranslated region (3´UTR) of the protein-coding gene *lin-14* [*24*, *25*]. In the year 2000,

let-7 was identified as second member of the miRNA family based on similar functions in *C. elegans* [*26*, *27*]. Initially thought to be a rarity in nematodes, the discovery that *let-7* is highly conserved across metazoa together with the newly identified RNA interference as widely existing mechanism for post-transcriptional gene regulation, gave rise to an entirely new research field [*28*]. By means of molecular cloning, hundreds of different miRNAs were identified and the name `microRNA´ was established for this class of ncRNAs [*29–38*]. Since then, miRNAs comprise the most studied and best characterized class of ncRNAs. According to the most recent release of the miRNA data bank *miRBase*, 38,589 mature miRNAs are listed in 271 different organisms, of which 1,917 miRNA members were identified in humans (*miRBase* release 22.1, October 2018; [*39*, *40*]). Bioinformatic analyses predicted that miRNAs regulate up to one third of all protein-coding genes in humans [*41*]. Therefore, it is hardly surprising that miRNAs participate in a broad range of cellular processes, such as development and differentiation, proliferation as well as cell metabolism, and apoptosis [*42–46*]. Moreover, the deregulation of the `miRNome´ (i.e. the entire set of miRNAs in a cell or organism) is associated with a plethora of malfunctions and diseases such as cancer, coronary heart disease, as well as metabolic and liver diseases [*47–56*]. In recent years the value of miRNAs as predictive and prognostic biomarkers on the one hand and as molecular targets for therapeutic intervention on the other hand were emphasized in various independent studies [*57–59*].

1.2 Biogenesis of microRNAs

1.2.1 The canonical miRNA biogenesis pathway

The expression of many miRNAs is highly specific in a temporal and a spatial manner [*28*, *60*]. Genomic sequences encoding for miRNAs can be found in three locations. Firstly, in intergenic regions [*61*, *62*], which may encode for either a single miRNA gene or for multiple miRNAs arranged in miRNA clusters [*29*, *30*, *63*], secondly in the introns (`intronic miRNAs´) or lastly, in the exons of protein-coding genes [*64*, *65*].

The transcription of miRNAs is typically performed by RNA polymerases II or III, which generate a hairpin-structured primary miRNA transcript (pri-miRNA) with up to several kilobase pairs in length [*66–68*]. Similar to mRNAs, pri-miRNAs that are transcribed by RNA polymerase II are frequently poly(A)-tailed and 5´-capped [*66*]. The processing of pri-miRNA

to mature miRNA is conducted in two distinct steps involving endonucleatic cleavages in the nucleus as well as in the cytoplasm (Figure 1.2).

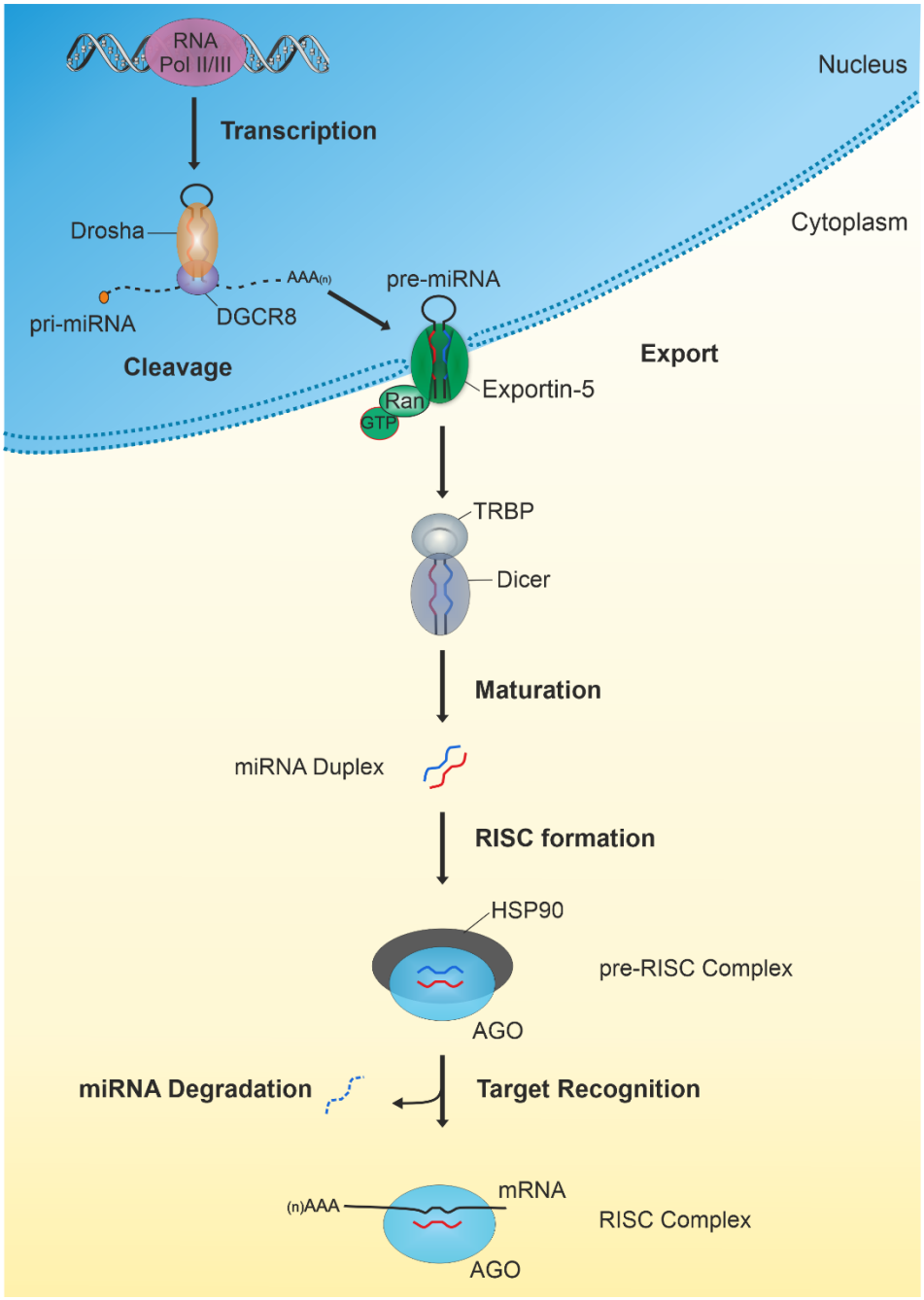

Figure 1.2: miRNA biogenesis via the `canonical´ pathway. (Modified and adapted by [*69*, *70*]). MicroRNAs are transcribed by RNA Polymerase II or III (RNA Pol II/ III) as long, primary hair-loop structured transcripts (pri-miRNAs). The maturation of miRNA involves the processing via the microprocessor complex (Drosha/ DGCR8) in the nucleus, which releases the shortened precursor microRNA (pre-miRNA). Following nuclear export via exportin-5, the stem-loop sequence of the pre-miRNA is cropped by the RNase Dicer, producing the mature miRNA duplex. The duplex is recruited to Argonaute proteins (AGO) and loaded into the RNA-induced silencing complex (RISC). The assembly of the RISC complex is an ATP-dependent process that requires heat shock proteins such as HSP90 as molecular chaperones. One of the mature miRNA strands remains assembled to the RISC complex to mediate target mRNA recognition, while the other strand is typically degraded.

The first maturation step of the `canonical´ miRNA biogenesis pathway is initiated in the nucleus by a protein complex termed microprocessor. It consists of a double-stranded RNA-binding protein DGCR8 (also known as Pasha in *D. melanogaster* and *C. elegans*) and the RNase III Drosha [*71*, *72*]. The microprocessor complex cleaves the base of the pri-miRNA stem and releases a cropped, stem-loop shaped RNA of roughly 65-70 bp in length, known as precursor-miRNA (pre-miRNA) [*73*, *74*]. Interestingly, it was reported that the DEAD-box RNA helicases p68 and p72 are associated subunits in the microprocessor complex of mice and required for the synthesis of a subset of, albeit not all, miRNAs [*75*]. While the processing of pri-miRNAs by the microprocessor was found to be crucial for the majority of miRNAs, intronic miRNA may also be produced independently of Drosha. This subset of miRNAs is typically generated from miRNA-coding introns (so called `mirtrons´) and is processed via the spliceosomal pathway [*76*, *77*].

The endonucleolytic cleavage by Drosha or the spliceosome creates a two nucleotide overhang at the 3´-end of the pre-miRNA which is necessary for the binding of pre-miRNAs to the nuclear transporter protein exportin-5. Subsequently, the pre-miRNA is translocated from the nucleus into the cytoplasm. This process requires the small G-protein RAN as cofactor that provides the energy for the exportin-5-mediated transport by hydrolyzing guanosine triphosphate (GTP) to guanosine diphosphate (GDP) [*78–81*]. Following nuclear export, the pre-miRNA is processed by a second endonuclease, Dicer, which acts as molecular ruler to produce a 21 – 25 nucleotide long miRNA duplex consisting of two mature miRNA strands [*82–85*]. The maturation of pre-miRNA by Dicer requires the double-stranded RNA binding proteins TAR RNA binding protein (TRBP) and protein activator of PKR (PACT) which serve as cofactors and regulators of Dicer activity [*86–88*]. The miRNA duplex is then loaded into the effector complex known as the RNA-induced silencing complex (RISC or miRISC) by binding to Argonaute family proteins (AGO) [*89*, *90*]. The assembly of miRNAs into the RISC complex is ATP-dependent and requires the assistance of heat shock proteins such as HSP90 or HSP70 [*91*]. Although the exact mechanism of how the miRNA duplex is incorporated into the RISC complex is still under debate, it is known that the unwinding of mature miRNA duplexes into single-stranded miRNAs depends on the activity of helicases such as p68 or the RNA helicase A [*69*, *92–94*].

Initially it was believed that only the thermodynamically less stable miRNA strand (`guide strand´ or `miR´) is loaded into the RISC to participate in target gene silencing, whereas

the miRNA strand with higher stability at the 5´-end (`passenger strand´ or `miR*´) was believed to be degraded [*95*, *96*]. However, in recent years this hypothesis was disproved due to compelling evidence indicating that both mature miRNA strands can be functional (reviewed by [*97*, *98*]). As a consequence, the nomenclature of identified miRNA species has changed and, nowadays, the mature miRNA is designated according to their position in the pre-miRNA sequence (located towards the 5´-end [miR-X-`5p´] or towards the 3´-end [miR-X-`3p´]) rather than based on miRNA stability [*99*].

1.2.2 Regulation of miRNA biogenesis

Considering the fact, that miRNA deregulation is frequently observed in human diseases, it becomes apparent that a tight control of the miRNA biogenesis is indispensable for the maintenance of cellular function. In addition, miRNAs are a mean to ensure a fast response to environmental changes by simultaneously modulating a broad number of targets without the requirement to synthesize proteins [*100*]. The cellular miRNA expression may be altered as a result of pathogen infection and immune response activity, in response to growth factor and cytokine signaling or cellular stressors [*100*–*104*]. For instance, increasing evidence suggest that oxidative stress affects the expression of redox-sensitive miRNAs, so called `redoximiRs´, which in turn orchestrate the cellular redox homeostasis [*105*]. This was shown for example for the miR-15/16 family members in perfused rat livers treated with either hyperosmotic medium or with the hepatotoxic bile acid glycochenodeoxycholate [*106*, *107*] or for the miR-326-3p in ammonia-treated astrocytes [*108*, *109*].

1.2.2.1 Regulation of miRNA transcription

The miRNA biogenesis is regulated on every level comprising the gene transcription, the maturation of the pri-miRNA and ultimately the miRNA decay. As for proteins, the expression of miRNA genes is coordinated by numerous mechanisms and highly depends on the genomic context of the miRNA. While genes encoding for intergenic miRNAs are under the regulation of autonomous promoters, the majority of intronic miRNAs are co-expressed together with their host protein-coding gene [*110*]. Intensive efforts were made to identify promoter sequences of intergenic miRNAs, which relied on the identification of well-known features of protein-coding genes including transcriptional starting sites (TSS), CpG islands, TATA box

sequences and characteristic histone modifications [*111–113*]. However, so far the promoters of only 80% of all validated miRNAs were identified in human and mouse genomes, respectively [*114*].

Similar to the promoters of protein-coding genes, promoters of miRNA-encoding genes are under the control of various transcription factors such as p53 [*115–117*], NFκB [*118*], c-Myc [*49*] or tissue-specific transcription factors like the liver-specific transcription factor HNF4α [*119*]. Surprisingly, although many intronic miRNAs are transcribed from the host gene promoter, the expression of intronic miRNA and protein-coding gene may also occur through distinct promoter regions, leading to a miRNA transcription independent of the host gene [*112*, *120*]. In addition to the regulation via promoter sequences, the gene expression of miRNAs is modulated epigenetically through genomic imprinting, DNA methylation and alterations in histone modifications [*121–123*].

1.2.2.2 Regulation of miRNA maturation

Numerous mechanisms exist to control the maturation of miRNAs on a transcriptional and post-transcriptional level. For instance, acetylation and phosphorylation of the processing factors Drosha and DGCR8 affect their protein stability, their nuclear localization and their substrate affinity [*124–127*]. The processing of pri-miRNAs by the microprocessor is also responsive towards several signaling pathways. Davis and coworkers revealed that the activation of SMAD proteins induced by stimulation with transforming growth factor β 1 (TGFβ1) or bone morphogenetic protein 4 (BMP4) increased the expression of several miRNAs [*128*, *129*]. As a consequence of receptor activation by TGFβ1 or BMP4, phosphorylated SMAD proteins translocate to the nucleus where they bind to specific motifs within the pri-miRNA stem region and thereby enhance the Drosha-mediated cleavage [*100*, *128*, *129*]. In response to DNA damage, the tumor suppressor p53 increases pri-miRNA processing by directly binding to the p68 helicase within the microprocessor complex [*130*, *131*]. In addition, the activation of the serine/ threonine kinase Ataxia Telangiectasia Mutate (ATM), a key enzyme of the DNA damage response and activator of p53 [*132*], promotes the translocation of pre-miRNA into the cytoplasm [*133*]. ATM activation triggers the phosphorylation of the nuclear complex core protein Nup153 which in turn associates with exportin-5 and accelerates pre-miRNA export [*133*]. In the cytoplasm, the endonuclease Dicer mediates the last step of the miRNA

maturation and its activity strongly depends on the expression of its cofactors TRBP and PACT [*87*, *134*, *135*]. Moreover, Dicer activity was shown to be sensitive to signaling pathways induced by cellular stress and by interferons (IFNs; [*136*]). While IFNα signaling increased Dicer-dependent pre-miRNA processing, IFNγ decreased Dicer activity [*136*]. Remarkably, a negative feedback mechanism exists between Dicer and its cleavage products. As shown for let-7a, *Dicer* mRNA harbors binding sites for miRNAs, which may prevent an overexpression of Dicer in order to maintain the equilibrium between Dicer activity and miRNA maturation [*137*, *138*].

1.2.2.3 Post-transcriptional regulation of miRNAs and their implication in miRNA decay

The stability of mature miRNAs is highly heterogeneous and may vary from several hours up to days, depending on the individual miRNA [*111*, *139*, *140*]. In the recent years multiple post-transcriptional miRNA modifications were identified, giving rise to various miRNA isoforms, which affect the half-life and/ or the target specificity of these so called `isomiRs´ [*141*, *142*]. The modification of adenosine (A) to inosine (I) (known as `miRNA editing´) was shown to affect the structures of pri-miRNAs as well as the target specificity of mature miRNAs [*143*–*145*]. Besides A-to-I editing, miRNAs may be subject to trimming events at the 5´- or the 3´-end, in which single nucleotides may be removed, or undergo miRNA tailing, a non-templated nucleotide addition [*70*, *146*]. Strikingly, oligo-U-tailing of the 3´-end of let-7a-5p decreased Dicer-mediated processing and increased miRNA decay [*147*]. In contrast, a single 3´-end adenylation of the liver-specific miR-122-5p was sufficient to prevent miRNA degradation and to increase miR-122-5p stability [*148*]. Furthermore, isomiRs with heterogeneous 3´- or 5´-ends may be produced as a result of imprecise cleavage by the nucleases Drosha and Dicer [*149*, *150*]. Due to the fact that the 5´-end was shown to be the most critical moiety for miRNA target gene recognition [*151*], it was proposed that editing of the 5´-end of miRNAs has a profound effect on the target specificity of isomiRs, whereas 3´-end modifications rather affect the miRNA processing and stability [*70*]. Independent studies suggest that the miRNA stability also depends in part on its association to target mRNAs [*111*]. However, contradictory findings show that miRNA-mRNA binding may prevent miRNA degradation [*152*, *153*], while other studies support the conclusion that mRNAs decrease the half-life of their regulating miRNAs [*154*, *155*].

Thus far, nucleases known to contribute to the degradation of a large number of miRNAs are only known in *A. thaliana* (RNA degrading nucleases SDN1-3; [*156*]) and *C. elegans* (5' - 3' exoribonuclease XRN2; [*152*]). In humans, several enzymes were proposed to mediate miRNA decay, such as XRN1 [*139*] and the polynucleotide phosphorylase PNPase [*157*]. Nevertheless, studies investigating the effect of XRN1 and PNPase focused on the expression of selected miRNAs and failed to demonstrate an involvement on the cellular miRNome [*139*, *157*].

1.3 Mechanism of miRNA-mediated target silencing

MicroRNAs direct Argonaute proteins to their target mRNAs in a sequence-specific manner [*158*, *159*], whereby the association of miRNAs to their targets is mediated through hydrogen bonds between complementary nucleobases [*24*, *25*]. The vast majority of miRNA recognition sites (MREs) are located in the 3´UTRs of the target mRNAs [*160*, *161*], but binding motifs may also reside in the coding sequence [*41*, *162*, *163*] or the 5´-untranslated region (5´UTR; [*164*, *165*]), albeit with lower prevalence [*166*]. The duplex formation of miRNA and target mRNA in the RISC complex may result in mRNA degradation or in translational repression. The mode of action depends on the complementarity between miRNA and mRNAs [*167*] as well as on the AGO isoform bound within the RISC complex [*158*, *168*, *169*]. The classical view of miRNA-induced target silencing suggests that perfect base pairing (which occurs mainly in plants) triggers the degradation of target mRNA, while imperfect base pairing (the major mechanism in animals) results in mRNA translational repression. [*45*]. Yet, a growing number of studies suggest that mRNA degradation and translational repression coexist in both, plants and animals [*170–172*]. Despite intense research efforts, it remains highly controversial which mode of action predominantly mediates target gene silencing [*173*].

1.3.1 Basic motifs of miRNA-target gene recognition

Early studies from 2003 identified that members of conserved miRNA families retain a high sequence homology at their 5´-end throughout evolution [*151*, *174*]. This moiety, located at position 2 – 7 in the mature miRNA and referred to as the `seed sequence´ [*151*], was shown to harbor the sequence that is most critical for the target mRNA recognition of a given miRNA [*163*, *170*]. Furthermore, within the 3´UTR of well-known miRNA target mRNAs, a widespread

conservation for sequences complementary to the miRNA seed motifs was identified [*41*, *161*]. Elaborate investigations on the conservation of seed sites across the eukaryotic lineage enabled the proposal of seed-pairing rules describing the requirement for functional miRNA-mRNA binding [*163*, *175–177*]. These rules, although complemented and refined during the last years [*178*, *179*], represent the fundament for the development of numerous miRNA target prediction tools [*151*, *180*].

Bartel and coworkers analyzed conserved MREs on the 3´UTR of target genes and identified several classes of target sites: `canonical sites´, `atypical canonical sites´, and `non-canonical sites´ [*166*, *181*]. The canonical binding motifs of miRNAs-mRNA duplexes have a 6 nucleotide long perfect Watson-Crick base pairing within the miRNAs´ seed sequence (`6mer´; Figure 1.3). This stretch may be shifted by one nucleotide to either 3´- or 5´-direction (`offset 6mer´; [*182*]), be prolonged by another perfect base match at position 8 and/ or harbor a conserved adenosine in the mRNA in the position across form the first nucleotide of the miRNA (`7mer´ or ` 8mer´ as illustrated in Figure 1.3; [*41*, *181*]).

The 7 – 8mer canonical sites were demonstrated to have strongest efficiency in gene repression compared to 6mer or offset 6mers [*182–185*]. Surprisingly, the occurrence of adenosines opposite from nucleotide 1 of the miRNA increases the repression efficacy independent of the miRNA sequence [*41*, *181*]. Later studies demonstrated that the first nucleotide at the 5´-end of the miRNA does not participate in the target recognition and that mRNAs with adenosines at this position are preferentially bound by the AGO proteins [*186*, *187*]. Apart from pairing to the miRNA seed, additional binding sites were identified between mRNA and the miRNA, typically involving the miRNAs´ position 13 – 16 at the 3´-end [*163*]. This binding motif (also known as `atypical canonical sites´; [*181*]) affects the binding affinity, stability of the RISC complex as well as the efficacy of the mRNA repression [*163*, *188*, *189*].

Perfect base matches within the seed sequence of the target site are not essential to retain a functional mRNA repression [*190*, *191*]. So-called `non-canonical´ miRNA target sites contain miss-match pairings in the seed sequence [*191*, *192*], which are compensated by extensive pairing encompassing at least 4 additional hydrogen bonds in the 3´-region (Figure 1.3; [*166*]). It is believed that non-canonical sites account for less than 2% of all miRNA sites [*182*] and trigger mRNA repression only with moderate effects [*193–196*]. Nonetheless, their discovery led to the refinement of the seed pairing rules and, subsequently, the target

prediction algorithms [*178*, *179*]. Moreover, target mRNA repression via atypical canonical or non-canonical sites may provide an explanation how isomiRs (which may differ in as few as a single nucleotide) achieve distinct target specificity.

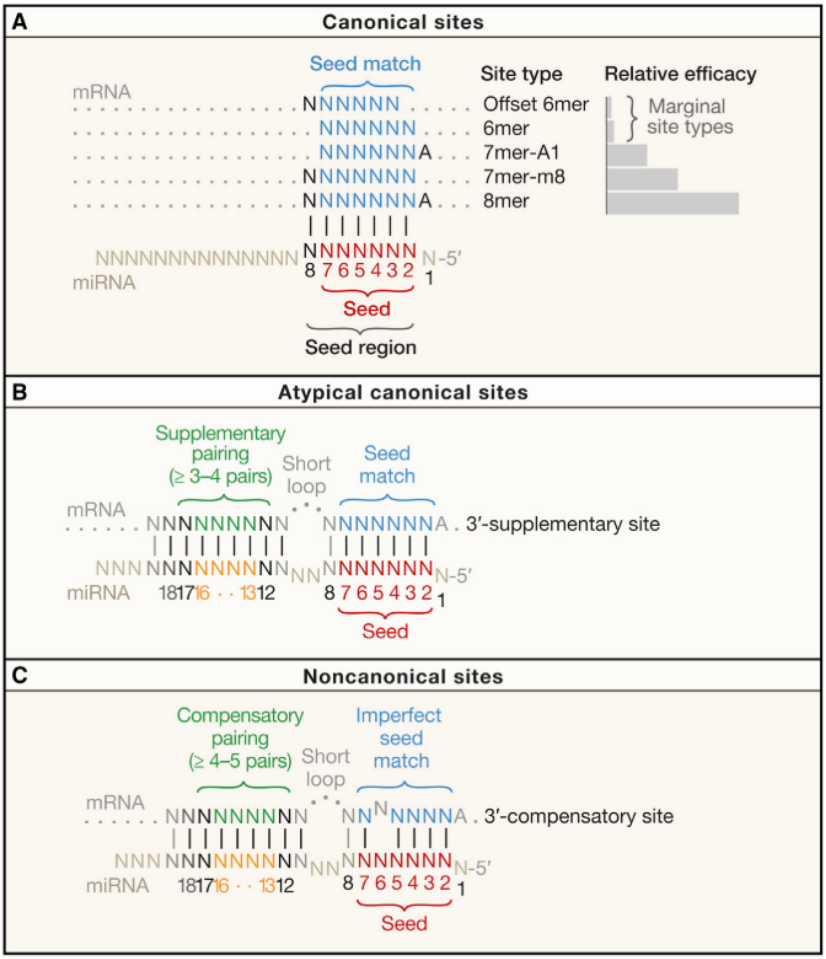

Figure 1.3.: Watson-Crick base pairing of mammalian miRNAs with their target mRNAs. (Adapted from David Bartel, 2018; [*181*])**.** Vertical lines indicate perfect base pairing between miRNA and mRNA. **A**) Canonical binding sites of miRNA bases in position 2 – 7 (`seed sequence´) and target mRNA. The relative efficiency of target mRNA inhibition by miRNA base pairing is illustrated as bar chart on the right hand side. Seed pairing may be shifted by one nucleotide to either direction (`offset 6mer´) or (`7mer´ and `8mer´, respectively). **B**) Atypical canonical site with extended sequence complementarity at position 13 – 16. **C**) Non-canonical sites compensate imperfect base pairing in the seed sequence by extensive base pairing with the 3´-end of the miRNA. (Reprinted by permission from Rightslink: Elsevier, Cell, David P. Bartel 2018; license no. 4697680786516).

1.3.2 Molecular mechanisms of target mRNA repression by microRNAs

Intensive studies were conducted to unravel the mechanisms leading to miRNA-mediated post-transcriptional gene regulation. Early findings already suggest that individual miRNAs modulate a great number of target genes [*170*], which is why even minor changes in the expression of certain miRNAs may have pronounced physiological effects [*100*].

The AGO proteins have often been referred to as the crucial components of the RISC effector complex, determining whether target mRNA is subject to degradation or to translational repression. However, although mRNA degradation is considered the main mechanism in animals, only AGO2 exerts endonucleolytic activity mediating mRNA degradation. Yet, all four family members (AGO1 – 4) participate in mRNA translational repression [*168*, *169*]. Nowadays, multiple studies indicate that miRNAs trigger mRNA inhibition in at least three different ways: the induction of mRNA degradation, the inhibition of translational initiation and the premature termination of mRNA translation (reviewed by [*173*, *177*]).

1.3.2.1 miRNA-mediated induction of mRNA decay

Similar to siRNAs, miRNAs may mediate the endonucleolytic cleavage of target messengers via the RNA interference machinery [*190*, *197*]. Following target recognition by the small RNA and assembly of the RISC complex, AGO proteins slice the targeted mRNA opposite of the miRNA nucleotides 10 – 11 (Figure 1.4 A; [*198*, *199*]). The resulting fragments are further degraded by the activity of 5´-to-3´exonucleases, such as XRN4, or by a multi-protein complex named exosome [*200*, *201*]. Structural analyses revealed that a fully complementary pairing of miRNA to its target is a prerequisite for this mechanism to occur [*186*, *202*]. In light of the fact that miRNA-mRNA duplexes in animals frequently occur through imperfect base pairing, endonucleolytic mRNA degradation is thought to be the dominant mechanism in plants rather than in animals [*197*, *203*].

Nonetheless, target degradation was also observed in metazoans through a different mechanism in which mRNAs are subject to progressive degradation by the action of exonucleases (Figure 1.4 B; [*204*, *205*]). This mechanism requires the association of the AGO C-terminus with GW182, a protein containing multiple glycine-tryptophan (GW)-repeats [*206*, *207*]. GW182 (or its mammalian counterpart TNRC6) serves as anchor to recruit additional effector proteins to the RISC complex, including the deadenylase complexes PAN2-PAN3 and CCR4-NOT, which in turn successively remove the poly(A) tail of the target mRNA [*208–211*]. Following deadenylation, mRNA is decapped in the miRISC complex by the decapping protein DCP2 [*209*, *212*]. Several cofactors, including DCP1, EDC4 and the helicase RCK are essential for proper 5´-cap removal, as the depletion of these factors suppressed miRNA-induced target

silencing [*213*, *214*]. Ultimately, the deadenylated and decapped mRNA is rapidly degraded by the cytoplasmic 5´ - 3´ exonuclease XRN1 (a paralog of the plant XRN4; [*200*, *204*, *215*]).

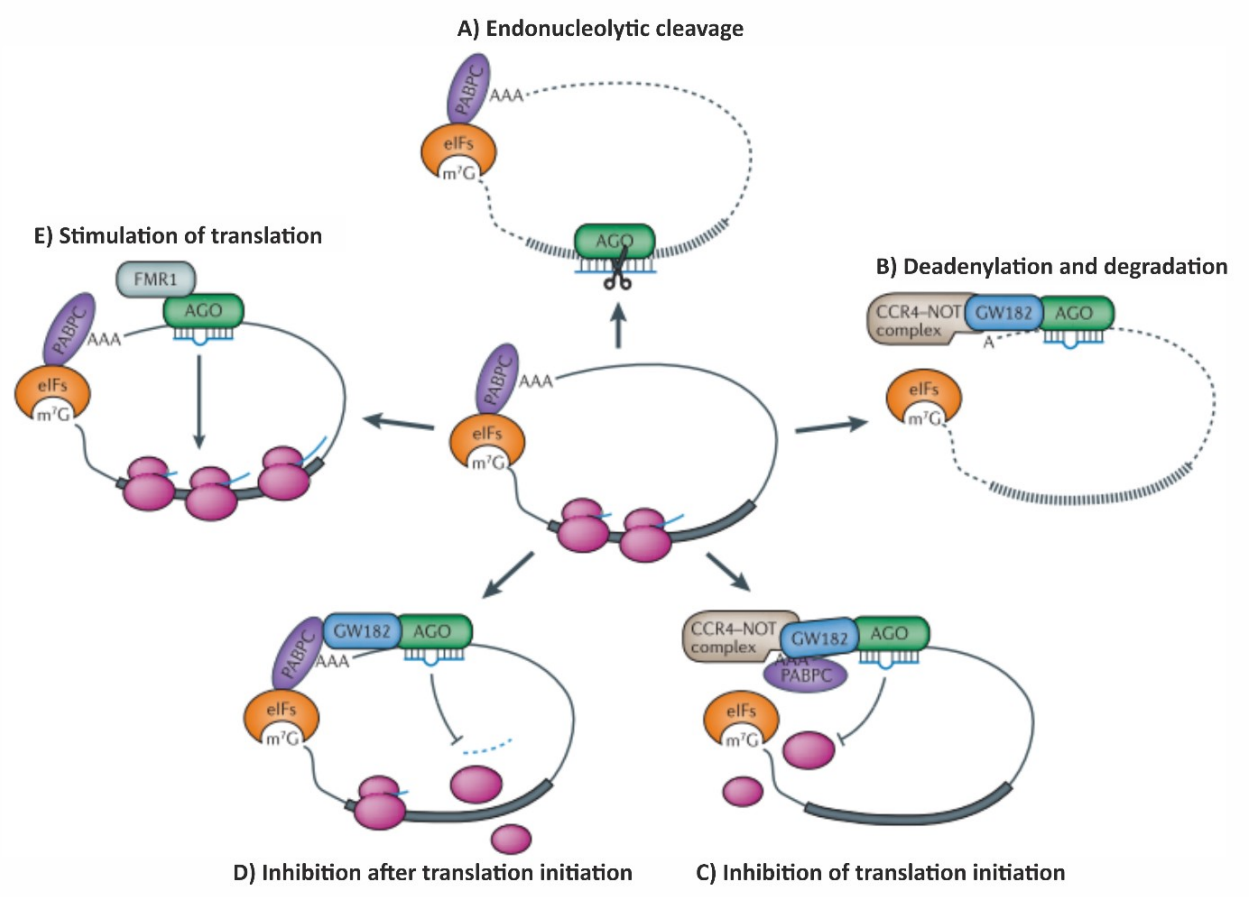

Figure 1.4: Potential mechanisms for target regulation by microRNAs. (Adapted from [*216*]). Multiple mechanisms were identified by which miRNAs achieve target mRNA repression. **A)** AGO-mediated endonucleolytic cleavage as result of perfect base pairing between miRNA and target mRNA (presumably the major mode of plant miRNAs). **B-E)** Imperfect base pairing as pivotal target recognition event in metazoan. **B)** GW182 protein interacts with the miRISC complex and recruits the protein complex CCR4-NOT that induces deadenylation and 5´-to-3´ exonucleolytic mRNA degradation. **C)** Association of GW182 anchor protein with poly(A)-binding protein (PABPC) inhibits mRNA circularization, a prerequisite for translational initiation. **D)** Translational repression induced at the elongation step by promoting premature termination (ribosome drop-off). **E)** miRNAs upregulate the mRNA translation by recruiting AGO and fragile X mental retardation protein 1 (FMR1) to AU-enriched elements in the 3´UTR of target mRNAs. (Reprinted by permission from Rightslink: Springer Nature, Nature Reviews Genetics, Pasquinelli *et al.*, 2012; license no 4701970535344).

1.3.2.2 Regulation of translational repression

The GW182-induced recruitment of CCR4-NOT and the deadenylation of mRNA do not necessarily lead to mRNA decay, but they also affect mRNA translation [*217*, *218*]. Typically, eukaryotic mRNA is activated for translation through the interaction with the initiation factor eIF4F to the 5´-cap structure and through association of the poly(A) binding protein PABPC to

the poly(A)-tailed mRNA as well as to eIF4G initiation factor (reviewed by [*219*]). These interactions result in the formation of a circular, activated mRNA as illustrated in Figure 1.4 (center panel; [*220*]). GW182 negatively affects the binding of PABPC to the eIF4G factor, thus, preventing mRNA circularization and subsequent ribosome assembly (Figure 1.4 C; [*221*, *222*]). Moreover, other studies support the hypothesis that miRNAs repress translation initiation by provoking the dissociation of initiation factors (including eIF4A, eIF4E or eIF4G) from the mRNA [*223*, *224*] or by impairing the recognition of the 5´-cap structure of target mRNAs [*225–227*]. Interestingly, structural analyses from Kiriakidou *et al.* identified several cap binding-like motifs in AGO2 proteins, indicating that AGO isoforms may compete with the eIF4 complex for 5´-cap binding and, thereby, suppress the translocation of the ribosomal subunits to the mRNA [*228*]. An involvement of AGOs in the translational initiation would also explain how AGO subtypes 1, 3, and 4, although lacking endonucleolytic activities, participate in target repression.

In order for eukaryotic translation to proceed, circularized mRNA is first loaded into 43S preinitiation complex and, after recognition of the first starting codon, attached to the 60S ribosomal subunit to form the 80S initiation complex [*219*]. During elongation, mRNAs polypeptide chains are successively produced by scanning the mRNA for base triplets and recruiting complementary aminoacyl-tRNAs to the 80S ribosomes [*229*]. To accelerate protein synthesis at the stage of the transcriptional elongation, a single mRNA molecule may be simultaneously attached to multiple 80S ribosomes and the resulting complexes are known as `polyribosomes´ or `polysomes´ [*230*, *231*]. Of note, miRNAs are attached to actively translated mRNAs on polysomes [*232–234*], thus indicating that miRNA-induced target repression may also occur after the initiation of translation. Maroney and coworkers provide evidence that miRNAs reduce the reaction rate of the translational elongation [*232*, *235*]. In contrast, Nottrott *et al.* proposed the hypothesis that miRNA-induced translational repression is based on the translocation of proteolytic enzymes to the nascent polypeptide chains, leading to co-translational degradation of the newly synthesized polypeptide [*236*]. A third model proposes that the association of mRNA to miRISC complexes recruits termination factors, such as eRF3, resulting in the dissociation of the ribosome subunits from target mRNAs and premature translational termination (termed `ribosome drop-off model´, Figure 1.4 D; [*235*]).

It is still under debate to which excess translational repression and mRNA decay contribute to the overall effects of miRNAs in metazoans. While the classical view on miRNA-mediated gene silencing favored translational repression as main mechanism, more recent works suggest that mRNA decay may account for up to 85% of all miRNA-induced silencing events [*237*–*239*]. Of note, the molecular mechanism may be time-dependent, as shown by Eichhorn *et al.* who revealed that translational repression is more often observed at early time points, whereas mRNA destabilization is the dominant effect at later time points [*239*]. It was therefore already speculated that the destabilization of mRNA is the ultimate consequence of translational inhibition, regardless of whether the inhibition occurs at the initiation or post-initiation steps [*239*, *240*].

1.3.2.3 MicroRNA-induced upregulation of target mRNAs

Novel insights from Vasudevan and coworkers draw attention to the fact that miRNAs are – under certain circumstances – capable to upregulate target gene expression [*241*]. For instance, the group reported that miR-369-3p and let-7a upregulate target genes in cell cycle-arrested, but not in proliferating human embryonic kidney cells HEK293. Comprehensive experiments revealed that the observed upregulation was triggered by a miR-369-3p-induced association of AGO2 to the RNA binding protein fragile X mental retardation–related protein 1 (FXR1), followed by a recruitment of the AGO2-FXR1 complex to AU-rich elements in the 3´UTR of *TNFα* mRNA (Figure 1.4 E; [*241*, *242*]). Furthermore, a strong GW182 downregulation was observed in quiescent cells and immature oocytes [*243*, *244*], suggesting that AGO2-FXR1 complex formation is performed preferably in the absence of GW182 [*245*]. The recruitment of AGO2-FXR1 to mRNA triggers the translational machinery through the activation of so called `non-canonical initiation factors´ PARN and p97/DAP5 [*246*]. Surprisingly, AGO2-FXR1 was shown to be localized in the nucleus, indicating that the selection of miRNA target genes via the non-canonical translation does not occur in the cytoplasm [*247*]. To date, it appears that target gene upregulation by miRNAs is rather a rare event, limited to certain cell types or specific cell condition (e.g. particular phases during the cell cycle; [*241*, *248*–*250*]). Yet, additional work is needed to address the questions whether further mechanisms contribute to miRNA-induced gene activation and how these mechanisms impact cellular function and homeostasis.

1.3.3 The significance of P-bodies in miRNA-induced mRNA silencing

There is a growing body of evidence pointing towards the fact that miRNA-mediated target suppression does not occur in the cytoplasm, but rather in discrete cytoplasmic foci known as processing (P)-bodies or GW-bodies [*251–253*]. These aggregates are mainly composed of mRNAs as well as proteins and are highly enriched in enzymes known to be involved in mRNA decay or repression pathways, e.g. the deadenylases CCR4-NOT, decapping factors DCP1 and DCP2, as well as XRN1 [*254–256*]. Notably, P-bodies are co-localized with AGO2, GW182 and miRNAs which is indicative for a functional connection between P-bodies and the miRNA silencing machinery [*225*, *252*, *253*, *257*, *258*]. In support of this, it was demonstrated that the inhibition of miRNA biogenesis or the depletion of GW182 impairs the formation or decreases the stability of P-bodies [*243*, *259*]. Ribosomes as well as the majority of translational factors are absent in P-bodies, leading to the conclusion that mRNAs resident in these compartments reflect a repressive state [*255*]. Later studies confirmed this conclusion by illustrating an inverse correlation between P-body- and polysome-association of miRNA-targeted mRNAs [*255*, *257*, *260*]. The group of Filipowicz demonstrated that under normal conditions, miR-122 represses its target gene *cationic amino acid transporter 1* (*CAT1*) mRNA, whereas both components are localized within P-bodies. In response to miR-122 inhibition, however, *CAT1* mRNA was translocated from the P-bodies to polyribosomes which was accompanied by a rapid increase in CAT1 protein levels [*257*].

P-bodies are highly dynamic aggregates whose size and number vary according to the translational activity of the cell [*254*, *255*, *261*]. It is conceivable that P-bodies function as scaffold to ensure the proper assembly of repressive complexes on mRNAs and to maintain the repressive state [*262*]. Furthermore, P-bodies are an elegant solution for the storage of repressed mRNAs, allowing for fast mRNA recycling and re-entrance of mRNA into the translational machinery in response to cellular changes, as shown for *CAT1* [*257*, *262*].

1.3.4 MicroRNA target identification: *In silico* prediction and experimental target gene validation

With the aim to identify potential target genes for the increasing number of validated miRNAs known so far, a magnitude of bioinformatic prediction tools were developed, including *miRanda* [*263*], *TargetScan* [*151*], *RNA22* [*264*], and *miRWalk* [*265*]. The algorithms underlying these prediction tools are based on different attributes, for instance sequence

complementarity between the miRNA and mRNA [*163*], cross-species conservation of the miRNA binding site [*41*], free energy gained during mRNA-miRNA duplex formation as well as the thermodynamic stability of the duplex [*180*, *263*]. Some algorithms consider structural aspects such as the accessibility of the miRNA binding site on the target mRNA or the three dimensional structure of the RISC complex [*266*, *267*]. Despite improved insights into the mechanisms of miRNA-induced target silencing, *in silico* target identification tools still suffer from high false positive (~40 – 66%) and false negative (~50 – 70%) results [*268*]. Therefore, it is imperative to experimentally validate the biological significance of putative miRNA targets.

High-throughput approaches upon miRNA overexpression or inhibition are frequently used for target gene identification for single miRNAs. The effects of manipulated miRNA levels are then measured by quantitative *real-time* PCR (qPCR), microarray or sequencing techniques to quantify effects on mRNA expression, or by applying mass spectrometry approaches for assessing changes in protein abundances [*170*, *269*, *270*]. Changes in transcriptional activity may also be identified by polysomal profiling [*231*, *271*]. This technique is based on the observation that a highly translated mRNA is simultaneously attached to a high number of ribosomes (heavy polysomes), while a poorly translated mRNA is bound to few ribosomes (light polysomes) [*272*, *273*]. By means of density gradient centrifugation of cytoplasmic extracts from cells treated with miRNA mimic or inhibitor, polysomes of different densities may be isolated and polysome-associated mRNA may be analyzed quantitatively [*272*, *273*]. An inhibition in mRNA translation is observed as shift from heavy to light polysomes, while a transcriptional activation of mRNA is characterized by a shift from light to heavy fractions [*273*]. Polysomal profiling has successfully been used for the identification of novel miRNA targets in various systems and cell types [*235*–*238*].

While the aforementioned methods allow for the identification of a great number of putative miRNA target candidates, they fail to distinguish between direct effects (due to miRNA-target interaction) and indirect side-effects. Therefore, immunoprecipitation-based methods were established to enable the pull-down of miRNA-mRNA duplexes associated with AGO proteins within the RISC complex. To prevent dissociation of RNA from protein during sample preparation, crosslinks are introduced using UV irradiation. This method (cross-linking and immunoprecipitation, shortly `CLIP´; [*274*]) may be combined with microarray analyses or high-throughput sequencing (`HITS-CLIP´; [*275*]). Another possibility for validating direct miRNA-target interactions is the utility of reporter gene assays. By this means, target

sequences encompassing the predicted miRNA binding sites are cloned in the 3´UTR of a reporter gene, e.g. *luciferase* [*151*] or *green fluorescence protein* [*276*]. The capability of an individual miRNA to bind to the cloned sequence, thus impairing the reporter protein synthesis, is investigated by transfecting the reporter gene plasmids in presence or absence of the miRNA of interest, respectively. Differences in reporter gene protein in cells transfected with or without the miRNA of interest are then assessed fluorometrically or by measuring the chemiluminescence of a substrate turnover.

1.4 The contribution of microRNA miR-122 to liver physiology

The first evidence for the existence of tissue-specific miRNAs came from the studies of the Tuschl group in 2002 which used a cloning strategy to identify small ncRNAs derived from distinct murine organs [*277*]. This way, Tuschl *et al.* identified the miRNA miR-122 as most abundant hepatic miRNA with an expression exclusive for the liver [*277*]. Later studies demonstrated that the liver-specific miR-122 is highly conserved across the vertebrate lineage, whereas miR-122 is not expressed in nematodes [*278*, *279*].

miR-122 is encoded by a single-genomic locus on chromosome 18 in human and mice, respectively, and is transcribed by RNA polymerase II as primary miR-122 transcript of roughly 4.5 kb in length. The pri-miR-122 is further processed to a 66 nucleotide long pre-miR-122 precursor that encodes for two mature miRNAs [*278*, *280*]. While levels of the miRNA positioned at the 3´-end (miR-122-3p, formerly `miR-122*´) are rather low, the miRNA located at the 5´-end of the precursor (miR-122-5p or `miR-122´) is the major product of the *MIR122* locus and is the research focus of most studies published to date [*281*]. Therefore, in this thesis the term `miR-122´ refers to the mature miR-122-5p, unless otherwise specified.

The transcription of the *MIR122* gene is under the control of a conserved RNA polymerase II promoter, characterized by the presence of a transcriptional starting site (TSS), TATA-box binding elements as well as CCAAT enhancer elements [*119*, *282*, *283*]. Several transcription factor binding sites were identified in the *MIR122* promoter, including binding motifs for the family of hepatocyte nuclear factors (HNFs), like HNF1α, HNF3β, HNF4α, HNF6 or the CCAAT-enhancer binding element protein C/EBPα [*119*, *282*, *284*]. The transcription of *MIR122* is also regulated epigenetically, whereby DNA methylation and specific histone

modifications may repress or enhance the transcriptional activity of the *MIR122* promoter under certain conditions [*285–288*].

During embryogenesis, levels of miR-122 successively increase with time of development, reaching a plateau shortly after birth [*278*]. The gradual increase in miR-122 is closely linked to hepatic expression of HNF members, but inversely correlates with levels of the miR-122 target gene *Cut-like homeobox 1* (*Cux1*) in developing livers [*282*]. Since *Cux1* is a transcriptional repressor highly expressed in undifferentiated tissue, miR-122 participates in liver development and in the maintenance of a differentiated state by successively degrading *Cux1* mRNA (Figure 1.5; [*289*, *290*]). In the adult liver, the expression of pri-miR-122 and pre-miR-122 underlies a circadian regulation, in which the orphan nuclear receptor REV-ERBα, a major regulator of circadian metabolism, represses miR-122 transcription [*280*]. In contrast to the precursor molecules, levels of miR-122 remain largely unaffected throughout the day, a finding which was attributed to the large stability of mature miR-122 [*280*]. This conclusion was supported by the fact that miR-122 is post-transcriptionally modified by the action of poly(A) polymerase GLD2, resulting in a single adenylation of the 3´-end accompanied by an increase in the miRNA half-life [*146*, *148*]. Despite the stable expression of mature miR-122, several miR-122 target genes are regulated anticyclical to the pri-miR-122 and pre-miR-122, indicating that *de novo* synthesis of miR-122 may effect target mRNA levels in a circadian manner [*280*].

First insights into the function of miR-122 were presented from knockdown experiments using miR-122-targeting antisense oligonucleotides injected in mice [*291*, *292*]. miR-122 silencing reduced plasma cholesterol levels but increased hepatic β-oxidation of fatty acids in the experimental animals compared to controls [*291*, *292*]. Microarray analyses of these animals uncovered significant downregulations in mRNA levels of genes involved in fatty acid synthesis (e.g. *fatty acid synthase (Fasn*) or *acetyl-CoA carboxylase 2* (*Acc2*); [*292*]) and cholesterol biosynthesis (e.g. the rate-limiting enzyme *HMG-CoA reductase* (*Hmgcr)*, *mevalonate kinase* (*Mvk*) or *farnesyl diphosphate synthase* (*Fdps);* [*291*]) after miR-122 downregulation. However, the decline in mRNA levels in response to miR-122 suppression is supposed to arise as a result of indirect effects of miR-122 silencing. To date, the molecular mechanism underlying miR-122-mediated regulation of lipid metabolism is still largely unknown, but the key enzymes AMP-activated protein kinase (AMPK) and the family of

peroxisome proliferator-activated receptors (PPARs) are believed to mediate the metabolic activity of miR-122 [*280*, *292*].

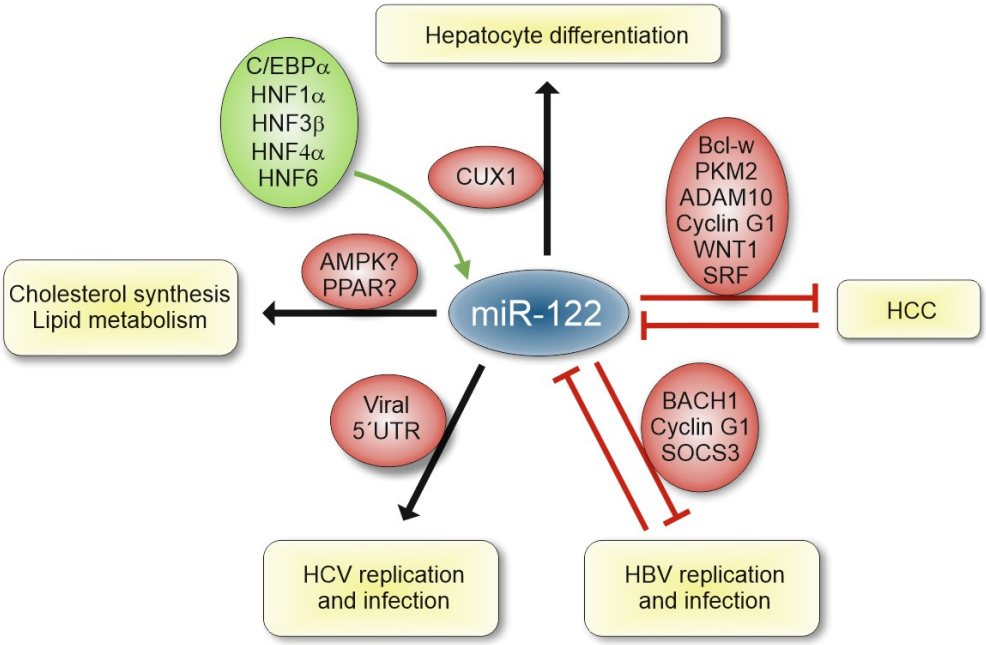

Figure 1.5: Role of miR-122 in hepatic functions and in liver diseases. (Modified from Hu *et al.* [*293*]). The biosynthesis of miR-122 is under the control of liver-enriched transcription factors (illustrated in green). miR-122 modulates hepatic functions such as differentiation as well as cholesterol and lipid synthesis. Moreover, it exerts tumor-suppressive effects through the inhibition of pro-oncogenes and prevention of angiogenesis. miR-122 has dual function in viral infections as it represses HBV but enhances HCV replication. Targets of miR-122 are depicted in red.

Systemic or liver-specific knockout of miR-122 in mice is accompanied by reduced plasma cholesterol and lipoproteins levels, an upregulation of genes involved in triglyceride biosynthesis and storage and, subsequently, an accumulation of hepatic triglycerides in *MIR122 KO* animals [*294*, *295*]. Apart from defects in lipid metabolism, *MIR122* transgenic animals develop hepatic microsteatosis and liver inflammation at early age [*294*]. The latter phenomenon is associated with an infiltration of inflammatory immune cells into the liver, which produce IL6 as well TNFα, thus triggering pro-oncogenic pathways [*294*]. Furthermore, the hepatic expression of various pro-fibrotic genes (i.e. *Klf6*, *Tgfb1* and *Ctgf*) and tumor marker genes (e.g. *Prom1*, *Thy1*, *Epcam*) is upregulated in miR-122 depleted mice which results in a high occurrence of fibrosis and hepatocellular carcinoma (HCC) in transgenic animals compared to the wild type control group [*294*, *295*]. Altogether these data point to an anti-inflammatory and tumor-suppressive effect of miR-122 [*294*].

Nowadays, the anti-tumorigenic properties of miR-122 have widely been confirmed in numerous experiments *in vitro* and *in vivo,* whereby distinct mechanisms contribute to tumor-suppressive effects of miR-122. For instance, miR-122 induces apoptosis in HCC cell lines by directly targeting anti-apoptotic and pro-proliferative genes, such as *Cyclin G1* and *Bcl-w* (Figure 1.5; [*296*, *297*]*).* The overexpression of miR-122 in HCC cell lines decreases cancer cell growth and renders them sensitive towards cytostatic drugs [*298*, *299*]. Interestingly, the repression of *Cyclin G1* by miR-122 triggers a complex regulatory circuit which activates the tumor suppressor p53 through repression of the p53-inhibitor Mdm-2 [*299*, *300*].

Besides affecting the cell survival and apoptosis, miR-122 inhibits cell migration, invasion and angiogenesis by targeting genes involved in the maintenance of the extracellular matrix, like laminin β2, or by suppressing genes involved in the remodeling of the extracellular matrix (e.g. *ADAM10* and *ADAM17*; [*298*, *301*, *302*]). A contribution of miR-122 in epithelial-to-mesenchymal transition (EMT) was also postulated based on the observation that miR-122 directly modulates genes of the WNT/ β-catenin pathway including *WNT1* or the EMT-related genes β-*cadherin, N-cadherin* and *vimentin* in human hepatoma cells (Figure 1.5; [*303*–*306*]).

In addition to its role in fine-tuning the hepatic transcriptome, miR-122 exerts relevant systemic effects by coordinating systemic iron homeostasis [*307*, *308*]. Injection of antisense oligonucleotides targeting miR-122 in mice engendered systemic iron deficiency, accompanied by depleted levels of iron in the plasma and the liver of treated animals, and impaired hematopoiesis [*307*]. Elaborate studies revealed that miR-122 indirectly regulates the key iron regulatory hormone hepcidine, through the regulation of hemochromatosis (*Hfe*) and hemojuvelin (*Hjv*) which are upstream activators of hepcidine expression [*307*]. Since iron withholding is a strategy of the innate immune system protecting against viral infections, the aforementioned study provides evidence for a link between miR-122 and immunity [*309*, *310*].

1.5 Deregulation of miR-122 in the pathogenesis of liver diseases

The hepatocyte-enriched miR-122 is a key regulator of liver physiology. Hence, it is not surprising that deregulation of miR-122 expression is linked to versatile hepatic malignancies and liver diseases. Hepatic miR-122 expression is reduced in patients with alcoholic liver disease (ALD; [*311*]), non-alcoholic steatohepatitis (NASH; [*312*, *313*]), primary biliary cholangitis (PBC; [*314*]), chronic hepatitis B (CHB; [*315*]), cirrhosis [*316*], as well as

hepatocellular carcinoma [*317–319*]. In contrast, levels of miR-122 circulating in the plasma are frequently elevated in patients with hepatitis B virus (HBV; [*320*, *321*]), hepatitis C virus (HCV; [*322*, *323*]), non-alcoholic fatty liver disease (NAFLD; [*322*, *324–326*]) and in response to drug-induced liver injuries [*327–329*]. Due to its high specificity for the liver, miR-122 is considered an interesting potential prognostic and predictive biomarker for liver diseases. For instance, miR-122 levels in HCC tissue may serve as prognostic marker for tumor invasiveness and overall survival, whereas higher miR-122 levels correlate with better prognosis [*306*, *318*, *330–332*]. In HCV infected patients, plasma miR-122 levels may predict the efficiency of interferon treatment, as lower treatment-naïve levels of circulating miR-122 were found in patients who did not respond well to IFN in comparison to IFN-responsive patients [*333*]. Ongoing investigations explore the possibility to target miR-122 therapeutically, and miRNA activators as well as miR-122 inhibitors are currently under revision for anticancer and antiviral therapies [*334*, *335*].

1.5.1 Role of miR-122 in hepatitis B virus infections

The hepatitis B virus, which belongs to the family of small, enveloped DNA viruses, causes acute or chronic infections of the liver [*336*]. According to the world health organization (WHO), approximately 257 million people worldwide suffered from chronic hepatitis B in 2015, which is a high risk factor for the development of secondary diseases, such as liver cirrhosis and HCC [*337*]. The WHO estimated that 887,000 deaths were related to complications of CHB in 2015, which is why CHB is considered as severe public health issue.

There is obvious evidence for a key role of miR-122 in hepatitis B infections from numerous investigations focusing on the link between miR-122 expression and HBV replication [*338*]. Significant deficiencies in hepatic miR-122 levels were observed in HBV transgenic mice compared to wild type controls as well as in CHB patients *versus* healthy individuals [*315*, *318*, *319*]. In addition, an inverse correlation between miR-122 levels and virus load was reported in HBV-infected patients [*315*]. *In vitro* studies conducted on HBV-expressing hepatoma cells HepG2.2.15 revealed that miR-122 overexpression inhibited HBV expression, whereas the depletion of miR-122 enhanced viral replication [*315*, *338*, *339*].

The virostatic effects of miR-122 against HBV are triggered by distinct mechanisms. For instance, miR-122 exerts antiviral effects by indirectly enhancing p53 downstream pathways

through the inhibition of *Cyclin G1* [*300*, *315*]. Activated p53 represses HBV transcription by interacting with enhancer elements in the viral genome, thus inhibiting gene transcription [*315*]. Apart from the p53-mediated antiviral effects, it was demonstrated that miR-122 directly targets *BACH1* mRNA, a repressor of *heme oxygenase-1* (*HO1*) transcription (Figure 1.5; [*340*]). HO1 protein in turn decreases HBV replication by binding to and reducing the stability of the HBV core protein and by activating the antiviral interferon response [*341*, *342*]. Moreover, miR-122 itself increases the activity of endogenous type I interferons by targeting *suppressor of cytokine signaling 3* (*SOCS3)* mRNA *in vitro* [*343*, *344*]. Viral infections with HCV and HBV are frequently accompanied by elevated *SOCS3* mRNA levels which is a viral defense mechanism to counteract the host innate immune system by repression of IFN signaling [*343*, *345*]. Hence, miR-122-induced suppression of *SOCS3* provides another possibility to antagonize viral infections (Figure 1.5; [*344*]).

The reduction in hepatic miR-122 in CHB carriers supports the conclusion that HBV escapes miR-122-mediated repression. Remarkably, all four viral mRNAs encoded by the HBV genome carry binding sites for miR-122 which functionally bind and sequester endogenous miR-122 [*346*]. In addition, the viral HBx protein affects miR-122 transcription epigenetically through interacting with the transcription factor PPARγ, followed by the recruitment of histone methyltransferases and deacetylases to the *MIR122* promoter. These events generate a repressive chromatin state and thereby suppress *MIR122* gene transcription [*286*, *347*]. Recent investigations further demonstrate that the viral HBx protein reduces miR-122 levels by decreasing the miRNA stability [*348*]. This effect was shown to include HBx-induced downregulation of GLD2, a poly(A) polymerase which typically stabilizes miR-122 by adenylation of the 3´-end [*148*, *348*].

1.5.2 Mechanism of miR-122-mediated enhancement of hepatitis C virus replication

In contrast to the antiviral effects of miR-122 counteracting HBV replication, miR-122 has a promoting effect on the replication of HCV [*349*]. The first indications pointing towards a pro-viral effect of miR-122 came from the observation that HCV only replicates in HCC cell line Huh-7 which express miR-122, but not in HepG2 cells lacking this miRNA [*349*, *350*]. A critical role for miR-122 in HCV replication was further confirmed as the sequestration of miR-122 in Huh-7 using antisense oligonucleotides was sufficient to diminish HCV RNA [*349*, *351*]. In

contrast, ectopic expression of miR-122 enhanced HCV replication even in non-hepatic cells [*352*].

The HCV genome harbors two functional miR-122 MREs in the 5´UTR of the viral genome, which are conserved across HCV subtypes (Figure 1.5; [*349*, *353*]). Comprehensive mechanistic analyses revealed that activation of miR-122 and the recruitment of the miRISC to the 5´UTR increase the stability of the targeted viral RNA. It was assumed that the miRISC complex bound to the 5´UTR acts as cap-like structure, thus protecting against exonuclease decay by XNR1 or XNR2 [*354–357*]. Interestingly, the stabilizing effect of miR-122 on mRNA was completely abolished when the MREs were cloned into the 3´UTR instead of the 5´UTR of a reporter plasmid, indicating that the location of the binding sites is a relevant factor dictating the activity of miR-122 [*349*, *353*]. By binding to the viral 5´UTR, miR-122 also enhances translation of the viral RNA [*358*, *359*]. Structural analyses provide evidence for a conformational change within the internal ribosome entry site of the viral RNA which is triggered by miR-122 and which facilitates the association with ribosomal subunits and transcriptional initiation factors [*360–362*].

Due to its pro-viral effects, inhibition of miR-122 was proposed as therapeutic strategy against chronic hepatitis C infections [*363–365*]. A locked nucleic acid (LNA)-modified antisense oligonucleotide (SPC3649 or Miravirsen) successfully suppressed HCV viremia in chronically HCV infected chimpanzees without severe side-effects and is currently undergoing phase IIa clinical trials to assess the antiviral activity in treatment-naïve HCV-infected patients [*363–365*]. Nonetheless, an important consideration is that miR-122 depletion is frequently observed in human HCC tissue, which is why anti-miR-122 treatment may not be useful as long-term therapeutic strategy [*366*]. Furthermore, due to the development of direct-acting antivirals (DAA) against HCV, which are novel inhibitors of viral proteases and polymerases that achieve high cure rates of more than 90%, miR-122 targeting strategies might be beneficial only for a minor percentage of patients which do not respond to DAA treatment [*367–370*].

1.5.3 Contribution of miR-122 in the pathogenesis of hepatocellular carcinoma

The incidence of HCC has raised considerably in the last decades and HCC is now one of the most prevalent cancer types worldwide and the second leading cause of cancer-related deaths [*371*]. The tumorigenesis leading to HCC is a complex multi-step process and is frequently accompanied by alterations in cell growth promoting and apoptotic signaling pathways, the activation of proto-oncogenic pathways and the induction of angiogenesis (reviewed by [*372*, *373*]). Tumorigenesis is also characterized by alterations in metabolic requirements, leading to decreased oxidative phosphorylation and enhanced anaerobic glycolysis in cancer cells, a phenomenon referred to as the `Warburg effect´ [*374, 375*].

In recent years, an overwhelming number of studies provided evidence for an involvement of miR-122 in HCC oncogenesis. Levels of miR-122 are downregulated in most primary HCC tumor tissues related to HBV and miR-122 levels inversely correlate with clinical parameters such as tumor size, differentiation status and etiology [*318*, *376*, *377*]. However, there are contradictory findings in the literature concerning the miR-122 status in HCV-related HCC, as some studies identified no alterations in HCC tissue compared to healthy liver tissue, while other studies observed elevated levels of hepatic miR-122 in cancer tissue compared to healthy liver tissue [*378–380*]. Recently, three single-nucleotide polymorphisms were identified in the human *MIR122* gene in a southern Chinese population, which was associated with a significantly increased risk for HCC [*381*]. Moreover, miR-122 was found to be transcriptionally repressed by the proto-oncogene c-Myc, whereby miR-122 and c-Myc levels are inversely correlated in HCC tissue [*382*].

The downregulation of the tumor-suppressive miR-122 induces the inhibition of apoptosis and the induction of pro-proliferative target genes such as *Cyclin G1, Bcl-w* and *Wnt1* as mentioned before [*296*, *297*, *303*]. In addition, *pyruvate kinase M2* (*PKM2*), encoding the rate-limiting enzyme of the glycolytic pathway, was identified as direct miR-122 target in HCC (Figure 1.5; [*331*, *383*, *384*]). As a functional consequence of PKM2-targeting, miR-122 may downregulate glycolytic activities in cancer cells, thus inhibiting tumor growth [*331*, *383*, *384*]. Of note, independent experiments suggest that overexpression of miR-122 increases sensitivity of cancer cells towards anti-cancer drugs, such as Sorafenib and Doxorubicin [*298*, *299*, *385*]. Weinstein *et al.* showed that miR-122 inhibits the expression of multi drug resistance genes *ABCB1* and *ABCF2*, which are transmembrane efflux pumps capable to export anticancer drugs out of the cells [*386*]. Another mechanism was proposed by Xu *et al*. who

demonstrated that miR-122 overexpression counteracts Sorafenib resistance by targeting *insulin-like growth factor 1 receptor* mRNA and inducing apoptosis [*385*]. Altogether, these data support the idea that miR-122 activation in combination with cytostatic agents may provide a new therapeutic tool to treat drug-resistant cancer types [*298*, *299*, *387*].

1.6 Research goals

The liver-enriched miR-122 is probably one of the best characterized miRNA so far. Although a number of miR-122 targets have already been identified in independent studies, only little is known about the molecular networks downstream to this miRNA. Therefore, the aim of this thesis was to gain more information about the genome-wide targets and the molecular networks downstream of miR-122. For this purpose, miR-122 was either overexpressed or inhibited in human hepatoma cells Huh-7 and translatome studies were conducted by polysome profiling, whereas proteome analyses were performed by mass spectrometry. Data sets were screened for miR-122 target gene candidates, which were validated by qPCR or by luciferase reporter assays.

Compelling evidence link miR-122 deregulation to the pathogenesis of liver diseases, such as liver inflammation, viral infections or HCC. Yet, little is known about the mechanisms leading to aberrant miR-122 levels in these malignancies. Liver diseases are frequently accompanied by a deregulation of pro- and anti-inflammatory cytokines and growth factors, which trigger diverse signaling pathways and regulate gene expression. This study therefore aimed to investigate whether cytokines and growth factors, which are involved in the pathophysiology of liver disease, may affect miR-122 biogenesis. To address this question, constructs of the human *MIR122* promoter were cloned into luciferase reporter plasmids and transfected in Huh-7 cells. Stimulation experiments of transfected Huh-7 cells were conducted to assess whether *MIR122* promoter constructs were responsive towards cytokine and growth factor treatment and to evaluate the possible effects of the aforementioned stimuli on miR-122 biogenesis.

Overall, data presented in this work contribute to our understanding of the role played by miR-122 in the maintenance of the liver homeostasis and the possible mechanisms leading to miR-122 deregulation at onset of liver diseases.

2. Materials and methods

2.1 Materials

Standard laboratory chemicals were purchased from Merck (Darmstadt, Germany), Thermo Fisher Scientific (Schwerte, Germany), VWR (Darmstadt, Germany) or Carl Roth (Karlsruhe, Germany). Cell culture dishes and plastic disposable materials were purchased from Greiner Bio-One (Frickenhausen, Germany) or Eppendorf (Hamburg, Germany). In the following sections, reagents and chemicals are listed that were used throughout the work for this thesis, i.e. enzymes, transfection reagents, miRNA mimics and inhibitors, antibodies, molecular biology kits, cell lines, cell culture media and supplements, growth factors and cytokines, bacteria and plasmids. Media and buffer compositions are itemized in Section 2.1.9. Clinical characterizations of patients donating HCC tissue samples are listed in Table 2.1 (Section 2.1.7). Primer sequences for qPCR are summarized in Tables 2.2 and 2.3 (Sections 2.1.10 and 2.1.11) and primer sequences used for molecular cloning are given in Table 2.4 (Section 2.1.12).

2.1.1 Enzymes

DNase I for RNA preparation (AS1260)	Promega GmbH, Mannheim, Germany
DNase I for polysomes (M303L)	New England BioLabs GmbH, Frankfurt a.M., Germany
GoTaq® DNA Polymerase (M3001)	Promega GmbH, Mannheim, Germany
GoTaq® qPCR Master Mix (A6002)	Promega GmbH, Mannheim, Germany
HindIII-HF® (R3104S)	New England BioLabs GmbH, Frankfurt a.M., Germany
KpnI-HF® (R3142S)	New England BioLabs GmbH, Frankfurt a.M., Germany
NheI-HF® (R3131S)	New England BioLabs GmbH, Frankfurt a.M., Germany
SacI-HF® (R3156S)	New England BioLabs GmbH, Frankfurt a.M., Germany
PrimeScript™ Reverse Transcriptase (2680A)	Takara Bio Europe S.A.S, Saint-Germain-en-Laye, France

Proteinase K (7528.5)	Carl Roth GmbH + Co. KG, Karlsruhe, Germany
Quick Ligation™ Kit (M2200L)	New England BioLabs GmbH, Frankfurt a.M., Germany
RNase Inhibitor (AM2682)	Thermo Fisher Scientific Inc, Schwerte, Germany
RNase Inhibitor (Roche, 335399001)	Sigma-Aldrich Chemie GmbH, Taufkirchen, Germany
StemPro™ Accutase™ Cell Dissociation Reagent (A1110501)	Thermo Fisher Scientific Inc, Schwerte, Germany
T4 RNA Ligase, truncated K227Q (M0351S)	New England BioLabs GmbH, Frankfurt a.M., Germany
0.05% Trypsin/ 0.02% EDTA (Invitrogen) (25300054)	Thermo Fisher Scientific Inc, Schwerte, Germany

2.1.2 Transfection reagents and miRNA mimics/ inhibitors

Ambion pre-miR™-122 miRNA precursor (AM17101; miR-122 mimic)	Thermo Fisher Scientific Inc, Schwerte, Germany
AntagomiR-122 (Miravirsen, SPC-3649)	Roche (fromerly Santaris Pharma), Mannheim, Germany
Lipofectamin™ RNAiMax (13778075)	Thermo Fisher Scientific Inc, Schwerte, Germany
Lipofectamin™ 3000 (L3000008)	Thermo Fisher Scientific Inc, Schwerte, Germany
Xfect™ MIRNA Transfection Reagent (631435)	Takara Bio Europe S.A.S, Saint-Germain-en-Laye, France
Xfect™ Transfection Reagent (631317)	Takara Bio Europe S.A.S, Saint-Germain-en-Laye, France

2.1.3 Antibodies

Mouse anti-β Actin antibody (ab8226)	Abcam plc., Cambridge, UK
Rabbit anti-G6PDH antibody (HPA000834)	Sigma-Aldrich Chemie GmbH, Taufkirchen, Germany
Rabbit anti-EPS15L1 antibody (ab53006)	Abcam plc., Cambridge, UK
Rabbit anti-CEP55 antibody (ab170414)	Abcam plc., Cambridge, UK

Goat anti-rabbit-HRP (P044801) (DakoCytomation)	Agilent Technologies Germany GmbH, Ratingen, Germany
Sheep anti-mouse-HRP (RPN4201) (GE Healthcare)	Sigma-Aldrich Chemie GmbH, Taufkirchen, Germany

2.1.4 Molecular biology kits

Dual-Luciferase® Reporter Assay (E1960)	Promega GmbH, Mannheim, Germany
Fast-n-Easy Plasmid Mini-Prep Kit (PP-204L)	Jena Bioscience GmbH, Jena, Germany
In-Fusion HD Cloning Plus for seamless DNA cloning (638920)	Takara Bio Europe S.A.S, Saint-Germain-en-Laye, France
Pierce™ 660nm Protein Assay (22660)	Thermo Fisher Scientific Inc, Schwerte, Germany
QIAgen miRNeasy Kit (217004)	Qiagen GmbH, Hilden, Germany
QIAGEN Plasmid Midi Kit (12145)	Qiagen GmbH, Hilden, Germany
QIAquick Gel Extraction Kit (28704)	Qiagen GmbH, Hilden, Germany
QIAquick PCR Purification Kit (28104)	Qiagen GmbH, Hilden, Germany
Qubit™ dsDNA HS Assay Kit (Q32854)	Thermo Fisher Scientific Inc, Schwerte, Germany
Qubit™ Protein Assay Kit (Q33211)	Thermo Fisher Scientific Inc, Schwerte, Germany
Qubit™ RNA HS Assay Kit (Q32852)	Thermo Fisher Scientific Inc, Schwerte, Germany
Western Lightning Plus-ECL, Enhanced Chemiluminescence Substrate (NEL103001EA)	PerkinElmer LAS (Germany) GmbH, Rodgau-Jügesheim, Germany

2.1.5 Cell lines, media and supplements

Cell lines:

Human embryonic kidney 293 cell (HEK293)	Kindly provided by Prof. Dr. Johannes Bode (Clinic for Gastroenterology, Hepatology and Infectious Diseases, Düsseldorf, Germany)
Human hepatoma cell line (Huh-7)	Kindly provided by Prof. Dr. Johannes Bode (Clinic for Gastroenterology, Hepatology and Infectious Diseases, Düsseldorf, Germany)

Media and supplements:

DMEM (Invitrogen)	Thermo Fisher Scientific Inc, Schwerte, Germany
DMEM/ Ham´s F-12 (Invitrogen)	Thermo Fisher Scientific Inc, Schwerte, Germany
Fetal calf serum (FCS)	Thermo Fisher Scientific Inc, Schwerte, Germany
Opti-MEM (Gibco)	Thermo Fisher Scientific Inc, Schwerte, Germany

2.1.6 Growth factors, cytokines and cytokine inhibitors

BMP6 (120-06)	PeproTech GmbH, Hamburg, Germany
IFNβ (IF011)	Thermo Fisher Scientific Inc, Schwerte, Germany
IL6 (I0406)	Sigma-Aldrich Chemie GmbH, Taufkirchen, Germany
IL10 (I9276)	Sigma-Aldrich Chemie GmbH, Taufkirchen, Germany
PDGF-BB (P4056)	Sigma-Aldrich Chemie GmbH, Taufkirchen, Germany
SB431542 (TGFβ receptor-I inhibitor)	Axon Medchem LLC, Groningen, Netherlands
TGFβ1 (100-21)	PeproTech GmbH, Hamburg, Germany
TNFα (ADI-908-066)	Enzo Life Sciences Inc, Famingdale (NY), USA

2.1.7 Human HCC biopsies

HCC tissue from 28 individuals with chronic HBV (n = 7) or without viral infections (n = 21) were kindly provided by Prof. Dr. Thomas Longerich (University Hospital Aachen, Germany). The ethic committee of the Medical Faculty of RWTH Aachen gave the approval for using human HCC tissue samples, in conformity with the Declaration of Helsinki ethical guidelines (reference no. EK122/16). All patients involved in this study provided their informed consent.

Table 2.1: Clinical characterizations of patients donating HCC tissue samples for miQPCR and qPCR.

No.	Sex	Age	Risk factors	Cirrhosis	Max. tumor size (cm)	No. of Nodules	Tumor Grading	Vascular invasion
1	♂	74	HBV	yes	4.2	1	3	1
2	♂	63	HBV	no	7.0	1	3	0
3	♂	62	HBV	no	17.5	multiple	3	1
4	♂	60	HBV	yes	6.7	2	1	0
5	♂	67	HBV	yes	8.0	1	3	0
6	♂	60	HBV	yes	1.3	1	3	1
7	♂	54	HBV	yes	5.9	1	2	1
8	♀	73	unknown, non-viral	no	7.0	1	1	0
9	♀	71	diabetes mellitus type 2	no	6.0	1	3	1
10	♂	60	unknown, non-viral	no	4.8	1	3	1
11	♂	67	unknown, non-viral	no	4.9	multiple	3	0
12	♀	75	ethanol abusus	yes	3.2	1	3	1
13	♂	63	diabetes mellitus type 2	yes	7.5	1	1	0
14	♂	60	unknown, non-viral	yes	5.5	2	2	0
15	♂	78	diabetes mellitus type 2	yes	3.8	3	3	0
16	♂	68	ethanol abusus	yes	4.8	1	2	1
17	♂	67	unknown, non-viral	no	3.5	1	2	1
18	♂	86	unknown, non-viral	no	9.0	3	2	1
19	♂	82	unknown, non-viral	no	12.0	multiple	3	0
20	♂	79	unknown, non-viral	no	6.0	1	2	0
21	♂	65	unknown, non-viral	yes	3.6	1	3	1
22	♂	52	unknown, non-viral	no	3.0	2	1	0
23	♀	79	unknown, non-viral	no	5.5	1	2	0
24	♀	68	unknown, non-viral	no	4.5	1	3	0
25	♂	63	NASH	yes	2.5	1	2	1
26	♂	61	unknown, non-viral	yes	4.9	1	2	0
27	♂	77	PBC	yes	3.0	1	2	0
28	♂	74	diabetes mellitus type 2	no	2.0	1	3	0

2.1.8 Bacteria and purchased plasmids

Stellar™ Competent Cells (provided with In-Fusion HD Cloning Kit)	Takara Bio Europe S.A.S, Saint-Germain-en-Laye, France
TOP-10 *E. coli*	Thermo Fisher Scientific Inc, Schwerte, Germany
pGL4[*luc*+] Promoter vector (E1761)	Promega GmbH, Mannheim, Germany
pGL4.10[*luc2*] Basic vector (E665A)	Promega GmbH, Mannheim, Germany
pRL-SV40 Vector	Promega GmbH, Mannheim, Germany

2.1.9 Media, buffer and solutions

For polysome fractionation:

lysis buffer	5 mM Tris-HCl pH 7.5 1.5 mM KCl 2.5 mM $MgCl_2$ 0.2 mM cycloheximide (CHX), 120 U/mL RNase inhibitor 120 U/µL DNase I 0.5% (w/v) sodium deoxycholate 0.5% (v/v) Triton X-100
hypotonic buffer	5 mM Tris-HCl pH 7.5 1.5 mM KCl 2.5 mM $MgCl_2$ 0.2 mM CHX
10% sucrose solution	10% (w/v) sucrose In hypotonic buffer
50% sucrose solution	50% (w/v) sucrose In hypotonic buffer
60% sucrose solution	60% (w/v) sucrose 0.01% (w/v) bromophenol blue In hypotonic buffer

For preparation of chemically competent *E. coli*:

TFB1 solution	30 mM KOAc 100 mM $RbCl_2$ 10 mM $CaCl_2$ 50 mM $MnCl_2$ 15% (v/v) glycerol pH adjusted to 5.8 with HOAc
TFB2 solution	10 mM MOPS 10 mM $RbCl_2$ 75 mM $CaCl_2$ 50 mM $MnCl_2$ 15% (v/v) glycerol pH adjusted to 6.5 with KOH

For RNA preparation from human HCC tissue

lysis buffer	50 mM Tris-HCl pH 7.4 10 mM EDTA pH 8.0 0.5% (w/v) SDS
DNase buffer	10 mM Tris-HCl pH 7.5 2.5 mM $MgCl_2$ 0.5 mM $CaCl_2$

Western blot buffers:

lysis buffer (for proteome analysis)	30 mM Tris base 7 M urea 2 M thiourea
RIPA buffer	50 mM Tris base pH 8.0 150 mM NaCl 1% (v/v) Nonidet P-40 0.5% (w/v) sodium deoxycholate 0.1% (w/v) sodium dodecyl sulfate 1 mM EDTA cOmplete™ Protease Inhibitor Cocktail (1 tablet/ 50 mL buffer)
2x SDS-loading dye	300 mM dithiothreitol 15% (v/v) glycerol 6% (w/v) SDS 75 mM Tris-HCl pH 7.0 0.0125% (w/v) bromophenol blue

MOPS buffer	50 mM MOPS 50 mM Tris base 0.1% (w/v) SDS 1 mM EDTA pH adjusted to 7.7
anode buffer	300 mM Tris base 100 mM tricine pH adjusted to 8.7 – 8.8
cathode buffer	300 mM aminocaproic acid 30 mM Tris base pH adjusted to 8.6 – 8.7

Miscellaneous:

TAE	40 mM Tris pH 7.6 20 mM acetic acid 1 mM EDTA pH 8.0
TBST	20 mM Tris pH 7.5 150 mM NaCl 0.1% (v/v) Tween-20

2.1.10 Oligonucleotide sequences for miQPCR

Table 2.2: Sequences of oligonucleotides for microRNA profiling using miQPCR. (As previously described by Benes *et al.* [*388*]).

miRNA Primer	Primer	Sequence 5´ – 3´
hsa-miR-122-5p	Forward	GTG ACA ATG GTG TTT GGG
hsa-miR-192-5p	Forward	TGA CCT ATG AAT TGA CAG CCG
Upm2A	Reverse	CCC AGT TAT GGC CGT TTA

2.1.11 Primers for quantitative *real-time* PCR

Table 2.3: Oligonucleotide sequences of qPCR primers for human mRNAs.

mRNA Primer	Primer	Sequence 5´ – 3´
hsa *ACTB*	Forward	CAG CAA GCA GGA GTA TGA CG
	Reverse	AAA GTC ATG CCA ATC TCA TC
hsa *BAG1*	Forward	CAT TTG GAG AAG TCT GTG GAG A
	Reverse	AAA TCC TTG GGC AGA AAA CC
hsa *BAX*	Forward	AGC AAA CTG GTG CTC AAG G
	Reverse	TCT TGG ATC CAG CCC AAC
hsa *CCDC43*	Forward	GAA GAG GAG AAG CAG AGA AAA GC
	Reverse	GCA CCT GAA TCA TCC TTC TCA

Table 2.3 (continued)

mRNA Primer	Primer	Sequence 5´ – 3´
hsa *CD47*	Forward	AGT GAC ACG GTA GCA CCA GTT
	Reverse	GAA CAC AGT GCT CTG AGA ACA AG
hsa *CEP55*	Forward	AGA AGA AGA GAT CCG AAG AGC
	Reverse	AGC AGA GAT GTG TAA AGA AAC TG
hsa *CLIC1*	Forward	CCT GTT GCC AAA GTT ACA CA
	Reverse	GTG AAT CCC CGG TAC TTC TT
hsa *CMTM7*	Forward	TAT CAG CTG GCC CCT GTC
	Reverse	CTT GGA AGC TGC CAC AAT G
hsa *DEDD*	Forward	AGC CCT CAG TGA TCC AGA AC
	Reverse	GGC AAC ACA CCA CAG GAT AG
hsa *DIXDC1*	Forward	TTA CGC CCT TCA TGG TCA AT
	Reverse	TCC TTC CCG ATC AAT AGC TG
hsa *DSG2*	Forward	AAT TGC GCT CAT GAT TTT GG
	Reverse	GCA ATG GCA CAT CAG CAG TA
hsa *E2F4*	Forward	GGT ATC GGG CTA ATC GAG AA
	Reverse	AAT CTC CCG GGT ATT GCA G
hsa *EEA1*	Forward	GAA TTG CAA AGA AAG CTG GAT AA
	Reverse	TTC AAC GCT TGT GTA TGT TTG A
hsa *EPS15L*	Forward	TTA CCT CGG ATC CAT TCA CG
	Reverse	TCA CTG GAT TCA AAG GGG TC
hsa *F2RL2*	Forward	CTA CGT CCA GGC CAC CTC TA
	Reverse	GTG AAG TGG TGG AGG GTA GG
hsa *G3BP2*	Forward	CCT GTT TCT CTG CCA CAA GA
	Reverse	GGA GGC AGG TTT TTA CTG GTC
hsa *G6PDH*	Forward	CTG GTG GCC ATG GAG AAG
	Reverse	TGC ATT TCA ACA CCT TGA CCT
hsa *HAMP*	Forward	CAA CAG ACG GGA CAA CTT GC
	Reverse	AGC AGA AAA TGC AGA TGG GGA
hsa *HCFC1*	Forward	CGC AAT GAG AAG GGC TAT G
	Reverse	TGG TGC CAG AGC TGT CTT TA
hsa *HPRT1*	Forward	AGG TCG CAA GCT TGC TGG
	Reverse	CCA ACA CTT CGT GGG GTC
hsa *KIF1B*	Forward	AAG GAC CTT CTT CGT GCT CA
	Reverse	GAG GGA CCC CAT GGA TGT A
hsa *KIF3A*	Forward	AAC TTC AAA GGG GAA AGC AAG
	Reverse	TTT CAG GCT TTG CAG AAC G
hsa *KPNA6*	Forward	CTT ATT GTG GCC TCA TAG AGG AA
	Reverse	GCC TTC TGG TAG ATC TCC TGG T
hsa *KPNB1*	Forward	CTG GAA TCG TCC AGG GAT TA
	Reverse	TCT GGG TTG TAC CAG CAT CA
hsa *MINK1*	Forward	AGT TCC TGT GTG AGC GGA AT
	Reverse	TGC AGT TAC GGT TCA GAG TCA
hsa *NRF1*	Forward	CAG TCA CTA TGG CGC TTA ACA
	Reverse	ATC TGT CCC CCA CCT TGT AA
hsa *NUP210*	Forward	GGA CAC AGC CCC CAC TAT T
	Reverse	CAT AGG CTG GGC TCC ACA

Table 2.3 (continued)

mRNA Primer	Primer	Sequence 5´ – 3´
hsa *P4HA1*	Forward	AAG ATC TAA CAG GAC TAG ATG TTT CCA
	Reverse	TCC TCC AAC TCC ATA ATT TGC
hsa *PCGF2*	Forward	TTC TCC GCA ACA AGA TGG AT
	Reverse	AGT GGC TCG TCC TCG TAC A
hsa *PDCD2*	Forward	TGG TGC CAA GAG AAT ATT GGA
	Reverse	CCC AGT CTG TCA GCC TTC A
hsa *PDCD4*	Forward	TGG AAA GCG TAA AGA TAG TGT GTG
	Reverse	AAT ATT CTT TCA GCA GCA TAT CAA TC
hsa *POLR2F*	Forward	GCG AAT CAC CAC ACC ATA CA
	Reverse	ACC ATC ACA GGG GCA CAC
hsa pri-miR-122	Forward	TTT CCT AGA CTG CAG AAT TGA TCA C
	Reverse	ATA ATC TGG CCG AAT GAA TGG ATA C
hsa *RNF26*	Forward	GGC GTT GGG GTT AGT ATC TCT
	Reverse	GCC TCA TCA GAC GAT CAC AG
hsa *RNMT*	Forward	TTG GAC CTG GGA TGT GGT
	Reverse	GAC AGA AAC ATC GGC AAT ATC A
hsa *SLC1A5*	Forward	GAT TCG TTC CTG GAT CTT GC
	Reverse	GGT AGA GTA TGA GCG AAA GG
hsa *SLC7A1*	Forward	TCA TCA CCG GCT GGA ACT
	Reverse	CCC TCG CTA CGC TTG AAG TA
hsa *SMAD7*	Forward	AAA CAG GGG GAA CGA ATT ATC
	Reverse	ACC ACG CAC CAG TGT GAC
hsa *SMG5*	Forward	GAT TTG CTG AAG AAG GAA CAC C
	Reverse	TTC TGG CAG CGA ATG TAC C
hsa *SPRED2*	Forward	GAG CAC CGG AGG ATT TAT ACC
	Reverse	GAA GCT CAC CTG GCG GTA G
hsa *TBC1D22B*	Forward	GAG GCT GAC AGC TTT TGG TG
	Reverse	CCT GGT TGT GCA AAG GTG TA
hsa *TFR2*	Forward	AAG CTG CGG CAG GAG ATC TA
	Reverse	GCG ACA CGT ACT GGG AAA GG
hsa *TK1*	Forward	GTC ATA GGC ATC GAC GAG G
	Reverse	GCA GAA CTC CAC GAT GTC A
hsa *TNPO1*	Forward	TGA TGA TAC AAT TTC TGA CTG GAA TC
	Reverse	GGC AGC AGT TCA TCA CGA TA
hsa *U2AF2*	Forward	CAG GCC TCA CGA CTA CCA G
	Reverse	GGG ACC ACA GTG GAC ACA A
hsa *WSB2*	Forward	TCC TAT GAC CAA TGG GCT TT
	Reverse	CGT GGC CAT CTC TTG TCC
hsa XRCC5	Forward	CAA AGA GGA AGC CTC TGG AA
	Reverse	AGC TGC TGT GTC TCC ACT TG
hsa *YY1*	Forward	TGG AGA GAA CTC ACC TCC TGA
	Reverse	TCT TTA ATT TTT CTT GGC TTC ATT C

2.1.12 Primer sequences for molecular cloning

Table 2.4: Oligonucleotide sequences for cloning of human *MIR122* promoter constructs and miR-122 target gene 3´UTRs. Recognition sequences for restriction enzymes (RE sites) were included to allow for site-specific cloning into reporter plasmids. 3´UTRs for *CEP55*, *CLIC1*, *EPS15L1*, *KIF11*, *SLC1A5*, and *TK1* were cloned using In-Fusion recombinase system, which requires sequence homology between the vector and insert (bold nucleotides).

Amplified sequence	Primer	Sequence 5´ – 3´	RE Site
hsa *MIR122* Pro 0.18kb	Forward	GAG CTA GCC TTG CTG AGT GTG TTT GAC CAA	NheI
	Reverse	AGA AAG CTT GCC TCT CCC CTC TCC CTT TA	HindIII
hsa *MIR122* Pro 0.75kb	Forward	GAG CTA GCG GCG TGA ACA AAG GAA TGC A	NheI
	Reverse	AGA AAG CTT CGC TGG GTG GCA TCT TTT	HindIII
hsa *MIR122* Pro 0.95kb	Forward	GAG CTA GCA AAT TAG TCA GGT GTG GGC A	NheI
	Reverse	AGA AAG CTT GCA TTC CTT TGT TCA CGC CA	HindIII
hsa *MIR122* Pro 1.7kb	Forward	GAG CTA GCA AAT TAG TCA GGT GTG GGC A	NheI
	Reverse	AGA AAG CTT TGG AAG ACA AAG TTA TGG TGT GT	HindIII
hsa *CEP55* 3´UTR	Forward	**AAT CGA TAG GTA CCG AGC TC**C AAA ATA AGT ATT TGT TTT G	SacI
	Reverse	**TCG AGC CCG GGC TAG C**TT AAA ACA TTA AAT AAT TTT ATT C	NheI
hsa *CLIC1* 3´UTR	Forward	**AAT CGA TAG GTA CCG AGC TC**G CCC CTC CTG GGA CTC CC	SacI
	Reverse	**TCG AGC CCG GGC TAG C**TT GCG TAA AAA CAC TTG ATT TTT	NheI
hsa *EPS15L1* 3´UTR	Forward	**AAT CGA TAG GTA CCG AGC TC**A GGA AAG CAG ATG AGG TGT G	SacI
	Reverse	**TCG AGC CCG GGC TAG C**TT TCA TTT CCC TTA GCA TTT TAT TT	NheI
hsa *G6PDH* 3´UTR	Forward	GAG GTA CCG GGT TTC CAG TAT GAG GGC A	KpnI
	Reverse	GAG CTA GCT TGC GGA TTT AAT GGC AGG G	NheI
hsa *KIF11* 3´UTR	Forward	**AAT CGA TAG GTA CCG AGC TC**T TCA CTT GGG GGT TGG CA	SacI
	Reverse	**TCG AGC CCG GGC TAG C**TT AAT GTA GAA ACC ACA TTT ATT AA	NheI
hsa *SLC1A5* 3´UTR	Forward	**AAT CGA TAG GTA CCG AGC TC**A CCC CGG GAG GGA CCT TC	SacI
	Reverse	**TCG AGC CCG GGC TAG C**TT AAA TAG TTG ACA CTC AAT TTT AT	NheI
hsa *TK1* 3´UTR	Forward	**AAT CGA TAG GTA CCG AGC TC**G GGA CCT GCG AGG GCC GC	SacI
	Reverse	**TCG AGC CCG GGC TAG C**TG CGT CCA CCA ACC AGT GAA TTT TC	NheI

2.2 Methods

2.2.1 Cell culture conditions for human hepatoma cell line Huh-7 and human embryonic kidney 293 cells

Human hepatoma cell line Huh-7 and human embryonic kidney 293 (HEK293) cells were kindly provided by Prof. Dr. Johannes Bode (Clinic for Gastroenterology, Hepatology and Infectious Diseases, Düsseldorf, Germany). Huh-7 cells were cultured in Dulbecco´s Modified Eagle Medium/ Nutrient F-12 Ham (DMEM/ Ham´s F12 1 : 1) supplemented with 10% (v/v) heat-inactivated and sterile filtered FCS, while HEK293 were maintained in Dulbecco´s Modified Eagle Medium (DMEM) in presence of 10% (v/v) FCS. Both cell lines were grown in sterile T75 cell culture flasks at 37 °C in a humidified atmosphere containing 5% CO_2. The cell growth as

well as the cell confluency were monitored using contrast-phase microscopy. Cell lines were subcultured at a confluency of 80 – 90%, typically two to three times a week.

2.2.2 Overexpression and inhibition of miR-122 in Huh-7 cells

Huh-7 cells were transfected with miR-122 mimic (Ambion pre-miR™-122 miRNA precursor, Thermo Fisher Scientific) or miR-122 inhibitor (antagomiR-122, Roche) using the transfection reagent Lipofectamin™ RNAiMAX. For this purpose, cells were transfected at ~80% confluency according to the manufacturer´s instructions. For proteome studies, 140,000 Huh-7 cells were cultured and transfected in 6 cm dishes. Before the transfection, cells were washed with PBS and kept in 5 mL fresh FCS-free cell culture medium. The transfection was performed with 56 pmoles miR-122 mimic per dish or 112 pmoles of either miR-122 inhibitor or scrambled oligo control per dish. The miRNA mimic, inhibitor or scrambled control were diluted in 250 µL OPTI-MEM, respectively. The transfection reagent (16.5 µL/ dish) was first diluted in 250 µL OPTI-MEM and then transferred to the diluted miRNA mimic, inhibitor or scrambled control, respectively. Following incubation for 5 min at room temperature (RT), 500 µL transfection solution were pipetted dropwise on top of the cells. Six hours after the transfections, cell culture medium was replaced by fresh FCS-containing DMEM/ Ham´s F-12 and cells were harvested 24 or 48 h post transfection. RNA was isolated by washing the cells once with 2 mL PBS, and thoroughly scraping the cells in 500 µL ice-cold PBS. To remove cell debris, cells were spun at 100 g/ 5 min/ 4 °C. The supernatants were completely removed and pellets were immediately snap-frozen in liquid nitrogen and stored at -80 °C. For transcriptome analyses of transfected Huh-7 cells, 400,000 Huh-7 cells were cultured in 10 cm dishes. Transfection was performed as described above with 150 pmoles miR-122 mimic or 300 pmoles miR-122 inhibitor using 45 µL Lipofectamin™ RNAiMAX per dish. Cells were processed for qPCR, Western blot or polysome analyses as described in the Sections 2.2.14, 2.2.20 and 2.2.21.

2.2.3 Stimulation of Huh-7 cells with TGFβ1 or TGFβ receptor type 1 inhibitor

Huh-7 were seeded on sterile 12-well plates with 60.000 cells/ well one day before the stimulation. In order to synchronize cells and to shut down growth factor-dependent signaling pathways, Huh-7 were starved in FCS-free DMEM/ Ham´s F-12 medium overnight. The medium was then removed and replaced by DMEM/ Ham´s F-12 supplemented with 5 ng/mL

or 10 ng/mL TGFβ1 for 3 – 6 h. For inhibition of TGFβ signaling pathways, cells were pre-treated for 3 h with TGFβ receptor type 1 inhibitor SB431542 (5 µM or 10 µM in DMEM/ Ham´s F-12) and then treated with 5 ng/mL TGFβ1 in presence of SB431542 for another 3 h. After the stimulation, cells were processed for RNA isolation as described in the Section 2.2.14.

2.2.4 Isolation of genomic DNA from Huh-7 cells

Huh-7 cells were grown on 10 cm culture dishes to approximately 90% confluency. DMEM/ Ham´s-F12 medium was aspirated, cells were washed twice with PBS and lysed in 1 mL DNAzol™ reagent (Thermo Fisher Scientific). The cell lysate was then collected in a reaction tube and genomic DNA was precipitated by addition of 0.5 mL 100% ethanol. After centrifugation (20,000 g/ 2 min/ RT), the supernatant was completely removed and the remaining DNA pellet was washed twice with 70% (v/v) ethanol. The pellet was allowed to dry for 1 – 5 minutes. Finally, genomic DNA was resuspended in 300 µL nuclease-free water and quantified fluorometrically using QuBit™ dsDNA Assay Kit (Section 2.2.9).

2.2.5 Primer design for polymerase chain reaction (PCR)

Oligonucleotide primers were designed for amplification of *MIR122* promoter constructs of different length as well as for the amplification of miR-122 target gene 3´UTR (e.g. *glucose-6-phosphate dehydrogenase* [*G6PDH*]) using genomic sequences obtained from *Ensembl Genome Browser* (human assembly GRCH38.p10; http://www.ensembl.org/index.html). The design was performed using *Primer3web* version 4.1.0 (http://primer3.ut.ee/). For cloning strategies with the In-Fusion Cloning system, the *Cloning Primer Design Tool* of Takara Bio Europe (https://www.takarabio.com/learning-centers/cloning/in-fusion-cloning-tools) was utilized. Oligonucleotide primers for qPCR were designed with *Roche Probe Library (https://lifescience.roche.com/en_de/brands/universal-probe-library.html#assay-design-center).* Melting temperatures for DNA primers as well as secondary structures and dimer formations were calculated by *OligoAnalyzer 3.1* (https://eu.idtdna.com/calc/analyzer). Restriction sites for NheI, HindIII (*MIR122* promoter constructs) or KpnI, NheI and SacI (miR-122 target gene 3´UTRs) for cloning into appropriate reporter vectors were included to the 5´-end of the respective primers (Table 2.4). Oligonucleotide primers were synthesized by Sigma-Aldrich.

2.2.6 PCR amplification of *MIR122* promoter constructs and miR-122 target gene 3´UTRs

PCR amplification was performed in a total volume of 50 µL, containing 25 ng genomic DNA isolated from Huh-7 cells, 1x GoTaq® reaction buffer, 0.2 µM of forward and reverse primer, 0.3 mM dNTP mix and 2.5 Units GoTaq® DNA Polymerase. Following an initial denaturation step of 2 min at 95 °C, a pre-amplification was performed for 10 cycles with the following profile: 95°C/ 30 s (denaturation), 55 °C/ 20 s (annealing), 68 °C/ 1 min (elongation). Next, the PCR was continued for another 40 cycles with 95°C/ 30 s (denaturation), 62 °C/ 20 s (annealing), 72 °C/ 1 min (elongation) per cycle. A final extension step was carried out at 72 °C/ 5 min. For PCR amplicons larger than 1 kb, the elongation steps were prolonged to 2 min. The PCR reactions were carried out in a PTC-200 Thermocycler (MJ Research, St. Bruno, Canada). PCR amplicons were subjected to agarose gel electrophoresis for product size analysis and purification.

2.2.7 Agarose gel electrophoresis

For detection and gel-purification of PCR amplicons, 1.2% (w/v) agarose gels were prepared in 1x TAE supplemented with 4 µL HD Green Plus DNA Stain (Intas Science Imaging Instruments, Göttingen, Germany) per 100 mL TAE. PCR reaction mixtures were mixed with 6x Mass Ruler DNA Loading Dye (R0621, Fermentas, Waltham, USA) and loaded on the agarose gel. For PCR size comparison, 5 – 10 µL of FastRuler Middle Range DNA Ladder (SM1113, Thermo Fisher Scientific) or GeneRuler 100bp DNA Ladder (SM0243, Thermo Fisher Scientific) were loaded on the gel. Electrophoresis was typically performed at 100 V for 30 – 60 min in a Sub-Cell® GT Cell electrophoresis cell (170–4403, Bio-Rad Laboratories, Feldkirchen, Germany) and 1x TAE solution as electrolyte. Following electrophoresis, DNA was visualized in a UV/ VIS Detector (Teledyne ISCO, Lincoln, USA).

2.2.8 Gel extraction and purification of PCR amplicons

The extraction and purification of DNA from agarose gels was carried out with QIAquick Gel Extraction Kit (Qiagen) according to the manufacturer´s instructions. Briefly, for gel extraction the DNA bands of interest were dissected from agarose gels. Agarose slices were melted in Qiagen´s solubilization buffer by incubating at 50 °C and the DNA-containing solutions were applied to spin columns. For PCR purification, 5x volumes of Qiagen´s PB buffer (typically

250 µL) were added to each PCR reaction before loading onto spin columns. Upon sample loading and centrifugation at 8,000 g/ 30 s/ RT, columns were first washed twice with 500 µL PE buffer and then dried by centrifuging at 8,000 g/ 2 min/ RT. The purified PCR amplicons were eluted in 50 µL nuclease-free water and the DNA content was quantified using Qubit™ dsDNA HS Assay Kit according to the manufacturer´s instructions (Section 2.2.9).

2.2.9 Quantification of nucleic acids with Qubit™ assays

Nucleic acids were quantified fluorescently with the Qubit™ system provided by Invitrogen (Thermo Fisher Scientific) according the manufacturer´s protocol. The Qubit™ system utilizes highly selective dyes which specifically bind to DNA, RNA or protein, respectively. The target-bound dye emits fluorescence light after excitation and the resulting signal is detected and quantified with high sensitivity by the Qubit™ Fluorometer 2.0. RNA isolated from Huh-7 or HCC tissue were quantified by Qubit™ RNA HS Assay Kit (Q32852, Invitrogen), while genomic DNA isolated from cell lines as well as bacterial plasmid DNA were quantified by Qubit™ dsDNA HS Assay Kit (Q32851, Invitrogen). In order to measure nucleic acid concentrations, RNA- or DNA-specific dye was diluted 1 : 200 in appropriate reaction buffer (Qubit™ DNA buffer or Qubit™ RNA buffer) and aliquoted in 190µL – 199 µL in thin-walled 0.5 µL assay tubes (Thermo Fisher Scientific). Two nucleic acid standards were included to generate a standard curve and to determine the amounts of nucleic acid concentrations in the samples. Next, 10 µL of each standard or 1 – 5 µL of DNA or RNA sample were added to assay tubes (total volume of 200 µL), shortly vortexted and incubated for 2 min/ RT to allow the binding of the dye to target nucleic acid. The fluorescence was then measured with the Qubit™ Fluorometer 2.0, whereas the two standards were measured first.

2.2.10 Preparation of chemically competent bacteria

Escherichia coli (*E. coli*) bacteria were purchased from Thermo Fisher Scientific (strain TOP-10). For the preparation of chemically competent bacteria on a large scale, 5 µL of bacteria suspension were plated on antibiotic-free Lysogeny Broth (LB) agar plates and incubated overnight at 37 °C. Then, single bacteria colonies were collected using a sterile 10 µL pipet tip, inoculated in 5 mL antibiotic-free LB medium and incubated overnight under constant shaking at 200 revolutions per minute (rpm). At the following day, the bacteria suspension was

transferred in 200 mL fresh LB medium and allowed to grow at 37 °C/ 200 rpm, whereby the bacterial growth was monitored photometrically by measuring the optical density (OD) at a wavelength of λ = 590 nm and stopped when a OD of 0.5 – 0.6 was reached. For this purpose, the bacteria suspension was immediately placed on ice, aliquoted into 50 mL reaction tubes and pelleted by centrifugation at 1,800 g/ 4 °C/ 10 min. In order to enable the bacteria to internalize plasmid DNA, pelleted bacteria were resuspended in 20 mL TFB1 solution and incubated for 1 h on ice. The suspension was then centrifuged at 1,400 g/ 4 °C/ 10 min, the supernatant was discarded and the bacteria were resuspended in TFB2 solution. The bacteria were kept on ice for another 15 min, aliquoted in 50 µL, snap-frozen in liquid nitrogen and stored at -80 °C until use.

2.2.11 Cloning of *MIR122* promoter constructs into pGL4.1 Basic luciferase reporter plasmid

MIR122 promoter sequences were generated by PCR amplification using human gDNA and sequence-specific primers containing recognition sites for restriction enzymes as described in Sections 2.2.4 – 2.2.8. To enable site-directed cloning of promoter sequences (inserts) into reporter plasmid (vector), amplified and purified *MIR122* promoter sequences as well as 1 µg of the pGL4.10[*luc2*] promoter-less luciferase plasmid were digested with 40 Units NheI-HF and HindIII-HF in 1x CutSmart buffer, respectively. To ensure a complete restriction digestion, reactions were carried out at 37 °C/ overnight. Following digestion, vectors and inserts were purified using QIAquick PCR Purification Kit and quantified fluorometrically (Sections 2.2.8 and 2.2.9). Subsequently, 50 ng of digested plasmid were ligated to one of the *MIR122* promoter sequences in a molecular ratio of 1 : 3 (vector : insert), respectively. The ligation reactions were catalyzed by DNA ligase provided with the Quick Ligation™ Kit in 1x Quick Ligase buffer for 30 min at RT. Thereafter, 2 – 5 µL of the ligation mixtures were directly transformed into TOP-10 chemically competent *E. coli*. The bacteria were incubated on ice for 30 min in presence of ligation mixtures, then heat-shocked for 45 s at 42 °C and immediately stored on ice for another 2 min. To initiate bacterial growth and allow bacteria to develop ampicillin-resistance, 200 µL LB-medium (Carl Roth) were added and bacteria were allowed to grow at 37 °C for 30 min under smooth agitation (180 rpm). Bacteria suspensions were then plated out on LB-agar plates supplemented with 100 µg/mL ampicillin (Sigma-Aldrich) and incubated at 37 °C/ overnight. The next day, bacterial colonies were picked using a sterile pipet tip and inoculated into 5 mL (for small-scale plasmid preparation) or 50 mL (for large-scale plasmid

preparation) ampicillin-containing LB-medium. Small-scale preparation of plasmid DNA was carried out with Fast-n-Easy Plasmid Mini-Prep Kit, large-scale preparation of plasmid DNA was performed using QIAGEN Plasmid Midi Kit according to the manufacturer's protocol. The isolated plasmids were sequenced by the Genomics and Transcriptomics Laboratory (GTL, Heinrich Heine University, Düsseldorf) by means of Sanger-Sequencing.

2.2.12 Cloning of *G6PDH* 3´UTRs into pMir(+) and pMir(-) luciferase reporter plasmids

The full length of the human *G6PDH* 3´UTR was cloned into pMir(+) and pMir(-) reporter plasmids with a similar approach as described in Section 2.2.11 and by Castoldi *et al.* [*307*]. Briefly, the desired sequence was amplified by PCR using human gDNA as template. Sequence-specific primers were designed with NheI recognition site in the 5´-end of the forward primer and KpnI recognition site at the 5´-end of the reverse primer in order to allow for the site-directed insertion of the desired sequence into the multiple-cloning site (MCS) of the reporter plasmids. The PCR products for the *G6PDH* 3´UTR were purified by gel extraction and digested by the restriction enzymes NheI-HF and KpnI-HF in 1x CutSmart buffer (New England BioLabs) at 37 °C overnight. Reporter plasmids pMir(+) and pMir(-) were likewise linearized by NheI-HF and KpnI-HF. Vectors and inserts were purified and quantified as described above (Section 2.2.11). The ligation was conducted using Quick DNA Ligase with 50 ng of linearized pMir(+) or pMir(-) and a 3-fold molecular excess of insert for 30 min and then immediately transformed into TOP-10 *E. coli* as described above. Large and small scale plasmid preparations were conducted using standard molecular biology kits and recombinant plasmids were sequenced by the Genomics and Transcriptomics Laboratory at the Heinrich Heine University (Düsseldorf).

2.2.13 Cloning of miR-122 target gene 3´UTRs into pMir(+) and pMir(-) using In-Fusion Cloning System

The full length 3´UTRs of human *CLIC1*, *CEP55*, *SLC1A5*, *KIF11*, *EPS15L1* and *TK1* were each cloned into pMir(+) and pMir(-) luciferase reporter plasmids with the In-Fusion Cloning Plus system (Takara Bio Europe), which utilizes recombinases to create recombinant plasmids. For this purpose, the *In-Fusion Cloning Primer Design Tool* was used to generate primers that allow for the amplification of 3´UTRs of the aforementioned human genes with homologous termini

to the linearized vectors (Table 2.4). The sequences of interest were PCR amplified using 25 ng genomic human DNA and CloneAmp HiFi PCR Premix (Takara Bio Europe) according to the manufacturer´s instructions and purified with QIAquick PCR Purification Kit (Qiagen). pMir(+) and pMir(-) vectors were linearized with NheI-HF and SacI-HF as described earlier (Section 2.2.11). In-Fusion cloning reactions were set up in a total volume of 10 µL consisting of 50 ng of linearized plasmid and a 5-molar excess of insert in 1x In-Fusion HD Enzyme Premix. The reactions were performed at 50 °C for 15 min and terminated by cooling on ice. An aliquot of 2.5 µL of In-Fusion reaction mixture was transformed in Stellar™ Competent Cells in accordance with the manufacturer´s instructions. Isolation of recombinant plasmids from bacteria colonies and Sanger sequencing were performed as described (Section 2.2.11).

2.2.14 RNA isolation from Huh-7 cells

Total RNA from Huh-7 cells was isolated by phenol/ chloroform extraction, followed by spin column clean up. For this purpose, culture medium was aspirated, the cell layer was shortly washed in cold PBS and cells were harvested in PBS by thoroughly deattaching the cells with a sterile cell scraper. The cells were transferred into clean reaction tubes, centrifugated at 1000 g/ 5 min/ 4 °C and the supernatant was discarded. The pelleted cells were lysed by addition of 500 µL Qiazol Lysis Reagent (79306, Qiagen) and vortexing for 3 min. The RNA was separated from protein and genomic DNA by extraction with 100 µL chloroform. Following invertion of the reaction tubes 4 – 6 times and centrifugation at 10,000 g/ 10 min/ 4 °C, the aqueous phase containing the RNA was carefully separated and transferred into clean reaction tubes. Next, the RNA was precipitated by addition of 1.5x volumes 100% ethanol. The whole sample was loaded on miRNeasy columns and spun at 5,500 g/ 30 s/ RT. The column was washed once with 250 µL RWT buffer (Qiagen), followed by two washing steps with 500 µL PE buffer (Qiagen), respectively. The RNA was then dried on the column by 2 min centrifugation at 8,000 g/ 2 min/ RT. Residual ethanol was allowed to evaporate by transferring the spin columns in clean reaction tubes and by incubation with open lid for 10 min. To elute the RNA, 50 µL RNase-free water was pipetted to the top of the column, incubated for 1 min, and eventually collected by centrifugation at 8,000 g/ 2 min. In order to increase the RNA yield, the flow-through was re-loaded on the spin column and eluted by centriguation at 20,000 g/ 2 min.

2.2.15 Extraction of RNA from formalin-fixed paraffin-embedded (FFPE) human HCC tissue

RNA isolation from human HCC tissue was performed with three 5 µm-thick FFPE sections for each individual sample (Table 2.1). Using a razor blade, sections were delicately scraped from objective slides and transferred to clean nuclease-free 2 mL reaction tubes. Slices were dewaxed by addition of 500 µL xylene and incubation at 50 °C for 3 min. To ensure a proper removal of paraffin, the sections were centrifuged at 20,000 g/ 2 min, fresh xylene was added and the incubation at 50 °C for 3 min was repeated two times. Sections were then washed twice with 500 µL 100% ethanol and centrifuged at 20,000 g/ 2 min. The supernatant was removed and the remaining tissue was allowed to dry at RT for up to 10 min. Following, the samples were digested with 100 µg/mL proteinase K in 400 µL lysis buffer for 2 h at 56 °C. To remove genomic DNA, tissue was treated with 11 µL DNase I in 80 µL DNase buffer for 15 min at RT. For the purification of RNA, a phenol/ chloroform extraction was applied by adding 500 µL Qiazol and 100 µL chloroform. The organic and the aqueous phase were separated by centrifugation (10,000 g/ 15 min/ 4 °C) and the aqueous phase was carefully collected in a clean reaction tube. RNA was precipitated with 1.5x volumes 100% ethanol and purified with miRNeasy spin columns as described above (Section 2.2.14).

2.2.16 Procedure of cDNA synthesis with random hexamers

Total RNA isolated from cell lines was reverse transcribed with random hexamers and PrimeScript™ reverse transcriptase (RTase). The cDNA was synthesized according to the recipe in Table 2.5 with 200 ng total RNA in a thermal cycler at 65 °C/ 5 min (annealing of random hexamers), 25 °C/ 10 min, 42 °C/ 60 min (first cDNA strand synthesis), followed by 70 °C/ 15 min (heat inactivation). The synthesized cDNA was diluted to 1 ng/µL with nuclease-free water and used as template for qPCR.

Table 2.5: Reaction for cDNA synthesis with random hexamers.

Components	Volumes [µL]
RNA (33.3 ng/µL)	6.0
Random hexamers (100 µM)	0.5
dNTPs (10 mM)	1.0
5x RTase buffer	4.0
PrimeScript™ RTase (200 U/µL)	0.5
Nuclease-free water	8.0
Total reaction volume	**20.0**

2.2.17 Gene-specific reverse transcription for RNA isolated from human HCC tissue

RNA isolated from human HCC tissue was reverse-transcribed with gene-specific primers (qPCR reverse primer, Table 2.3) and PrimeScript™ reverse transcriptase (RTase). Table 2.6 depicts the reaction mixture for 200 ng of total RNA and pooled gene-specific RT primer (each at 5 µM). Reaction was performed at 65 °C/ 5 min, 25 °C/ 10 min, 42 °C/ 30 min, followed by 70 °C/ 15 min. The synthesized cDNA was diluted to 1 ng/µL with nuclease-free water.

Table 2.6: Reaction mixture for gene-specific reverse transcription for *G6PDH* and *HPRT1* mRNA.

Components	Volumes [µL]
RNA (33.3 ng/µL)	6.0
Pooled gene-specific primers (5 µM each)	0.4
dNTPs (10 mM)	1.0
5x RTase buffer	4.0
PrimeScript™ RTase (200 U/µL)	0.5
Nuclease-free water	8.1
Total reaction volume	**20.0**

2.2.18 Quantitative *real-time* PCR for relative mRNA quantification

Relative quantification of mRNA was performed in a ViiA7™ Real-Time PCR Cycler (Applied Biosystems, Darmstadt, Germany) with GoTaq® qPCR Master Mix (A6002, Promega) using the reaction mixture indicated in the Table 2.7:

Table 2.7: Reaction mixture for qPCR of messenger RNA.

Components	Volumes [µL]
cDNA (1 ng/µL)	2.50
Forward primer (10 µM)	0.21
Reverse primer (10 µM)	0.21
2x GoTaq® qPCR Master Mix	7.50
Nuclease-free water	4.58
Total reaction volume	**15.0**

For each gene of interest, one master mix containing gene-specific primers, 2x GoTaq® qPCR Master Mix and water was prepared and aliquoted in 12.5 µL in appropriate 96-well plates (Applied Biosystems). Next, 2.5 ng (2.5 µL) of the respective cDNA was added, whereby each sample was measured in at least two technical replicates. The 96-well plate was sealed with a clear sealing foil (Applied Biosystems) and centrifuged at 1,000 g/ 2 min/ RT to collect

the whole reaction volume at the bottom of the wells. The plate was transferred to the cycler and qPCR was started using the settings shown in Table 2.8:

Table 2.8: QPCR program for relative quantification of mRNA.

Step	Temperature [°C]	Time [s]	Cycles
Heat-activation	94	120	
Denaturation	94	15	40x
Annealing/ elongation	60	60	
Melting curve analysis			1x

At the end of the last qPCR cycle, melting curve analysis was carried out to evaluate the presence of qPCR byproducts or primer dimers. To quantify relative mRNA amounts, a signal intensity threshold within the linear range of the amplification curves was set. The threshold cycles (C_t-values), defined as the intersection of the amplification curves and the intensity threshold, were exported and relative mRNA quantities were calculated based on the delta-delta C_t ($\Delta\Delta C_t$) method [*389*]. Appropriate reference genes were selected based on *GeNorm* algorithm using *qBase* software v 1.3.5 [*390*]. The statistical analysis of qPCR data was conducted by unpaired student´s t-test or one-way analysis of variance (ANOVA) with a significance level of $p < 0.05$.

2.2.19 Relative quantifications of microRNAs by miQPCR

In this thesis, relative quantification of miRNAs was performed by miQPCR [*388*]. To cope with the difficulties of miRNA quantification by qPCR, which is the short length of miRNAs and the lack of poly(A) tails, miQPCR uses the activity of T4 RNA Ligase to uniformly elongate the 3´-ends of small RNAs to a short oligonucleotide adaptor (miLINKER). In the next step, a universe reverse transcription is performed using PrimeScript™ RTase and a reverse-transcription primer (mQ-RT) that specifically hybridizes to the miLINKER adaptor sequence. The universal reverse transcription allows for the quantification of numerous miRNAs of interest, without the need to generate individual cDNAs for each miRNA. Relative miRNA quantification is then carried out by qPCR using SYBR Green-based approaches with miRNA-specific forward primers and a universal reverse primer (Upm2A).

miQPCR was conducted as previously described [*106*–*109*, *388*]. For the elongation of RNA according to the miQPCR protocol, 10 ng of diluted RNA were mixed with 7 µL elongation

mix (Table 2.9), incubated at 25 °C/ 30 min and then cooled down to 10 °C. The elongated RNA was mixed with 7 µL cDNA Mix 1 (Table 2.9) heated up to 85 °C for 2 min in order to allow mQ-RT primer annealing and incubated at 46 °C (the temperature optimum of the reverse transcriptase). Next, 5 µL of cDNA Mix 2 (Table 2.9) were added and samples were incubated at 46 °C for 30 min to complete the first strand reverse transcription. Finally, samples were heat-inactivated at 85 °C/ 2 min and cooled down to 10 °C.

Table 2.9: Composition of master mixes required for cDNA synthesis by miQPCR [*388*]. The table lists compounds required for preparation of three master mixes.

Components	Volumes [µL]
1) Elongation mix	
10x T4 Rnl2 Buffer (New England BioLabs)	0.9
$MgCl_2$ (450 mM)	0.1
PEG 8000 (50%)	3.1
miLINKER (5 mM)	0.1
RNase inhibitor (40 U/µL, Roche)	0.1
Truncated T4 RNA Ligase (K227Q) (New England BioLabs)	0.2
Nuclease-free water	3.1
2) cDNA Mix 1	
dNTPs (10 mM)	0.5
mQ-RT primer (10 mM)	0.25
Nuclease-free water	7.0
2) cDNA Mix 2	
5x RT Buffer (Takara Bio Europe)	4.4
PrimeScript™ RTase (Takara Bio Europe)	0.14
Nuclease-free water	0.85

The miQPCR was performed in PTC-200 thermal cyclers (MJ Research) to ensure appropriate temperature control. The synthesized cDNA was diluted to 50 pg/µL by addition of 180 µL nuclease-free water. QPCR assays were typically conducted with 2 – 5 µL cDNA (i.e. 100 pg – 250 pg cDNA) in a total volume of 15 µL as follows:

Table 2.10: Reaction mixture for qPCR quantification of miRNAs.

Components	Volumes [µL]
cDNA (50 pg/µL)	2.00 – 5.00
Forward primer (10 µM)	0.21
Reverse primer (10 µM)	0.21
2x GoTaq® qPCR Master Mix	7.50
Nuclease-free water	2.08 – 5.08
Total reaction volume	**15.0**

One master mix containing miRNA-specific primers, universal Upm2A primer, 2x GoTaq® qPCR Master Mix and water was prepared for each miRNA to be measured. The mixes were aliquoted in 10 µL – 13 µL in appropriate 96-well plates and 100 pg – 250 pg cDNA (2 – 5 µL) were added. All samples were measured in at least two technical replicates. 96-well plates were then sealed with sealing foil and centrifuged at 1,000 g/ 2 min/ RT. QPCR was carried out with the following protocol:

Table 2.11: QPCR program for relative quantification of miRNA.

Step	Temperature [°C]	Time [s]	Cycles
Heat-activation	94	120	
Denaturation	94	15	50x
Annealing/ elongation	60	30	
Melting curve analysis			1x

As for mRNA quantification, melting curve analysis was performed at the end of the qPCR to exclude the presence of byproducts or primer dimers. Relative miRNA quantity was calculated with *qBase* software version 1.3.5 [*390*] based on the ΔΔCt method [*389*]. The microRNA miR-192 was identified as most stable miRNA using the *GeNorm* algorithm and was therefore selected as reference gene for data normalization. Statistical analysis of qPCR data was carried out by unpaired student´s t-test with a significance level of $p < 0.05$.

2.2.20 Western blot and proteome analyses

Preparation of protein lysates from Huh-7 cells

Protein lysates and proteome analysis of Huh-7 cells were prepared by Jessica Schira (Molecular Proteomics Laboratory, Heinrich Heine University Düssedorf). Cell lysation was carried out in lysis buffer containing 30 mM Tris base, 7 M urea, 2 M thiourea, cells were disrupted by high-speed shaking using a TissueLyser (Qiagen) and by sonication for 10 s six times. Cell debris was removed by centrifugation 16,000 g/ 15 min/ 4 °C and the supernatant was collected in a fresh reaction tube. Protein content was quantified by Pierce™ 660 nm Protein Assay (Thermo Fisher Scientific) according to the manufacturer´s instructions. For Western blot analyses, cells were washed with cold PBS, harvested in RIPA buffer and collected in clean reaction tubes on ice. To remove cell debris, cells were centrifuged at 10,000 g/ 4 °C/ 10 min and the supernatant was collected in a fresh reaction tube. This

procedure was repeated twice. Protein amounts were quantified by Qubit™ Protein Assay Kit according to the manufacturer´s instructions.

Preparation of polyacrylamide gel electrophoresis (PAGE)

Sodium dodecyl sulfate (SDS)-PAGE were conducted with purchased Bolt™ 4-12% Bis-Tris Plus Gels (NW04120BOX, Invitrogen) in a Mini-PROTEAN Electrophoresis Cells (4400-110-01, Bio-Rad Laboratories). Protein lysates containing 20 µg total protein were transferred to reaction tubes, mixed with 1x volume of 2x loading dye and denatured by heating to 40 °C/ 10 min. The samples were shortly centrifuged and loaded on the Bis-Tris Plus Gel using a Hamilton pipette. For protein size comparison, 10 µL of protein standards (PageRuler™ Prestained Protein Ladder, 10 to 180 kDa, 26616, Thermo Fisher Scientific) were loaded on each gel. The electrophoresis cell was then flooded with 1x MOPS buffer and electrophoresis was conducted with a voltage of 50 V for 15 min and 200 V for another hour.

Protein transfer on PVDF membranes

Proteins were blotted on PVDF membranes (GE Medical Systems, Solingen, Germany) using a semidry blotting approach in a Trans-Blot® SD Semi-Dry Transfer Cell (Bio-Rad Laboratories). Two Whatmann papers (Sigma-Aldrich) were moistened in anode buffer and applied on the bottom of the transfer assembly. The PVDF membrane (Sigma-Aldrich) was shortly moistered in anode buffer and gently laid on top of the Whatman papers, followed by the polyacryl amide gel. Two Whatman papers were shortly incubated with cathode buffer and carefully placed on top of the polyacrylamide gel. The transfer of proteins was carried out with constant current strength of 128 mA for 2 h.

Protein detection and densitometric quantification of proteins

Subsequent to protein blotting, the PVDF membranes were washed with TBST for 10 min/ RT and blocked with 10% (v/v) bovine serum albumin (BSA) in TBST (blocking buffer) for 2 h/ RT. Antibody incubation with rabbit anti-G6PDH (1 : 2,000) and mouse anti-β actin (1 : 20,000) were carried out simultaneously in 10% BSA/ TBST blocking buffer for 2 h/ RT. For measurement of EPS15L1 or CEP55, membrane blocking and antibody incubation with rabbit anti-EPS15L1 (1 : 5,000) or rabbit anti-CEP55 (1 : 20,000) were conducted in 5% milk powder/ TBST. After incubation with primary antibodies, the membranes were washed three

times with TBST for 20 min/ RT. Secondary antibodies (goat anti-rabbit-HRP or sheep anti-mouse-HRP) were diluted at 1 : 10,000 in either 10% BSA/ TBST or 5% milk powder/ TBST. Membranes were incubated with secondary antibody solutions for 2 h at RT and washed three times with TBST for 10 min/ RT. Western Lightning Plus-ECL was used according to the manufacturer´s instructions as a substrate for the HRP. The resulting chemiluminescence was detected with ChemiDoc™ Imaging Systems (Bio-Rad Laboratories) using appropriate exposure times (typically within 30 – 120 s). Densitometric evaluation of signal intensities was carried out with *Image J* software using β-actin for normalization.

2.2.21 Polyribosomal profiling for miR-122 target identification

Polyribosomes (also referred to as polysomes) are a complex consisting of mRNA, ribosomes and nascent polypeptide chains that are assembled during mRNA translation (Figure 2.1). The density of this complex depends on the translational activity of a given mRNA. Highly translated mRNA is simultaneously bound by many ribosomes, leading to a high polysome density (`heavy polysomes´). On the other hand, mRNAs that are poorly translated only bind few ribosomes and the resulting polysomal complex is less dense (`light polysomes´).

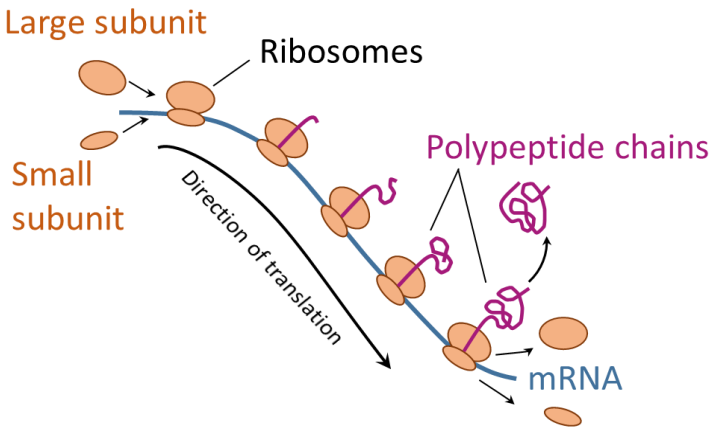

Figure 2.1: Schematic illustration of mRNA translation and polyribosome content. (Adapted from Freeman *et al.* 2004 [*391*]).

Depending on their density, polysomes can be fractionated on a sucrose gradient by centrifugal force. Heavy polysomes co-sediment in the high sucrose percentage area, while light polysomes associate with the lower sucrose percentage area of the gradient (Figure 2.2).

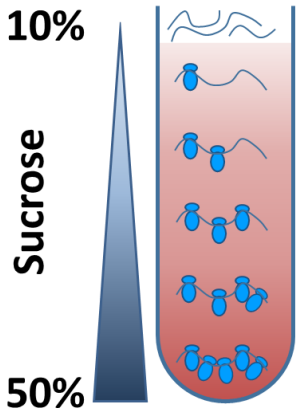

Figure 2.2: Scheme of polysome sedimentation using linear 10 – 50% sucrose gradients.

It has been demonstrated that miRNAs cosediment with their target mRNAs [*232*], which makes it possible to study miRNA targets on polyribosomes isolated from cells with manipulated miRNA content (i.e cells treated with miRNA mimics or inhibitors). In order to avoid polysome dissociation, cells are treated with cycloheximide (CHX) and lysed in the presence of CHX. The cytosolic extracts are loaded on top of a sucrose gradient and centrifuged to allow for the polysome separation. Using a fractionator, polysome fractions of varying density are collected and polysome-associated mRNAs are isolated by phenol/ chloroform extraction and ethanol precipitation.

Preparation of sucrose gradients

Sucrose gradients used for polysome isolation were prepared in plastic round-bottom polyallomer tubes (13 x 51 mm) suitable for ultracentrifugation (Beckman Coulter, Krefeld, Germany). Two sucrose solutions were prepared with 10 % (w/v) and 50% (w/v) sucrose in hypotonic buffer, respectively. Five mL of 10% (w/v) sucrose solution were placed on the bottom of the polyallomer tube using a 20 mL syringe and a long metal needle. Next, 5 mL of the 50% (w/v) sucrose solution were filled into the 20 mL syringe and the solution was layered underneath the 10% (w/v) sucrose solution by gently moving down the metal needle to the very bottom of the polyallomer tube and slowly releasing the liquid from the syringe. In this way, two layers of sucrose were created in the tube with a visible border in between the layers. The tube was then delicately placed in a gradient maker (Gradient Master 108, BioComp Instruments, Fredericton, Canada) and a linear 10 – 50% sucrose gradient was created by tilting and rotating the tubes following a standardized protocol of the manufacturer (BioComp Instruments).

Preparation of cell lysates and fractionation of polyribosomes

Polysomes were isolated from Huh-7 transfected with miR-122 mimic and miR-122 inhibitor, respectively, as described in paragraph 2.2.2. In order to prevent the disassembly of polysomes, cells were treated with 200 µg/mL CHX for 10 min/ 37 °C in the incubator. Then, cells were washed with PBS supplemented with 100 µg/mL CHX (PBS-CHX) for 5 min/ RT. Afterwards, PBS was removed and cells were detached from culture dishes by incubating in 1 mL accutase supplemented with 200 µg/mL CHX for 5 min at 37 °C. The cell suspensions were collected in clean reaction tubes and cells were pelleted by centrifugal force at 1,000 g/ 5 min/ 4 °C. The supernatants were discarded and cells were lysed in 750 µL lysis buffer. To ensure complete cell disruption, lysates were gently passed through a 25G canula and the cell nuclei were removed by centrifugation at 20,000 g/ 10 min/ 4 °C. For total RNA analysis, 50 µL of lysate were transferred to a fresh reaction tube, while the remaining lysate was carefully layered on top of the linear sucrose gradient. To separate polysomes depending on their density, tubes were placed in a SW40 Ti swinging-bucket rotor (Beckman Coulter) and centrifuged in an Optima XPN-80 ultracentrifuge (Beckman Coulter) at 200,000 g/ 3 h/ 4 °C with brakes turned off to prevent gradient disruption upon completion of the centrifugation. Then, the polyallomer tubes were cautiously removed from the swinging-bucket rotor and assembled in a fraction collector (Fraction collector FoxyR1, Teledyne ISCO). The bottom of the polyallomer tube was gently pierced with a metal canula. To elute the sucrose gradients, 60% (w/v) sucrose solutions (supplemented with 0.01% bromophenol blue) were pumped very slowly through the canula into the bottom of the polyallomer tubes using a peristaltic pump (Minipuls 3 peristaltic pump; Gilson Inc, Middleton, USA). The sucrose gradient was eluted into a fraction collector, thereby nucleic acids passing a preinstalled UV recorder were detected at a wavelength of λ = 254 nm. Fractions of roughly 650 µL were collected in reaction tubes (up to 17 fractions) and the RNA from each fraction was recovered with 1x volume 25 : 24 : 1 (v/v/v) phenol : chloroform : isoamyl alcohol (P2609, Sigma-Aldrich). Following a centrifugation at 10,000 g/ 10 min/ 4 °C, the aqueous phase was collected in clean tubes. The RNA was precipitated with 1.5x volumes 100% ethanol and pelleted at 20,000 g/ 30 min/ 4 °C. The RNA pellet was washed once with ice-cold 70% ethanol, air dried for up to 5 min and then resuspended in 50 µL nuclease-free water.

Affymetrix microarray hybridization and data analysis

With the purpose to identify potential targets of human miR-122 at a genome-wide level, RNA isolated from different polyribosomal fractions were pooled to generate heavy polysome (fractions A2 – A5), middle density polysome (fractions A6 – A9) and light polysome (fractions A10 – 13) pooled samples. The profiling of RNA by Bioanalyzer as well as microarray analyses were conducted by the Genomics Core Facility at the European Molecular Biology Laboratories (EMBL, Heidelberg). Sample preparation and raw data analyses for microarrays were performed by Dr. Castoldi (Clinic for Gastroenterology, Hepatology and Infectious Disease). The raw data from Affymetrix Human Gene Chip 1.0 ST were analyzed with *AltAnalyze* software [*392*] by applying thresholds for gene expression changes with fold change (FC) ≥ 1.5 and a statistical significance niveau of $p < 0.05$.

2.2.22 *MIR122* promoter analysis by luciferase reporter assay

Luciferase reporter assays are a tool for the investigation of gene expression changes at the transcriptional or post-transcriptional level. One of the main applications for which luciferase reporter assays are used, is the analysis of cloned promoter DNA fragments. This approach allows to evaluate whether a cloned fragment may drive or inhibit the expression of luciferase in a given environment (e.g. in a specific cell-type or under a certain treatment). The output of the luciferase assay is a chemiluminescent signal, measured from the lysates of cells which were transfected with a luciferase reporter plasmid. The signal intensity of the luminescence can be considered as proportional to the amount of luciferase in the samples. Typically, two luciferase plasmids are used in this type of assay: The *Firefly* luciferase plasmid serves as the actual reporter plasmid that encodes the DNA sequence of interest, while *Renilla* luciferase plasmid is co-transfected for data normalization. *Firefly* and *Renilla* luciferases both catalyze related enzymatic reactions, but they differ in their substrate specificity and they catalyze reactions at different pH. The luciferase reporter plasmid pGL4.10[*luc2*] that was used in this study encodes for a *Firefly* luciferase but lacks an active promoter. To study the activity of different constructs of the human *MIR122* promoter, cloning of the desired sequences into the *Firefly* plasmid was conducted as described in paragraph 2.2.11. The recombinant plasmids were then transfected together with pRL-SV40 (*Renilla* plasmid) into Huh-7 and luciferase activity was measured after stimulation of cells with a panel of different cytokines and growth factors.

Promoter analysis by Dual-Luciferase® Reporter Assay

The responsiveness of human *MIR122* promoter constructs to treatment with a panel of cytokines and growth factors was investigated in Huh-7. For this purpose, 1 µg of promoter plasmid was co-transfected with 10 ng pRL-SV40 in presence of 3 µg linear 25 kDa polyethyleneimine (PEI, Polysciences Inc., Warrington, USA) as transfection reagent. Hereby, PEI (1 mg/mL in water, sterile filtered) was diluted in 50 µL Tris-buffered saline (TBS, 50 mM Tris base pH 8.2, 150 mM NaCl, sterile filtered) and pipetted on top of plasmid DNA. The transfection solution was gently flickered to ensure proper mixing of the reagents, incubated 15 min/ RT and diluted with 450 µL FCS-free DMEM/ Ham´s F-12 medium. Huh-7 cells cultured in 12-well plates (60,000 cells/ well) were prepared for transfection by washing with 1 mL PBS and addition of 0.5 mL FCS-free transfection medium. The transfection mixtures were pipetted dropwise on top of the cell layer. After 5 h incubation time, transfection medium was replaced by fresh culturing medium. The next day, cells were synchronized in starvation medium (FCS-free DMEM/ Ham´s F-12) for another 24 h. Then, Huh-7 cells were stimulated with growth factors and cytokines as listed in Table 2.12. Control cells were kept in starvation medium for the same period. Following stimulation for 24 h, Huh-7 cells were subjected to lysis and Dual-Luciferase® Reporter Assay as described below.

Table 2.12: Growth factors and cytokines for Huh-7 cell stimulation.

Cytokine	Concentration [ng/mL]	Cat. no.	Manufacturer
Transforming growth factor beta 1 (TGFβ1)	10	100-21	PeproTech
Bone morphogenetic protein 6 (BMP6)	50	120-06	PeproTech
Interleukin 6 (IL6)	50	I0406	Sigma-Aldrich
Interleukin 10 (IL10)	10	I9276	Sigma-Aldrich
Tumor necrosis factor alpha (TNFα)	10	ADI-908-066	Enzo Life Sciences
Interferon beta (IFNβ)	1.000 [U/µL]	IF011	Merck Millipore
Platelet-derived growth factor-BB (PDGF-BB)	20	P4056	Sigma-Aldrich

Dual-Luciferase® Reporter Assay

Promega´s Dual-Luciferase® Reporter Assay was conducted in accordance with the manufacturer´s instructions. For this purpose, Huh-7 cells were washed with PBS and lysed in 150 µL 1x Passive Lysis Buffer (Promega) for 15 min/ RT. The cell lysates were collected in reaction tubes, centrifuged at 10,000 g/ 2 min/ 4 °C to remove cell debris and supernatants were transferred in fresh reaction tubes. The chemiluminescence assay was performed in

white opaque 96-well plates with 50 µL cell lysate and 50 µL of both, LARII reagent (*Firefly* luciferase substrate) and Stop and Glo reagent (*Renilla* luciferase substrate), in a GloMax® Multi Plus Multiplate Reader (Promega) according to the preset protocol with an integrity time of 10 seconds for each read. Data were normalized by calculating ratios of *Firefly*/ *Renilla* activities to correct for possible variations in transfection efficiencies.

2.2.23 Validation of miR-122 target genes using Dual-Luciferase® Reporter Assay

A luciferase reporter-based approach was applied in this thesis to verify a direct miR-122-target 3´UTR interaction. This assay utilizes a modified *Firefly* luciferase plasmid derived from pGL3 Promoter Vector (Promega) that allows for basal luciferase mRNA and protein expression. Previously, the reporter plasmid was modified in a way that the multiple cloning site (MCS) of the vector was re-cloned to the 3´-end of the *Firefly* luciferase mRNA (schematically depicted in Figure 2.3; and described by Castoldi *et al.* [*307*]).

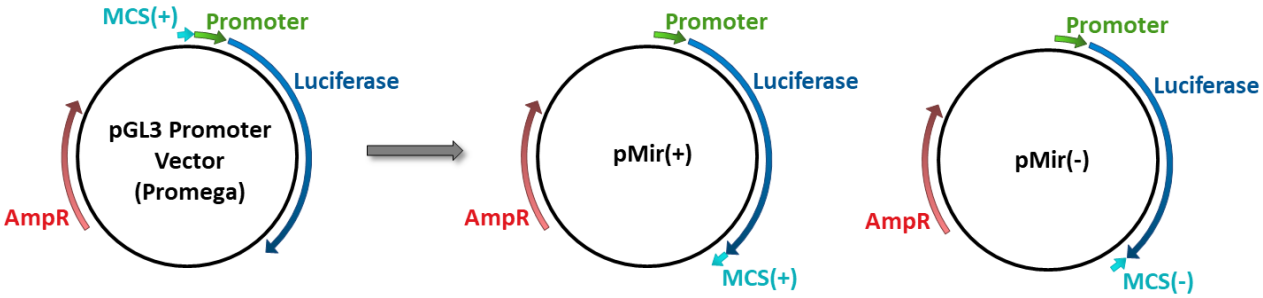

Figure 2.3: Illustration of pMir(+) and pMir(-) *Firefly* luciferase plasmids for miR-122 target gene validation. The multiple cloning site (MCS) of pGL3 Promoter Vector was cloned to the 3´-end of the *Firefly luciferase* gene as described by Castoldi *et al.* [*307*]. The pMir(+) vector contains the MCS in original orientation, while the pMir(-) harbors the MCS in inverse orientation. AmpR: ampicillin-resistance gene.

In this way, two plasmids were generated, one with the MCS in original sense orientation [pMir(+)] and the other with the MCS in antisense orientation [pMir(-)] serving as negative control vector [*307*]. Following cloning of recombinant plasmids encoding the 3´UTRs of putative miRNA target genes (Sections 2.2.12 and 2.2.13), the plasmids were transfected into human embryonic kidney cells (HEK293) in presence or in absence of miR-122 mimic, respectively. If the cloned 3´UTR of the putative target gene harbors functional binding sites for miR-122, *luciferase* mRNA is silenced by miR-122. As a result, in comparison to cells transfected with plasmid only, a reduction of luciferase protein level is observed,

accompanied by reduced chemiluminescence measured in lysates of cells simultaneously transfected with plasmid and miR-122 mimic. Recombinant pMir(-) plasmids were also transfected in presence or absence of miR-122 to exclude unspecific effects of miR-122 on luciferase translation. HEK293 were chosen as model organism, because they lack endogenous miR-122 and, therefore, changes in luciferase activity can clearly be attributed to overexpression of miR-122 with miR-122 mimic.

Co-transfection of luciferase reporter plasmids and miR-122 mimics into HEK293 cells

For co-transfection of luciferase reporter plasmids in presence or absence of miR-122 mimics, HEK293 cells were seeded in sterile 12-well plates to a confluency of ~60% (typically 70,000 cells/ well). Transfection was performed with either Lipofectamin™ 3000 (Thermo Fisher Scientific) or with Xfect™ MIRNA Transfection Reagent and Xfect™ Tranfection Reagent (Takara Bio Europe). The transfection was carried out with 300 ng *Firefly* plasmid DNA, 6.25 ng pRL-SV40 *Renilla* luciferase plasmid in presence or absence of 25 pmoles miR-122 mimic according to the manufacturer´s instructions. The transfection medium was replaced by fresh culturing medium after 5 h. HEK293 cells were incubated for 24 or 48 h and then harvested for Dual-Luciferase® Reporter Assay as described in the Section 2.2.22.

2.2.24 Bioinformatic tools and online databases

Genomic DNA sequences of human *MIR122* gene, its promoter regions as well as sequences of miR-122 target gene 3´UTRs were downloaded from *Ensembl Genome Browser* (release GRCh38.p3 at http://www.ensembl.org/index.html). miRNA sequences were acquired from *miRBASE* (release 22.1, October 2018, www.mirbase.org). Virtual cloning and analysis of nucleic acid sequences were performed with *CLC Genomics Workbench* (Version 3.6.5). Primer sequences for the cloning of *MIR122* promoter constructs and *G6PDH* 3´UTRs were designed with *Primer3web version 4.1.0* software (http://primer3.ut.ee/). Cloning primers for In-Fusion Cloning Plus system were designed using Takara´s web-based *In-Fusion Cloning Primer Design Tool* (https://www.takarabio.com/learning-centers/cloning/in-fusion-cloning-tools). The sequences for qPCR primers were received from *Universal ProbeLibrary Assay Design Center (*https://lifescience.roche.com/ en_de/brands/universal-probe-library.html#assay-design-center*)*. The melting temperatures for all miRNA and mRNA primers were calculated with *OligoAnalyzer 3.1* (https://eu.idtdna.com/calc/analyzer). Primers for PCR amplification were

designed with respect to their secondary structure and the potential occurrence of homo- or heterodimers. The qPCR data were exported with *QuantStudio™ Real-Time PCR Software* or with *StepOne Software v2.3* (Thermo Fisher Scientific). QPCR data sets were analyzed using *qBase* software v 1.3.5 and reference genes were selected based on the *GeNorm* algorithm [*390*]. *miRWalk* (http://www.umm.uni-heidelberg.de/apps/zmf/mirwalk/) and *RNA22 version 2.0* (https://cm.jefferson.edu/rna22/) were used for target prediction of human miR-122 [*264*]. Microarray data obtained from hepatic RNA isolated from *MIR122* transgenic mice (GSE27713 and GSE31453; [*295*]) as well as from tumor tissue and adjacent non-tumor tissue of HCC patients (GEO repository; GSE45050; [*393*]) were downloaded from the Gene Expression Omnibus (GEO) repository (https://www.ncbi.nlm.nih.gov/geo/). Microarray raw data were analyzed with *AltAnalyze* software version 2.0.8.1 by Dr. Castoldi [*392*]. Gene Ontology term analysis for microarray data were performed using the *GO-Elite* algorithm implemented in *AltAnalyze*, while GO-term analysis for proteome data were received from *GOrilla* (http://cbl-gorilla.cs.technion.ac.il/) [*394*]. Conservation of human *MIR122* promoter sequence and flanking sequence was visualized with *ECR Browser* (https://ecrbrowser.dcode.org). Data from luciferase assays were exported using *Instinct®* Software (version 3.1.3, Promega).

2.2.25 Statistical information

Statistical analyses were carried out by using *GraphPad Prism 5.03* software. Quantitative variables were described as percentages or means ± standard error of the mean (SEM). Statistical analyses for the comparisons between two groups were performed by applying unpaired, two-tailed student´s t-test (parametric test). Correlation between two groups was calculated using Pearson correlation. Comparison between three (or more groups) were carried out by using one-way ANOVA (parametric test) or by applying multiple t-test when appropriate. Analyses resulting in p-values $p < 0.05$ were considered as statistically significant. For the statistical evaluation of *MIR122* promoter assays, multiple t-test was applied with a false discovery rate (FDR) of 0.5% ($p < 0.005$).

3. Results

3.1 *De novo* identification of miRNA targets by polysomal profiling

With the aim to identify novel miR-122 target gene candidates on a transcriptome-wide scale, polysomal profiling was conducted. This method allows for the investigation of differences in the translational turnover of mRNAs and was already described as useful tool for miRNA target identification [*235*–*238*]. For this purpose, polysomes were fractionated from Huh-7 cells after miR-122 overexpression or miR-122 inhibition as described in Section 2.2.21. During the fractionation of the individual samples, nucleic acids were monitored photometrically. Figure 3.1 A shows one representative illustration of the UV_{254} profile of fractionated polysomes isolated from cytosolic extracts of miR-122 overexpressing Huh-7 cells. Nucleic acids were present in the fractions A2 – A17. While fractions A2 to A9 contained polysomes of different density, monosomes were present in fraction A9 – A13. (Figure 3.1 A).

Eukaryotic mRNA translation is initiated by the recruitment of the 40S ribosomal subunit together with various transcription factors to the mRNA, resulting in the formation of the 48S initiation complex [*219*]. Therefore, to study the miR-122-mediated effects on the translatome of Huh-7 cells, the sucrose fractions containing monosomes as well as the ribosomal subunits were collected together with the fractions carrying polysomes of different density. Hence, RNA from fractions A2 – A13 were recovered from the sucrose gradients and visualized by capillary electrophoresis (Bioanalyzer). Total RNA isolated from mammalian samples typically generates two prominent peaks in the Bioanalyzer electropherogram, representing the cytoplasmic 28S ribosomal RNA (peak size ~4700 nucleotides) and the 18S ribosomal RNA (~1900 nucleotides). Figure 3.1 B illustrates a representative Bioanalyzer electropherogram of RNAs isolated from polysomal fractions A2 to A13 of Huh-7 cells. Remarkably, the amounts of 28S and 18S RNA differed in between the polysomal fractions. The signal intensity of 28S RNA declined in the sucrose fractions with lower density (from A2 to A12). On the other hand, only minor amounts of 18S RNA were present in fractions A3 – A5, while amounts of 18S RNA increased from A6 – A12. In the lower molecular size range, 5S RNA was most prominently present in fraction A13. The electropherogram indicated that polysomes of different density may be differentially composed.

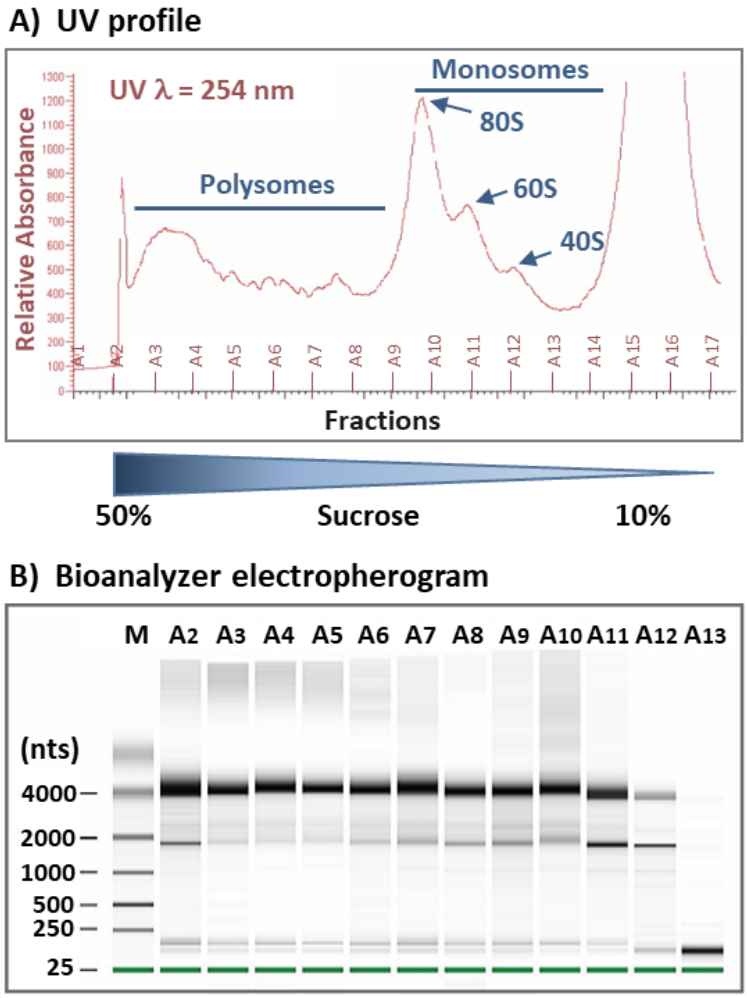

Figure 3.1: Isolation and fractionation of polysomes from Huh-7 cells. Polysomes were isolated from Huh-7 cells transfected with miR-122 mimic for 48 h. Cells were lysed in presence of cycloheximide and cytosolic extracts were separated on 10 – 50% sucrose gradients by ultracentrifugation. Polyribosomes were fractionated and RNA was isolated from each fraction and subsequently quantified. **A**) Representative UV absorbance profile (λ = 254 nm) of nucleic acids associated with polyribosomes. The collected fractions are depicted as A1 – A17. The sucrose gradient is indicated as blue color scale. **B**) Electropherogram from Agilent Bioanalyzer illustrates the presence of ribosomal RNAs in fractions A2 – A13.

3.1.1 Detection of polysome-associated microRNAs and mRNAs from miR-122 overexpressing and miR-122 inhibited Huh-7

To evaluate whether manipulation of cellular miR-122 levels changes the association of miRNAs to polysome fractions, RNA was isolated from fraction A2 – A13 and the miRNA content was quantified by miQPCR.

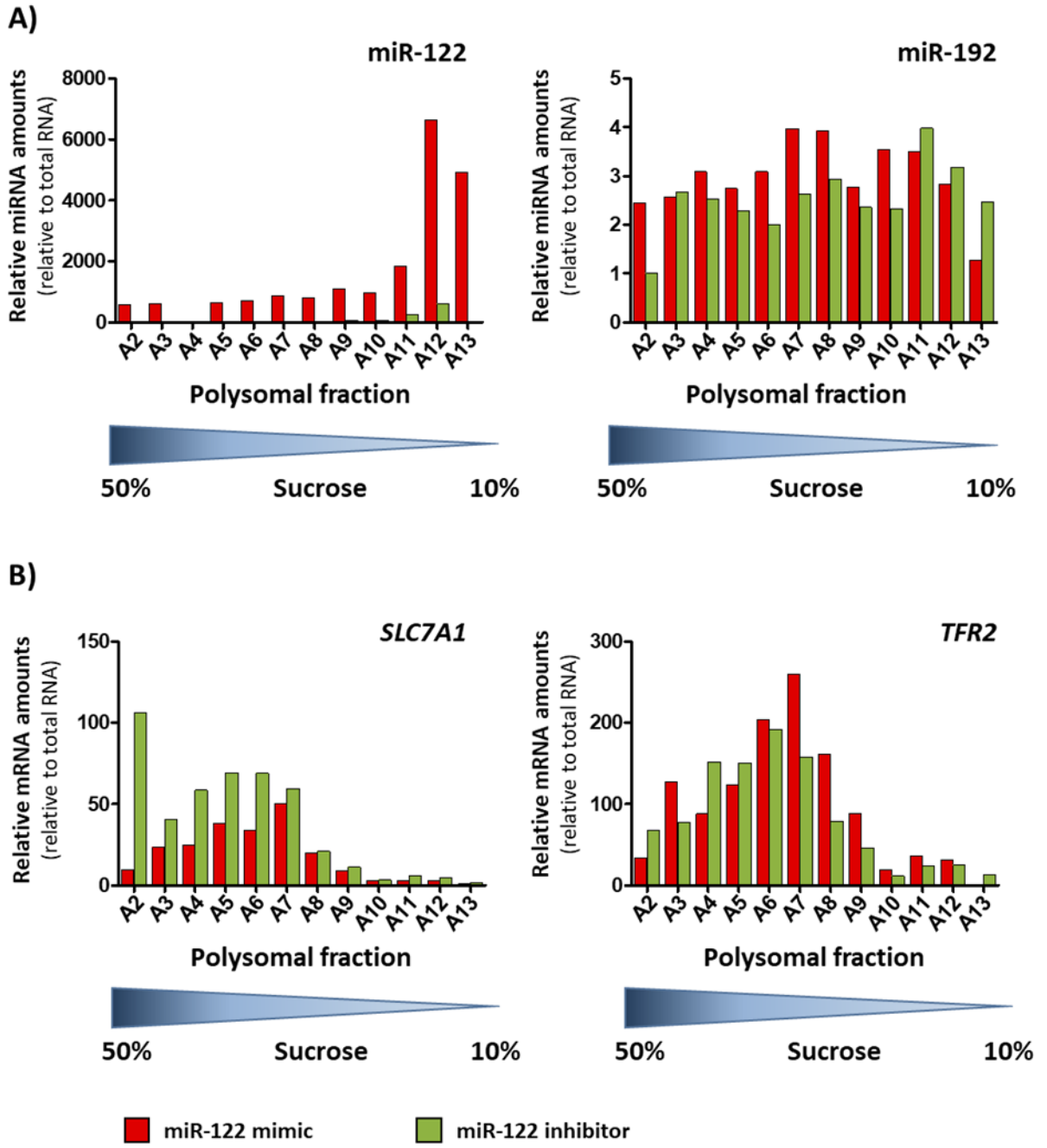

Figure 3.2: Analysis of miRNA and mRNA distribution across polysomes isolated from Huh-7 treated with miR-122 mimic or miR-122 inhibitor. Polysome-associated RNAs from Huh-7 cells treated with miR-122 mimic **(red)** or miR-122 inhibitor **(green)** were isolated 48 h post transfection, purified and quantified by qPCR. **A)** Analysis of miR-122 and miR-192 distribution across polysome fractions. **B)** Relative distribution of miRNA-122 target mRNA *SLC7A1* (left) and control transcript *TFR2* mRNA (right). Representative illustration of a single experiment out of three experiments performed for microarray analyses. Blue color scales illustrate the direction of the sucrose gradients.

Figure 3.2 A illustrates the relative amounts of miR-122 and miR-192 across polysomal fractions isolated from Huh-7 after miR-122 overexpression or miR-122 inhibition. The overexpression of miR-122 in Huh-7 efficiently increased the amount of polysome-associated

miR-122 in every fraction. Moreover, in miR-122 overexpressing cells, this miRNA was highly enriched in light polysomal fractions (A10 – A13), indicating that miR-122 mainly co-sediments with poorly translated mRNAs. On the other hand, no substantial differences in the levels or the relative distribution of polysome-associated miR-192 were found when comparing polysome fractions isolated from miR-122 overexpressing to those isolated from miR-122 inhibitor (antagomiR-122) treated Huh-7 cells. These data indicate that miR-122 overexpression increased the levels of polysome-bound miR-122, but did not essentially affect the association of other miRNAs to polysomes.

The suitability of the polysomal profiling for miRNA target gene identification was investigated by measuring the amount and the distribution of polyribosome-associated mRNAs. For this purpose, mRNA levels of the validated miR-122 target *high affinity cationic amino acid transporter 1* (*SLC7A1*, also known as *CAT1*) were assessed across polysomes isolated from miR-122 mimic and antagomiR-122 treated Huh-7 cells. As control, mRNA levels of the *transferrin receptor 2* (*TFR2*), which is known to be unaffected by miR-122 [*278*, *307*], were likewise quantified (Figure 3.2 B). Higher levels of *SLC7A1* mRNA were measured in all polysomal fractions isolated from Huh-7 cells treated with miR-122 inhibitor compared to those fractions isolated from miR-122 mimic transfected cells (Figure 3.2 B, left panel). In addition to that, *SLC7A1* mRNA was highly present in fractions derived from heavier polysomes (fraction A2) upon miR-122 knockdown with antagomiR-122 inhibitor. In contrast, as depicted in Figure 3.2 B neither the total amount of *TFR2* mRNA nor its relative distribution across the polysomes were substantially affected by overexpressing or by inhibiting cellular miR-122.

The increase of the *SLC7A1* mRNA in the polysomal fractions in response to miR-122 inhibition compared to miR-122 overexpression indicated that higher amounts of *SLC7A1* mRNA were actively transcribed. Moreover, the enrichment of *SLC7A1* mRNA in the fractions derived from heavier polysomes implied that mRNA translation was relatively enhanced in the cells with reduced miR-122 content compared to miR-122 overexpressing cells. Overall, the presented data demonstrated that the analysis of polysomes is a suitable tool for identifying miRNA targets.

3.1.2 Microarray analysis of polyribosomal pools for genome-wide identification of miR-122 target gene candidates

With the aim to gain insight into the molecular networks which are regulated by miR-122, transcriptome analysis of polysome-bound mRNA was conducted. For this purpose, polysomes were fractionated from Huh-7 transfected with miR-122 mimic (overexpression) or miR-122 inhibitor (antagomiR), respectively. RNAs isolated from individual fractions were pooled as illustrated in Figure 3.3 A and are herein referred to as `heavy´ polysomal pools (fractions A2 – A5), `middle´ polysomal pools (fractions A6 – A9) and `light´ pools (fractions A10 – A13). The RNAs pooled from miR-122 mimic or from antagomiR-122 transfected Huh-7 cells were then subjected to microarray analyses. The levels of polysome-associated mRNAs in a given polysomal pool were compared in cells treated with miR-122 mimic to those treated with antagomiR-122. Furthermore, levels of mRNAs across the polysomal pools were compared with regard to their relative distribution across light, middle or heavy polysomal pools in a given treatment (i.e. in miR-122 mimic or in antagomiR-122 transfected cells).

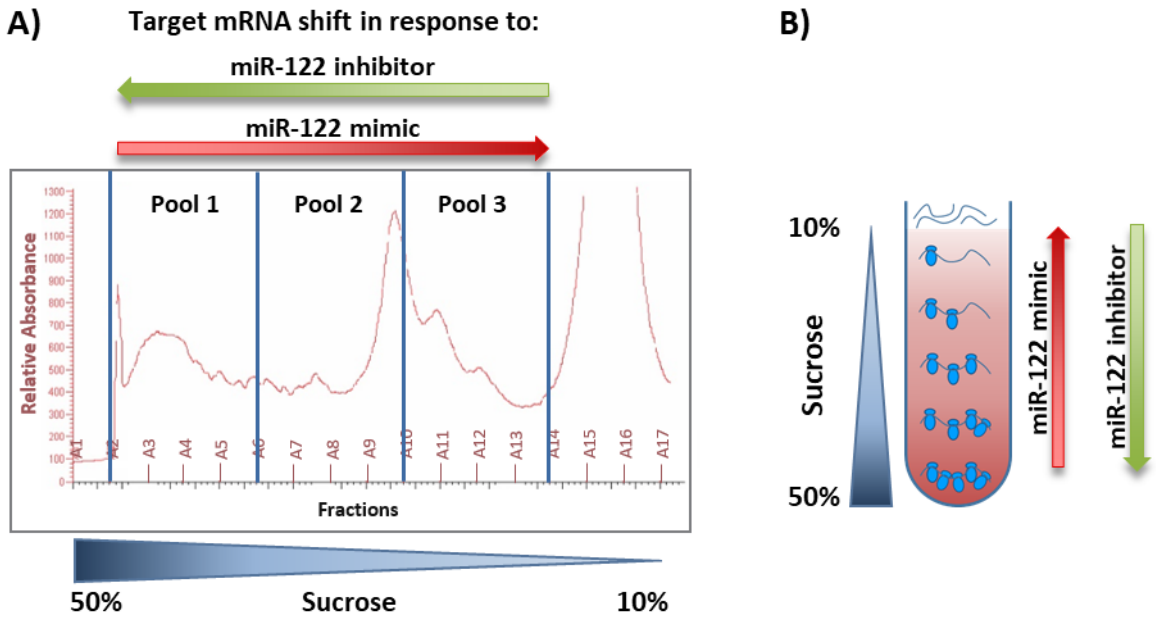

Figure 3.3: Illustration of expected target mRNA shift on polysomes in response to miR-122 modulation. Polysomes from Huh-7 cells treated with miR-122 mimic and miR-122 inhibitors were analyzed for *de novo* identification of miR-122 target gene candidates. Overexpression of miR-122 causes translational repression of miR-122 target mRNA, initiating a shift of mRNAs from heavier to lighter polysomes (indicated as red arrow). In contrast, the inhibition of miR-122 releases target transcripts from miR-122-mediated repression, accompanied by an increase in mRNA translation. Target mRNAs, therefore, shift from lighter towards heavier polysomes (direction indicated as green arrow). **A)** Scheme of the mRNA distribution shift on fractionated polysomes of Huh-7 cells after overexpression **(red arrow)** and inhibition **(green arrow)** of miR-122. **B)** Schematic illustration of polyribosomes in sucrose gradients with shifting miR-122 target amounts.

Potential miR-122 targets shift from high-density (highly transcribed) towards lower-density pools (less transcribed) upon miR-122 overexpression or from lower-density (low transcribed) towards higher density pools (higher transcribed) in response to antagomiR-122 treatment. Alternatively, miR-122 target candidates might be associated in lower abundance in polysomal pools isolated from miR-122 overexpressing compared to miR-122 downregulated cells, illustrating a lower overall transcriptional activity in response to high miR-122 levels (Figure 3.3).

3.1.3 Transcriptome analysis of polysome-associated mRNAs isolated from Huh-7 cells overexpressing miR-122

Microarray analyses were conducted on RNAs isolated from polysomal pools of miR-122 mimic transfected cells to study the changes of the Huh-7 translatome in response to elevated miR-122 levels. Since miR-122 overexpression was expected to lower the translation of its target transcripts, target mRNA candidates were expected to be more abundant in light polysomal fractions. Therefore, levels of polysome-bound mRNAs in miR-122 mimic treated Huh-7 cells were evaluated with a specific focus on those transcripts that revealed a reduced translational activity.

The heat maps presented in Figure 3.4 A indicate that miR-122 overexpression in Huh-7 profoundly affected the cellular translatome. When comparing mRNA levels in the middle (pool 2) against the heavy (pool 1) polysomal pool, 532 mRNAs were associated with heavier polysomes, 2,023 mRNAs co-sedimented with lighter polysomes, while 22,415 transcripts did not show any differential distribution (Figure 3.4 B, left panel). The evaluation of transcripts in middle and light (pool 3) polysomes revealed that 3,144 messengers associated with heavier polysomes, while 3,111 transcripts co-sedimented with lighter polyribosomes and no changes were observed for 18,715 transcripts (Figure 3.4 B, middle panel). The direct comparison of the heavy to the light polysomal pools showed that 912 transcripts were associated with heavier polysomes, 1,992 transcripts were found with higher abundance in the light polysomal pools, and the distribution of 22,066 transcripts was found unchanged (Figure 3.4 B, right panel).

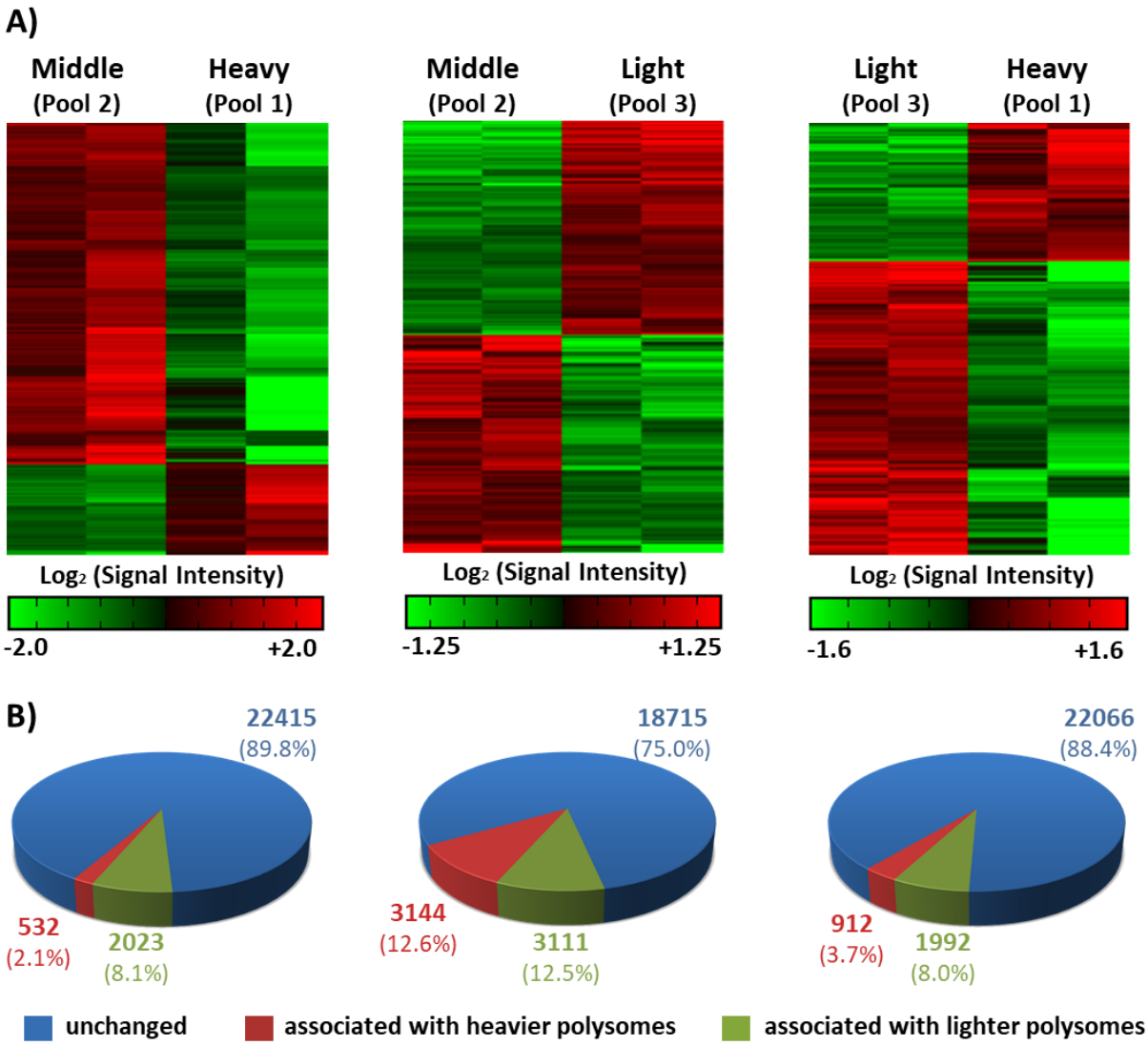

Figure 3.4: Microarray analysis of mRNA distribution across polysomes isolated from miR-122 overexpressing Huh-7 cells. Polysomes were fractionated from Huh-7 cells treated with miR-122 mimic for 48 h. Following RNA isolation from the purified fractions, RNA was pooled to create a heavy polysomal RNA pools (pool 1, fractions A2 – A5), middle polysomal RNA pools (pool 2, fractions A6 – A9) and light polysomal RNA pools (pool 3, fractions A10 – A13). RNA from the polysomal pools was hybridized to Affymetrix arrays (human Genechip 1.0 ST Array, n = 2). Data were analyzed by *AltAnalyze* using a cut-off of 1.5-fold change and significance level of $p < 0.05$ (one-way ANOVA). **A)** Heat map representing the differential distribution of mRNAs in polysomal pools using a Cousine Matrix to generate hierarchical tree of gene clusters. Signal intensities are expressed on a logarithmic scale (base 2). **B)** Pie charts representing the numbers of transcripts significantly regulated between different pool comparisons. **Left** pool 2 *vs.* pool 1, **middle** pool 2 *vs.* pool 3, **right** pool 3 *vs.* pool 1.

Potential miR-122 target genes co-sediment with lighter polysomal pools in response to miR-122 overexpression. Therefore, those mRNAs that were identified to be more abundant in the lighter polysomal pools were further analyzed. The *miRWalk* prediction tool was utilized to correlate all predicted miR-122 targets to those mRNAs that were found in the lighter polysomes after miR-122 overexpression. For this purpose, a data set from *miRWalk*

was downloaded which lists all predicted miR-122 target genes that were identified by at least two independent prediction algorithms and that may be targeted by miR-122 at their 3´UTR, their 5´UTR or their coding-sequence. Using these criteria, a large proportion of mRNAs found in the lighter polysomal pools in response to miR-122 overexpression were identified as predicted miR-122 target by *miRWalk* (Appendix Figure 7.1 A). In total, 37.8% genes identified from the heavy *vs.* the middle polysomal pool (pool 1 *vs*. pool 2), 25.8% of the genes identified from comparing middle *versus* light pools (pool 2 *vs*. pool 3), and 31.3% analyzed in the heavy compared to the light polysomal pools (pool 1 *vs*. pool 3) were annotated as predicted miR-122 target genes by the chosen algorithm (Appendix Figure 7.1 A).

3.1.4 Transcriptome analysis of polysome-associated mRNAs isolated from antagomiR-122 transfected Huh-7 cells

Transfection of antagomiR-122 in Huh-7 cells strongly reduces the cellular miR-122 availability (Appendix Figure 7.2), thus releasing target messengers from the translational inhibition. Subsequently, the translation of miRNA target transcripts is increased and this change in the translational turnover is observed as shift of mRNA from lighter towards heavier polysomes (displayed in Figure 3.3).

The changes of the Huh-7 translatome in response to antagomiR-122 transfections of Huh-7 cells are visualized in Figure 3.5. Microarray analysis of the polysome-associated mRNAs in the heavy (pool 1) compared to the middle (pool 2) polysomal pools identified that 879 messengers associated with the heavier polysomes and 1,484 transcripts co-sedimented together with the lighter polysomes (Figure 3.5 B, left panel). Differential mRNA distributions in the middle compared to the light (pool 3) polysomal pool was found for 2,308 transcripts, which associated with heavier polysomes, and for 2,135 mRNAs which co-sedimented with the lighter polysomal pools (Figure 3.5 B, middle panel). The most pronounced changes were observed in light compared to heavy polysomal pools, with 3,066 transcripts associated with heavier polysomes and 2,972 transcripts with lighter polysomes (Figure 3.5 B, right panel). Target mRNA candidates for miR-122 are believed to associate with heavier polysomes in response to miR-122 overexpression. In order to assess whether predicted miR-122 target genes were identified in the group of mRNAs co-sedimented in the heavier polysomal pools, an intersection with the predicted miR-122 target genes from the *miRWalk* algorithm was performed. Remarkably, among the transcripts associated with heavier polysomes in the

comparison of heavy to middle polysomal pool, 52.6% of transcripts were identified as predicted miR-122 target genes by the *miRWalk* prediction tool (Appendix Figure 7.1 B). In the comparison of middle to heavy polysomes 52.9% of transcripts were assigned as predicted miR-122 target genes. Among the transcripts associated with heavy polysomes identified from comparing heavy to light polysomal pools, 54.4% of all genes were predicted miR-122 target (Appendix Figure 7.1 B).

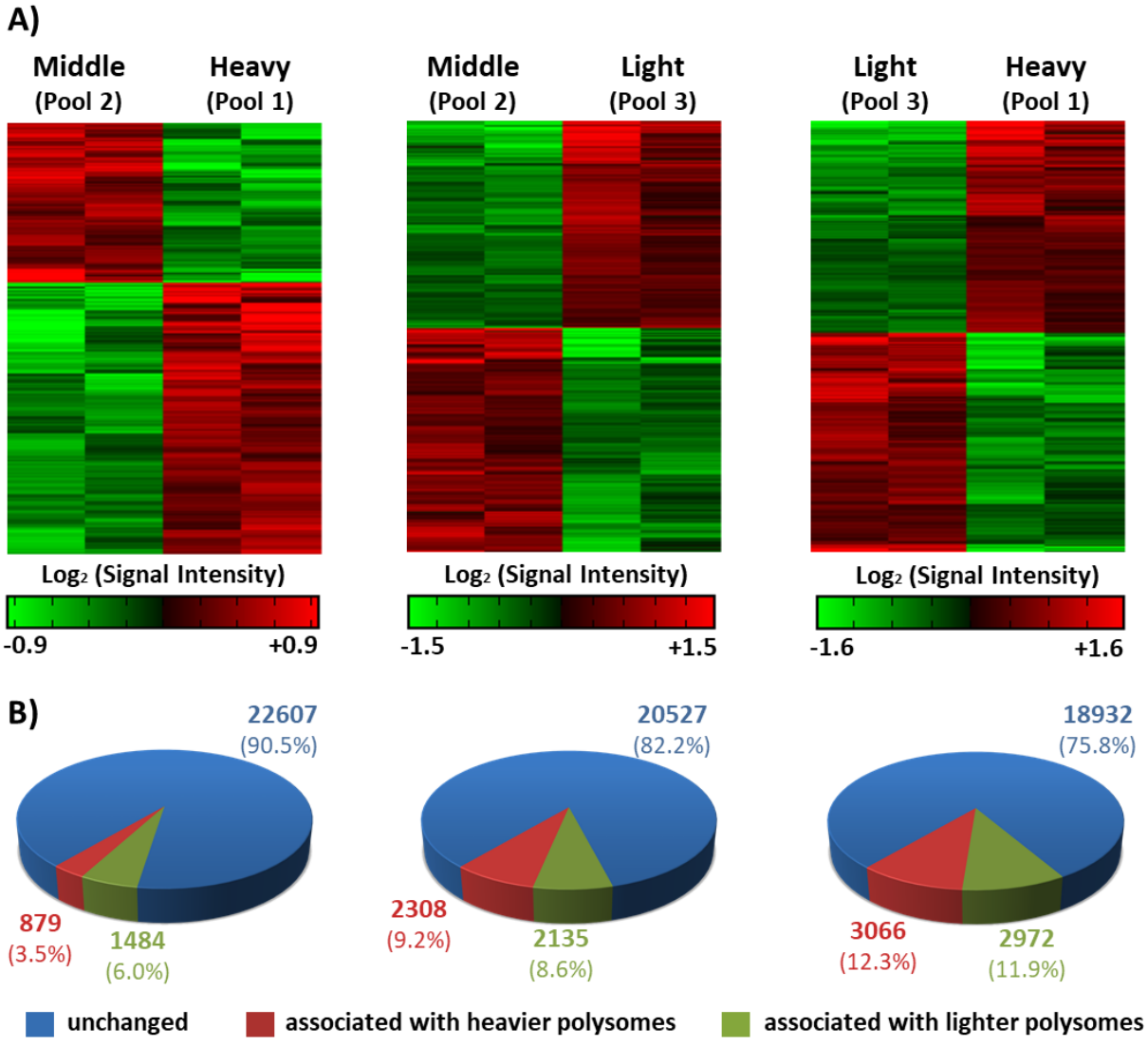

Figure 3.5: Microarray analysis of mRNA distribution across polysomes isolated from Huh-7 cells treated with miR-122 inhibitor. Polysome-associated RNA was recovered from Huh-7 cells treated with miR-122 inhibitor for 48 h. The RNA was pooled to generate heavy polysomal RNA pools (pool 1), middle polysomal RNA pools (pool 2) and light polysomal RNA pools (pool 3) and hybridized to Affymetrix arrays (human Genechip 1.0 ST Array, n = 2). Data analysis was carried out by *AltAnalyze* (fold change > 1.5, significance level $p < 0.05$ using one-way ANOVA). **A)** Differential distribution of mRNAs associated with polysomal pools in antagomiR-122 transfected Huh-7 cells illustrated as heat map. Signal intensities are expressed on a logarithmic scale (base 2). **B)** Pie charts representing the numbers of transcripts significantly regulated between different pool comparisons. **Left** pool 1 *vs.* pool 2, **middle** pool 2 *vs.* pool 3, **right** pool 1 *vs.* pool 3.

3.1.5 Comparison of mRNA distribution across polysomal pools derived from miR-122 enriched and miR-122 inhibited Huh-7 cells

As shown for *SLC7A1* mRNA (Figure 3.2), an upregulation of miR-122 is accompanied by a reduction of target mRNA levels bound to individual polysomal fractions. Therefore, the microarray data received from polysomal profiling were further analyzed, whereby the composition of individual pools was compared in miR-122 mimic transfected to antagomiR-122 transfected cells.

Figure 3.6 visualizes the altered mRNA distribution in the individual polysomal pools isolated from Huh-7 cells after miR-122 overexpression or miR-122 inhibition. In the heavy pool, 609 messengers were downregulated in miR-122 overexpressing cells, while 315 were upregulated in response to miR-122 overexpression compared to miR-122 inhibition (Figure 3.6 B, left panel). In the polysomal pool of middle density, 221 mRNAs were upregulated and 164 transcripts were downregulated in miR-122 overexpressing compared to miR-122 inhibited cells (Figure 3.6 B, middle panel). The transcript distribution in the light density pool identified 331 upregulated and 304 downregulated transcripts (Figure 3.6 B, right panel).

The intersection of all downregulated transcripts in response to miR-122 overexpression with the *miRWalk* prediction algorithm identified that 37.8% (heavy pool), 43.2% (middle pool), and 42.8% (light pool) of all transcripts were assigned as predicted miR-122 target genes, respectively (Appendix Figure 7.1 C).

In summary, microarray analysis identified a large number of transcripts with altered mRNA levels across polysomes isolated from Huh-7 transfected with either miR-122 mimic or with antagomiR-122.

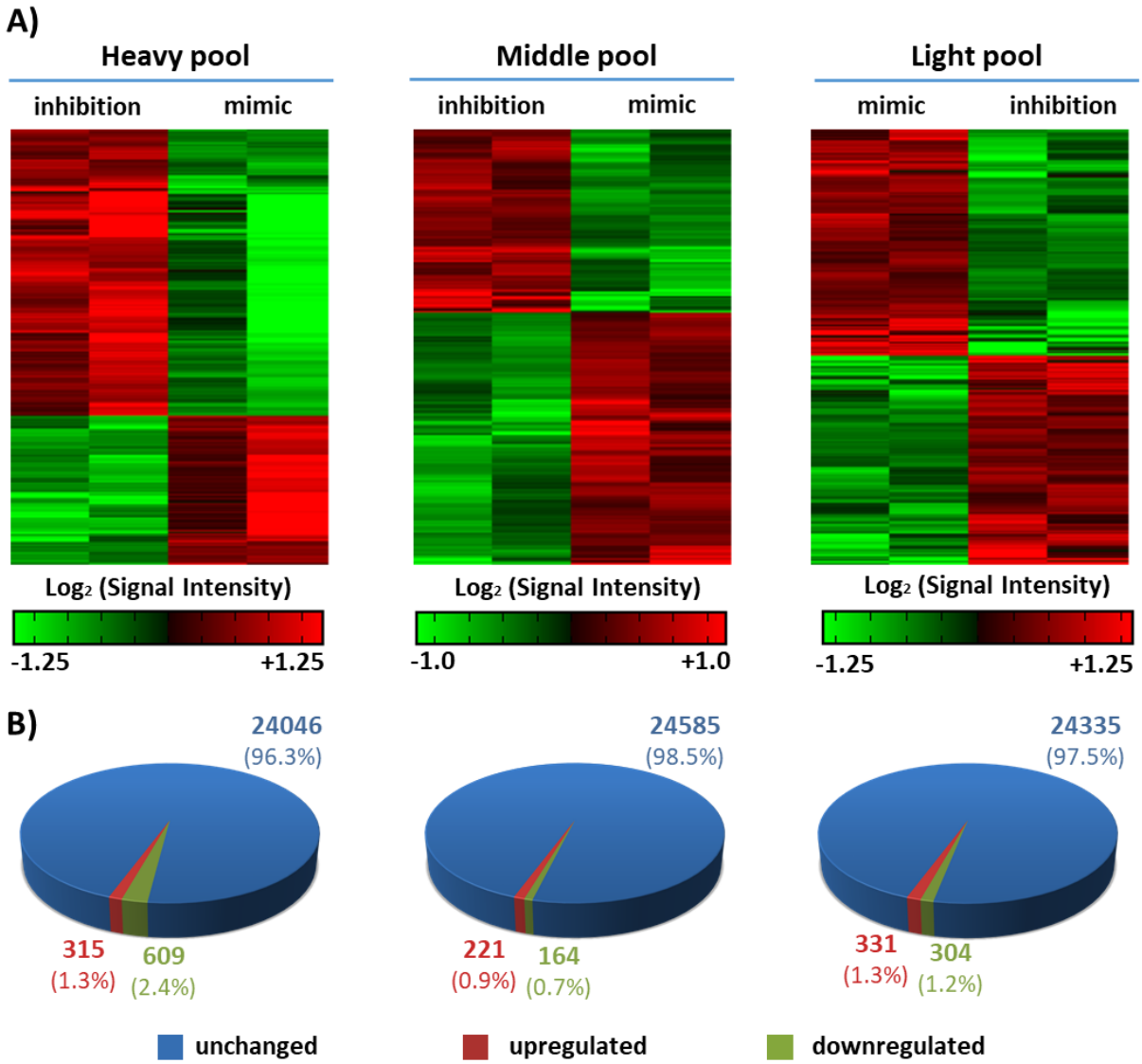

Figure 3.6: Microarray analysis of mRNA associated with heavy, middle or light polysomes isolated from Huh-7 cell treated with miR-122 mimic or inhibitor. Polysomes were fractionated from Huh-7 cells treated with miR-122 mimic or miR-122 inhibitor for 48 h. RNA isolated from individual polysomal fractions was pooled into heavy (pool 1), middle (pool 2) and light polysomal RNA pools (pool 3). RNA was then hybridized to Affymetrix arrays (human Genechip 1.0 ST Array, n = 2). Data analysis was performed using *AltAnalyze* by applying a cut-off of 1.5-fold change and significance level of $p < 0.05$ (one-way ANOVA). **A)** Heat map representing the differential association of mRNAs to polysomal pools using a Cousine Matrix to generate hierarchical tree of gene clusters. **Left panel** heavy pool (pool 1), **middle panel** middle polysomes (pool 2), **right panel** light polysomal pool (pool 3). Signal intensities are expressed on a logarithmic scale (base 2). **B)** Pie charts representing the numbers of transcripts significantly regulated in polysomal pools upon miR-122 overexpression compared to inhibition.

3.1.6 Gene Ontology analysis identified gene networks which are regulated by miR-122

Overall, the polysomal profiling by microarray identified a total of 12,877 unique transcripts which showed the expected target mRNA shift across the polysomes, indicating a direct or an indirect regulation by miR-122. With the aim to gain a better understanding of the functional

consequences accompanied by changes of endogenous miR-122 levels, a Gene Ontology enrichment (GO) analysis was performed for miR-122-responsive genes using *GO-Elite*. This algorithm identifies genetic networks by determing common transcription factors which modulate the expression of a subset of regulated genes (in this case the miR-122-responsive genes identified by polysome profiling).

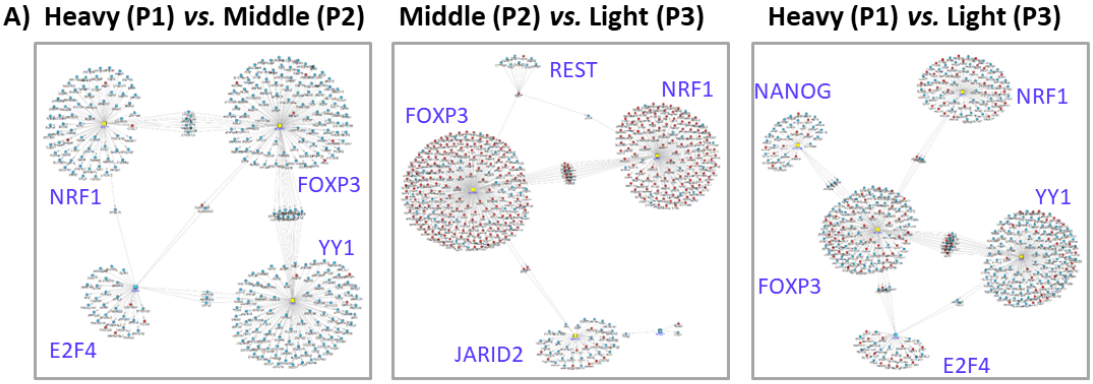

***GO-Elite* analysis of regulated transcripts on polysomes isolated from miR-122 overexpressing cells**

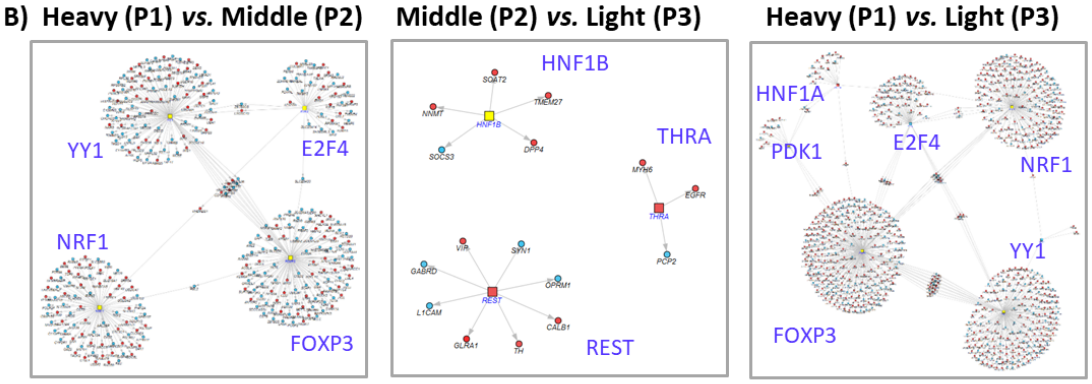

***GO-Elite* analysis of regulated transcripts on polysomes isolated from miR-122 inhibited cells**

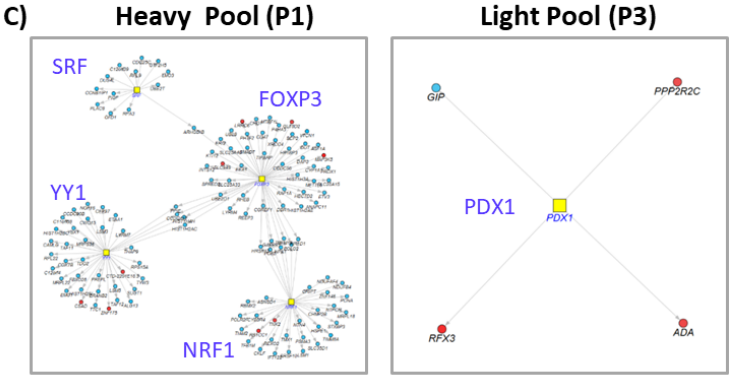

***GO-Elite* analysis of regulated transcripts on polysomes isolated from cells treated with miR-122 mimic and inhibitor**

Figure 3.7: *GO-Elite* analysis of regulated transcripts across polysomal pools in response to changes of miR-122 levels in Huh-7 cells. *GO-Elite* searches for connections between regulated transcripts to a number of validated transcription factors. **A)** GO analysis of regulated mRNAs on polysomes isolated from miR-122 overexpressing Huh-7. **B)** GO analysis of regulated transcripts on polysomes isolated from antagomiR-122 treated Huh-7. **C)** GO-Elite analysis of regulated transcripts in heavy pool 1 (**left**) and light pool 3 (**right**) isolated from miR-122 overexpressing *versus* miR-122 inhibited Huh-7 cells.

As illustrated in Figure 3.7, *GO-Elite* identified that a substantial number of miR-122-responsive transcripts are regulated by common transcription factors (TFs), such as Yin Yang 1 (YY1), Forkhead box P3 (FOXP3), E2F transcription factor 4 (E2F4), and nuclear respiratory factor 1 (NRF1). These transcription factors appear to control a large network of genes which are responsive to changes in cellular miR-122 levels (Figure 3.7). Therefore, the function of the identified TFs was further studied by applying literature mining research (Table 3.1). Notably, screening recent publications revealed that all of the identified TFs have previously been described to play role in the pathogenesis of diverse liver diseases. For instance, the transcription factors E2F4, FOXP3, HNF1A and B, JARID2, NANOG, NRF1, PDK1, SRF, THRA and YY1 are involved in the pathogenesis of hepatocellular carcinoma. NANOG, PDK1, SRF and YY1 are linked to viral hepatitis type B or C infections (Table 3.1). In light of the fact that miR-122 is deregulated in these kind of liver malignancies, the presented data may be indicative for a link between abberations of miR-122 levels and dysregulations of the transcription factor-mediated networks in the context of liver diseases.

Table 3.1: Literature mining research for identifying links between transcription factors upstream to miR-122-responsive transcripts and liver diseases. *GO-Elite* analysis revealed that miR-122 regulates a high number of transcripts that are regulated by certain transcription factors. Recent publications were screened to reveal a possible association between these transcription factors and liver diseases known to be accompanied by changes of endogenous miR-122 levels.

Transcription factor	Symbol	Association with liver disease	References
E2F transcription factor 4	E2F4	HCC	[*395–397*]
Forkhead box P3	FOXP3	liver Inflammation hepatic fibrosis HCC	[*398*, *399*] [*398*] [*400*]
HNF1 homeobox A	HNF1A	hepatic neoplasm/ adenomas HCC HCV	[*401–403*] [*404–408*] [*409*]
HNF1 homeobox B	HNF1B	HCC cholestasis	[*404*, *410–412*] [*413–415*]
Jumonji and AT-rich interaction domain containing 2	JARID2	HCC	[*416*]
Nanog homeobox	NANOG	HCC HCV HBV	[*417–419*] [*420*] [*421*]
Nuclear respiratory factor 1	NRF1	NASH NAFLD hepatic neoplasia HCC	[*422*, *423*] [*423*, *424*] [*422*] [*425*]
Pyruvate dehydrogenase kinase 1	PDK1	HCC HBV HCV	[*426–428*] [*428*] [*429*, *430*]

Table 3.1 (continued)

Transcription factor	Symbol	Association with liver disease	References
RE1 silencing transcription factor	REST	cholangiocellular carcinoma	[*431*]
Serum response factor	SRF	HCC fibrosis	[*432–436*] [*437*, *438*]
Thyroid hormone receptor, alpha	THRA	HCC	[*439–442*]
Yin Yang 1	YY1	steatosis HCC HBV NAFLD	[*443–446*] [*447–450*] [*451–453*] [*446*]

With the purpose to investigate whether similar networks may be affected by changes of miR-122 levels in other experimental conditions, microarray data sets of *MIR122* transgenic mice were downloaded from the Gene Expression Omnibus (GEO) repository and analyzed by *GO-Elite*. One data set compared the gene expression profiles of healthy liver tissues from 2 months old *MIR122* KO animals compared to healthy liver tissues from wild type mice (data set GSE27713; [*295*]). Another data set investigated the expression profiles of HCC tumor tissues from *MIR122* KO mice (11 or 14 months of age) to those of healthy liver tissues from matching wild type animals (data set GSE31453, Table 3.2 C; [*295*]). Of note, the genetic networks downstream to the transcription factors YY1 and FOXP3 were found altered in all animal models. While networks downstream to E2F4 were found deregulated in HCC tissue *vs.* healthy liver tissue in 14 months old mice, NRF1-regulatory networks were only altered in 11 months old mice (Table 3.2 C).

miR-122 is known to be downregulated in the liver of HCC patients [*317*, *318*]. Therefore, it was aimed to assess whether a link between the aforementioned transcription factors could also be identified in human HCC samples. A genome-wide study comparing gene expression profiles of human grade III HCC to surrounding non-tumor liver tissue (data set GSE45050; [*393*]) was downloaded and accordingly analyzed. In agreement with the data obtained from polysomal profiling and from the re-analysis of *MIR122* KO mice, a significant enrichment for genes regulated by the transcription factors YY1, FOXP3 and NFR1 was found in the HCC tissue compared to adjacent non-tumor tissue (Table 3.2 D). Altogether, these data reveal that conserved molecular networks are similarly regulated in response to altered miR-122 levels in both, human and mouse livers, as well as in human hepatoma cells (Huh-7) transfected with either miR-122 mimic or inhibitor.

Table 3.2. Regulation of transcription factor-driven molecular networks in response to alterations of miR-122 levels and in mouse or human HCC. *GO-Elite* algorithm was utilized to identify transcription factors that regulate subsets of miR-122-responsive genes. Analysis of gene expression profiles on polyribosomes isolated from **A)** miR-122 mimic or **B)** antagomiR-122 transfected Huh-7 cells. **C)** Re-analysis of microarray data of RNA isolated from *MIR122 KO* or wild type mice. **(left)** Healthy liver tissues of *MIR122* KO *versus* wild type mice before tumor development (GEO repository: GSE31453; [*295*]). HCC tissue of *MIR122* KO mice compared to healthy liver tissue of wild type control animals of **(middle)** 11 months or **(right)** 14 months old animals (GSE27713; [*295*]). **D)** Re-analysis of gene expression changes in tumor tissue compared to adjacent non-tumor tissue isolated from HCC patients (GEO repository: GSE45050; [*393*]). The table summarizes the total number of regulated genes downstream to the individual transcription factors (indicated as n). The relative amount of miR-122-responsive genes in relation to the total number of genes associated with transcription factors is expressed in %. Statistical analysis was carried out by Fisher's test.

A)	**Polysomes isolated from miR-122 overexpressing Huh-7**		
	heavy *vs.* middle	**heavy *vs.* light**	**middle *vs.* light**
YY1	n = 114 (14.6%)	n = 111 (14.2%)	n = 113 (14.5%)
E2F4	n = 30 (13.6%)	n.s.	n = 43 (19.5%)
FOXP3	n = 120 (12.9%)	n = 81 (8.7%)	n = 190 (20.5%)
NRF1	n = 77 (12.6%)	n.s.	n = 133 (21.7%)

B)	**Polysomes isolated from antagomiR-122 treated Huh-7**		
	heavy *vs.* middle	**heavy *vs.* light**	**middle *vs.* light**
YY1	n = 43 (5.5%)	n = 131 (16.8%)	n = 14 (1.8%)
E2F4	n = 16 (7.2%)	n = 44 (19.9%)	n = 6 (2.7%)
FOXP3	n.s.	n = 177 (19.1%)	n = 29 (3.1%)
NRF1	n = 43 (7.0%)	n = 125 (20.4%)	n = 15 (2.5%)

C)	***MIR122* KO mice (GEO repository accession no. GSE31453 and GSE27713; [*295*])**		
	***KO vs.* wild type (healthy liver tissue, 2 months)**	**HCC tissue *KO* mice *vs.* healthy liver wild type (11 months)**	**HCC tissue *KO* mice *vs.* healthy liver wild type (14 months)**
YY1	n = 18 (2.9%)	n = 5 (0.8%)	n = 28 (4.5%)
E2F4	n.s.	n.s.	n = 10 (5.1%)
FOXP3	n = 78 (8.2%)	n = 47 (4.5%)	n = 113 (11.9%)
NRF1	n.s.	n = 10 (2.0%)	n.s.

D)	**Human grade III HCC (GEO repository accession no. GSE45050; [*393*])**
	HCC tissue *vs.* adjacent non-tumor tissue
YY1	n = 67 (9.3%)
E2F4	n.s.
FOXP3	n = 98 (11.0%)
NRF1	n = 70 (12.5%)

3.1.7 Functional link between miR-122-responsive transcripts

By means of *GO-Elite* analysis, it was identified that a large number of genes downstream to the transcription factors E2F4, FOXP3, YY1, and NRF1 were responsive towards changes of cellular miR-122 levels (Figure 3.7 and Table 3.2). Interestingly, molecular networks regulated by these transcription factors appear to be concordantly affected on Huh-7 polysomes as well as in murine and human HCC tumors. Hence, the microarray data obtained from polysome profiling were studied with a focus on those miR-122-responsive mRNAs which were under the control of FOXP3, YY1, NRF1 or E2F4 (as visualized in Figure 3.8).

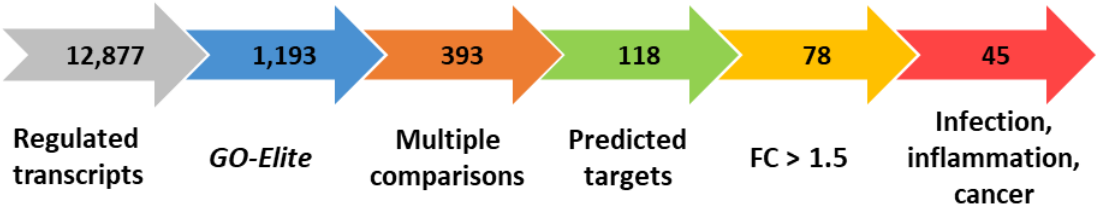

Figure 3.8: Workflow for the evaluation of polysome analysis for *de novo* identification of miR-122 target candidates. Overall 12,877 regulated transcripts were identified by polysomal profiling, whereby 1,193 were under the control of the transcription factors E2F4, YY1, NRF1, and FOXP3. Out of these genes, 393 transcripts showed the expected target gene shift in two or more comparisons of polysomal pools. Using the *miRWalk* target prediction tool, 118 predicted miR-122 target candidates were identified, whereas 78 showed changes of mRNA levels higher than 1.5-fold (FC > 1.5). Recent publications revealed a connection between putative miR-122 target genes and processes which are known to involve miR-122, such as `liver disease', `cancer', `inflammation' or `infection'.

Overall, 1,193 out of 12,877 unique transcripts were found to be under the control of E2F3, FOXP3, YY1 or NRF1. Of those, 393 transcripts were significantly altered in at least two polysome comparisons (i.e. in different polysomal pools) or conditions (i.e. upon miR-122 overexpression *vs.* depletion). Among this subset of genes, 30.0% (118) were predicted as miR-122 target transcripts by the *miRWalk* algorithm, of which 78 transcripts showed a fold change of at least 1.5. In order to investigate whether the remaining genes were linked to the known functions of miR-122, a literature mining research was conducted. Specifically, text mining included processes such as the regulation of lipid or cholesterol metabolism, iron homeostasis or the regulation of cell cycle, in which miR-122 plays a central role [*292*, *297*, *307*]. Furthermore, pathological processes such as viral infections [*338*, *349*], liver disease [*316*, *454*] or processes associated with the pathogenesis of cancer [*317*] were included in the research. As miR-122 was found to play a role in hepatic inflammation [*294*], it was also investigated whether target gene candidates were associated with signaling pathways that contribute to either pro- or anti-inflammatory liver phenotypes, including the TGFβ signaling

pathways or the antiviral interferon signaling pathway. Overall, 45 miR-122 target gene candidates were found associated with the aforementioned biological processes as summarized by Table 3.3.

Table 3.3: miR-122-responsive target gene candidates and processes associated with miR-122 function such as `inflammation´, `infection´, `liver disease´ or `cancer´ according to the literature.

Gene symbol	ENSEMBL ID	Transcription factor	Association with key words	References
ATRX	ENSG00000085224	YY1	carcinogenesis HCC	[*455–459*] [*460*]
BAG1	ENSG00000107262	YY1	carcinogenesis HCC	[*461–463*] [*464*]
BAX	ENSG00000087088	YY1	HCC NASH HCV	[*465–467*] [*468*, *469*] [*470*, *471*]
CCDC43	ENSG00000180329	YY1	carcinogenesis	[*472*]
CD47	ENSG00000196776	FOXP3	HCC	[*473–476*]
CMTM7	ENSG00000153551	FOXP3	cancer HCC	[*477–480*] [*478*, *481*]
DEDD	ENSG00000158796	YY1	cancer metastasis TGFβ signaling	[*482*, *483*] [*484*]
DIXDC1	ENSG00000150764	FOXP3	cancer cell, invasion, metastasis, proliferation HCC	[*485–488*] [*489*]
DSG2	ENSG00000046604	FOXP3	HCC HBV cancer	[*490*, *491*] [*490*] [*492–494*]
EEA1	ENSG00000102189	FOXP3	HCV	[*495–497*]
F2RL2	ENSG00000164220	FOXP3	HCC	[*498*, *499*]
FKBP1A	ENSG00000088832	FOXP3	HCC HCV iron homeostasis TGFβ signaling	[*500*] [*501*] [*502*] [*503*]
G3BP2	ENSG00000138757	NRF1	carcinogenesis HCV HCC	[*504–506*] [*507*] [*508*]
GOLGA2	ENSG00000167110	NRF1	HCC cancer cell invasion	[*509*] [*510*, *511*]
HCFC1	ENSG00000172534	YY1	NASH cell cycle	[*512*] [*513*]
HSPE1	ENSG00000115541	NRF1	HCC HBV cancer	[*514*, *515*] [*515*] [*516*, *517*]
JAK1	ENSG00000162434	NRF1	HCC HBV	[*518–520*] [*519*, *521*]
KIF1B	ENSG00000054523	E2F4	HCC HBV	[*522–524*] [*525*]
KIF3A	ENSG00000131437	NRF1	cancer HCC	[*526*, *527*] [*528*]

Table 3.3 (continued)

Gene symbol	ENSEMBL ID	Transcription factor	Association with key words	References
KPNA6	ENSG00000025800	YY1	cytokine signaling oxidative stress HBV	[*529*] [*530*] [*531*]
KPNB1	ENSG00000108424	FOXP3	HCC HCV HBV	[*532*, *533*] [*534*, *535*] [*536*]
MINK1	ENSG00000141503	FOXP3	TGFβ signaling oxidative stress Wnt signaling	[*537*, *538*] [*538*, *539*] [*540*, *541*]
NUP210	ENSG00000132182	FOXP3	PBC	[*542–545*]
P4HA1	ENSG00000122884	NRF1	fibrosis	[*546*]
PCGF2	ENSG00000277258	FOXP3	cancer	[*547–550*]
PDCD2	ENSG00000071994	FOXP3	cytokine signaling cancer cell proliferation EMT	[*551*] [*552*, *553*] [*554*]
PDCD4	ENSG00000150593	NRF1	HCC fibrosis HBV	[*555–557*] [*558*] [*559*]
POLR2F	ENSG00000100142	NRF1	cancer	[*560*, *561*]
RAD50	ENSG00000113522	NRF1	tumorigenesis HCC HCV	[*562*] [*455*, *563*] [*564*]
RNF26	ENSG00000173456	YY1	cancer IFN signaling	[*565*] [*566*]
RNMT	ENSG00000101654	FOXP3	HCC	[*567*]
ROCK2	ENSG00000134318	FOXP3	HCC CCC HCV	[*568–571*] [*572*] [*496*]
SMAD7	ENSG00000101665	FOXP3	TGFβ signaling HCC HBV	[*573*, *574*] [*575–577*] [*574*, *578*]
SMAP2	ENSG00000084070	FOXP3	HCV HBV	[*579*] [*580*]
SMG5	ENSG00000198952	YY1	viral infection P-bodies	[*581*] [*212*]
SPRED2	ENSG00000198369	FOXP3	HCC TGβ signaling liver injury	[*582*, *583*] [*584*] [*585*, *586*]
STAT6	ENSG00000166888	FOXP3	inflammation HCV HCC	[*587*] [*588*] [*589*]
TBC1D22B	ENSG00000065491	YY1	HCV	[*590*]
TNPO1	ENSG00000083312	FOXP3	fibrosis Wnt signaling HCV HCC	[*591*] [*591*] [*534*, *592*] [*593–595*]

Table 3.3 (continued)

Gene symbol	ENSEMBL ID	Transcription factor	Association with key words	References
U2AF2	ENSG00000063244	NRF1	HCC tumorigenesis	[*596*] [*597*]
UBIAD1	ENSG00000120942	YY1	cancer cholesterol/ lipid metabolism	[*598–600*] [*599*, *601*]
UQCRB	ENSG00000156467	YY1	HCC mitochondria function	[*602*, *603*] [*603*]
WNK4	ENSG00000126562	FOXP3	tumorigenesis TGFβ signaling	[*604*] [*605*]
WSB2	ENSG00000176871	FOXP3, YY1	cytokine signaling cancer	[*606*, *607*] [*608*]
XRCC5	ENSG00000079246	NRF1	HBV HCC	[*609*] [*563*, *609–612*]

3.1.8 Analysis of miR-122 target gene candidates in response to miR-122 overexpression

In this study, microarray analysis of polyribosomal RNA was employed for *de novo* identification of miR-122 target gene candidates. By means of GO analysis and by screening the recent literature, 45 potential miR-122 target candidates were determined of which 32 were randomly selected for qPCR analysis. The levels of those selected mRNAs were studied in Huh-7 transfected with miR-122 mimic for either 24 or 48 h.

The Figure 3.9 indicates successful overexpression of miR-122 in the target cells. Cellular levels of miR-122 were elevated by 306.6-fold ($p = 0.006$) at 24 h and by 48.6-fold ($p = 0.029$) at 48 h post transfection.

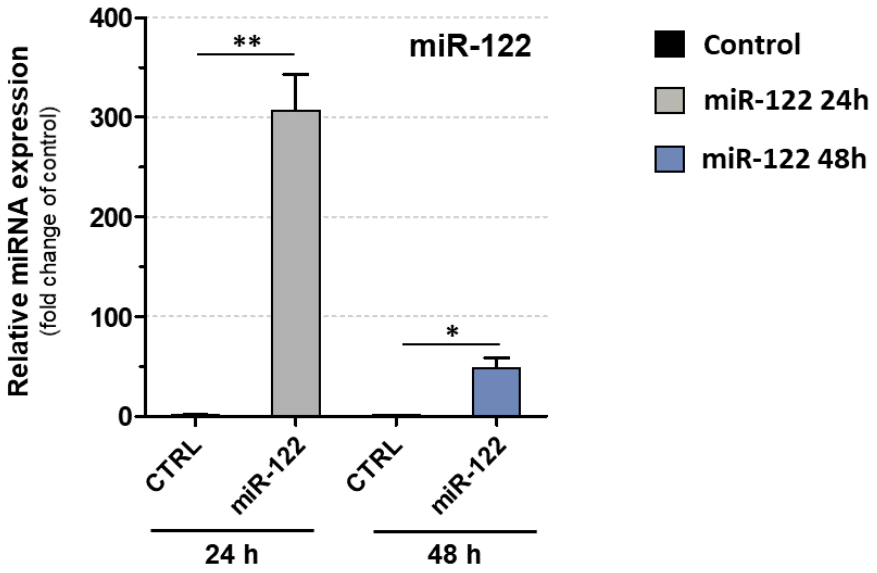

Figure 3.9: Quantitative analysis of cellular miR-122 levels in miR-122 mimic transfected Huh-7 cells. Huh-7 cells were transfected with miR-122 mimic for 24 or 48 h. Control cells were mock-transfected in absence of miR-122 mimic. Following RNA isolation, miRNAs were quantified by miQPCR. Levels of miR-122 were normalized to miR-192 for each sample and are displayed as fold change (± standard error of the mean [SEM]) relative to control of 5 independent experiments. Asterisks indicate significant differences to control (student´s t-test with significance level * $p < 0.05$; ** $p < 0.01$).

Next, the levels of selected target mRNAs were investigated by qPCR. miR-122 overexpression in Huh-7 cells caused a reduction of the relative amount of a number of mRNAs after 24 h (Figure 3.10 A) or after 48 h (Figure 3.10 B). The validated miR-122 target *SLC7A1* (alias *CAT1*) mRNA was downregulated to 27.7% (± 5.1%; $p < 0.001$) and to 22.3% (± 3.6%; $p < 0.001$) relative to the respective mock-transfected control after 24 h or 48 h, respectively.

Furthermore, the mRNA expression of *BAG1*, *BAX*, *CCDC43*, *CD47*, *DIXDC1*, *DSG2*, *F2RL2*, *G3BP2*, *KPNA6*, *KPNB1*, *NUP210*, *P4HA1*, *PCGF2*, *PDCD4*, and of *TBC1D22B* were significantly downregulated in miR-122 overexpressing cells 24 h post transfection compared to control cells. A tendency towards downregulation was further observed for *HCFC1* (91.1% ± 3.2%; $p = 0.071$). Moreover, 48 h after miR-122 mimic transfection, a significant downregulation of the transcript levels of *CMTM7*, *HCFC1, KIF3A*, *PCGF2*, *PDCD2*, *RNF26*, *SPRED2*, and *TNPO1* was measured, whereas *KPNA6* ($p = 0.080$), *KIF1B* ($p = 0.080$) and *MINK1* ($p = 0.074$) mRNA levels tended to decrease.

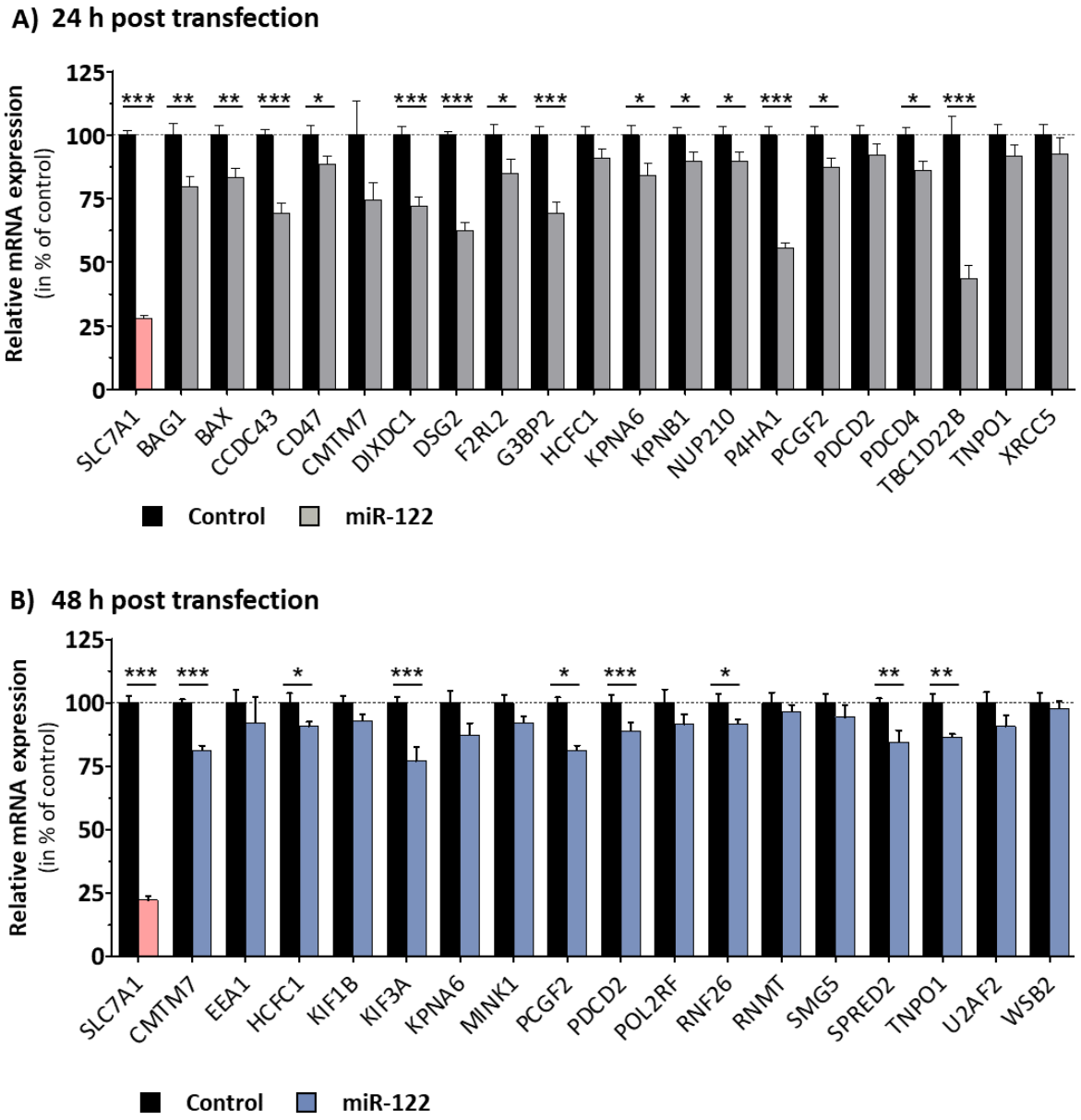

Figure 3.10: Levels of putative miR-122 target mRNAs in Huh-7 cells treated with miR-122 mimic. Huh-7 cells were transfected with miR-122 mimic for **A**) 24 h or **B**) 48 h, while control cells were mock-transfected in absence of miR-122 mimic. RNA was isolated and mRNAs were quantified by using qPCR. Levels of selected transcripts were normalized to *death effector domain containing* (*DEDD*) mRNA, which was identified as most stable gene based on *GeNorm* algorithm. Relative mRNA levels are expressed as percentage to control. Data represent average ± SEM of 4 – 5 independent experiments. Asterisks indicate significant differences to control (student´s t-test with significance level * $p < 0.05$; ** $p < 0.01$; *** $p < 0.001$).

In order to investigate whether the target gene candidates mentioned above contain binding motifs for miR-122, a binding site analysis was conducted. For this purpose, the 3´UTRs of the aforementioned mRNAs were analyzed using *RNA22.* Based on the complementarity of the miRNA and the transcript, the folding energy released upon formation of the miRNA-mRNA heteroduplex, and to a lesser extent the cross-species conservation of the

3´UTR, *RNA22* screens for potential MREs in a given target sequence [*264*]. Multiple potential binding sites were identified in the 3´UTRs of miR-122 target gene candidates. While the majority of MREs contain non-canonical or atypical binding sites, a number of canonical binding sites were also identified, including two in the 3´UTR of *DIXDC1* (Appendix Figure 7.3).

Altogether, these data suggest that miR-122 overexpression in Huh-7 resulted in the downregulation of transcript levels of 22 individual genes, thus indicating that these transcripts may be directly targeted by miR-122.

3.1.9 Analysis of *E2F4*, *NRF1,* and *YY1* mRNA levels in response to miR-122 overexpression

The data presented in this work indicated that 22 mRNAs may be directly regulated by miR-122. As shown by GO analysis, the expression of genes encoding for these identified target candidates is known to be under the control of the transcription factors E2F4, NRF1, FOXP3 or YY1. In order to assess whether miR-122 overexpression may also exert a direct effect on the expression of these transcription factors, mRNA levels of *E2F4*, *YY1* and *NRF1* were quantified in Huh-7 transfected with miR-122 mimic. Due to very low levels of *FOXP3* mRNA, relative quantification by qPCR failed to produce reliable data and is, therefore, not shown here.

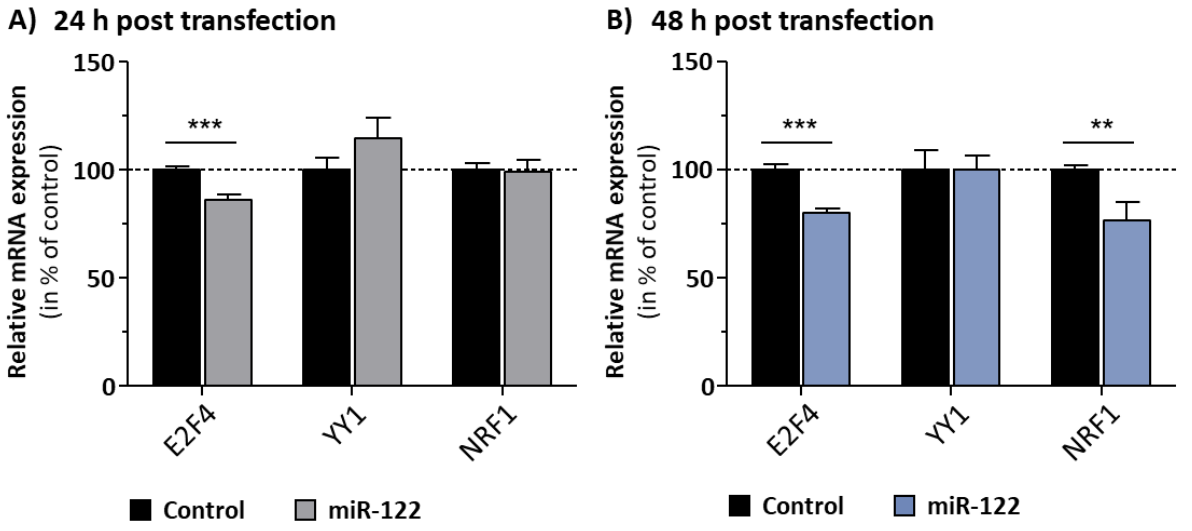

Figure 3.11: Analysis of *E2F4*, *YY1*, and *NRF1* mRNA in miR-122 overexpressing Huh-7 cells. RNA was isolated from miR-122 mimic or mock transfected control cells **A)** 24 h and **B)** 48 h post transfection and mRNA levels of the transcription factors *E2F4*, *YY1,* and *NRF1* were quantified by qPCR. Levels of selected transcripts were normalized to *DEDD* and the relative mRNA amounts are expressed as percentage to control. Data represent average ± SEM of 6 independent experiments. Asterisks indicate significant differences to control (student´s t-test with significance level ** $p < 0.01$; *** $p < 0.001$).

As shown in Figure 3.11, mRNA levels of *E2F4* were significantly downregulated 24 h (86.1% ± 2.6%; p = 0.002) and 48 h (87.2% ± 3.6%; p = 0.016) after transfection with miR-122 mimic compared to control. A significant reduction of *NRF1* mRNA (69.7% ± 10.1%; p = 0.033) was observed 48 h after miR-122 transfection. In contrast, the relative amount of *YY1* mRNA remained unaffected by miR-122 overexpression at both time points (Figure 3.11). Altogether, the data presented herein suggested that miR-122 may regulate the mRNA of *E2F4* and *NRF1*, but not of *YY1*. However, it remained unclear whether the observed effects were triggered by a direct interaction of miR-122 with the mRNAs of *E2F4* and *NRF1*, or whether other yet unknown mechanisms might be involved.

3.2 Proteome analysis of miR-122 overexpressing and miR-122 down-regulated Huh-7 cells

3.2.1 Identification of miR-122-responsive proteins using mass spectrometry

Several studies reported that changes in the transcriptome do not mandatorily mirror the exact changes in the cellular proteome [*613*], making it hardly possible to predict functional consequences only on the basis of transcriptome studies. Therefore, mass spectrometry was conducted to study the effect of miR-122 mimic or antagomiR-122 treatment on the cellular proteome in Huh-7 cells.

Overall, 1,960 proteins were quantified in Huh-7 as visualized in Figure 3.12 A. As evident from the hierarchical clustering, the overexpression of miR-122 caused distinct alterations in the protein abundances in the investigated cell line compared to scrambled oligonucleotide transfected control. In contrast, only minor differences were observed in Huh-7 treated with antagomiR-122 compared to scrambled control. As a result, the Euclidean algorithm was not capable of discriminating between scrambled control and antagomiR-122 treated samples (Figure 3.12 A).

The alterations in protein abundancies in response to changes of miR-122 levels are shown in Figure 3.12 B. Overall, 504 proteins showed significant alterations among the three conditions (false discovery rate [FDR] < 5%). The proteomic data are separately displayed to show changes in the protein abundance in miR-122 overexpression compared to control samples (mimic *vs.* scrambled), the effect of miR-122 inhibition *versus* control (antagomiR *vs.*

scrambled), and changes in protein amounts in miR-122 enriched *vs.* miR-122 downregulated cells (mimic *vs.* antagomiR-122).

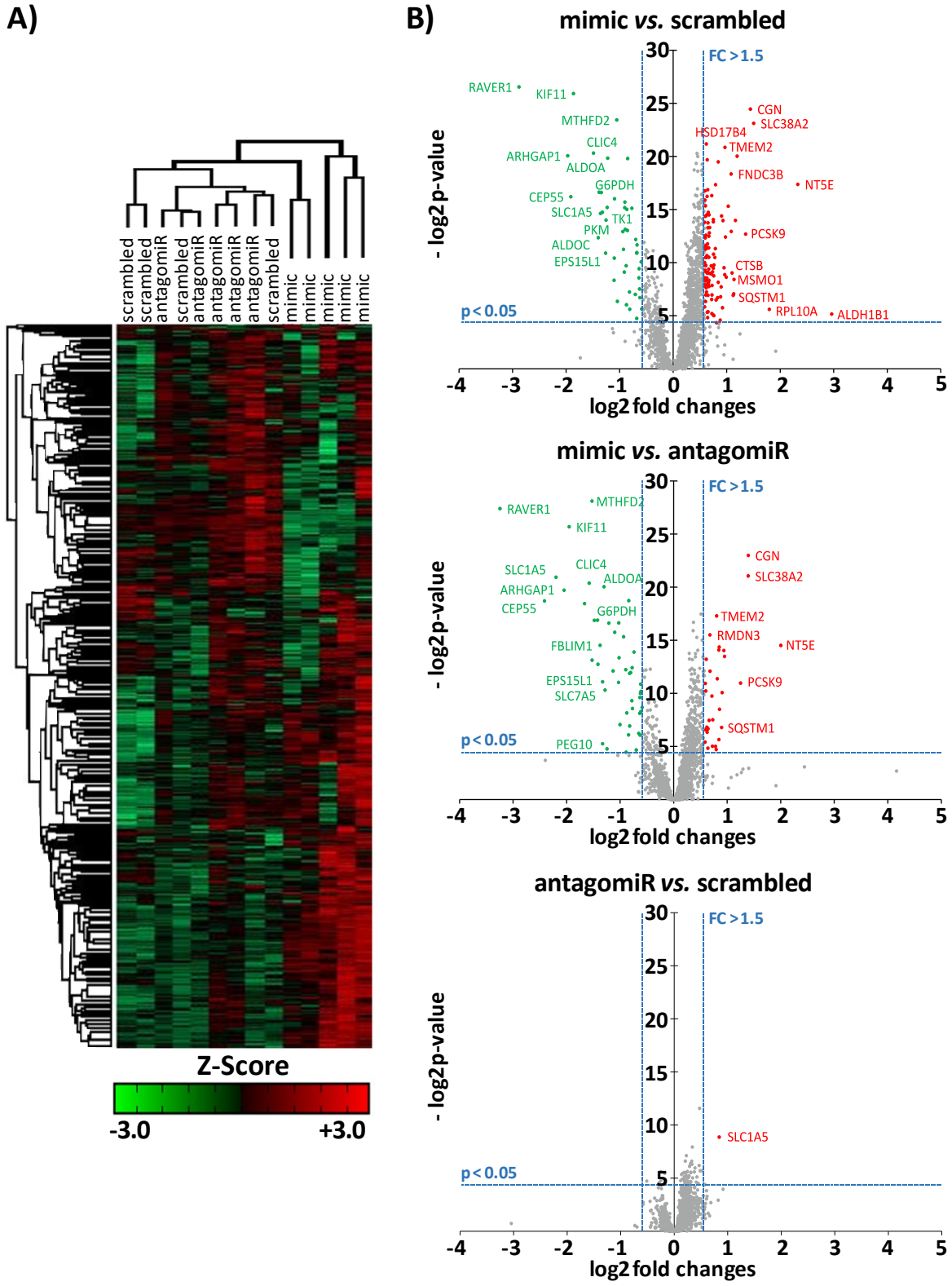

Figure 3.12: Quantitative proteomic analysis of Huh-7 cells transfected with miR-122 mimics, miR-122 inhibitor (antagomiR) or scrambled oligos. Cells were transfected with miR-122 mimic, inhibitor or scrambled oligo for 48 h. Following purification and quantification, proteins were subjected to liquid chromatography-tandem mass spectrometry (LC-MS/MS). **A)** Unsupervised hierarchical clustering of the quantified proteins. Z-Score shows downregulated proteins in green

shades, while upregulated proteins are displayed in red shades. **B)** Volcano blots demonstrating differential protein levels in Huh-7 cells treated with miR-122 mimic *vs.* scrambled control **(upper panel)**, miR-122 mimic *vs.* antagomiR treatment **(middle panel)**, and antagomiR *vs.* scrambled control **(lower panel)**. Protein levels are presented on a logarithmic scale (base 2) on the abscissa, while p-values are illustrated as negative $\log_2$ value on the ordinate. Cut-off levels for fold changes are depicted as perpendicular blue line (FC > 1.5), while the cut-off for statistical significance ($p < 0.05$ [FDR]) is depicted as horizontal blue line. Significantly downregulated proteins are labeled in green and significantly upregulated proteins are labeled in red.

Albeit the majority of proteins showed only minor changes in the relative protein abundance, the treatment of Huh-7 cells with miR-122 mimic was accompanied by a significant elevation of the relative amounts of 405 proteins and a reduction of 86 proteins (mimic *vs.* scrambled; $p < 0.05$). When protein amounts of miR-122 overexpressing to miR-122 downregulated cells were compared, 275 proteins were found significantly upregulated, while 86 proteins were found with lower abundance (mimic *vs.* antagomiR; $p < 0.05$). In contrast, miR-122 inhibition had minor effects and only caused the significant upregulation of 42 proteins and downregulation of 3 proteins (scrambled *vs.* antagomiR; $p < 0.05$). When applying a threshold of at least 1.5-fold for the changes in relative protein abundancies (proteins highlighted in red or green in Figure 3.12 B), 95 significantly upregulated proteins and 45 significantly downregulated proteins were identified in miR-122 enriched cells (mimic *vs.* scrambled; $FC > 1.5$, $p < 0.05$). When comparing miR-122 overexpressing to miR-122 inhibited cells, 32 proteins were found more abundant and 43 proteins less abundant (mimic *vs.* antagomiR; $FC > 1.5$, $p < 0.05$). The transporter protein SLC1A5 was the only protein to be significantly upregulated more than 1.5-fold in miR-122 depleted cells compared to scrambled controls (scrambled *vs* antagomiR; $FC > 1.5$, $p < 0.05$), indicating that the miR-122 inhibition had only minor effects on the cellular proteome in Huh-7. Of note, endogenous miR-122 levels in Huh-7 were relatively low, so it was assumed that the inhibition of miR-122 had negligible effects on cellular protein content compared to miR-122 overexpression.

In order to evaluate whether similar or distinct proteins were altered in response to miR-122 mimic and to antagomiR treatment, a comparison of all regulated proteins was conducted. For this purpose, proteins which were inversely correlated with miR-122 (i.e. proteins found with lower abundance in miR-122 overexpressing cells or proteins which were upregulated in response to miR-122 inhibition, Figure 3.13 A) and proteins found to be concordantly regulated with miR-122 were overlapped (Figure 3.13 B). In total, 133 unique proteins were found inversely correlated with the levels of miR-122. The relative abundance

of 86 proteins was significantly lower in miR-122 enriched cells compared to either scrambled control (mimic *vs.* scrambled) or to antagomiR-122 treated cells (mimic *vs.* antagomiR), respectively (Figure 3.13 A). Furthermore, 42 proteins were found in higher abundance in antagomiR *vs.* scrambled treated controls (Figure 3.12 and Figure 3.13 A). Interestingly, very similar protein changes were observed in miR-122 mimic *versus* scrambled control as well as in miR-122 mimic *versus* to antagomiR treated cells. In contrast, proteins modulated in response to miR-122 inhibition (antagomiR) compared to scrambled control were different from those protein changes induced by miR-122 overexpression.

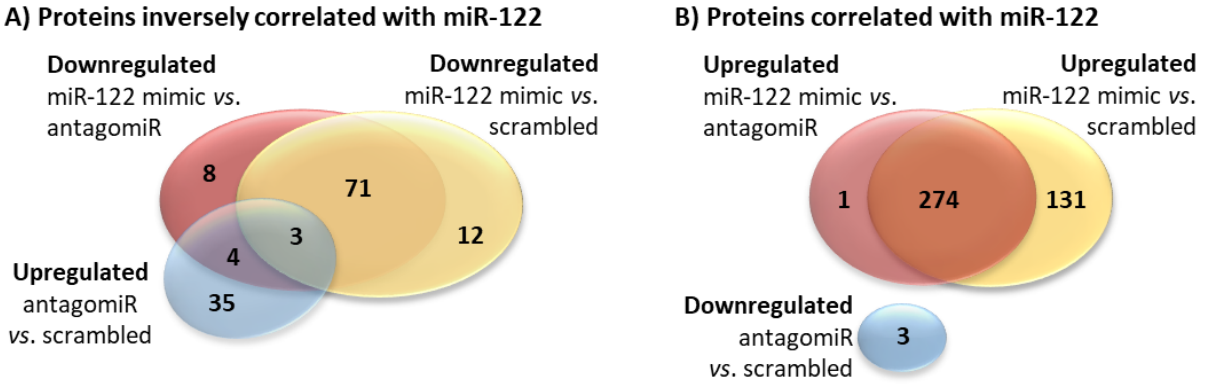

Figure 3.13: Intersections of miR-122-responsive proteins identified by mass spectrometry in Huh-7 cells. A) Number of proteins that were found inversely correlated with miR-122 in Huh-7 cells treated with either miR-122 mimic, miR-122 inhibitor (antagomiR) or scrambled control. **B)** Overlap of proteins which exhibited a positive correlation with miR-122 (i.e. proteins with higher abundance upon miR-122 overexpression or lower abundance in response to miR-122 depletion).

3.2.2 Gene Ontology analysis of miR-122-responsive proteins

To gain a better understanding of the functions of miR-122 and the possible consequences associated with miR-122 deregulation, GO term enrichment analysis was performed using the *GOrilla* software. Since miRNAs are considered as fine-tuning mechanism for gene expression, all proteins identified as significantly regulated were included in this study ($p < 0.05$), independent of the fold change. The GO enrichment was carried out with an emphasis on common biological process and cellular components associated with the altered proteins.

GO analysis revealed that in particular processes linked to metabolic functions were substantially affected in response to miR-122 overexpression (Figure 3.14). Specifically, processes associated with glucose metabolism, as well as nucleoside monophosphate and carboxylic acid metabolic processes were significantly reduced in cells transfected with

miR-122 mimic *versus* antagomiR-122 (Figure 3.14 A). On the other hand, terms associated with metabolic processes involving small molecule or organic substances were highly enriched in miR-122 mimic compared to antagomiR-122 treated cells (Figure 3.14 A).

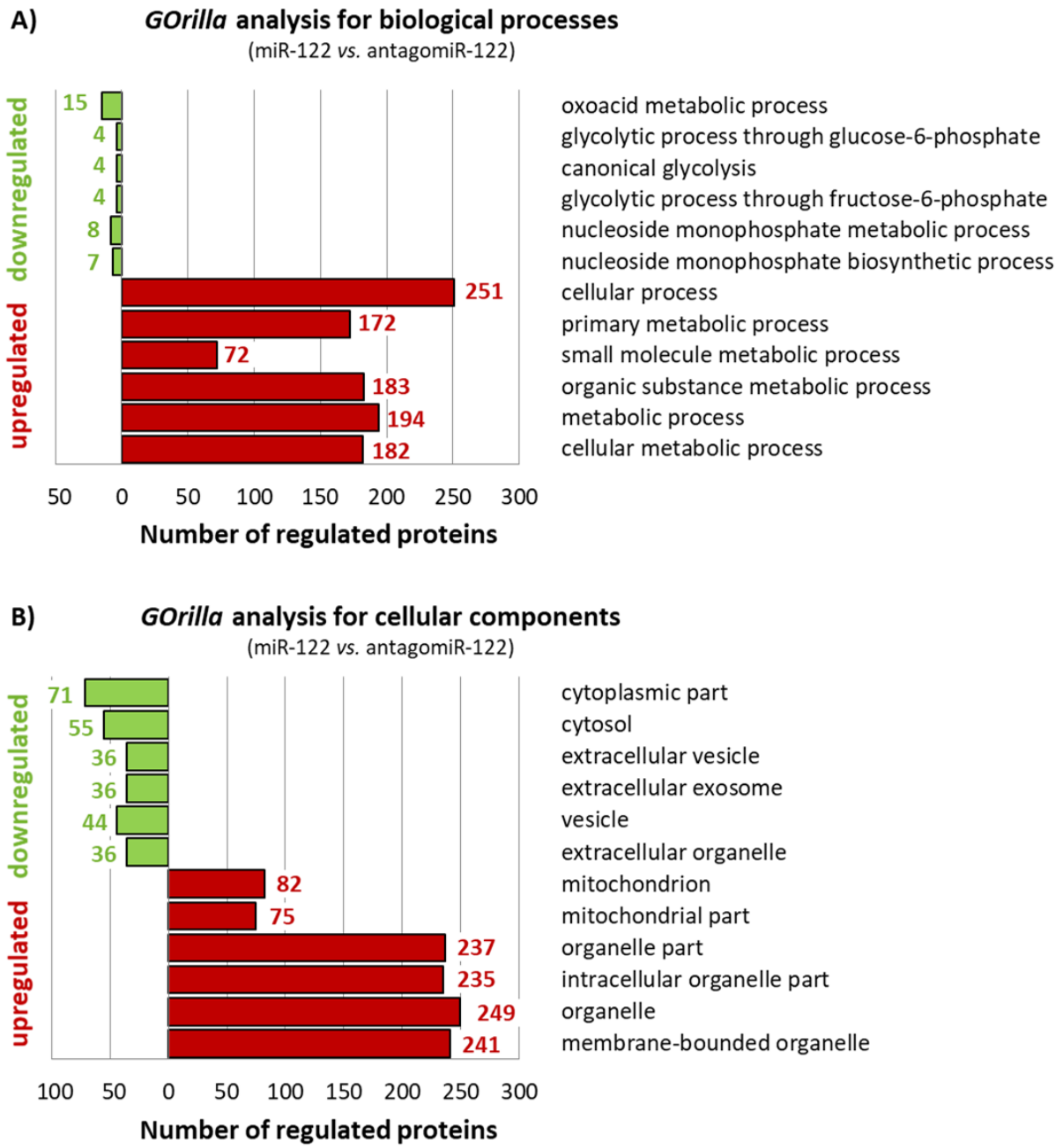

Figure 3.14: Gene Ontology (GO) analysis of significantly regulated proteins in miR-122 overexpressing (mimic) *versus* miR-122 reduced (antagomiR) Huh-7 cells. *GOrilla* Gene Ontology enrichment tool was utilized to investigate the six most significantly depleted **(green)** and enriched **(red)** GO terms. Numbers of proteins associated with a given term are illustrated in green (downregulated term) and red (upregulated term). **A)** GO analysis with respect to biological processes. **B)** GO analysis with an emphasis on cellular components.

The cellular component analysis indicated that miR-122 overexpression negatively affected the proportion of GO terms associated with the cytoplasmic parts and the cytosol, as well as extracellular components, such as vesicles, exosomes and organelles (Figure 3.14 B). On the other hand, GO terms associated with mitochondria and intracellular as well as membrane-bound organelles were significantly enriched in response to miR-122 overexpression (Figure 3.14 B). Overall, the presented analyses point to a so far unknown role for miR-122 in controlling the cellular secretome as well as suggesting a possible role for this miRNA in modulating diverse metabolic processes associated with oxidative and energetic metabolism.

Remarkably, the analysis of proteins altered in miR-122 mimic compared to scrambled oligonucleotide transfections (mimic *vs.* scrambled) delivered very similar GO terms regarding the cellular components and the biological processes affected by miR-122 overexpression *versus* antagomiR-122 (Appendix Figure 7.4).

3.2.3 Functional analysis of miR-122-responsive proteins in Huh-7

The evaluation of the Huh-7 proteome in response to changes of the cellular miR-122 allowed for the quantification of 1,960 proteins and enabled the assessment of the functional alterations accompanied by deregulation of miR-122. In order to identify potential miR-122 target candidates, the focus of further analysis was set to the 133 proteins found to be significantly and inversely correlated with the miR-122 levels, as given by Figure 3.12 and 3.13 A. Among those, the prediction algorithm *miRWalk* identified 97 significantly regulated proteins as potential miR-122 target candidates, whereby 50 proteins were characterized by fold changes larger than 1.5 (Figure 3.15).

Figure 3.15: Workflow for the analysis of proteomic data from Huh-7 cells treated with miR-122 mimic, miR-122 inhibitor and scrambled oligo transfected controls. In total, 133 proteins were inversely correlated with miR-122. Among those, 97 were identified as target candidates by the *miRWalk* target prediction algorithm. In order to screen for the most pronounced changes, a cut-off for the fold change was set to 1.5 (FC > 1.5) and proteins were further selected with respect to their known association to those liver diseases that are accompanied by deregulated levels of miR-122.

Various liver diseases are accompanied by aberrant levels of the liver-specific miR-122, such as hepatic inflammation [*294*], viral infection [*338*, *349*], liver fibrosis and cirrhosis [*316*, *454*] as well as hepatocellular carcinoma [*317*, *318*]. To gain a better understanding of the potential contribution of miR-122 dysregulation in the pathogenesis of chronic liver diseases, literature mining was carried out to evaluate links between the 50 selected proteins and the aforementioned diseases (summarized in Table 3.4).

Table 3.4: Functional association of miR-122-responsive proteins and liver pathogenesis. Proteins identified by mass spectrometry showing inverse correlation with miR-122 were selected for further analysis. Among those proteins, 97 were identified as predicted miR-122 targets by *miRWalk* algorithm. Literature mining research was carried out to unravel functional links between miR-122-responsive proteins, whereby 20 proteins were found to be deregulated in liver diseases.

UniProt ID	Symbol	Gene name	Disease	Reference
Q53EZ4	**CEP55**	centrosomal protein 55	HCC	[*614*]
O00299	**CLIC1**	chloride intracellular channel 1	HCC	[*615*, *616*]
P21291	**CSRP1**	cysteine and glycine rich protein 1	HCC	[*617*]
Q9UBC2	**EPS15L1**	epidermal growth factor receptor pathway substrate 15 like 1	HCC	[*618*]
P07148	**FABP1**	fatty acid binding protein 1	HCC	[*619*, *620*]
Q8WUP2	**FBLIM1**	filamin binding LIM protein 1	HCC metastasis	[*621*]
P11413	**G6PDH**	glucose-6-phosphate dehydrogenase	HCC HBV	[*594*, *622*, *623*]
P21266	**GSTM3**	glutathione S-transferase mu 3	HCC ASH	[*624–626*]
P46940	**IQGAP1**	IQ motif containing GTPase activating protein 1	HCC	[*627*, *628*]
P52732	**KIF11**	kinesin family member 11	HCC	[*526*, *629–631*]
P18858	**LIG1**	DNA ligase 1	HCC HCV	[*632*, *633*]
Q13952	**NFYC**	nuclear transcription factor Y subunit gamma	HBV	[*634*]
P55786	**NPEPPS**	aminopeptidase puromycin sensitive	HCC	[*632*]
P14618	**PKM**	pyruvate kinase, muscle	HCC	[*383*, *635–637*]
Q15758	**SLC1A5**	solute carrier family 1 member 5	HCC	[*638*, *639*]
Q01650	**SLC7A5**	solute carrier family 7 member 5	HCC	[*639–642*]
Q99523	**SORT1**	sortilin 1	HBV	[*643*, *644*]
O14907	**TAX1BP3**	tax1 binding protein 3	NAFLD	[*645*]
P04183	**TK1**	thymidine kinase 1	HCC	[*646*, *647*]
P04818	**TYMS**	thymidylate synthetase	HCC	[*648–650*]

Abbreviation: ASH: alcoholic steatohepatitis

Overall, a total of 20 proteins was described as associated with liver diseases. More specifically, independent studies indicated that 16 of these proteins have been reported as linked to the pathogenesis of HCC.

3.2.4 QPCR and Western blot analyses of miR-122-responsive proteins in Huh-7

Among those proteins identified by mass spectrometry, seven proteins (CLIC1, CEP55, EPS15L1, G6PDH, KIF11, SLC1A5, and TK1) were reported as significantly upregulated in the tumor tissue of HCC patients (see Table 3.4). This observation reinforces the hypothesis that miR-122 deregulation might play a direct role in the pathogenesis of HCC. In order to evaluate whether miR-122 may directly regulate the levels of those target candidates, Huh-7 cells were transfected with miR-122 mimic and the mRNA levels of potential targets were assessed 48 h post transfection (Figure 3.16).

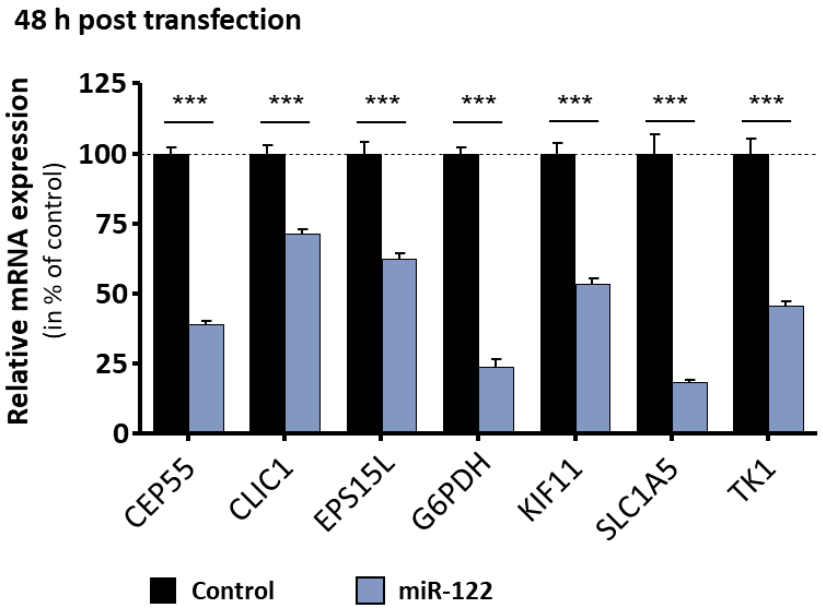

Figure 3.16: Analysis of mRNA levels of miR-122 target candidates identified by proteomics in Huh-7 cells treated with miR-122 mimic. Huh-7 cells were transfected with miR-122 mimic or mock transfected for 48 h. RNA was isolated and mRNAs were quantified by qPCR. Levels of selected transcripts were normalized to *DEDD* mRNA and expressed as percentage of control. Data represent average ± SEM of 3 independent experiments. Asterisks indicate significant differences to control (unpaired student´s t-test with a significance level *** $p < 0.001$).

As detailed in Figure 3.16, compared to control treated cells, the relative mRNA amounts of all seven investigated miR-122 target gene candidates were significantly lower in miR-122 mimic transfected Huh-7 cells. The levels of *CEP55* mRNA decreased to 38.9%

(± 1.3%; p < 0.001), *CLIC1* to 71.3% (± 1.7%; p < 0.001), *EPS15L1* to 62.5% (± 2.1%; p < 0.001), *G6PDH* to 23.8% (± 2.6%; p < 0.001), *KIF11* to 53.6% (± 2.0%; p < 0.001), *SLC1A5* to 18.5% (± 0.8%; p < 0.001), and *TK1* to 45.5% (± 1.9%; p < 0.001).

Furthermore, to assess the effect of miR-122 overexpression on the protein levels as well as to further validate the proteome data obtained from mass spectrometry, Western blot analyses were carried out to evaluate the differential protein amounts of G6PDH, EPS15L1, and CEP55 (Figure 3.17).

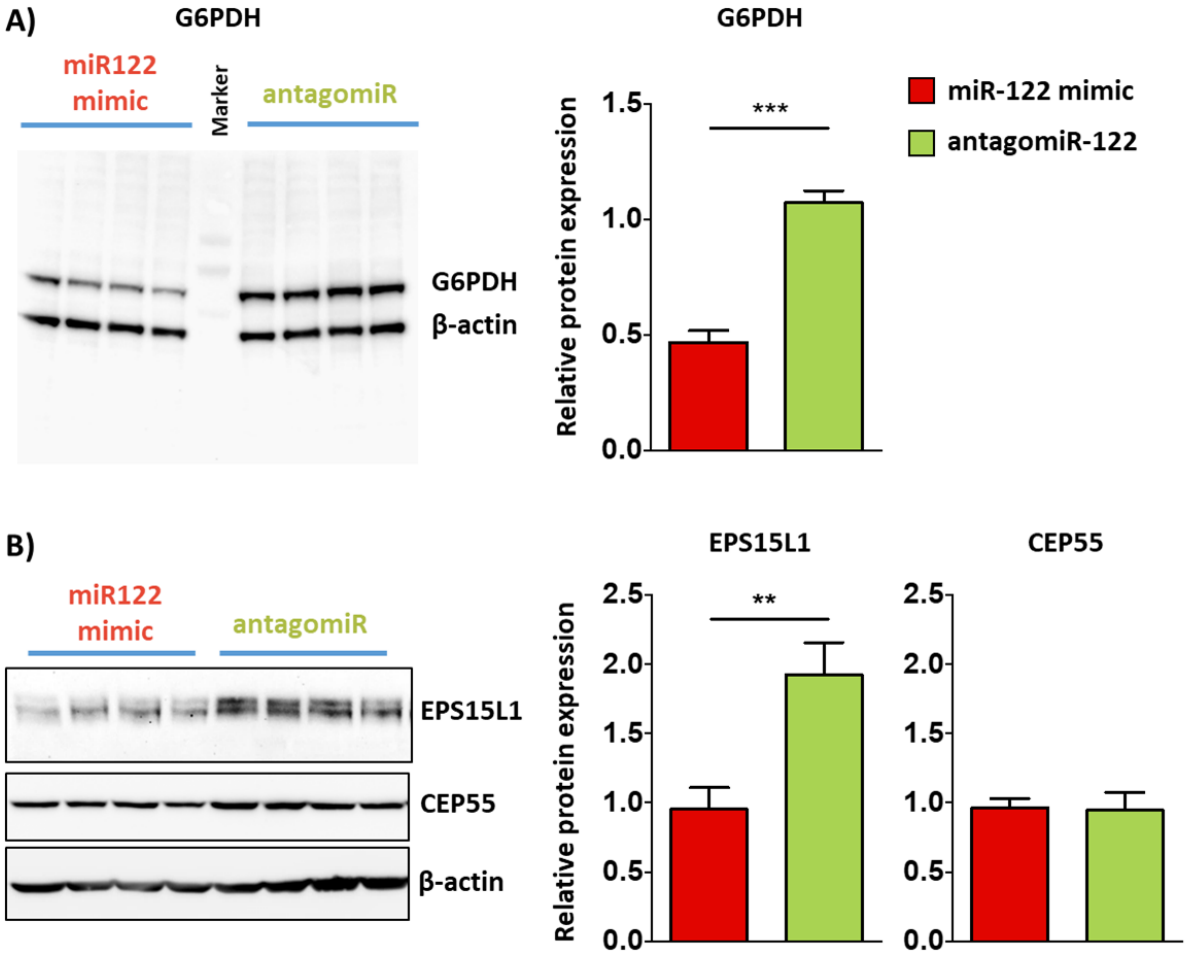

Figure 3.17: Analysis of G6PDH, EPS15L1, and CEP55 protein amounts in response to changes of miR-122 levels in Huh-7. Cells treated with miR-122 mimic (red) or miR-122 inhibitor (green) were harvested 48 h post transfection. Protein lysates were quantified and subjected to Western blot analysis. **A)** Immunoblot for human G6PDH in lysates from miR-122 overexpressing **(red)** and miR-122 inhibited **(green)** Huh-7 cells (left panel). Quantification of protein expression changes for G6PDH (right panel). **B)** Representative immunoblot and relative quantification of EPS15L1 and CEP55 protein in response to miR-122 modulation in Huh-7 cells. Signal intensity for G6PDH, EPS15L1 and CEP55 were normalized to β-actin for each sample. Data represent average ± SEM of 4 – 7 biological replicates per group. Asterisks indicate significant differences between groups (student´s t-test with significance level ** p < 0.01; *** p < 0.001).

The immunoblotting analyses from Figure 3.17 showed a significant downregulation of G6PDH and EPS15L1 protein levels in response to miR-122 overexpression compared to miR-122 inhibition. The evaluation of signal intensities indicated a 2.3-fold ($p < 0.001$) downregulation of G6PDH as well as a downregulation of 2.1-fold ($p = 0.005$) for EPS15L in response to miR-122 overexpression, respectively. In contrast, protein levels of CEP55 were not altered in Huh-7 treated with miR-122 mimic or miR-122 inhibitor. This latter finding could either indicate that CEP55 has a long half-life and reduction in protein levels is not yet detectable at 48 h time point or that small changes in protein levels may not be detected by immunoblotting and different methodological approaches must be employed.

3.3 Validation of miR-122 target gene candidates

3.3.1 Binding site analysis for miR-122 in the 3´UTRs of target gene candidates

By means of proteome analysis and immunoblotting, several miR-122 target gene candidates could be identified, which have been described in association with either the development or the progression of HCC in human (e.g. *G6PDH*, *CLIC1*, *CEP55*, *EPS15L1*, *KIF11*, *SLC1A5*, and *TK1*; Table 3.4). In order to investigate whether these target gene candidates harbor functional miR-122 binding sites in the 3´UTRs of their mRNAs, binding site analysis was conducted using the miRNA target discovery algorithm *RNA22*.

Importantly, *RNA22* computed 15 predicted MREs in the human 3´UTR sequences of the putative target gene candidates. Figure 3.18 illustrates the computationally predicted heteroduplex consisting of miR-122 and the predicted MRE in the analyzed 3´UTR of the given transcript. Several distinct binding motifs were identified for miR-122, including `canonical´, `atypical´, and `non-canonical´ binding motifs. Notably, 4 predicted binding sites were identified in the human 3´UTR of *G6PDH* mRNA and in the 3´UTR of *EPS15L1* mRNA, respectively. The 3´UTR of the human *SLC1A5* mRNA harbored three predicted miR-122 MREs, while human 3´UTR of *KIF11* encompassed two miR-122 MREs. Moreover, in the 3´UTRs of human *CEP55*, *CLIC1,* and *TK1*, one miR-122 binding site was found for each transcript.

Binding site analyses of miR-122 with predicted target mRNAs

Binding partners	Heteroduplex	p-value	Folding energy
miR-122-5p human *G6PDH* 3´UTR; Position: 21	3´-GUUUGUGGUAAC AG**UGUGAGG**U-5´ 5´-CCCCCGCCACGGCCACCCUCC U-3´	p=0.02	-15.6 kcal/mol
miR-122-5p human *G6PDH* 3´UTR; Position: 83	3´-GUUUGUGGU - AACAG**UGUGAGG**U-5´ 5´-UUGACCUCAGCUG-CACAUUCCU-3´	p=0.01	-15.1 kcal/mol
miR-122-5p human *G6PDH* 3´UTR; Position: 154	3´-GUUUGUGGUAACAG**UGUGAGG**U-5´ 5´-CGAGC-CCA--GCUACAUUCCU-3´	p=0.05	-16.3 kcal/mol
miR-122-5p human *G6PDH* 3´UTR; Position: 479	3´-GUUUGUGGUAACAG-**UGUGAGG**U-5´ 5´-GUCCCACCA-ACUCUGCACUCCA-3´	p=0.01	-18.1 kcal/mol
miR-122-5p human *CEP55* 3´UTR; Position 669	3´-GUUUGUGGUAACAG**UGUGAGG**U-5´ 5´-UGAAUUACAUUAGCACAUUCUG-3´	p=0.37	-13.7 kcal/mol
miR-122-5p human *CLIC1* 3´UTR; Position 66	3´-GUUUGUGGUA AC - AG**UGUGAGG**U-5´ 5´-GCUAC - CCAAUGGACACACUCCA-3´	p=0.02	-19.9 kcal/mol
miR-122-5p human *EPS15L1* 3´UTR; Position 346	3´-GUUUGUGG - UAACAG**UGUGAGG**U-5´ 5´-CAGACAUCCCCACCCGCCCUCCC-3´	p=0.06	-15.2 kcal/mol
miR-122-5p human *EPS15L1* 3´UTR; Position 368	3´-GUUUGUGGUAAC AG--**UGUGAGG**U-5´ 5´-CACGCAUCA--GUCAGACACUCCC-3´	p=0.16	-17.3 kcal/mol
miR-122-5p human *EPS15L1* 3´UTR; Position 695	3´-GUUUG - UGGUA - ACAG**UGUGAGG** U-5´ 5´-AAGGCCUCCAUCCCUCAUAUGCCA-3´	p=0.08	-12.7 kcal/mol
miR-122-5p human *EPS15L1* 3´UTR; Position 815	3´-GUUUGUGGUA ACAG**UGUGAGG**U-5´ 5´-GCCACACGGUGGCAGCAGUCCC-3´	p=0.36	-13.5 kcal/mol
miR-122-5p human *EPS15L1* 3´UTR; Position 1037	3´-GUUUGUGGUAA CAG**UGUGAGG**U-5´ 5´-CAGA-GCC--GGUCUCACUUCC-3´	p=0.16	-15.0 kcal/mol
miR-122-5p human *KIF11* 3´UTR; Position 66	3´-GUUUGUGG-UAACA-G**UGUGAGG**U-5´ 5´-CUUGAGCCUUGUGUAUAGAUUUUA-3´	p=0.10	-7.5 kcal/mol
miR-122-5p human *KIF11* 3´UTR; Position 1435	3´-GUUUGUGGUAA CAG**UGUGAGG**U-5´ 5´-UGAAUAU--AUG-C-UACUUCA-3´	p=0.14	-8.1 kcal/mol
miR-122-5p human *SLC1A5* 3´UTR; Position 92	3´-GUUUGUGGUAA CAG**UGUGAGG**U-5´ 5´-GGUCUGCC--UG-CACACUCUG-3´	p=0.17	-15.3 kcal/mol
miR-122-5p human *SLC1A5* 3´UTR; Position 117	3´-GUUUGUGGUAAC AG**UGUGAGG**U-5´ 5´-CAGGGGCC-CCAGCACCCUCCA-3´	p=0.17	-16.7 kcal/mol
miR-122-5p human *SLC1A5* 3´UTR; Position 3222	3´-GUUUGUGGUAACAG**UGUGAGG**U-5´ 5´-AGGUCACCAUGG-GGAAUUCUA-3´	p=0.19	-13.2 kcal/mol
miR-122-5p human *TK1* 3´UTR; Position 256	3´-GUUUGUGGUAACAG**UGUGAGG**U-5´ 5´-CUGGGAUC-UGG-CACACUCCC-3´	p=0.01	-14.7 kcal/mol

Figure 3.18: Analysis of putative miR-122 binding sites on the 3´UTRs of human *G6PDH*, *CEP55*, *CLIC1*, *EPS15L1*, *KIF11*, *SLC1A5*, and *TK1*. *RNA22* computed several miR-122 MREs in the 3´UTRs of human miR-122 target candidates. Blue lines indicate predicted base pairing between miRNA and target sequence, dashed blue lines indicate weaker hydrogen bonds between the nucleobases. The seed sequence of miR-122 is illustrated in grey boxes and corresponding nucleic acids are displayed in red font.

Taken together, binding site prediction conducted by *RNA22* identified numerous potential miR-122 binding sites, suggesting that the translation of the genes of interest may be directly modulated by miR-122.

3.3.2 Direct validation of putative miR-122 target gene candidates in HEK293

Previous analyses presented in this study revealed that miR-122 overexpression reduced the mRNA and the protein levels of several target gene candidates (Figure 3.16 and Figure 3.17). Taken together with the findings that several putative miR-122 MREs were found in the 3´UTRs of the genes of interest (Figure 3.18), it was hypothesized that the levels of those mRNAs may be directly modulated by miR-122 in humans. In order to experimentally verify the direct interaction between miR-122 and the 3´UTRs, a luciferase-based reporter assay was conducted (as described in detail in Section 2.2.23). The full length sequences of *G6PDH*, *CLIC1*, *CEP55*, *EPS15L1*, *KIF11*, *SLC1A5,* and *TK1* 3´UTRs were cloned into pMir(+) reporter plasmids as well as into pMir(-) negative control plasmids. The recombinant luciferase plasmids were then transiently transfected into HEK293 in presence or in absence of miR-122, respectively.

Figure 3.19 shows that the luciferase activity in cells co-transfected with pMir(+)_122 (positive control) in presence of miR-122 mimic was significantly reduced to 11.4% (± 1.7%; $p < 0.001$) after 24 h and to 24.2% (± 6.0%; $p < 0.001$) after 48 h compared to the cells which were transfected with pMir(+)_122 in absence of miR-122 mimic (Figure 3.19). These data indicated that the product of pMir(+)_122 vector, which encodes for a *luciferase* mRNA harboring a functional miR-122 MRE in its 3´UTR, was subjected to translational repression by increased miR-122 expression. In contrast, the translation of the product of pMir(-)_122 vector, which harbored the miR-122 binding site in the inverse orientation (negative control), was not translationally inhibited by the co-transfection with the miR-122 mimic at both, 24 and 48 h. (Figure 3.19).

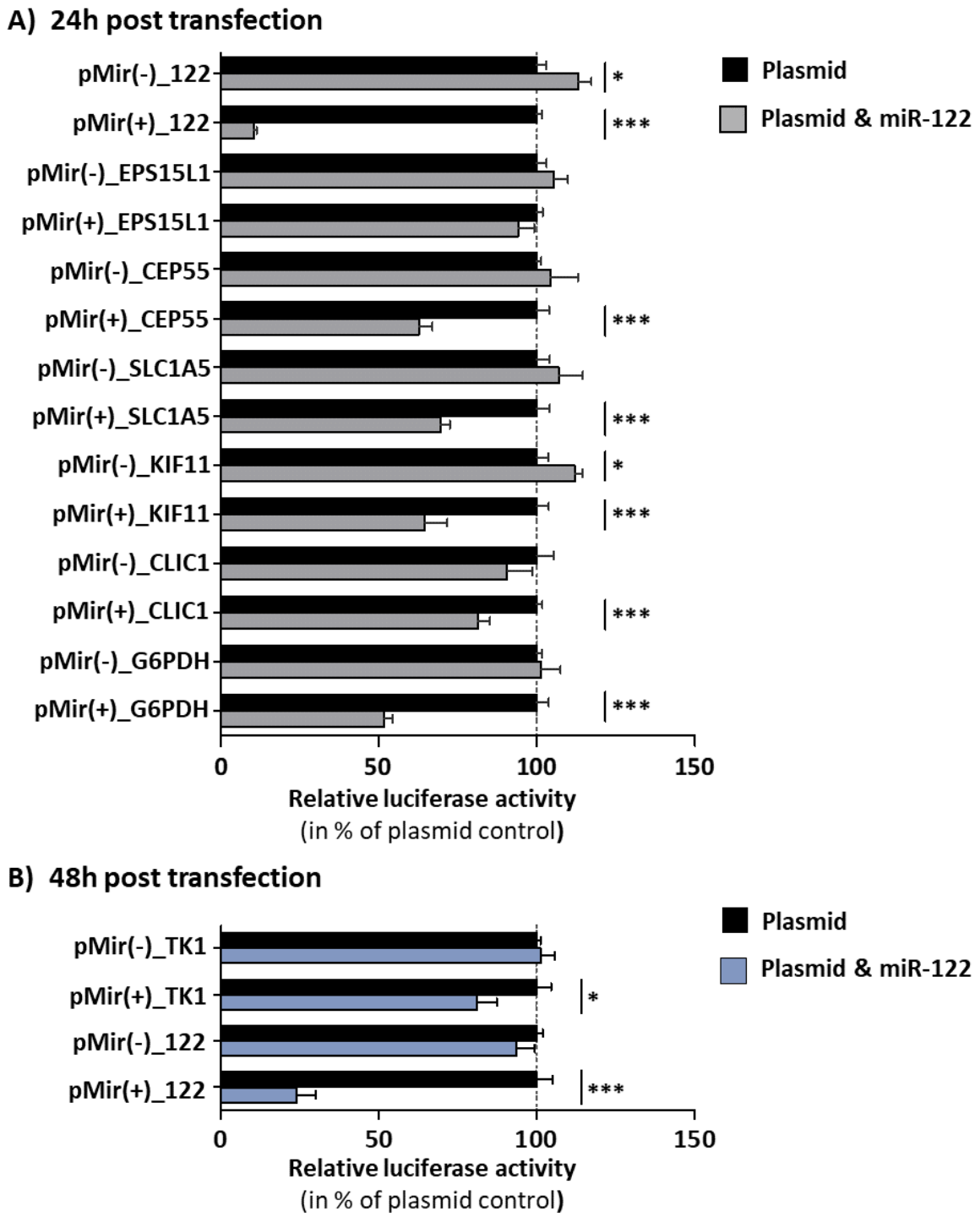

Figure 3.19: Validation of human 3´UTRs as direct miR-122 target sites by luciferase assay. Full length 3´UTRs of human genes were cloned into luciferase plasmid pMir(+) and control plasmid with MCS in inverse orientation pMir(-). As controls, the miR-122 perfect binding site was cloned in both plasmids (pMir(+)_122 and pMir(-)_122). Recombinant plasmids were transfected in HEK293 cells either in absence **(black)** or in presence of miR-122 **(pale grey or blue)**. Luciferase activity was measured from cell lysates **A)** 24 h or **B)** 48 h post transfection. Data are represented as percentage ± SEM of 3 – 5 independent experiments. The luciferase activity for each plasmid transfection in absence of miR-122 was set to 100%. Asterisks indicate significant differences between groups (student´s t-test with significance level * $p < 0.05$; *** $p < 0.001$).

Moreover, a significant effect of miR-122 on the luciferase activity was observed in cells transfected with pMir(+)_G6PDH plasmid for 24 h, but not in cells transfected with the negative orientated pMir(-)_G6PDH plasmid. Compared to HEK293 cells transfected with pMir(+)_G6PDH alone, the luciferase activity in cells overexpressing miR-122 was declined to 51.8% (± 2.5%; $p = 0.002$). Likewise, the overexpression of miR-122 significantly decreased luciferase activity derived from pMir(+)_CEP55 (62.8% ± 4.2%; $p < 0.001$), pMir(+)_SLC1A5 (69.6% ± 3.0%; $p < 0.001$), and pMir(+)_CLIC1 (81.4% ± 3.9%; $p < 0.001$) after 24 h. Of note, while in presence of miR-122 the luciferase count from pMir(+)_KIF11 was reduced to (64.6% ± 7.1%; $p < 0.001$) compared to control, the negative control plasmide pMir(-)_KIF11-derived luciferase was slightly increased after 24 h (112% ± 2.7%). Furthermore, the luciferase encoded by pMir(+)_TK1 was significantly downregulated (24.3% ± 5.9%; $p = 0.03$) in presence of miR-122 after 48 h but not after 24 h. In contrast, the luciferase count from pMir(+)_EPS15L1 was not significantly affect by simultaneous overexpression of miR-122.

To summarize, the observed changes in luciferase activity were attributed to the binding of miR-122 to the luciferase transcript, leading to miRNA-mediated repression and, thus, to reduced luciferase protein levels. Therefore, the luciferase data provided compelling evidence for a direct interaction between miR-122 and the cloned 3´UTRs as illustrated in Figure 3.19.

3.3.3 Analysis of miR-122 and *G6PDH* mRNA levels in human hepatocellular carcinoma tissue

One of the identified miR-122 targets, glucose-phosphate dehydrogenase (G6PDH), was of particular interest, since this gene encodes for the rate-limiting enzyme in the pentose phosphate pathway [*651*, *652*]. Numerous studies reported the upregulation of G6PDH in various cancer types, including HCC [*653*, *654*]. Strikingly, G6PDH was found significantly upregulated in the liver of patients suffering from chronic HBV infection [*655*], a disease which is considered as main risk factors for the development of HCC [*656*]. In contrast, the hepatic expression of miR-122 is frequently downregulated in patients chronically infected with HBV as well as in HCC patients [*317*, *318*, *346*, *657*]. Therefore, it was investigated whether a correlation between miR-122 and G6PDH exist. For this purpose, RNA was isolated from 7 tumour tissue samples of CHB patients (referred to as `HBV-HCC´) and from 21 tumor samples

of HCC patients without viral infection (subsequently termed as `non-viral HCC´; Table 2.1) and levels of miR-122 and *G6PDH* mRNA were determined by qPCR (Figure 3.20).

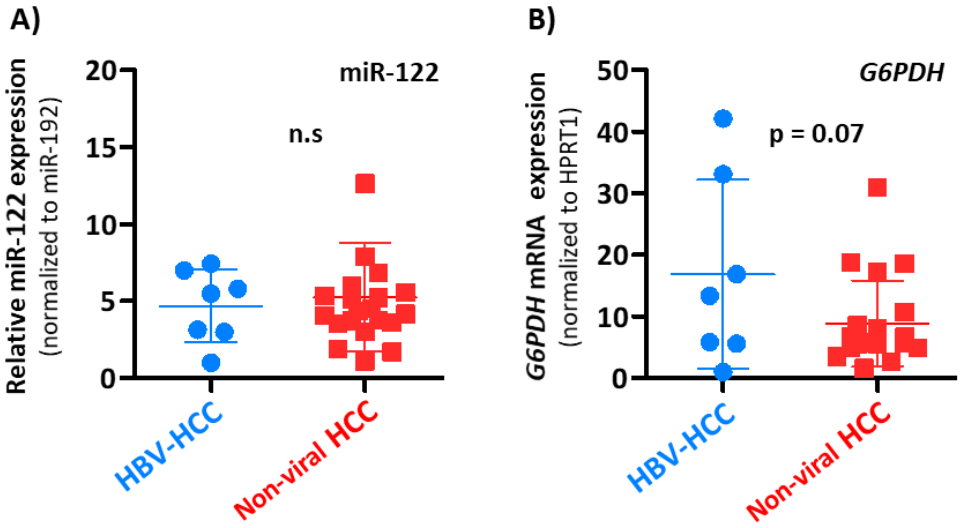

Figure 3.20: Quantification of hepatic miR-122 and *G6PDH* mRNA levels in HCC tissue of patients with or without HBV infection. Total RNAs were isolated from HCC tissue of patients with HBV infection (HBV-HCC; n = 7) or without viral infections (non-viral HCC: n = 21). **A)** Relative expression of miR-122 in HCC patients with or without HBV infection. Levels of miR-122 were normalized to miR-192 for each sample. **B)** Profiling of *G6PDH* mRNA normalized to *HPRT1* as reference gene. Statistical analysis was conducted by using unpaired student´s t-test.

Although the levels of *G6PDH* mRNA in the HCC tissue of HBV-HCC patients showed a tendency towards upregulation compared to the non-viral HCC cohort (Figure 3.20 B), no significant changes of the hepatic miR-122 levels were measured in the two groups (Figure 3.20 A). A possible explanation for this could reside in the limited number of samples which could be introduced in these studies. However, when miR-122 and *G6PDH* mRNA levels were directly correlated using linear regression as illustrated in Figure 3.21, significant changes between the HBV-HCC and the non-viral HCC group were found. While an inverse correlation between miR-122 and *G6PDH* mRNA levels was determined in HCC tissues of patients with viral hepatitis type B ($R^2 = 0.610$; $p = 0.038$), neither negative nor positive correlation was found in cancer specimens of patients suffering from HCC without viral infection ($R^2 < 0.001$, not significant).

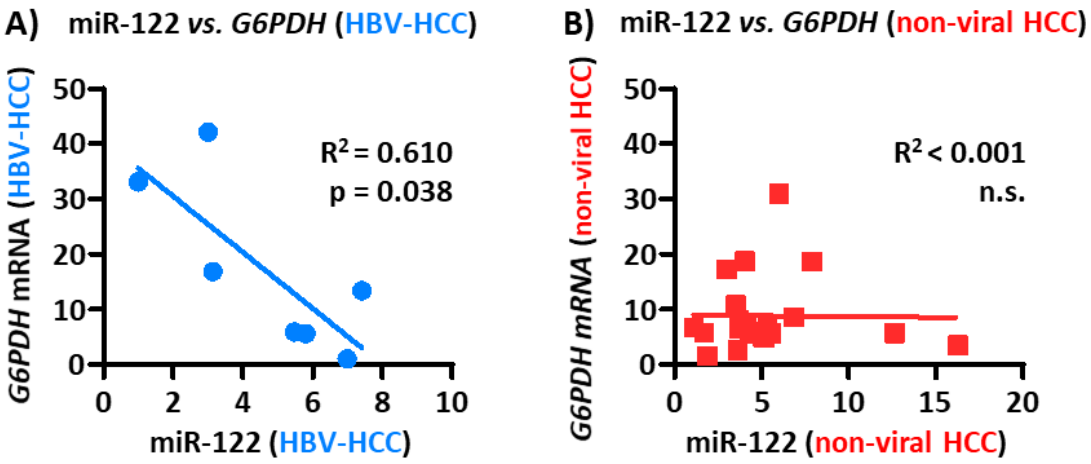

Figure 3.21: Correlation between miR-122 and *G6PDH* levels in HCC tissue of patients with or without HBV infection. Total RNAs were isolated from HCC tissue from patients with HBV (HBV-HCC; n = 7) or without HBV infection (non-viral HCC; n = 21) and analyzed by qPCR. **A)** Correlation in tumor tissue from HCC patients with HBV infection. **B)** Correlation of miR-122 and *G6PDH* mRNA in tumor tissue obtained from HCC patients without viral infection.

In summary, the data presented here support the hypothesis that miR-122 directly regulates *G6PDH* mRNA (Figure 3.19). Moreover, an inverse correlation of miR-122 and *G6PDH* messenger levels was identified in tumor tissue of HCC patients with HBV infection, but not in HCC tissue of individuals without HBV infections.

3.4 Regulation of miR-122 by cytokines and growth factors

The liver-specific miR-122 is mainly expressed in hepatocytes and regulated by a number of liver-enriched transcription factors such as the family of hepatocyte nuclear factors HNF4α and HNF3 [*119*, *658*]. In humans, the gene encoding for miR-122 is located on chromosome 18, and – in contrast to many other miRNAs – *MIR122* encodes for a monocystronic primary transcript whose expression is driven by its own promoter [*119*, *282*, *659*]. Despite the amount of studies focusing on the complex mechanisms by which miR-122 is regulated, only little is known about the mechanisms that may contribute to miR-122 dysregulation at the onset of liver diseases. It is well known that acute or chronic liver diseases are characterized by alterations in various growth factors and anti- or pro-inflammatory cytokines such as TNFα, TGFβ or cytokines of the interleukin family (e.g. IL6 or IL10; [*660*]). Therefore, the aim of this study was to elucidate the effects of immunoregulatory cytokines and growth factors on the activity of the human *MIR122* promoter and, subsequently, on the miR-122 biosynthesis.

3.4.1 Characterization of the human *MIR122* promoter

With the aim to improve our understandings of the miR-122 regulation, promoter constructs of the human *MIR122* gene were designed. For this purpose, the *MIR122* promoter as described by Li *et al.* (pGL4_hsa 0.75kb; [*119*]) was cloned into luciferase reporter plasmids lacking a functional promoter (pGL4.1 Basic vector). Moreover, three additional promoter constructs were cloned; one encompassing the most conserved moiety of the *MIR122* promoter (pGL4_hsa 0.18kb; Appendix Figure 7.5) and constructs encompassing the promoters´ upstream flanking sequences with (pGL4_hsa 1.7kb) or without the promoter (pGL4_hsa 0.95kb) as illustrated in Figure 3.22 and Appendix Figure 7.5. The recombinant plasmids encoding the human *MIR122* promoter constructs were transfected into Huh-7 cells and the basal activities of the inserted promoter fragments were assessed by monitoring the luciferase activity in the transfected cells after 24 h. The luciferase activity, which is proportional to the relative amounts of luciferase produced in the transfected cells, was calculated based on a chemiluminescent signal measured from cell lysates upon addition of luciferase substrate.

Figure 3.22 illustrates the basal promoter activities of the human *MIR122* constructs. The basal luciferase activity of the promoter encompassing the promoter element increased with the length of the inserted promoter relative to the pGL4.1 Basic vector. While the activity of pGL4_hsa 0.18kb only tendencially raised to 262% (± 73%) without reaching significance, the activity of pGL4_hsa 0.75kb significantly increased to 1447% (± 436%; $p = 0.011$), and the activity of pGL_hsa 1.7kb was significantly elevated to 18,734% (± 3,473%; $p < 0.001$) relative to the promoter-less pGL4.1 Basic vector. However, the promoter activity of the core-promoter-less construct pGL_hsa 0.95kb was not affected in comparison to the pGL4.1 Basic vector, indicating that the 0.75kb promoter fragment is crucial for driving *luciferase* gene expression.

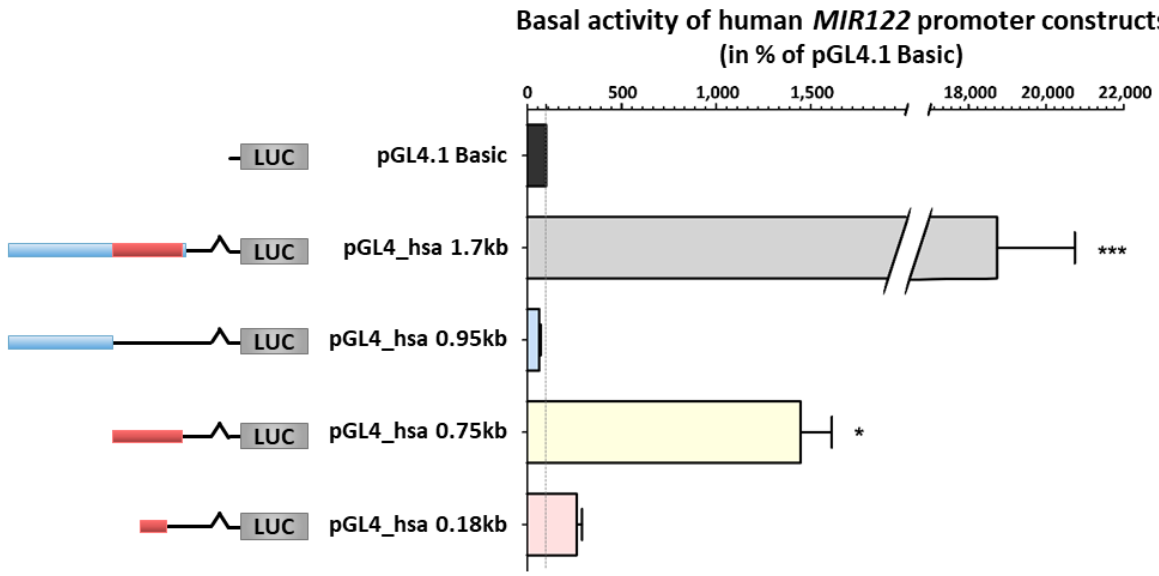

Figure 3.22: Basal activity of human *MIR122* promoter constructs. Promoter constructs encoding different lengths of the human *MIR122* promoter (0.18kb, 0.75kb, 0.95kb, 1.7kb) were generated by PCR amplification and cloned into promoter-less luciferase reporter plasmids (pGL4.1 Basic). The promoter sequence of the human *MIR122* gene as identified by Li *et al.* [*119*] is illustrated as red bar, while the flanking sequence is illustrated as blue bar. Promoter plasmids were transfected in Huh-7 cells and basal promoter activities were measured 24 h after transfection by quantifying luciferase activity using the Dual-Luciferase® Reporter Assay Kit. Data represent average luciferase activity in percentage of pGL4.1 Basic vector ± SEM for 3 – 4 independent experiments. Asterisks indicate significant differences to pGL4.1 Basic vector (one-way ANOVA with Dunnett´s multiple comparison test with significance level * $p < 0.05$; *** $p < 0.001$).

In order to explore signaling pathways that potentially regulate the activity of the human *MIR122* promoter constructs and, thereby, the miR-122 expression, the effects of liver disease-associated cytokines and growth factors on the activity of the promoter constructs were assessed. For this, cells were transfected with vectors encompassing the different promoter constructs and stimulated with either TGFβ1, BMP6, IL6, IL10, TNFα, IFNβ, or PDGF-BB, respectively.

The activity of the highly conserved promoter construct pGL4_hsa 0.18kb was not significantly affected by any of the cytokines or growth factors included in this study (Figure 3.23). The promoter-less construct pGL4_hsa 0.95kb showed a significant response to PDGF-BB treatment which reduced the promoter activity to 93.1% (± 2.7%; $p = 7.8 \times 10^{-5}$ [FDR]). In contrast, the activity of the promoter containing construct pGL4_hsa 0.75kb increased in response to IL10 by 24.0% (± 9.3%; $p = 6.2 \times 10^{-5}$ [FDR]) and TNFα stimulation by 16.6% (± 5.3%; $p = 1.1 \times 10^{-5}$ [FDR]), respectively. Moreover, the pGL4_hsa 0.75kb as well as the longest construct pGL4_hsa 1.7kb responded to TGFβ1 treatment with reduced promoter activity of

63.2% (± 13.4%; p = 3.3x10^{-5} [FDR]; pGL4_hsa 0.75kb) and 52.6% (± 8.0%; p = 4.9x10^{-4} [FDR]; pGL4_hsa 1.7kb). In contrast, the bone morphogenetic protein 6 (BMP6), which belongs to the TGFβ family, tendencially increased the activity of pGL4_hsa 1.7kb to 127.0% (± 11.6%), although significance was not reached (p = 0.02 [FDR]).

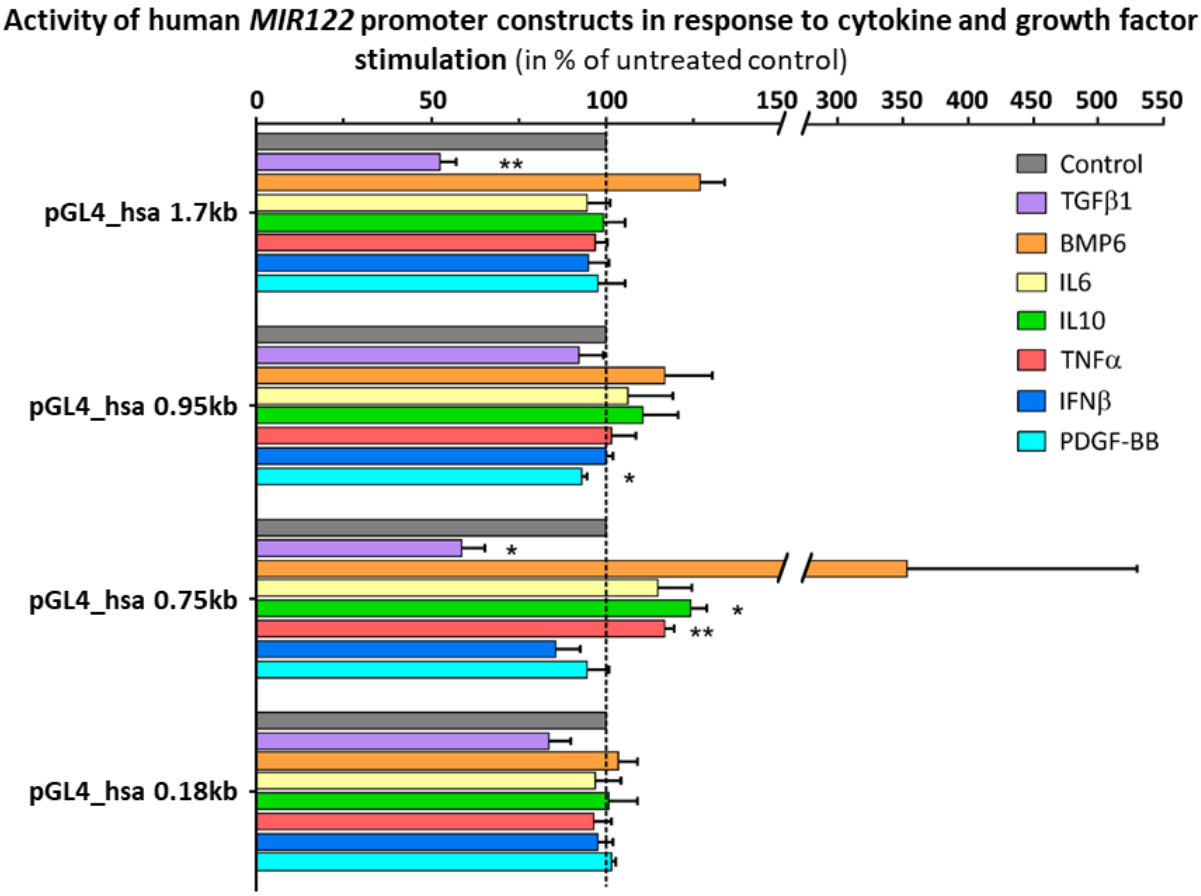

Figure 3.23: Response of the human *MIR122* promoter to cytokine and growth factor stimulations. Four promoter constructs encompassing different lengths of the human *MIR122* promoter were transfected into Huh-7 cells. After transfection, cells were synchronized by starvation in FCS-free medium for 24 h and then treated with selected cytokines TGFβ1 (10 ng/mL), BMP6 (50 ng/mL), IL6 (50 ng/mL), IL10 (10 ng/mL), TNFα (10 ng/mL), IFNβ (10^6 U/mL), and PDGF-BB (20 ng/mL) for another 24 h. Control cells were kept in serum-free medium (untreated control). Cells were lysed and luciferase activities were quantified by using Promega´s Dual-Luciferase® Reporter Assay Kit. Data represent average luciferase activity for each plasmid in percentage of untreated control ± SEM of 3 independent experiments. Asterisks indicate significant differences to control (grouped analysis using unpaired multiple t-test applying a false discovery rate (FDR) * p < 0.005; **p < 0.001).

Taken together, these data indicate that cytokines and growth factors differentially affected the promoter activity of the human *MIR122* gene. While the data suggested that IL10, TNFα and to some extent BMP6 rather exerted an activating effect on the *MIR122* promoter, TGFβ1 inhibited the activity of the *MIR122* promoter.

3.4.2 Investigation of miR-122 biogenesis in human hepatoma cells in response to TGFβ1 stimulation

The promoter analyses conducted in this study indicated that cytokines and growth factors may differentially regulate the activity of the human *MIR122* promoter. However, as gene transcription is a highly complex process with multiple regulatory levels, changes in promoter activity may not necessarily reflect the alterations of miR-122 at the transcriptional level. Therefore, relative expression changes of both, the primary miR-122 transcript (pri-miR-122) as well as the mature miR-122, were investigated upon stimulation of human hepatoma cells Huh-7 with TGFβ1.

As illustrated in Figure 3.24, The mRNA levels of the TGFβ-responsive gene *Hepcidin* (*HAMP*) were significantly upregulated in Huh-7 cells after stimulation with 5 ng/mL TGFβ1 (290.7% ± 38.9%; $p < 0.001$) or 10 ng/mL TGFβ1 (267.1% ± 52.6; $p < 0.001$) compared to control cells. The mRNA of the TGFβ-responsive gene *SMAD family member 7* (*SMAD7*) was significantly elevated to 332.1% (± 45.1%; $p < 0.001$) in response to 5 ng/mL TGFβ1 and to 274.2% (± 27.3%; $p < 0.001$) in response to 10 ng/mL TGFβ1 compared to control treated cells after 3 h. Moreover, a significant upregulation of *SMAD7* mRNA was observed after 6 h, reaching mRNA levels of 262.8% (± 52.0%; $p < 0.001$) and 278.1% (± 65.7%; $p < 0.001$) in response to 5 ng/mL or 10 ng/mL TGFβ1, respectively. While, levels of mature miR-122 were not altered after 3 or 6 h of TGFβ1 stimulation, the relative expression of primary miR-122 transcript was reduced to 71.3% (± 9.5%; $p < 0.001$) after treatment with 5 ng/mL TGFβ1, and to 65.4% (± 13.0%; $p < 0.001$) after treatment with 10 ng/mL TGFβ1 for 3 h. The observed downregulation of pri-miR-122 was sustained after 6 h in TGFβ1-stimulated cells compared to control cells, whereby 5 ng/mL TGFβ1 resulted in downregulation of pri-miR-122 to 59.4% (± 4.6%; $p < 0.001$) and 10 ng/mL TGFβ1 caused reduction of pri-miR-122 levels to 58.7% (± 6.4%; $p < 0.001$).

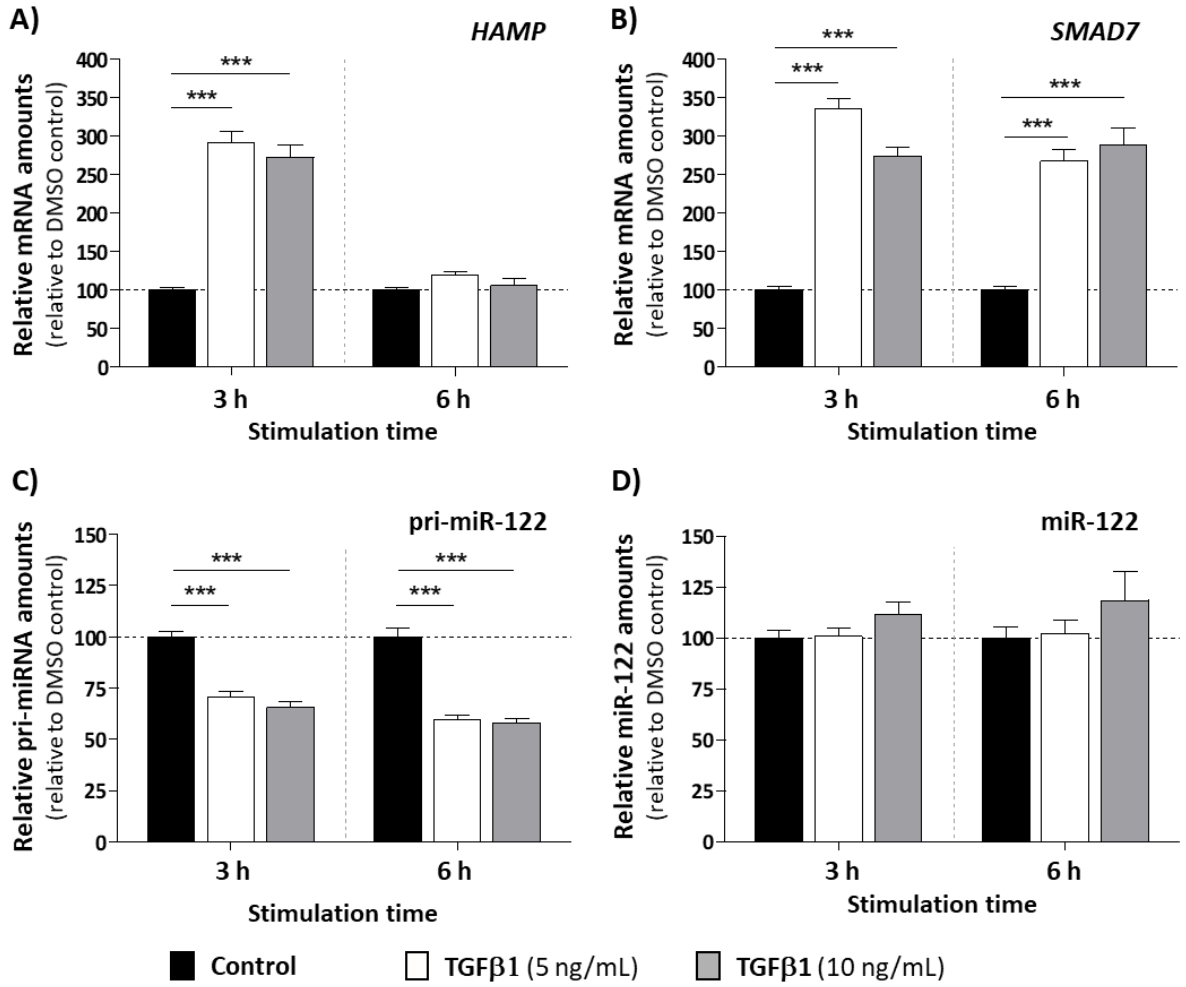

Figure 3.24: Analysis of pri-miR-122 levels upon stimulation of Huh-7 cells with TGFβ1. Huh-7 cells were synchronized in serum-free medium for 24 h and incubated with TGFβ1 (5 or 10 ng/mL) for 3 h or 6 h, respectively. Control cells were kept in serum-free medium for the same duration. Following RNA isolation, relative mRNA levels were quantified using qPCR. **A)** *Hepcidin* (*HAMP*) mRNA, **B)** *SMAD family member 7* (*SMAD7*) mRNA, **C)** pri-miR-122, and **D)** mature miR-122. QPCR data were normalized to the most stable gene identified in the data set (β-actin) using *qBase* software, while miR-122 was measured by miQPCR and normalized to miR-192 levels. Values are illustrated as relative expression in percentage of control ± SEM of 5 independent experiments. Asterisks indicate significant differences to control (one-way ANOVA using Dunnett´s multiple comparison test with significance level *** $p < 0.001$).

Altogether, the presented data indicated that the transcription of pri-miR-122, was reduced in response to TGFβ1 stimulation of Huh-7 cells, albeit no alterations in the relative expression of the mature miR-122 were observed after 3 or 6 h. Based on these observations, it was hypothesized that TGFβ1 may affect the *de novo* transcription of miR-122 rather than modulating the stability of the mature miR-122.

3.4.3 Effects of TGFβ receptor 1 inhibition on the biogenesis of miR-122 in Huh-7 cells

To address the question whether the canonical TGFβ receptor-mediated signaling pathway is involved in promoting the observed downregulation of pri-miR-122, the effect of a TGFβ receptor inhibitor was tested in Huh-7 cells. For this purpose, Huh-7 cells were treated with SB431542, a small molecule inhibitor that selectively inhibits TGFβ receptors type 1 [*661*]. Following pre-incubation with SB431542, cells were stimulated with TGFβ1 in presence of inhibitor for 3 hours and mRNA levels of *HAMP*, *SMAD7*, and pri-miR-122 were assessed.

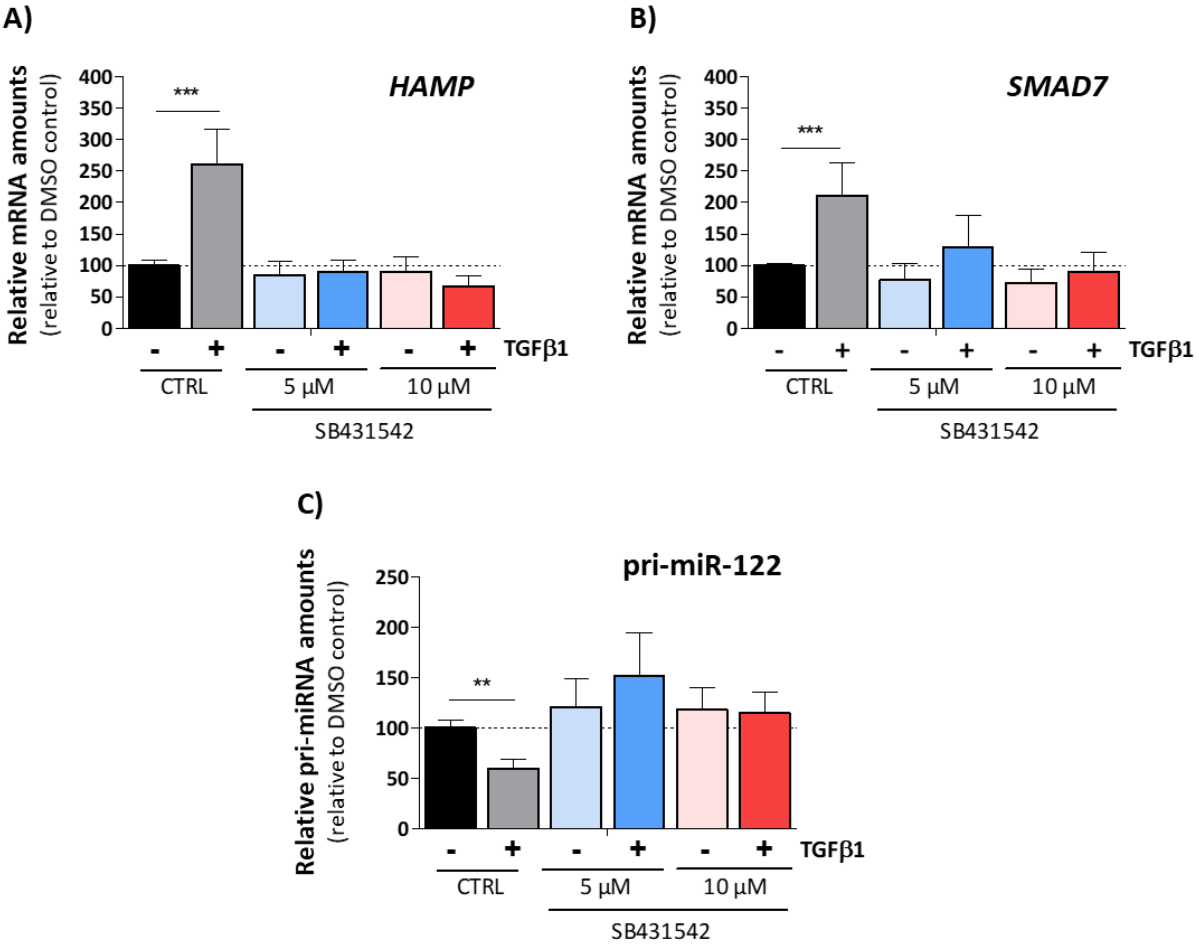

Figure 3.25: Inhibition of TGFβ1 signaling pathway in human hepatoma cells. Huh-7 cells were starved in serum-free medium for 24 h and incubated with TGFβ receptor type 1 inhibitor SB431542 (5 µM or 10 µM) for 3 h. The cells were then stimulated with TGFβ1 (5 ng/mL) in presence of inhibitor for another 3 h, respectively. Control cells were treated with DMSO, the solvent of SB431542, in serum-free medium as vehicle control. The mRNA levels for **A)** *HAMP*, **B)** *SMAD7* and **C)** pri-miR-122 were measured by qPCR. Data were normalized to β-actin using *qBase* software. Values are illustrated as relative expression in percentage of control ± SEM of 5 independent experiments. Asterisks indicate significant differences to control (one-way ANOVA using Dunnett´s multiple comparison test with significance level ** $p < 0.01$; *** $p < 0.001$).

As presented in Figure 3.25, the significant upregulation of *HAMP* mRNA after 3 h stimulation with 5 ng/mL TGFβ1 (254.8% ± 45.5%; $p < 0.001$) was abolished in the presence of 5 µM or 10 µM of SB431542. Likewise, TGFβ1-induced upregulation of *SMAD7* mRNA (229.3% ± 51.5%; $p < 0.001$) was inhibited in the presence of 5 and 10 µM SB431542. In addition, the downregulation of pri-miR-122 to 59.2% (± 9.1%; $p < 0.001$) observed upon stimulation with 5 ng/mL TGFβ1 for 3 h was completely prevented in Huh-7 stimulated in presence of SB431542.

Taken together, the presented data indicate that TGFβ1-mediated downregulation of pri-miR-122 was sensitive to inhibition of TGFβ receptors type 1, indicating that the canonical TGFβ signaling pathway might play role in regulating miR-122 transcription in human Huh-7 cells.

4. Discussion

The discovery of the `miRNome´ in the early 2000s, has fundamentally changed our understanding of post-transcriptional gene regulation and has drawn considerable attention to the function of individual miRNAs. One prominent member of this family of short ncRNAs is miR-122, a miRNA highly enriched in liver that accounts for up to 46% of all miRNAs in hepatocytes according to most recent sequencing data [*662*]. Yet, the expression of miR-122 is not limited to hepatocytes but also occurs in different cell types like hepatic stellate cells or primary fibroblasts, albeit in low abundances [*546*, *663*].

The function of miR-122 has intensively been studied in the past two decades. miR-122 modulates diverse liver processes including the biosynthesis of hepatic lipids and the cholesterol metabolism as well as the function of mitochondria, thus contributing to liver homeostasis [*292*, *319*]. Moreover, there is compelling evidence that miR-122 dysregulation directly contributes to the development and progression of chronic liver diseases [*312*, *313*, *315*, *317*, *318*]. For instance, miR-122 exerts pronounced tumor-suppressive effects *in vitro* and a lowering of miR-122 is frequently observed in liver tumor tissue of HCC patients [*294*, *317*, *658*].

So far, the molecular mechanisms linking aberrant miR-122 expression to the pathogenesis of liver diseases remain largely elusive. The present study was therefore carried out to gain insight into the mechanisms modulating miR-122 transcription, as well as to identify gene networks which are regulated by miR-122. For this purpose, transcriptome as well as proteome analyses were conducted in Huh-7 cells after transfection of miR-122 mimic or miR-122 inhibitor. Furthermore, the responsiveness of the human *MIR122* promoter constructs to stimulation with liver disease-associated cytokines and growth factors was investigated by reporter gene assays.

4.1 Regulation of miR-122 biosynthesis in response to cytokines and growth factors

The miRNA-122 is encoded by a single genetic locus located on chromosome 18 in humans as well as in mice [*278*]. Its transcription is controlled by a RNA polymerase II promoter which encompasses binding motifs for several transcription factors of the hepatocyte nuclear factor family, such as HNF1α, HNF3β, HNF4α, HNF6, and CCAAT-enhancer binding element protein

C/EBPα [*119*, *282*, *284*]. *MIR122* gene expression is further controlled via epigenetic mechanisms including DNA methylation and histone modifications [*285–288*]. Albeit being among the best characterized miRNAs, the detailed mechanisms causing a decline of miR-122 expression in individuals suffering from acute or chronic liver diseases are not fully understood.

Cytokines are proteins that are produced mainly by immune cells and that regulate the immune response in health and disease. Acute as well as chronic liver diseases are frequently accompanied by an upregulation of cytokine or growth factor serum levels, including TNFα, IL10 and TGFβ [*664*]. Several studies reported that miR-122 regulates cytokine-mediated signaling pathways. For instance, miR-122 enhances endogenous type I interferon (IFN) signaling by targeting *suppressor of cytokine signaling 3* (*SOCS3)*, thus promoting antiviral defense mechanisms triggered by IFNs [*343*, *344*]. A recent study further suggests that miR-122 amplifies IFN signaling by targeting tyrosine kinases that activate STAT3, which in turn counteracts IFN signaling [*665*, *666*]. Moreover, in hepatic stellate cells miR-122 inhibits the production of pro-inflammatory cytokines, such as IL6 and IL1β, through silencing PKR-activating protein (PACT) [*667*]. Despite these evidences supporting the effect of miR-122 on cytokine signaling, the regulatory activity of cytokines on miR-122 expression is largely unknown.

This study therefore aimed to investigate whether immunoregulatory cytokines and growth factors affect miR-122 biogenesis. It was shown that TNFα, IL10, and to some extent BMP6 increase the activity of the human *MIR122* promoter (Figure 3.23). In contrast, TGFβ1 significantly reduced the promoter activity of the human *MIR122*, whereby IFNβ showed a tendency to decrease the activity of the same promoter construct (Figure 3.23). Of particular interest are the findings that TGFβ1 administration to Huh-7 cells significantly decreased miR-122 *de novo* transcription, although levels of mature miR-122 remained constant within the time course of the experiments (Figure 3.24). Similar differences between miR-122 and pri-miR-122 expression changes were shown by Gatfield and collaborators who demonstrated a circadian regulation of pri-miR-122 transcription accompanied by inverse changes in miR-122 targets [*280*]. Yet, miR-122 levels stayed unchanged throughout the day, probably due to the high stability of the mature miR-122 [*280*]. As possible explanation, Gatfield *et al.* proposed that miRNAs remain stably assembled to RISC complexes once they are bound to target mRNA. Thus, it was speculated that the amount of newly synthesized miR-122, rather

than the total levels of cellular miR-122, may be the crucial factor determining the efficiency of miRNA-mediated gene silencing [*280*].

The TGFβ1-induced downregulation of pri-miR-122 was blocked in the presence of TGFβ receptor type 1 inhibitor SB431542, indicating that the canonical signaling through TGFβ receptor type 1 may contribute to the inhibition of miR-122 transcription (Figure 3.25). The molecular mechanism underlying the repressive effects of TGFβ1 on *MIR122* transcription will require further examination, but it was recently reported that TGFβ1 suppresses the transcription factor HNF4α [*668*]. Thus, it could be hypothesized that TGFβ1-induced inhibition of HNF4α may contribute to the reduced transcription of miR-122. Of note, a recent study showed that miR-122 antagonizes TGFβ signaling by targeting either *TGFβ1* mRNA (in human) or *TGFβ receptor* mRNA (in mice) [*669*]. Taken together with the results presented here, it is proposed that miR-122 and TGFβ1 regulate one another through a regulatory circuit (Figure 4.1).

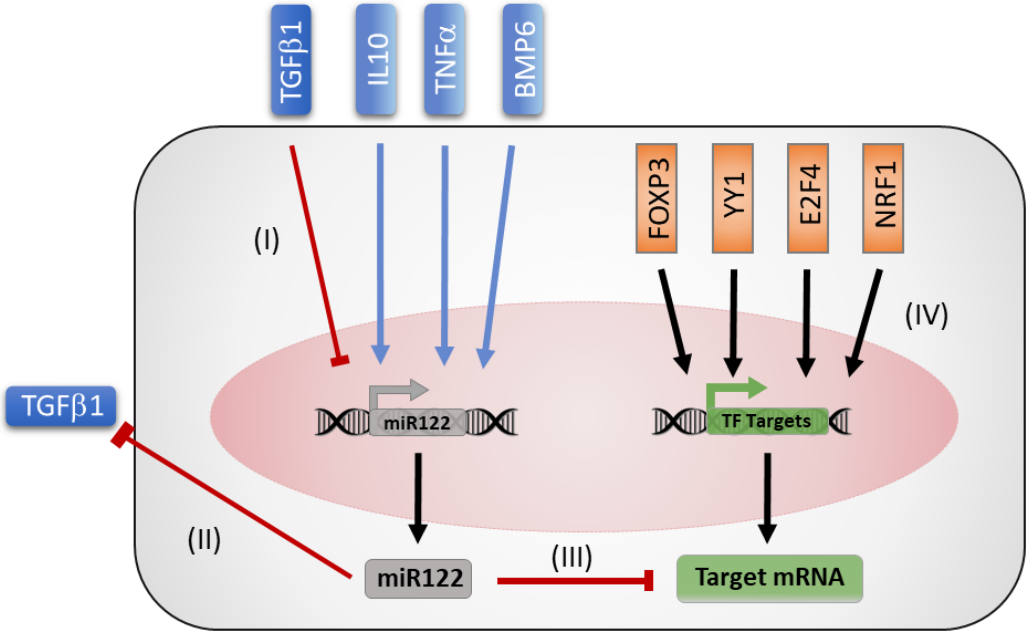

Figure 4.1: Proposed model for the modulation of miR-122. (I) miR-122 transcription is under the control of cytokines and growth factors, e.g. IL10, TNFα, BMP6 and TGFβ. miR-122 was shown to inhibit TGFβ signaling pathway by directly targeting TGFβ1 or TGFβ receptor mRNA [*669*]. **(II)** Thus, it is suggested that TGFβ1 and miR-122 may regulate one another. **(III)** Following its biogenesis, mature miR-122 accumulates in the cytosol where it inhibits the translation of target genes. **(IV)** Data presented in this study indicate that miR-122 fine-tunes the expression of genes downstream to the transcription factors Forkhead box P3 (FOXP3), Yin Yang 1 (YY1), nuclear respiratory factor 1 (NRF1), and E2F transcription factor 4 (E2F4).

Remarkably, a literature mining suggests that levels of miR-122 and TGFβ1 are inversely correlated in patients with liver diseases, such as NAFLD, PBC, HCC, and viral hepatitis (Table 4.1). Based on these findings, one could hypothesize that the upregulation of TGFβ1 that occurs during acute or chronic liver injury may contribute to a downregulation of miR-122. In line with this, it was shown that TGFβ1-exposure of hepatic stellate cells significantly reduced miR-122 levels which was accompanied by an elevation of pro-fibrogenic gene expression and a pro-fibrotic phenotype [*437*]. Moreover, TGFβ1 is known to promote HCC invasion as well as metastatic potential of HCC cells and phase II trials are ongoing to assess the safety of TGFβ1 inhibitors in cohorts of HCC patients [*670*]. It would be of great interest to assess the effect of these inhibitors on miR-122 levels and to evaluate the potential contribution of miR-122 towards counteracting HCC growth and development *in vivo*. Initial studies demonstrate that miR-122 overexpression sensitizes hepatoma cells to anti-cancer drugs, such as Sorafenib or Doxorubicin [*298*, *299*, *385*], thus the upregulation of miR-122 could offer a promising tool for inhibiting tumor growth.

Table 4.1: Aberrant expression of miR-122 and TGFβ1 in human diseases based on recent publications. Downregulation of miR-122 levels (↓) and increased *TGFβ1* mRNA levels (↑) are illustrated as arrows.

Disease	miR-122	Reference	TGFβ1	Reference
HBV	↓	[*346*]	↑	[*578*, *671*, *672*]
HCC/ HBV	↓	[*318*, *319*]	↑	[*673*, *674*]
NAFLD	↓	[*312*, *326*, *675*]	↑	[*578*, *676*]
Fibrosis	↓	[*316*]	↑	[*677*, *678*]
HCC	↓	[*297*, *317*, *318*, *376*]	↑	[*679*, *680*]
PBC	↓	[*314*]	↑	[*681*]

Despite novel insights into the regulation of miR-122 biogenesis presented here, the regulatory activities of cytokines on miR-122 expression remain contradictory. While Rivkin *et al.* demonstrated that TNFα activates miR-122 promoter [*682*], which is in agreement to the increased promoter activity in response to TNFα administration illustrated in this work, Li *et al.* have reported that TNFα indirectly inhibits miR-122 expression through the repression of C/EBPα [*683*]. Overall, these contradictory findings indicate that complex interactions are at play and more comprehensive studies are required to decipher the regulatory interactions linking miR-122 biogenesis and signaling pathways triggered by cytokines. In addition, the

physiological function of pri-miR-122 upregulation in response to BMP6, TNFα, and IL10 as observed in this study require further investigation. Elevated levels of BMP6 ameliorate fibrosis in NAFLD patients [*684*]. Hence, it would be of interest to investigate whether BMP6-induced upregulation of miR-122 expression may contribute to the reported anti-fibrotic effect of BMP6 in patients with NAFLD.

4.2 Polysome profiling identified large regulatory networks downstream to miR-122

Polyribosomes are a complex consisting of ribosomes bound to actively-translated mRNA and the nascent polypeptide chains [*230*, *231*]. Polysomes associated with highly translated mRNAs are denser than polysomes associated with poorly translated mRNAs. The fractionation of polyribosomes is a widely-used technique to study the cellular translatome in various samples and experimental settings [*271*, *685–687*]. Importantly, miRNAs cosediment with their polyribosome-associated target mRNAs, which makes the analysis of polysomes a useful technique to determine potential miRNA target genes on a genome-wide scale [*232*, *235–238*]**.**

In the work presented in this thesis, polyribosomal profiling combined with genome-wide microarray analyses of polysome-associated mRNAs were conducted to study the effect of miR-122 overexpression or miR-122 inhibition on the translatome of Huh-7 cells (Figures 3.4 – 3.6). Altogether, 12,877 transcripts (51.6% of all transcripts identified by microarray chip analyses) were found significantly regulated across the different polysomal pools. An intersection with the *miRWalk* target prediction tool recognized that a subset of 25.8 – 54.5% of regulated transcripts were potential miR-122 targets (Appendix Figure 7.1). These findings indicated that the modulation of miR-122 levels had the potential to affect the translation of a large number of transcripts in Huh-7 cells. Using bioinformatic tools, it was identified that a substantial number of miR-122-responsive genes were under the transcriptional control of common transcription factors, among others the hepatocyte nuclear factors HNF1α or HNF1β (Figure 3.7 and Table 3.1). Interestingly, the expression of miR-122 itself is modulated by the activity of liver-enriched transcription factors such as HNF1α which directly bind to the *MIR122* promoter and trigger pri-miR-122 transcription [*119*, *282*]. This positive regulation is crucial for the gradual activation of miR-122 transcription during liver development [*278*, *282*]. Taken together with the observation that miR-122 modulates the

expression of genes downstream to HNF1α (Figure 3.7 B), it is conceivable that one of the functions of miR-122 is to fine-tune the action of liver-enriched transcription factors in order to balance out the hepatic gene expression during embryogenesis and in the adult liver.

The relevance of miR-122 for the maintenance of liver physiology is further strengthened by the fact that deregulation of this miRNA is associated to the pathogenesis of liver diseases [*312*, *313*, *315*, *317*, *318*]. In line with this, data presented in this study indicate that miR-122-responsive genes as well as the transcription factors that regulate subsets of these genes are tightly related to liver malignancies such as fibrosis, hepatic inflammation, viral infections, and HCC (Table 3.1 and Table 3.3). For instance, in mouse models of liver fibrosis, the transcription factor serum response factor (SRF) promotes the production of reactive oxygen species and drives the expression of pro-fibrotic genes (e.g. collagen type I or alpha smooth muscle actin) in hepatic stellate cells [*437*, *688*]. This pro-fibrotic phenotype was attenuated by hepatic stellate cell-specific knockout of SRF [*437*, *438*]. Moreover, SRF was identified as direct target for miR-122 in hepatic stellate cells as well an in human hepatoma cell lines [*298*, *437*]. These data point towards a link between miR-122 downregulation and SRF upregulation during fibrogenesis [*316*, *437*].

A detailed analysis of the miR-122-responsive network by polysomal profiling identified 1,193 genes that were controlled by the transcription factors YY1, E2F4, FOXP3, and NRF1 (Figure 3.7 and Figure 3.8). These transcription factors as well as their target genes, are frequently upregulated and hence inversely correlated with hepatic miR-122 levels in patients with chronic liver diseases (Table 3.1). Hepatic *FOXP3* mRNA levels for example are elevated during liver inflammation in patients with chronic HBV and HCV as well as in NAFLD patients and individuals suffering from autoimmune disease [*398*]. Interestingly, *FOXP3* mRNA levels correlate with the degree of inflammation and significantly decrease in the remission state compared to the diseased state [*398*, *399*]. Wang *et al.* described that FOXP3 protein is undetectable in healthy liver tissue, but present in 70% of HCC tumor tissues associated with liver cirrhosis, indicating a potential role in the progression of HCC [*400*]. In addition to FOXP3, the transcription factor E2F4 was also described in the context of liver cancer. E2F4 modulates the cell cycle progression by acting as translational repressor to maintain cell cycle arrest, whereas in cancer tissue E2F4 was described to function primarily as oncogene [*397*]. Several genetic and epigenetic alterations were associated with E2F4 in HCC and a recent study reported that *E2F4* mRNA is significantly elevated in HCC tissue and associated with poor

prognosis [*395–397*]. While mRNA levels of *FOXP3* were too low for proper quantification in Huh-7 cells, in this study it was shown that miR-122 overexpression significantly reduced mRNA abundance of *E2F4* mRNA after 24 and 48 h (Figure 3.11). Collectively, these data support the conclusion that miR-122 and E2F4 regulatory networks are tightly linked to each other.

Another transcription factor identified to regulate miR-122-responsive genes is YY1. The upregulation of YY1 contributes to the development of fatty liver diseases in obese mouse through the inhibition of the farnesoid X receptor (FXR), which in turn transcriptionally regulates enzymes of the triglyceride metabolism [*443*, *689*]. Both, the overexpression of YY1 as well as the downregulation of FXR were confirmed in the liver of NAFLD patients [*443*, *689*]. Interestingly, He *et al.* demonstrated a significant correlation between FXR downregulation and miR-122 suppression in HCC tissue as well as in cancer cell lines, and further validated miR-122 as transcriptional target gene of farnesoid X receptor [*690*]. In addition, a significant upregulation of YY1 occurs in HCC tissue compared to para-tumor tissue and YY1 was found to facilitate lipid metabolism in HCC cell lines [*447*, *450*]. Based on these studies, it is conceivable that the upregulation of YY1 and the downregulation of FXR accompanied by the reduction of miR-122 may be interconnected in the pathogenesis of fatty liver diseases and liver cancer. A recent study suggests that miR-122 directly targets *YY1* mRNA at the 3´UTR [*445*], indicating that YY1 and miR-122 might constitute a regulatory circuit. However, the data presented here did not confirm a direct effect of miR-122 on the relative expression of *YY1* mRNA (Figure 3.11). These inconsistent findings may be explained by different concentrations that were used for studying the effect of miR-122 on target gene expression, since a 8-fold higher concentration of miR-122 mimic was used in the study of Wu *et al.* compared to the experiments performed for this thesis [*445*].

As illustrated in Figure 3.7, modulation of miR-122 levels affects the expression of genes downstream to the nuclear respiratory factor NRF1. Knockout studies in mice provide evidence for a crucial role of murine NRF1 during embryogenesis due to high embryonic lethality in transgenic animals [*422*]. Moreover, in the adult liver, the inactivation of NRF1 results in liver steatosis, inflammation, fibrosis, and tumor development [*422*]. NRF1 is a key regulator of mitochondrial biogenesis and an important player of the antioxidant defense [*691*, *692*]. Interestingly, the overexpression of miR-122 triggered a significant downregulation of *NRF1* mRNA expression in Huh-7 after 48 h (Figure 3.11). Together with the fact that

miR-122 regulated genetic networks downstream to NRF1 as shown in this work, these findings shed new light on the function of miR-122 in the regulation of oxidative stress response as well as the maintenance of mitochondria function [*288*, *319*].

With the purpose of seeking corroboration for the findings presented in this thesis, microarray data from *MIR122* knockout and wild type mice [*295*] as well as from human HCC tissue and adjacent healthy tissue [*393*] were downloaded from the GEO repository. The data sets were reanalyzed using the identical parameters employed for the analysis of the polysomal profiling. As outlined in Table 3.2 C, the hepatic expression of genes regulated by YY1 and FOXP3, E2F4, and NRF1 was significantly altered in healthy liver tissue from *MIR122* knockout mice *versus* wild type control. Moreover, similar networks were enriched in HCC specimen of *MIR122* knockout mice compared to healthy liver tissue of matching wild-type controls. In good agreement with this, re-analysis of transcriptome data from human HCC tissue *versus* surrounding healthy liver tissue revealed that the expression of genes downstream to FOXP3, NRF1, and YY1 was significantly enriched in tumor tissue (Table 3.2 D; [*393*]). Based on these results, it is proposed that very similar regulatory networks are affected in miR-122 depleted animals, in human HCC tissue and in the human hepatoma cell line Huh-7 following modulation of miR-122 levels with miRNA mimics or inhibitors. These data also suggest that the regulation of transcription factor-driven networks may be partially conserved across human and mice.

To further study the effect of miR-122 on the genes downstream to the aforementioned transcription factors, mRNA levels of selected target gene candidates were assessed in response to miR-122 overexpression (Figure 3.10). Overall the majority of genes were found significantly or tendentially reduced at the mRNA level after miR-122 mimic transfection. Using *RNA22*, numerous potential binding motifs were determined in the 3´UTRs of the selected target gene candidates (Appendix Figure 7.3), encouraging the idea that miR-122 may directly regulate these transcripts. Of note, among the putative target genes identified by polysomal profiling included in this thesis, a few genes have already been validated as direct miR-122 target genes. For instance, *P4HA1* that encodes for the alpha-1 subunit of the prolyl 4-hydroxylase and that participates in collagen maturation is directly downregulated by miR-122 in hepatic stellate cells, thus preventing excessive collagen production [*546*]. A decline of miR-122 accompanied by an increase in P4HA1 at the mRNA and the protein level was further observed in the liver of CCl_4-induced fibrotic mice [*546*].

Taken together, the results obtained from polysomal profiling suggest that miR-122 regulates large networks comprising the genes downstream to the transcription factors YY1, E2F4, FOXP3, and NRF1. Based on these data, it is hypothesized that miR-122 downregulation as observed in patients with chronic liver diseases, together with a consequent dysregulation of YY1, E2F4, FOXP3, and NRF1-dependent transcription, may be one of the molecular mechanisms linking miR-122 to the pathogenesis of liver diseases (Figure 4.1). Nevertheless, future studies are required to elucidate the downstream networks of miR-122 in detail. It would be of special interest to investigate which mechanisms drive the debalancing of the miR-122 regulatory network. Furthermore, intensive work will be necessary to discriminate which miR-122-responsive genes are directly targeted by miR-122 and which are deregulated based on indirect mechanisms.

4.3 Direct targeting of disease-associated proteins by miR-122

The miRNA-mediated target gene repression results in the reduction of target protein. Since the underlying mechanisms are diverse and may imply either a translational repression or the degradation of messengers, miRNA target identification is hardly possible based only on transcriptome analyses. Moreover, changes of the cellular transcriptome and the cellular proteome may not be identical due to different kinetics underlying the synthesis as well as the degradation of both, mRNA and protein [*613*]. To investigate the effects of miR-122 overexpression and miR-122 inhibition on the protein level of Huh-7, proteome analyses were carried out in this study. Altogether 504 proteins were quantified in Huh-7 of which 133 proteins were inversely correlated with respect to the cellular levels of miR-122, meaning that they were found in higher abundance in response to miR-122 inhibition or in lower abundance after miR-122 overexpression (Figure 3.12 and 3.13). Of note, the comparison of microarray data with proteome data revealed a partial overlap of the two approaches. For instance, the miR-122-responsive proteins G6PDH, FBLIM1, LAMC1, SORT1, CLIC1, and SLC1A5 were also identified as miR-122-responsive genes by microarray analyses conducted on polyribosomes isolated from Huh-7 (Appendix Figure 7.6).

A Gene Ontology term enrichment analysis with regard to biological processes as well as cellular components was conducted to gain insight into the functional consequences of miR-122 deregulation (Figure 3.14 and Appendix Figure 7.4). The GO analysis of the identified miR-122-responsive proteins suggested that overexpression of miR-122 downregulates

proteins participating in glycolysis, and oxoacid metabolic processes. The latter includes all processes involving keto acids such as pyruvate according to the *Gene Ontology Browser* [*693*]. These findings are in line with already known functions of miR-122, since miR-122 targets glycolytic genes such as *pyruvate kinase M2*, *aldolase A*, or *phosphofructokinase 2* [*383*]. Among the proteins found to be upregulated in miR-122 mimic transfected cells, an enrichment for proteins of metabolic processes was noted. These data compare well with previous studies showing a decline in hepatic fatty acid and cholesterol synthesis in miR-122 knockout animals [*292*, *694*]. The GO enrichment analysis for terms regarding cellular components revealed an involvement of miR-122-responsive proteins in the modulation of mitochondria functionality or biogenesis. These findings are consistent with a recent publication illustrating that miR-122 is crucial for the maintenance of mitochondrial metabolic functions and that a reduction of miR-122 expression as found in HCC specimen heavily impairs mitochondria integrity [*319*]. It was further demonstrated that the overexpression of miR-122 downregulates proteins associated with extracellular vesicles and exosomes. Albeit the implication of this finding remains elusive, it is interesting to note that levels of extracellular miR-122 are upregulated in rat serum following partial hepatectomy and that elevated serum levels of miR-122 are considered as promising biomarker for drug-induced liver injuries and HCC in humans [*695–697*].

Next, the proteins with an inverse correlation with miR-122 levels were further investigated as these encompass proteins that are potentially silenced by miR-122 through direct interactions. Remarkably, among those 133 proteins, 73% were identified as predicted miR-122 targets by the target prediction algorithm *miRWalk.* A substantial number of these proteins has been described as dysregulated in the livers of patients with different types of liver diseases, e.g. HCC (Table 3.4). For instance, kinesin family member 11 (KIF11) and the centrosomal protein CEP55 which are involved in mitosis or in cytokinesis, respectively, are significantly upregulated in HCC tissue compared to healthy liver tissue [*614*, *629*]. Thymidine kinase 1 (TK1), an enzyme participating in DNA synthesis expressed during the S phase of cell division [*698*], is elevated in serum and in cancerous tissue of HCC patients [*646*, *647*]. The increase of serum TK1 levels is already detected at early clinical stage, making TK1 an attractive biomarker for early diagnostic and prognosis of cancer progression [*699*, *700*]. Moreover, the epidermal growth factor receptor (EGFR) substrate EPS15L1 (or EPS15R; [*701*]) was downregulated at the protein level in response to miR-122 overexpression in Huh-7 cells.

EPS15L1 as well as the EGFR substrate EPS15 are concordantly induced in human HCC tissue, probably via the action of HNF4α [*618*]. Niehof *et al.* hypothesized that EPS15L1 and EPS15 trigger receptor internalization of activated EGFR, thus increasing its recycling and turnover and thereby amplifying EGFR-driven tumorigenesis [*618*, *702*]. Furthermore, a number of transporter proteins were identified as miR-122-responsive proteins. For instance, the intracellular chloride channel 1 (CLIC1) was shown to act as oncogene by promoting cancer cell proliferation [*616*, *703*, *704*]. Another member of the group of transporter proteins is the neutral amino acid transporter SLC1A5 (ASCT2), an importer that preferentially uptakes glutamine into cells [*705*, *706*]. Glutamine is not only a substrate for protein synthesis, but also a critical regulator of cell growth and proliferation [*707*]. The underlying mechanisms mediating the proliferative effect of glutamine are highly diverse and embrace the induction of volume-sensitive signaling cascades and of antioxidant defense strategies via glutathione synthesis [*707*–*709*]. Therefore, the availability of glutamine may be an essential factor determining the growth and the metastatic potential of cancer cells [*707*]. Besides glutamine, rapidly dividing cancer cells consume great amounts of nucleosides for nucleic acid synthesis and NADPH for oxidative stress defense. Remarkably, proteome analysis revealed an inverse correlation between miR-122 and glucose-6-phophate dehydrogenase (G6PDH), the key enzyme of the pentose phosphate pathway [*651*, *652*]. The major products of this pathway are ribose-5-phosphate, NADPH and glutathione, hence G6PDH is a crucial factor limiting the nucleic acid synthesis and the oxidative stress defense [*651*, *652*]. G6PDH is a well-known oncogene and elevated G6PDH levels are observed in various cancer types, including breast, lung, colon, and liver cancers [*654*, *710*]. Notably, G6PDH has been proposed as therapeutic target in HCC as suppression of G6PDH is sufficient to inhibit cancer cell migration and invasion [*622*].

These data collectively indicate that miR-122 may modulate the expression of various processes that, if unbalanced, may contribute to either cancer development or progression or both, such as cytokinesis, signal transduction as well as cellular metabolism. This hypothesis is strengthened by the observation that miR-122 overexpression results in the decline of mRNA levels and partially of protein levels of the aforementioned target gene candidates (Figure 3.16 and Figure 3.17). Reporter gene assays provide evidence for a direct interaction of miR-122 with the 3´UTRs of human *G6PDH*, *TK1*, *CLIC1*, *CEP55*, *KIF11* and *SLC1A5* (Figure 3.19). These findings are in agreement with studies proposing SLC1A5 as miR-122

target gene candidate [*711*, *712*] and with a very recent publication validating G6PDH as direct target of miR-122 in Huh-7 cells [*713*]. In contrast, albeit downregulation of EPS15L1 on mRNA and protein levels was observed, and even though various predicted miR-122 binding motifs were identified in the *EPS15L1* 3´UTR (Figure 3.18), the luciferase assay did not confirm a direct effect of miR-122 (Figure 3.19). However, it must be considered that the functional interaction of miRNA-mRNA depends in part on the ratio of both components as well as the binding affinity to one another [*714*, *715*]. Since levels of target 3´UTR sequences are relatively high abundant in cells transfected with recombinant reporter plasmids, one could speculate that efficient miR-122 repression of EPS15L1 3´UTR may require higher amounts of miR-122 mimic.

4.4 Possible implications of miR-122 mediated *G6PDH* regulation in hepatitis B virus infections

Hepatitis B is a contagious liver disease with worldwide distribution. While the majority of adults recover from acute hepatitis B infection, 5% are at risk of developing a chronic manifestation of hepatitis B. The likelihood for a chronic hepatitis B (CHB) is strongly correlated with young age at first exposure to the virus and HBV infections in early childhood may become chronic in up to 90% of all cases [*716*]. CHB patients have a significantly elevated probability to develop secondary chronic liver diseases such as cirrhosis and subsequently HCC [*717*].

A growing number of evidence points to a virostatic effect of miR-122 on hepatitis B replication *in vitro* and *in vivo* [*315*, *318*, *319*, *338*, *339*]. Different aspects of the antiviral effect of miR-122 have already been described, such as the activation of p53 signaling pathways via the suppression of Cyclin G1, or the induction of IFN signaling through silencing of *SOCS3* [*315*, *344*]. However, the downregulation of hepatic miR-122 expression in CHB carriers suggest that HBV is able to circumvent miR-122-mediated antiviral defense by decreasing miR-122 stability. This is achieved by HBV through suppressing poly(A) polymerase Gld2 and by sequestering miR-122 through binding to viral mRNA [*338*, *346*, *348*]. Moreover, independent studies have shown that the viral HBx protein has the ability to amplify TGFβ-induced signaling pathways [*718–720*]. Liu and colleagues demonstrated that HBx protein triggers the proteasomal degradation of protein phosphatase magnesium dependent 1A (PPM1A) which terminates TGFβ-dependent signaling cascades by dephosphorylating the effectors proteins SMAD2 and SMAD3 [*720*]. Taken together with the observed TGFβ-mediated downregulation of miR-122

transcription in this study (Figure 3.24), it is now proposed that HBV-driven enhancement of TGFβ1 signaling could be one of the factors contributing to miR-122 deficiency in the liver of CHB patients (Figure 4.2). Furthermore, the downregulation of miR-122 may further amplify TGFβ1 signaling, since miR-122 was shown to target TGFβ1 or TGFβ receptor in mouse and human (Figure 4.1 and Figure 4.2) [*669*].

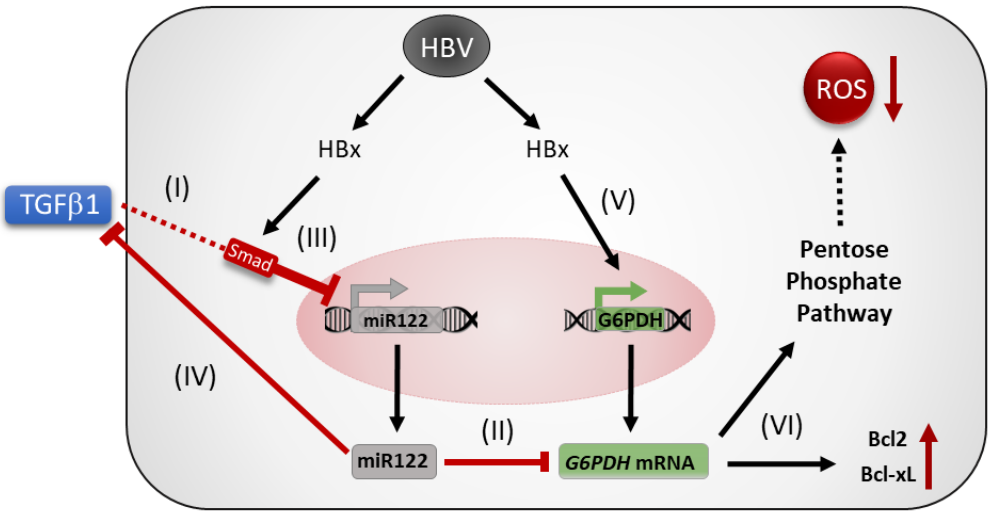

Figure 4.2: Proposed contribution of miR-122 in the pathogenesis of HBV-associated HCC. (I) Data presented in this thesis indicate that miR-122 transcription is inhibited by TGFβ1 and **(II)** that miR-122 targets the oncogene *glucose-6-phosphate dehydrogenase* (*G6PDH*) mRNA. **(III)** In HBV infected hepatocytes, it was shown that the viral HBx protein enhances TGFβ1 signaling [*718–720*], which may result in depression of endogenous miR-122 in HBV infected hepatocytes. Through this mechanism, HBx may indirectly downregulate miR-122 levels and reduce the antiviral effects of miR-122 [*338*, *346*, *348*]. **(IV)** The downregulation of miR-122 may release *TGFβ1* mRNA from miR-122-mediated inhibition, thus amplifying TGFβ1-dependent signaling cascades [*669*]. **(V)** It was reported that HBx activates *G6PDH* expression via the induction of the transcription factor NRF2 [*655*]. **(VI)** The upregulation of G6PDH enhances cell survival via the activation of anti-apoptotic proteins like Bcl2/ Bcl-xL and by accelerating the pentose phosphate pathway [*651*, *652*, *721*]. The downregulation of miR-122 and the coincident upregulation of *G6PDH* may be one of the mechanisms promoting the transformation of hepatocytes to a malignant phenotype.

The present study adds novel insights into the functional role played by miR-122 in the regulation of G6PDH in CHB patients. In hepatocytes, the viral HBx protein triggers *G6PDH* expression by induction of the transcription factor NRF2 [*655*]. The expression of G6PDH is significantly elevated in the liver of CHB patients [*655*]. G6PDH is a well-known oncogene which mediates metabolic changes observed in cancer cells via the activation of the pentose phosphate pathway [*651*, *652*]. In addition, an enhancement of G6PDH results in an increased expression of anti-apoptotic factors including Bcl-2 and Bcl-xl [*721*], hence further promoting cell growth and tumor development [*721*]. Therefore, G6PDH has been proposed as

therapeutic target in HCC, since suppression of G6PDH is sufficient to inhibit tumor progression [*622*]. In line with this, Dore *et al.* examined that G6PDH deficiency decreases the risk for HCC development in humans [*710*]. Here, it was demonstrated that miR-122 levels inversely correlate in tumor specimen of HCC patients with viral hepatitis B infection, whereas no correlation was found in patients without viral infections (Figure 3.21). Furthermore, G6PDH was shown to be a direct target of miR-122 (this study and [*713*]).

Taken together, the deficiency of hepatic miR-122 as observed in CHB carriers may be another mechanism contributing to an increase of G6PDH levels in the liver of CHB patients. As a possible consequence of G6PDH elevation, metabolic changes may be triggered which participate in the early events of hepatocyte transformation and eventually increase the likelihood for the development of HCC (Figure 4.2).

4.5 Outlook

In conclusion, the present study places miR-122 into a central position in the regulation and fine-tuning of liver homeostasis. It is proposed that alterations in the signaling pathways driven by cytokines and growth factors may be one of the factors contributing to miR-122 dysregulation. As a possible result, the decoupling of miR-122 from its regulatory networks including those controlled by YY1, FOXP3, NRF1, and E2F4 may be one of the molecular mechanisms participating in the complex cellular changes that are involved in the pathogenesis of chronic liver diseases. The work presented in this thesis provides new insights into the molecular mechanisms governing the transcription of human *MIR122* and the potential consequences for the liver function that may result from alterations of hepatic miR-122 levels. Yet, more work is required to understand the effects of miR-122 in the liver and the contribution of miR-122 dysregulation at the onset of liver disease. Specifically, it would be necessary to develop experimental models dedicated to evaluate how the biogenesis of miR-122 is affected during the pathogenesis of chronic liver diseases. In addition, new studies and methodological approaches would be required to elucidate in detail the effects of alterations of miR-122 levels on the hepatic homeostasis.

5. Literature

[1] Morris KV, Mattick JS (2014). The rise of regulatory RNA. *Nat. Rev. Genet.* **15**, 423–437.

[2] Crick F (1970). Central dogma of molecular biology. *Nature*. **227**, 561–563.

[3] Kapranov P, Cawley SE, Drenkow J, Bekiranov S, Strausberg RL, Fodor SPA, Gingeras TR (2002). Large-scale transcriptional activity in chromosomes 21 and 22. *Science.* **296**, 916–919.

[4] The FANTOM Consortium and the RIKEN Genome Exploration Research Group Phase I & II Team (2002). Analysis of the mouse transcriptome based on functional annotation of 60,770 full-length cDNAs. *Nature*. **420**, 563–573.

[5] Rinn JL, Euskirchen G, Bertone P, Martone R, Luscombe NM, Hartman S, Harrison PM, Nelson FK, Miller P, Gerstein M, Weissman S, Snyder M (2003). The transcriptional activity of human chromosome 22. *Genes Dev.* **17**, 529–540.

[6] Bertone P, Stolc V, Royce TE, Rozowsky JS, Urban AE, Zhu X, Rinn JL, Tongprasit W, Samanta M, Weissman S, Gerstein M, Snyder M (2004). Global identification of human transcribed sequences with genome tiling arrays. *Science.* **306**, 2242–2246.

[7] Cheng J, Kapranov P, Drenkow J, Dike S, Brubaker S, Patel S, Long J, Stern D, Tammana H, Helt G, Sementchenko V, Piccolboni A, Bekiranov S, Bailey DK, Ganesh M, Ghosh S, Bell I, Gerhard DS, Gingeras TR (2005). Transcriptional maps of 10 human chromosomes at 5-nucleotide resolution. *Science.* **308**, 1149–1154.

[8] The ENCODE Project Consortium (2012). An integrated encyclopedia of DNA elements in the human genome. *Nature*. **489**, 57–74.

[9] The ENCODE Project Consortium (2007). Identification and analysis of functional elements in 1% of the human genome by the ENCODE pilot project. *Nature*. **447**, 799–816.

[10] Palazzo AF, Lee ES (2015). Non-coding RNA: What is functional and what is junk? *Front. Genet.* **6**, 2.

[11] Goodrich JA, Kugel JF (2006). Non-coding-RNA regulators of RNA polymerase II transcription. *Nat. Rev. Mol. Cell Biol.* **7**, 612–616.

[12] Mattick JS (1994). Introns: Evolution and function. *Curr. Opin. Genet. Dev.* **4**, 823–831.

[13] Sana J, Faltejskova P, Svoboda M, Slaby O (2012). Novel classes of non-coding RNAs and cancer. *J. Transl. Med.* **10**, 103.

[14] Diamantopoulos MA, Tsiakanikas P, Scorilas A (2018). Non-coding RNAs: The riddle of the transcriptome and their perspectives in cancer. *Ann. Transl. Med.* **6**, 241.

[15] Qu Z, Adelson DL (2012). Evolutionary conservation and functional roles of ncRNA. *Front. Genet.* **3**, 205.

[16] Palade GE (1955). A small particulate component of the cytoplasm. *J. Biophys. Biochem. Cytol.* **1**, 59–68.

[17] Hoagland MB, Stephson ML, Scott JF, Hecht LI, Zamecnik PC (1958). A soluble ribonucleic acid intermediate in protein synthesis. *J. Biol. Chem.* **231**, 241–257.

[18] Weinberg R, Penman S (1968). Small molecular weight monodisperse nuclear RNA. *J. Mol. Biol.* **38**, 289–304.

[19] Weinberg R, Penman S (1969). Metabolism of small molecular weight monodisperse nuclear RNA. *Biochim. Biophys. Acta*. **190**, 10–29.

[20] Jarmolowski A, Zagorski J, Li H V., Fournier MJ (1990). Identification of essential elements in U14 RNA of *Saccharomyces cerevisiae*. *EMBO J.* **9**, 4503–4509.

[21] Batagov AO, Yarmishyn AA, Jenjaroenpun P, Tan JZ, Nishida Y, Kurochkin I V. (2013). Role of genomic architecture in the expression dynamics of long noncoding RNAs during differentiation of human neuroblastoma cells. *BMC Syst. Biol.* **16**, S11.

[22] Laurent GS, Wahlestedt C, Kapranov P (2015). The landscape of long non-coding RNA classification. *Trends Genet.* **31**, 239–251.

[23] Brosnan CA, Voinnet O (2009). The long and the short of noncoding RNAs. *Curr. Opin. Cell Biol.* **21**, 416–425.

[24] Lee RC, Feinbaum RL, Ambros V (1993). The *C. elegans* heterochronic gene *lin-4* encodes small RNAs with antisense complementarity to *lin-14*. *Cell*. **75**, 843–854.

[25] Wightman B, Ha I, Ruvkun G (1993). Posttranscriptional regulation of the heterochronic gene *lin-14* by *lin-4* mediates temporal pattern formation in *C. elegans*. *Cell*. **75**, 855–862.

[26] Reinhart BJ, Slack FJ, Basson M, Pasquienelli AE, Bettlnger JC, Rougvle AE, Horvitz HR, Ruvkun G (2000). The 21-nucleotide *let-7* RNA regulates developmental timing in *Caenorhabditis elegans*. *Nature*. **403**, 901–906.

[27] Slack FJ, Basson M, Liu Z, Ambros V, Horvitz HR, Ruvkun G (2000). The *lin-41* RBCC gene acts in the *C. elegans* heterochronic pathway between the *let-7* regulatory RNA and the LIN-29 transcription factor. *Mol. Cell*. **5**, 659–669.

[28] Pasquinelli AE, Reinhart BJ, Slack F, Martindale MQ, Kuroda MI, Maller B, Hayward DC, Ball EE, Degnan B, Müller P, Spring J, Srinivasan A, Fishman M, Finnerty J, Corbo J, Levine M, Leahy P, Davidson E, Ruvkun G (2000). Conservation of the sequence and temporal expression of *let-7* heterochronic regulatory RNA. *Nature*. **408**, 86–89.

[29] Lau NC, Lim LP, Weinstein EG, Bartel DP (2001). An abundant class of tiny RNAs with probable regulatory roles in *Caenorhabditis elegans*. *Science.* **294**, 858–862.

[30] Lagos-Quintana M, Rauhut R, Lendeckel W, Tuschl T (2001). Identification of novel genes coding for small expressed RNAs. *Science.* **294**, 853–858.

[31] Lee RC, Ambros V (2001). An extensive class of small RNAs in *Caenorhabditis elegans*. *Science.* **294**, 862–864.

[32] Babak T, Zhang W, Morris Q, Blencowe BJ, Hughes TR (2004). Probing microRNAs with microarrays: Tissue specificity and functional inference. *RNA*. **10**, 1813–1819.

[33] Barad O, Meiri E, Avniel A, Aharonov R, Barzilai A, Bentwich I, Einav U, Gilad S, Hurban P, Karov Y, Lobenhofer EK, Sharon E, Shiboleth YM, Shtutman M, Bentwich Z, Einat P (2004). MicroRNA expression detected by oligonucleotide microarrays: System establishment and expression profiling in human tissues. *Genome Res.* **14**, 2486–2494.

[34] Liu CG, Calin GA, Meloon B, Gamliel N, Sevignani C, Ferracin M, Dumitru CD, Shimizu M, Zupo S, Dono M, Alder H, Bullrich F, Negrini M, Croce CM (2004). An oligonucleotide microchip for genome-wide microRNA profiling in human and mouse tissues. *Proc. Natl. Acad. Sci. U. S. A.* **101**, 9740–9744.

[35] Nelson PT, Baldwin DA, Scearce LM, Oberholtzer JC, Tobias JW, Mourelatos Z (2004). Microarray-based, high-throughput gene expression profiling of microRNAs. *Nat. Methods*. **1**, 155–161.

[36] Thomson JM, Parker J, Perou CM, Hammond SM (2004). A custom microarray platform for analysis of microRNA gene expression. *Nat. Methods*. **1**, 47–53.

[37] Lu C, Tej SS, Luo S, Haudenschild CD, Meyers BC, Green PJ (2005). Elucidation of the small RNA component of the transcriptome. *Science*. **309**, 1567–1569.

[38] Ruby JG, Jan C, Player C, Axtell MJ, Lee W, Nusbaum C, Ge H, Bartel DP (2006). Large-scale sequencing reveals 21U-RNAs and additional microRNAs and endogenous siRNAs in *C. elegans*. *Cell*. **127**, 1193–1207.

[39] Griffiths-Jones S, Grocock R, Van Dongen S, Bateman A, Enright A (2006). miRBase: MicroRNA sequences, targets and gene nomenclature. *Nucleic Acids Res.* **34**, D140-4.

[40] Kozomara A, Birgaoanu M, Griffiths-Jones S (2019). miRBase: From microRNA sequences to function. *Nucleic Acids Res.* **47**, D155–D162.

[41] Lewis BP, Burge CB, Bartel DP (2005). Conserved seed pairing, often flanked by adenosines, indicates that thousands of human genes are microRNA targets. *Cell*. **120**, 15–20.

[42] Ambros V (2003). MicroRNA pathways in flies and worms: Growth, death, fat, stress, and timing. *Cell*. **113**, 673–676.

[43] Xu P, Vernooy SY, Guo M, Hay BA (2003). The *Drosophila* microRNA mir-14 suppresses cell death and is required for normal fat metabolism. *Curr. Biol.* **13**, 790–795.

[44] Houbaviy HB, Murray MF, Sharp PA (2003). Embryonic stem cell-specific microRNAs. *Dev. Cell*. **5**, 351–358.

[45] Bartel DP (2004). MicroRNAs: Genomics , biogenesis, mechanism, and function. *Cell*. **116**, 281–297.

[46] Brennecke J, Hipfner DR, Stark A, Russell RB, Cohen SM (2003). *bantam* encodes a developmentally regulated microRNA that controls cell proliferation and regulates the proapoptotic gene *hid* in *Drosophila*. *Cell*. **113**, 25–36.

[47] Calin GA, Sevignani C, Dumitru CD, Hyslop T, Noch E, Yendamuri S, Shimizu M, Rattan S, Bullrich F, Negrini M, Croce CM (2004). Human microRNA genes are frequently located at fragile sites and genomic regions involved in cancers. *Proc. Natl. Acad. Sci. U. S. A.* **101**, 2999–3004.

[48] Lu J, Getz G, Miska EA, Alvarez-Saavedra E, Lamb J, Peck D, Sweet-Cordero A, Ebert BL, Mak RH, Ferrando AA, Downing JR, Jacks T, Horvitz HR, Golub TR (2005). MicroRNA expression profiles classify human cancers. *Nature*. **435**, 834–838.

[49] O'Donnell KA, Wentzel EA, Zeller KI, Dang C V., Mendell JT (2005). c-Myc-regulated microRNAs modulate E2F1 expression. *Nature*. **435**, 839–843.

[50] He L, Thomson JM, Hemann MT, Hernando-Monge E, Mu D, Goodson S, Powers S, Cordon-Cardo C, Lowe SW, Hannon GJ, Hammond SM (2005). A microRNA polycistron as a potential human oncogene. *Nature*. **435**, 828–833.

[51] van Rooij E, Sutherland LB, Liu N, Williams AH, McAnally J, Gerard RD, Richardson JA, Olson EN (2006). A signature pattern of stress-responsive microRNAs that can evoke cardiac hypertrophy and heart failure. *Proc. Natl. Acad. Sci. U. S. A.* **103**, 18255–18260.

[52] Rane S, He M, Sayed D, Vashistha H, Malhotra A, Sadoshima J, Vatner DE, Vatner SF, Abdellatif M (2009). Downregulation of miR-199a derepresses hypoxia-inducible factor-1α and sirtuin 1 and recapitulates hypoxia preconditioning in cardiac myocytes. *Circ. Res.* **104**, 879–886.

[53] Rottiers V, Näär AM (2012). MicroRNAs in metabolism and metabolic disorders. *Nat. Rev. Mol. Cell Biol.* **13**, 239–250.

[54] Fernández-Hernando C, Ramírez CM, Goedeke L, Suárez Y (2013). MicroRNAs in metabolic disease. *Arterioscler. Thromb. Vasc. Biol.* **33**, 178–185.

[55] Wang XW, Heegaard NHH, Orum H (2012). MicroRNAs in liver disease. *Gastroenterology*. **142**, 1431–1443.

[56] Szabo G, Bala S (2013). MicroRNAs in liver disease. *Nat. Rev. Gastroenterol. Hepatol.* **10**, 542–552.

[57] Wang J, Chen J, Sen S (2016). MicroRNA as biomarkers and diagnostics. *J. Cell. Physiol.* **231**, 25–30.

[58] Pal MK, Jaiswar SP, Dwivedi VN, Tripathi AK, Dwivedi A, Sankhwar P (2015). MicroRNA: A new and promising potential biomarker for diagnosis and prognosis of ovarian cancer. *Cancer Biol. Med.* **12**, 328–341.

[59] Christopher AF, Kaur RP, Kaur G, Kaur A, Gupta V, Bansal P (2016). MicroRNA therapeutics: Discovering novel targets and developing specific therapy. *Perspect. Clin. Res.* **7**, 68–74.

[60] Eun JL, Baek M, Gusev Y, Brackett DJ, Nuovo GJ, Schmittgen TD (2008). Systematic evaluation of microRNA processing patterns in tissues, cell lines, and tumors. *RNA*. **14**, 35–42.

[61] Saini HK, Griffiths-Jones S, Enright AJ (2007). Genomic analysis of human microRNA transcripts. *Proc. Natl. Acad. Sci.* **104**, 17719–17724.

[62] Saini HK, Enright AJ, Griffiths-Jones S (2008). Annotation of mammalian primary microRNAs. *BMC Genomics*. **9**, 564.

[63] Lai EC, Tomancak P, Williams RW, Rubin GM (2003). Computational identification of *Drosophila* microRNA genes. *Genome Biol.* **4**, R42.

[64] Lin SL, Chang D, Wu DY, Ying SY (2003). A novel RNA splicing-mediated gene silencing mechanism potential for genome evolution. *Biochem. Biophys. Res. Commun.* **310**, 754–760.

[65] Rodriguez A, Griffiths-Jones S, Ashurst JL, Bradley A (2004). Identification of mammalian microRNA host genes and transcription units. *Genome Res.* **14**, 1902–1910.

[66] Cai X, Hagedorn CH, Cullen BR (2004). Human microRNAs are processed from capped, polyadenylated transcripts that can also function as mRNAs. *RNA*. **10**, 1957–1966.

[67] Lee Y, Kim M, Han J, Yeom K-H, Lee S, Baek SH, Kim VN (2004). MicroRNA genes are transcribed by RNA polymerase II. *EMBO J.* **23**, 4051–4060.

[68] Borchert GM, Lanier W, Davidson BL (2006). RNA polymerase III transcribes human microRNAs. *Nat. Struct. Mol. Biol.* **13**, 1097–1101.

[69] Winter J, Jung S, Keller S, Gregory RI, Diederichs S (2009). Many roads to maturity: MicroRNA biogenesis pathways and their regulation. *Nat. Cell Biol.* **11**, 228–234.

[70] Ameres SL, Zamore PD (2013). Diversifying microRNA sequence and function. *Nat. Rev. Mol. Cell Biol.* **14**, 475–488.

[71] Denli AM, Tops BBJ, Plasterk RHA, Ketting RF, Hannon GJ (2004). Processing of primary microRNAs by the Microprocessor complex. *Nature*. **432**, 231–235.

[72] Gregory RI, Yan KP, Amuthan G, Chendrimada T, Doratotaj B, Cooch N, Shiekhattar R (2004). The Microprocessor complex mediates the genesis of microRNAs. *Nature*. **432**, 235–240.

[73] Lee Y, Ahn C, Han J, Choi H, Kim J, Yim J, Lee J, Provost P, Rådmark O, Kim S, Kim VN (2003). The nuclear RNase III Drosha initiates microRNA processing. *Nature*. **425**, 415–419.

[74] Han J, Lee Y, Yeom KH, Kim YK, Jin H, Kim VN (2004). The Drosha-DGCR8 complex in primary microRNA processing. *Genes Dev.* **18**, 3016–3027.

[75] Fukuda T, Yamagata K, Fujiyama S, Matsumoto T, Koshida I, Yoshimura K, Mihara M, Naitou M, Endoh H, Nakamura T, Akimoto C, Yamamoto Y, Katagiri T, Foulds C, Takezawa S, Kitagawa H, Takeyama KI, O'Malley BW, Kato S (2007). DEAD-box RNA helicase subunits of the Drosha complex are required for processing of rRNA and a subset of microRNAs. *Nat. Cell Biol.* **9**, 604–611.

[76] Ruby JG, Jan CH, Bartel DP (2007). Intronic microRNA precursors that bypass Drosha processing. *Nature*. **448**, 83–86.

[77] Okamura K, Hagen JW, Duan H, Tyler DM, Lai EC (2007). The mirtron pathway generates microRNA-class regulatory RNAs in *Drosophila*. *Cell*. **130**, 89–100.

[78] Zeng Y, Cullen BR (2004). Structural requirements for pre-microRNA binding and nuclear export by Exportin 5. *Nucleic Acids Res.* **32**, 4776–4785.

[79] Yi R, Qin Y, Macara IG, Cullen BR (2003). Exportin-5 mediates the nuclear export of pre-microRNAs and short hairpin RNAs. *Genes Dev.* **17**, 3011–3016.

[80] Bohnsack MT, Czaplinski K, Görlich D (2004). Exportin 5 is a RanGTP-dependent dsRNA-binding protein that mediates nuclear export of pre-miRNAs. *RNA*. **10**, 185–191.

[81] Lund E, Güttinger S, Calado A, Dahlberg JE, Kutay U (2004). Nuclear export of microRNA precursors. *Science.* **303**, 95–98.

[82] Hutvágner G, McLachlan J, Pasquinelli AE, Bálint É, Tuschl T, Zamore PD (2001). A cellular function for the RNA-interference enzyme Dicer in the maturation of the *let-7* small temporal RNA. *Science.* **293**, 834–838.

[83] Bernstein E, Caudy AA, Hammond SM, Hannon GJ (2001). Role for a bidentate ribonuclease in the initiation step of RNA interference. *Nature*. **409**, 363–366.

[84] Ketting RF, Fischer SEJ, Bernstein E, Sijen T, Hannon GJ, Plasterk RHA (2001). Dicer functions in RNA interference and in synthesis of small RNA involved in developmental timing in *C. elegans*. *Genes Dev.* **15**, 2654–2659.

[85] Knight SW, Bass BL (2001). A role for the RNase III enzyme dcr-1 in RNA interference and germ line development in *Caenorhabditis elegans*. *Science.* **293**, 2269–2271.

[86] Ma E, MacRae IJ, Kirsch JF, Doudna JA (2008). Auto-inhibition of human Dicer by its internal helicase domain. *J. Mol. Biol.* **380**, 237–243.

[87] Lee Y, Hur I, Park SY, Kim YK, Mi RS, Kim VN, Suh MR, Kim VN (2006). The role of PACT in the RNA silencing pathway. *EMBO J.* **25**, 522–532.

[88] Lee HY, Zhou K, Smith AM, Noland CL, Doudna JA (2013). Differential roles of human Dicer-binding proteins TRBP and PACT in small RNA processing. *Nucleic Acids Res.* **41**, 6568–6576.

[89] Hammond SM, Boettcher S, Caudy AA, Kobayashi R, Hannon GJ (2001). Argonaute2, a link between genetic and biochemical analyses of RNAi. *Science.* **293**, 1146–1150.

[90] Mourelatos Z, Dostie J, Paushkin S, Sharma A, Charroux B, Abel L, Rappsilber J, Mann M, Dreyfuss G (2002). miRNPs: A novel class of ribonucleoproteins containing numerous microRNAs. *Genes Dev.* **16**, 720–728.

[91] Iwasaki S, Kobayashi M, Yoda M, Sakaguchi Y, Katsuma S, Suzuki T, Tomari Y (2010). Hsc70/ Hsp90 chaperone machinery mediates ATP-dependent RISC loading of small RNA duplexes. *Mol. Cell*. **39**, 292–299.

[92] Kawamata T, Tomari Y (2010). Making RISC. *Trends Biochem. Sci.* **35**, 368–376.

[93] Salzman DW, Shubert-Coleman J, Furneaux H (2007). P68 RNA helicase unwinds the human let-7 microRNA precursor duplex and is required for let-7-directed silencing of gene expression. *J. Biol. Chem.* **282**, 32773–32779.

[94] Robb GB, Rana TM (2007). RNA helicase A interacts with RISC in human cells and functions in RISC loading. *Mol. Cell*. **26**, 523–537.

[95] Schwarz DS, Hutvágner G, Du T, Xu Z, Aronin N, Zamore PD (2003). Asymmetry in the assembly of the RNAi enzyme complex. *Cell*. **115**, 199–208.

[96] Khvorova A, Reynolds A, Jayasena SD (2003). Functional siRNAs and miRNAs exhibit strand bias. *Cell*. **115**, 209–216.

[97] Guo L, Lu Z (2010). The fate of miRNA* strand through evolutionary analysis: Implication for degradation as merely carrier strand or potential regulatory molecule? *PLoS One*. **5**, e11387.

[98] Mah S, Buske C, Humphries R, Kuchenbauer F (2010). miRNA*: A passenger stranded in RNA-induced silencing complex. *Crit. Rev. Eukaryot. Gene Expr.* **20**, 141–148.

[99] Desvignes T, Batzel P, Berezikov E, Eilbeck K, Eppig JT, McAndrews MS, Singer A, Postlethwait JH (2015). miRNA nomenclature: A view incorporating genetic origins, biosynthetic pathways, and sequence variants. *Trends Genet.* **31**, 613–626.

[100] Olejniczak M, Kotowska-Zimmer A, Krzyzosiak W (2018). Stress-induced changes in miRNA biogenesis and functioning. *Cell. Mol. Life Sci.* **75**, 177–191.

[101] Forster SC, Tate MD, Hertzog PJ (2015). MicroRNA as type I interferon-regulated transcripts and modulators of the innate immune response. *Front. Immunol.* **6**, 334.

[102] Zhou X, Li X, Wu M (2018). miRNAs reshape immunity and inflammatory responses in bacterial infection. *Signal Transduct. Target. Ther.* **3**, 14.

[103] Leung AKL, Sharp PA (2010). MicroRNA functions in stress responses. *Mol. Cell*. **40**, 205–215.

[104] Mendell JT, Olson EN (2012). MicroRNAs in stress signaling and human disease. *Cell*. **148**, 1172–1187.

[105] Cheng X, Ku CH, Siow RCM (2013). Regulation of the Nrf2 antioxidant pathway by microRNAs: New players in micromanaging redox homeostasis. *Free Radic. Biol. Med.* **64**, 4–11.

[106] Santosa D, Castoldi M, Paluschinski M, Sommerfeld A, Häussinger D (2015). Hyperosmotic stress activates the expression of members of the miR-15/107 family and induces downregulation of anti-apoptotic genes in rat liver. *Sci. Rep.* **5**, 12292.

[107] Paluschinski M, Castoldi M, Schöler D, Bardeck N, Oenarto J, Görg B, Häussinger D (2019). Tauroursodeoxycholate protects from glycochenodeoxycholate-induced gene expression changes in perfused rat liver. *Biol. Chem.* **400**, 1551–1565.

[108] Oenarto J, Karababa A, Castoldi M, Bidmon HJ, Görg B, Häussinger D (2016). Ammonia-induced miRNA expression changes in cultured rat astrocytes. *Sci. Rep.* **6**, 18493.

[109] Görg B, Karababa A, Schütz E, Paluschinski M, Schrimpf A, Shafigullina A, Castoldi M, Bidmon HJ, Häussinger D (2019). *O*-GlcNAcylation-dependent upregulation of HO1 triggers ammonia-induced oxidative stress and senescence in hepatic encephalopathy. *J. Hepatol.* **71**, 930–941.

[110] Boivin V, Deschamps-Francoeur G, Scott MS (2018). Protein coding genes as hosts for noncoding RNA expression. *Semin. Cell Dev. Biol.* **75**, 3–12.

[111] Krol J, Loedige I, Filipowicz W (2010). The widespread regulation of microRNA biogenesis, function and decay. *Nat. Rev. Genet.* **11**, 597–610.

[112] Ozsolak F, Poling LL, Wang Z, Liu H, Liu XS, Roeder RG, Zhang X, Song JS, Fisher DE (2008). Chromatin structure analyses identify miRNA promoters. *Genes Dev.* **22**, 3172–3183.

[113] Corcoran DL, Pandit KV, Gordon B, Bhattacharjee A, Kaminski N, Benos P V. (2009). Features of mammalian microRNA promoters emerge from polymerase II chromatin immunoprecipitation data. *PLoS One*. **4**, e5279.

[114] Marson A, Levine SS, Cole MF, Frampton GM, Brambrick T, Johnstone S, Guenther MG, Johnston WK, Wernig M, Newman J, Calabrese JM, Dennis LM, Volkert TL, Gupta S, Love J, Hannett N, Sharp PA, Bartel DP, Jaenisch R, Young RA (2008). Connecting microRNA genes to the core transcriptional regulatory circuitry of embryonic stem cell. *Cell*. **134**, 521–533.

[115] Bommer GT, Gerin I, Feng Y, Kaczorowski AJ, Kuick R, Love RE, Zhai Y, Giordano TJ, Qin ZS, Moore BB, MacDougald OA, Cho KR, Fearon ER (2007). p53-mediated activation of miRNA34 candidate tumor-suppressor genes. *Curr. Biol.* **17**, 1298–1307.

[116] Chang TC, Wentzel EA, Kent OA, Ramachandran K, Mullendore M, Lee KH, Feldmann G, Yamakuchi M, Ferlito M, Lowenstein CJ, Arking DE, Beer MA, Maitra A, Mendell JT (2007). Transactivation of miR-34a by p53 broadly influences gene expression and promotes apoptosis. *Mol. Cell*. **26**, 745–752.

[117] He L, He X, Lim LP, De Stanchina E, Xuan Z, Liang Y, Xue W, Zender L, Magnus J, Ridzon D, Jackson AL, Linsley PS, Chen C, Lowe SW, Cleary MA, Hannon GJ (2007). A microRNA component of the p53 tumour suppressor network. *Nature*. **447**, 1130–1134.

[118] Niu J, Shi Y, Tan G, Yang CH, Fan M, Pfeffer LM, Wu ZH (2012). DNA damage induces NF-κB-dependent microRNA-21 up-regulation and promotes breast cancer cell invasion. *J. Biol. Chem.* **287**, 21783–21795.

[119] Li ZY, Xi Y, Zhu WN, Zeng C, Zhang ZQ, Guo ZC, Hao DL, Liu G, Feng L, Chen HZ, Chen F, Lv X, Liu DP, Liang CC (2011). Positive regulation of hepatic miR-122 expression by HNF4α. *J. Hepatol.* **55**, 602–611.

[120] Monteys AM, Spengler RM, Wan J, Tecedor L, Lennox KA, Xing Y, Davidson BL (2010). Structure and activity of putative intronic miRNA promoters. *RNA*. **16**, 495–505.

[121] Seitz H, Royo H, Bortolin ML, Lin SP, Ferguson-Smith AC, Cavaillé J (2004). A large imprinted microRNA gene cluster at the mouse Dlk1-Gtl2 domain. *Genome Res.* **14**, 1741–1748.

[122] Saito Y, Jones PA (2006). Epigenetic activation of tumor suppressor microRNAs in human cancer cells. *Cell Cycle*. **5**, 2220–2222.

[123] Lujambio A, Esteller M (2007). CpG island hypermethylation of tumor suppressor microRNAs in human cancer. *Cell Cycle*. **6**, 1455–1459.

[124] Tang X, Zhang Y, Tucker L, Ramratnam B (2010). Phosphorylation of the RNase III enzyme Drosha at Serine300 or Serine302 is required for its nuclear localization. *Nucleic Acids Res.* **38**, 6610–6619.

[125] Wada T, Kikuchi J, Furukawa Y (2012). Histone deacetylase 1 enhances microRNA processing via deacetylation of DGCR8. *EMBO Rep.* **13**, 142–149.

[126] Tang X, Wen S, Zheng D, Tucker L, Cao L, Pantazatos D, Moss SF, Ramratnam B (2013). Acetylation of Drosha on the N-terminus inhibits its degradation by ubiquitination. *PLoS One*. **8**, e72503.

[127] Herbert KM, Pimienta G, DeGregorio SJ, Alexandrov A, Steitz JA (2013). Phosphorylation of DGCR8 increases its intracellular stability and induces a progrowth miRNA profile. *Cell Rep.* **5**, 1070–1081.

[128] Davis BN, Hilyard AC, Lagna G, Hata A (2008). SMAD proteins control DROSHA-mediated microRNA maturation. *Nature*. **454**, 56–61.

[129] Davis BN, Hilyard AC, Nguyen PH, Lagna G, Hata A (2010). Smad proteins bind a conserved RNA sequence to promote microRNA maturation by Drosha. *Mol. Cell*. **39**, 373–384.

[130] Suzuki HI, Yamagata K, Sugimoto K, Iwamoto T, Kato S, Miyazono K (2009). Modulation of microRNA processing by p53. *Nature*. **460**, 529–533.

[131] Kawai S, Amano A (2012). BRCA1 regulates microRNA biogenesis via the DROSHA microprocessor complex. *J. Cell Biol.* **197**, 201–208.

[132] Banin S, Moyal L, Shieh SY, Taya Y, Anderson CW, Chessa L, Smorodinsky NI, Prives C, Reiss Y, Shiloh Y, Ziv Y (1998). Enhanced phosphorylation of p53 by ATM in response to DNA damage. *Science.* **281**, 1674–1677.

[133] Wan G, Zhang X, Langley RR, Liu Y, Hu X, Han C, Peng G, Ellis LM, Jones SN, Lu X (2013). DNA-damage-induced nuclear export of precursor microRNAs is regulated by the ATM-AKT pathway. *Cell Rep.* **3**, 2100–2112.

[134] Haase AD, Jaskiewicz L, Zhang H, Lainé S, Sack R, Gatignol A, Filipowicz W (2005). TRBP, a regulator of cellular PKR and HIV-1 virus expression, interacts with Dicer and functions in RNA silencing. *EMBO Rep.* **6**, 961–967.

[135] Chendrimada TP, Gregory RI, Kumaraswamy E, Norman J, Cooch N, Nishikura K, Shiekhattar R (2005). TRBP recruits the Dicer complex to Ago2 for microRNA processing and gene silencing. *Nature*. **436**, 740–744.

[136] Wiesen JL, Tomasi TB (2009). Dicer is regulated by cellular stresses and interferons. *Mol. Immunol.* **46**, 1222–1228.

[137] Tokumaru S, Suzuki M, Yamada H, Nagino M, Takahashi T (2008). *let-7* regulates Dicer expression and constitutes a negative feedback loop. *Carcinogenesis*. **29**, 2073–2077.

[138] Forman JJ, Legesse-Miller A, Coller HA (2008). A search for conserved sequences in coding regions reveals that the *let-7* microRNA targets Dicer within its coding sequence. *Proc. Natl. Acad. Sci. U. S. A.* **105**, 14879–14884.

[139] Bail S, Swerdel M, Liu H, Jiao X, Goff LA, Hart RP, Kiledjian M (2010). Differential regulation of microRNA stability. *RNA*. **16**, 1032–1039.

[140] Gantier MP, McCoy CE, Rusinova I, Saulep D, Wang D, Xu D, Irving AT, Behlke MA, Hertzog PJ, MacKay F, Williams BRG (2011). Analysis of microRNA turnover in mammalian cells following *Dicer1* ablation. *Nucleic Acids Res.* **39**, 5692–5703.

[141] Wu H, Neilson JR, Kumar P, Manocha M, Shankar P, Sharp PA, Manjunath N (2007). miRNA profiling of naïve, effector and memory CD8 T cells. *PLoS One*. **2**, e1020.

[142] Morin RD, O'Connor MD, Griffith M, Kuchenbauer F, Delaney A, Prabhu AL, Zhao Y, McDonald H, Zeng T, Hirst M, Eaves CJ, Marra MA (2008). Application of massively parallel sequencing to microRNA profiling and discovery in human embryonic stem cells. *Genome Res.* **18**, 610–621.

[143] Yang W, Chendrimada TP, Wang Q, Higuchi M, Seeburg PH, Shiekhattar R, Nishikura K (2006). Modulation of microRNA processing and expression through RNA editing by ADAR deaminases. *Nat. Struct. Mol. Biol.* **13**, 13–21.

[144] Kawahara Y, Zinshteyn B, Sethupathy P, Iizasa H, Hatzigeorgiou AG, Nishikura K (2007). Redirection of silencing targets by adenosine-to-inosine editing of miRNAs. *Science.* **315**, 1137–1140.

[145] Kawahara Y, Megraw M, Kreider E, Iizasa H, Valente L, Hatzigeorgiou AG, Nishikura K (2008). Frequency and fate of microRNA editing in human brain. *Nucleic Acids Res.* **36**, 5270–5280.

[146] Burroughs AM, Ando Y, De Hoon MJ, Tomaru Y, Nishibu T, Ukekawa R, Funakoshi T, Kurokawa T, Suzuki H, Hayashizaki Y, Daub CO (2010). A comprehensive survey of 3' animal miRNA modification events and a possible role for 3' adenylation in modulating miRNA targeting effectiveness. *Genome Res.* **20**, 1398–1410.

[147] Heo I, Joo C, Cho J, Ha M, Han J, Kim VN (2008). Lin28 mediates the terminal uridylation of let-7 precursor microRNA. *Mol. Cell*. **32**, 276–284.

[148] Katoh T, Sakaguchi Y, Miyauchi K, Suzuki T, Kashiwabara SI, Baba T, Suzuki T (2009). Selective stabilization of mammalian microRNAs by 3' adenylation mediated by the cytoplasmic poly(A) polymerase GLD-2. *Genes Dev.* **23**, 433–438.

[149] Starega-Roslan J, Krol J, Koscianska E, Kozlowski P, Szlachcic WJ, Sobczak K, Krzyzosiak WJ (2011). Structural basis of microRNA length variety. *Nucleic Acids Res.* **39**, 257–268.

[150] Warf MB, Johnson WE, Bass BL (2011). Improved annotation of *C. elegans* microRNAs by deep sequencing reveals structures associated with processing by Drosha and Dicer. *RNA*. **17**, 563–577.

[151] Lewis BP, Shih IH, Jones-Rhoades MW, Bartel DP, Burge CB (2003). Prediction of mammalian microRNA targets. *Cell*. **115**, 787–798.

[152] Chatterjee S, Großhans H (2009). Active turnover modulates mature microRNA activity in *Caenorhabditis elegans*. *Nature*. **461**, 546–549.

[153] Chatterjee S, Fasler M, Büssing I, Großhans H (2011). Target-mediated protection of endogenous microRNAs in *C. elegans*. *Dev. Cell*. **20**, 388–396.

[154] Ameres SL, Horwich MD, Hung JH, Xu J, Ghildiyal M, Weng Z, Zamore PD (2010). Target RNA-directed trimming and tailing of small silencing RNAs. *Science.* **328**, 1534–1539.

[155] Baccarini A, Chauhan H, Gardner TJ, Jayaprakash AD, Sachidanandam R, Brown BD (2011). Kinetic analysis reveals the fate of a microRNA following target regulation in mammalian cells. *Curr. Biol.* **21**, 369–376.

[156] Ramachandran V, Chen X (2008). Degradation of microRNAs by a family of exoribonucleases in *Arabidopsis*. *Science.* **321**, 1490–1492.

[157] Das SK, Sokhi UK, Bhutia SK, Azab B, Su ZZ, Sarkar D, Fisher PB (2010). Human polynucleotide phosphorylase selectively and preferentially degrades microRNA-221 in human melanoma cells. *Proc. Natl. Acad. Sci. U. S. A.* **107**, 11948–11953.

[158] Pillai RS, Artus CG, Filipowicz W (2004). Tethering of human Ago proteins to mRNA mimics the miRNA-mediated repression of protein synthesis. *RNA*. **10**, 1518–1525.

[159] Hutvágner G, Simard MJ (2008). Argonaute proteins: Key players in RNA silencing. *Nat. Rev. Mol. Cell Biol.* **9**, 22–32.

[160] Lai EC (2002). MicroRNAs are complementary to 3' UTR sequence motifs that mediate negative post-transcriptional regulation. *Nat. Genet.* **30**, 363–364.

[161] Xie X, Lu J, Kulbokas EJ, Golub TR, Mootha V, Lindblad-Toh K, Lander ES, Kellis M (2005). Systematic discovery of regulatory motifs in human promoters and 3' UTRs by comparison of several mammals. *Nature*. **434**, 338–345.

[162] Easow G, Teleman AA, Cohen SM (2007). Isolation of microRNA targets by miRNP immunopurification. *RNA*. **13**, 1198–1204.

[163] Grimson A, Farh KK, Johnston WK, Garrett-Engele P, Lim LP, Bartel DP (2007). MicroRNA targeting specificity in mammals: Determinants beyond seed pairing. *Mol. Cell*. **27**, 91–105.

[164] Kloosterman WP, Wienholds E, Ketting RF, Plasterk RH (2004). Substrate requirements for *let-7* function in the developing zebrafish embryo. *Nucleic Acids Res.* **32**, 6284–6291.

[165] Lytle JR, Yario TA, Steitz JA (2007). Target mRNAs are repressed as efficiently by microRNA-binding sites in the 5′ UTR as in the 3′ UTR. *Proc. Natl. Acad. Sci. U. S. A.* **104**, 9667–9672.

[166] Bartel DP (2009). MicroRNA target recognition and regulatory functions. *Cell*. **136**, 215–233.

[167] Hutvágner G, Zamore PD (2002). A microRNA in a multiple-turnover RNAi enzyme complex. *Science.* **297**, 2056–2060.

[168] Meister G, Landthaler M, Patkaniowska A, Dorsett Y, Teng G, Tuschl T (2004). Human Argonaute2 mediates RNA cleavage targeted by miRNAs and siRNAs. *Mol. Cell*. **15**, 185–197.

[169] Liu J, Carmell MA, Rivas FV, Marsden CG, Thomson JM, Song JJ, Hammond SM, Joshua-Tor L, Hannon GJ (2004). Argonaute2 is the catalytic engine of mammalian RNAi. *Science.* **305**, 1437–1441.

[170] Lim LP, Lau NC, Garrett-Engele P, Grimson A, Schelter JM, Castle J, Bartel DP, Linsley PS, Johnson JM (2005). Microarray analysis shows that some microRNAs downregulate large numbers of target mRNAs. *Nature*. **433**, 769–773.

[171] Brodersen P, Sakvarelidze-Achard L, Bruun-Rasmussen M, Dunoyer P, Yamamoto YY, Sieburth L, Voinnet O (2008). Widespread translational inhibition by plant miRNAs and siRNAs. *Science.* **320**, 1185–1190.

[172] Carthew RW, Sontheimer EJ (2009). Origins and mechanisms of miRNAs and siRNAs. *Cell*. **136**, 642–655.

[173] Huntzinger E, Izaurralde E (2011). Gene silencing by microRNAs: Contributions of translational repression and mRNA decay. *Nat. Rev. Genet.* **12**, 99–110.

[174] Lim LP, Lau NC, Weinstein EG, Abdelhakim A, Yekta S, Rhoades MW, Burge CB, Bartel DP (2003). The microRNAs of *Caenorhabditis elegans*. *Genes Dev.* **17**, 991–1008.

[175] Doench JG, Sharp PA (2004). Specificity of microRNA target selection in translational repression. *Genes Dev.* **18**, 504–511.

[176] Brennecke J, Stark A, Russell RB, Cohen SM (2005). Principles of microRNA-target recognition. *PLoS Biol.* **3**, e85.

[177] Filipowicz W, Bhattacharyya SN, Sonenberg N (2008). Mechanisms of post-transcriptional regulation by microRNAs: Are the answers in sight? *Nat. Rev. Genet.* **9**, 102–114.

[178] Stefani G, Slack FJ (2012). A `pivotal´ new rule for microRNA-mRNA interactions. *Nat. Struct. Mol. Biol.* **19**, 265–266.

[179] Kim KK, Ham J, Chi SW (2013). miRTCat: A comprehensive map of human and mouse microRNA target sites including non-canonical nucleation bulges. *Bioinformatics.* **29**, 1898–1899.

[180] Krek A, Grün D, Poy MN, Wolf R, Rosenberg L, Epstein EJ, MacMenamin P, Da Piedade I, Gunsalus KC, Stoffel M, Rajewsky N (2005). Combinatorial microRNA target predictions. *Nat. Genet.* **37**, 495–500.

[181] Bartel DP (2018). Metazoan microRNAs. *Cell*. **173**, 20–51.

[182] Friedman RC, Farh KK, Burge CB, Bartel DP (2009). Most mammalian mRNAs are conserved targets of microRNAs. *Genome Res.* **19**, 92–105.

[183] Jan CH, Friedman RC, Ruby JG, Bartel DP (2011). Formation, regulation and evolution of *Caenorhabditis elegans* 3'UTRs. *Nature*. **469**, 97–101.

[184] Agarwal V, Bell GW, Nam JW, Bartel DP (2015). Predicting effective microRNA target sites in mammalian mRNAs. *Elife*. **Aug 12**, 4.

[185] Kim D, Sung YM, Park J, Kim S, Kim J, Park J, Ha H, Bae JY, Kim S, Baek D (2016). General rules for functional microRNA targeting. *Nat. Genet.* **48**, 1517–1526.

[186] Ma JB, Yuan YR, Meister G, Pei Y, Tuschl T, Patel DJ (2005). Structural basis for 5'-end-specific recognition of guide RNA by the *A. fulgidus* Piwi protein. *Nature*. **434**, 666–670.

[187] Schirle NT, Sheu-Gruttadauria J, Chandradoss SD, Joo C, MacRae IJ (2015). Water-mediated recognition of t1-adenosine anchors Argonaute2 to microRNA targets. *Elife*. **Sep 11**, 4.

[188] Wee LM, Flores-Jasso CF, Salomon WE, Zamore PD (2012). Argonaute divides its RNA guide into domains with distinct functions and RNA-binding properties. *Cell*. **151**, 1055–1067.

[189] Salomon WE, Jolly SM, Moore MJ, Zamore PD, Serebrov V (2015). Single-molecule imaging reveals that Argonaute reshapes the binding properties of its nucleic acid guides. *Cell*. **162**, 84–95.

[190] Yekta S, Shih IH, Bartel DP (2004). MicroRNA-directed cleavage of *HOXB8* mRNA. *Science.* **304**, 594–596.

[191] Brodersen P, Voinnet O (2009). Revisiting the principles of microRNA target recognition and mode of action. *Nat. Rev. Mol. Cell Biol.* **10**, 141–148.

[192] Tay Y, Zhang J, Thomson AM, Lim B, Rigoutsos I (2008). MicroRNAs to *Nanog*, *Oct4* and *Sox2* coding regions modulate embryonic stem cell differentiation. *Nature*. **455**, 1124–1128.

[193] Lal A, Navarro F, Maher C, Maliszewski LE, Yan N, O´Day E, Chowdhury D, Dykxhoorn DM, Tsai P, Hofman O, Becker KG, Gorospe M, Hide W, Lieberman J (2009). miR-24 inhibits cell proliferation by suppressing expression of *E2F2*, *MYC* and other cell cycle regulatory genes by binding to `seedless´ 3´UTR microRNA recognition elements. *Mol. Cell*. **35**, 610–625.

[194] Chi SW, Hannon GJ, Darnell RB (2012). An alternative mode of microRNA target recognition. *Nat. Struct. Mol. Biol.* **19**, 321–327.

[195] Loeb GB, Khan AA, Canner D, Hiatt JB, Shendure J, Darnell RB, Leslie CS, Rudensky AY (2012). Transcriptome-wide miR-155 binding map reveals widespread noncanonical microRNA targeting. *Mol. Cell*. **48**, 760–770.

[196] Helwak A, Kudla G, Dudnakova T, Tollervey D (2013). Mapping the human miRNA interactome by CLASH reveals frequent noncanonical binding. *Cell*. **153**, 654–665.

[197] Llave C, Xie Z, Kasschau KD, Carrington JC (2002). Cleavage of *Scarecrow-like* mRNA targets directed by a class of *Arabidopsis* miRNA. *Science.* **297**, 2053–2056.

[198] Wang Y, Juranek S, Li H, Sheng G, Tuschl T, Patel DJ (2008). Structure of an argonaute silencing complex with a seed-containing guide DNA and target RNA duplex. *Nature*. **456**, 921–926.

[199] Jinek M, Doudna JA (2009). A three-dimensional view of the molecular machinery of RNA interference. *Nature*. **457**, 405–412.

[200] Souret FF, Kastenmayer JP, Green PJ (2004). AtXRN4 degrades mRNA in *Arabidopsis* and its substrates include selected miRNA targets. *Mol. Cell*. **15**, 173–183.

[201] Parker R, Song H (2004). The enzymes and control of eukaryotic mRNA turnover. *Nat. Struct. Mol. Biol.* **11**, 121–127.

[202] Chiu YL, Rana TM (2003). siRNA function in RNAi: A chemical modification analysis. *RNA*. **9**, 1034–1048.

[203] Rhoades MW, Reinhart BJ, Lim LP, Burge CB, Bartel B, Bartel DP (2002). Prediction of plant microRNA targets. *Cell*. **10**, 513–520.

[204] Bagga S, Bracht J, Hunter S, Massirer K, Holtz J, Eachus R, Pasquinelli AE (2005). Regulation by *let-7* and *lin-4* miRNAs results in target mRNA degradation. *Cell*. **122**, 553–563.

[205] Schmitter D, Filkowski J, Sewer A, Pillai RS, Oakeley EJ, Zavolan M, Svoboda P, Filipowicz W (2006). Effects of Dicer and Argonaute down-regulation on mRNA levels in human HEK293 cells. *Nucleic Acids Res.* **34**, 4801–4815.

[206] Takimoto K, Wakiyama M, Yokoyama S (2009). Mammalian GW182 contains multiple Argonaute-binding sites and functions in microRNA-mediated translational repression. *RNA*. **15**, 1078–1089.

[207] Lian SL, Li S, Abadal GX, Pauley BA, Fritzler MJ, Chan EK (2009). The C-terminal half of human Ago2 binds to multiple GW-rich regions of GW182 and requires GW182 to mediate silencing. *RNA*. **155**, 804–813.

[208] Yamashita A, Chang TC, Yamashita Y, Zhu W, Zhong Z, Chen CY, Shyu AB (2005). Concerted action of poly(A) nucleases and decapping enzyme in mammalian mRNA turnover. *Nat. Struct. Mol. Biol.* **12**, 1054–1063.

[209] Behm-Ansmant I, Rehwinkel J, Doerks T, Stark A, Bork P, Izaurralde E (2006). mRNA degradation by miRNAs and GW182 requires both CCR4:NOT deadenylase and DCP1:DCP2 decapping complexes. *Genes Dev.* **20**, 1885–1898.

[210] Chen CY, Zheng D, Xia Z, Shyu AB (2009). Ago-TNRC6 triggers microRNA-mediated decay by promoting two deadenylation steps. *Nat. Struct. Mol. Biol.* **16**, 1160–1166.

[211] Braun JE, Huntzinger E, Fauser M, Izaurralde E (2011). GW182 proteins directly recruit cytoplasmic deadenylase complexes to miRNA targets. *Mol. Cell*. **44**, 120–133.

[212] Rehwinkel J, Behm-Ansmant I, Gatfield D, Izaurralde E (2005). A crucial role for GW182 and the DCP1:DCP2 decapping complex in miRNA-mediated gene silencing. *RNA*. **11**, 1640–1647.

[213] Eulalio A, Rehwinkel J, Stricker M, Huntzinger E, Yang SF, Doerks T, Dorner S, Bork P, Boutros M, Izaurralde E (2007). Target-specific requirements for enhancers of decapping in miRNA-mediated gene silencing. *Genes Dev.* **21**, 2558–2570.

[214] Jonas S, Izaurralde E (2013). The role of disordered protein regions in the assembly of decapping complexes and RNP granules. *Genes Dev.* **27**, 2628–2641.

[215] Orban TI, Izaurralde E (2005). Decay of mRNAs targeted by RISC requires XRN1, the Ski complex, and the exosome. *RNA*. **11**, 459–469.

[216] Pasquinelli AE (2012). MicroRNAs and their targets: Recognition, regulation and an emerging reciprocal relationship. *Nat. Rev. Genet.* **13**, 271–282.

[217] Cooke A, Prigge A, Wickens M (2010). Translational repression by deadenylases. *J. Biol. Chem.* **285**, 28506–28513.

[218] Chekulaeva M, Mathys H, Zipprich JT, Attig J, Colic M, Parker R, Filipowicz W (2011). miRNA repression involves GW182-mediated recruitment of CCR4-NOT through conserved W-containing motifs. *Nat. Struct. Mol. Biol.* **18**, 1218–1226.

[219] Jackson RJ, Hellen CU, Pestova TV (2010). The mechanism of eukaryotic translation initiation and principles of its regulation. *Nat. Rev. Mol. Cell Biol.* **11**, 113–127.

[220] Wells SE, Hillner PE, Vale RD, Sachs AB (1998). Circularization of mRNA by eukaryotic translation initiation factors. *Mol. Cell*. **2**, 135–140.

[221] Fabian MR, Mathonnet G, Sundermeier T, Mathys H, Zipprich JT, Svitkin YV, Rivas F, Jinek M, Wohlschlegel J, Doudna JA, Chen CY, Shyu AB, Yates JR, Hannon GJ, Filipowicz W, Duchaine TF, Sonenberg N (2009). Mammalian miRNA RISC recruits CAF1 and PABP to affect PABP-dependent deadenylation. *Mol. Cell*. **35**, 868–880.

[222] Zekri L, Huntzinger E, Heimstadt S, Izaurralde E (2009). The silencing domain of GW182 interacts with PABPC1 to promote translational repression and degradation of microRNA targets and is required for target release. *Mol. Cell. Biol.* **29**, 6220–6231.

[223] Fukao A, Mishima Y, Takizawa N, Oka S, Imataka H, Pelletier J, Sonenberg N, Thoma C, Fujiwara T (2014). MicroRNAs trigger dissociation of eIF4AI and eIF4AII from target mRNAs in humans. *Mol. Cell*. **56**, 79–89.

[224] Fukaya T, Iwakawa HO, Tomari Y (2014). MicroRNAs block assembly of eIF4F translation initiation complex in *Drosophila*. *Mol. Cell*. **56**, 67–78.

[225] Pillai RS, Bhattacharyya SN, Artus CG, Zoller T, Cougot N, Basyuk E, Bertrand E, Filipowicz W (2005). Inhibition of translational initiation by let-7 microRNA in human cells. *Science.* **309**, 1573–1576.

[226] Humphreys DT, Westman BJ, Martin DIK, Preiss T (2005). MicroRNAs control translation initiation by inhibiting eukaryotic initiation factor 4E/ cap and poly(A) tail function. *Proc. Natl. Acad. Sci. U. S. A.* **102**, 16961–16966.

[227] Mathonnet G, Fabian MR, Svitkin Y V., Parsyan A, Huck L, Murata T, Biffo S, Merrick WC, Darzynkiewicz E, Pillai RS, Filipowicz W, Duchaine TF, Sonenberg N (2007). MicroRNA inhibition of translation initiation *in vitro* by targeting the cap-binding complex eIF4F. *Science.* **317**, 1764–1767.

[228] Kiriakidou M, Tan GS, Lamprinaki S, De Planell-Saguer M, Nelson PT, Mourelatos Z (2007). An mRNA m^7G cap binding-like motif within human Ago2 represses translation. *Cell*. **129**, 1141–1151.

[229] Dever TE, Green R (2012). The elongation, termination, and recycling phases of translation in eukaryotes. *Cold String Harb. Perspect. Biol.* **4**, a013706.

[230] Wettstein FO, Staehelin T, Noll H (1963). Ribosomal aggregate engaged in protein synthesis: Characterization of the ergosome. *Nature*. **197**, 430–435.

[231] Warner JR, Knopf PM, Rich A (1963). A multiple ribosomal structure in protein synthesis. *Proc. Natl. Acad. Sci. U. S. A.* **49**, 122–129.

[232] Maroney PA, Yu Y, Fisher J, Nilsen TW (2006). Evidence that microRNAs are associated with translating messenger RNAs in human cells. *Nat. Struct. Mol. Biol.* **13**, 1102–1107.

[233] Kim J, Krichevsky A, Grad Y, Hayes GD, Kosik KS, Church GM, Ruvkun G (2004). Identification of many microRNAs that copurify with polyribosomes in mammalian neurons. *Proc. Natl. Acad. Sci. U. S. A.* **101**, 360–365.

[234] Nelson PT, Hatzigeorgiou AG, Mourelatos Z (2004). miRNP:mRNA association in polyribosomes in a human neuronal cell line. *RNA*. **10**, 387–394.

[235] Petersen CP, Bordeleau ME, Pelletier J, Sharp PA (2006). Short RNAs repress translation after initiation in mammalian cells. *Mol. Cell*. **21**, 533–542.

[236] Nottrott S, Simard MJ, Richter JD (2006). Human let-7a miRNA blocks protein production on actively translating polyribosomes. *Nat. Struct. Mol. Biol.* **13**, 1108–1114.

[237] Hendrickson DG, Hogan DJ, McCullough HL, Myers JW, Herschlag D, Ferrell JE, Brown PO (2009). Concordant regulation of translation and mRNA abundance for hundreds of targets of a human microRNA. *PLoS Biol.* **7**, e1000238.

[238] Guo H, Ingolia NT, Weissman JS, Bartel DP (2010). Mammalian microRNAs predominantly act to decrease target mRNA levels. *Nature*. **466**, 835–840.

[239] Eichhorn SW, Guo H, McGeary SE, Rodriguez-Mias RA, Shin C, Baek D, Hsu S hao, Ghoshal K, Villén J, Bartel DP (2014). mRNA destabilization is the dominant effect of mammalian microRNAs by the time substantial repression ensues. *Mol. Cell*. **56**, 104–115.

[240] Djuranovic S, Nahvi A, Green R (2012). miRNA-mediated gene silencing by translational repression followed by mRNA deadenylation and decay. *Science.* **336**, 237–240.

[241] Vasudevan S, Tong Y, Steitz JA (2007). Switching from repression to activation: MicroRNAs can up-regulate translation. *Science.* **318**, 1931–1934.

[242] Bhattacharyya SN, Filipowicz W (2007). Argonautes and company: Sailing against the wind. *Cell*. **128**, 1027–1028.

[243] Yang Z, Jakymiw A, Wood MR, Eystathioy T, Rubin RL, Fritzler MJ, Chan EK (2004). GW182 is critical for the stability of GW bodies expressed during the cell cycle and cell proliferation. *J. Cell Sci.* **117**, 5567–5578.

[244] Flemr M, Ma J, Schultz RM, Svoboda P (2010). P-body loss is concomitant with formation of a messenger RNA storage domain in mouse oocytes. *Biol. Reprod.* **82**, 1008–1017.

[245] Valinezhad Orang A, Safaralizadeh R, Kazemzadeh-Bavili M (2014). Mechanisms of miRNA-mediated gene regulation from common downregulation to mRNA-specific upregulation. *Int. J. Genomics*. **2014**,.

[246] Bukhari SIA, Truesdell SS, Lee S, Kollu S, Classon A, Boukhali M, Jain E, Mortensen RD, Yanagiya A, Sadreyev RI, Haas W, Vasudevan S (2016). A specialized mechanism of translation mediated by FXR1a-associated microRNP in cellular quiescence. *Mol. Cell*. **61**, 760–773.

[247] Truesdell SS, Mortensen RD, Seo M, Schroeder JC, Lee JH, Letonqueze O, Vasudevan SV (2012). MicroRNA-mediated mRNA translation activation in quiescent cells and oocytes involves recruitment of a nuclear microRNP. *Sci. Rep.* **2**, 842.

[248] Vasudevan S, Tong Y, Steitz JA (2008). Cell cycle control of microRNA-mediated translation regulation. *Cell Cycle*. **7**, 1545–1549.

[249] Lin CC, Liu LZ, Addison JB, Wonderlin WF, Ivanov AV, Ruppert JM (2011). A KLF4-miRNA-206 autoregulatory feedback loop can promote or inhibit protein translation depending upon cell context. *Mol. Cell. Biol.* **31**, 2513–2527.

[250] Mortensen RD, Serra M, Steitz JA, Vasudevan S (2011). Posttranscriptional activation of gene expression in *Xenopus laevis* oocytes by microRNA-protein complexes (microRNPs). *Proc. Natl. Acad. Sci. U. S. A.* **108**, 8281–8216.

[251] Sen GL, Blau HM (2005). Argonaute 2/ RISC resides in sites of mammalian mRNA decay known as cytoplasmic bodies. *Nat. Cell Biol.* **7**, 633–636.

[252] Meister G, Landthaler M, Peters L, Chen PY, Urlaub H, Lührmann R, Tuschl T (2005). Identification of novel Argonaute-associated proteins. *Curr. Biol.* **15**, 2149–2155.

[253] Liu J, Valencia-Sanchez MA, Hannon GJ, Parker R (2005). MicroRNA-dependent localization of targeted mRNAs to mammalian P-bodies. *Nat. Cell Biol.* **7**, 719–723.

[254] Sheth U, Parker R (2003). Decapping and decay of messenger RNA occur in cytoplasmic processing bodies. *Science.* **300**, 805–808.

[255] Teixeira D, Sheth U, Valencia-Sanchez MA, Brengues M, Parker R (2005). Processing bodies require RNA for assembly and contain nontranslating mRNAs. *RNA*. **11**, 371–382.

[256] Parker R, Sheth U (2007). P bodies and the control of mRNA translation and degradation. *Mol. Cell*. **25**, 635–46.

[257] Bhattacharyya SN, Habermacher R, Martine U, Closs EI, Filipowicz W (2006). Relief of microRNA-mediated translational repression in human cells subjected to stress. *Cell*. **125**, 1111–1124.

[258] Jakymiw A, Lian S, Eystathioy T, Li S, Satoh M, Hamel JC, Fritzler MJ, Chan EK (2005). Disruption of GW bodies impairs mammalian RNA interference. *Nat. Cell Biol.* **7**, 1267–1274.

[259] Pauley KM, Eystathioy T, Jakymiw A, Hamel JC, Fritzler MJ, Chan EK (2006). Formation of GW bodies is a consequence of microRNA genesis. *EMBO Rep.* **7**, 904–910.

[260] Brengues M, Teixeira D, Parker R (2005). Movement of eukaryotic mRNAs between polysomes and cytoplasmic processing bodies. *Science.* **310**, 486–489.

[261] Cougot N, Babajko S, Séraphin B (2004). Cytoplasmic foci are sites of mRNA decay in human cells. *J. Cell Biol.* **165**, 31–40.

[262] Pillai RS, Bhattacharyya SN, Filipowicz W (2007). Repression of protein synthesis by miRNAs: How many mechanisms? *Trends Cell Biol.* **17**, 118–126.

[263] John B, Enright AJ, Aravin A, Tuschl T, Sander C, Marks DS (2004). Human microRNA targets. *PLoS Biol.* **2**, e363.

[264] Miranda KC, Huynh T, Tay Y, Ang YS, Tam WL, Thomson AM, Lim B, Rigoutsos I (2006). A pattern-based method for the identification of microRNA binding sites and their corresponding heteroduplexes. *Cell*. **126**, 1203–1217.

[265] Dweep H, Sticht C, Pandey P, Gretz N (2011). miRWalk - Database: Prediction of possible miRNA binding sites by `walking´ the genes of three genomes. *J. Biomed. Inform.* **44**, 839–847.

[266] Long D, Lee R, Williams P, Chan CY, Ambros V, Ding Y (2007). Potent effect of target structure on microRNA function. *Nat. Struct. Mol. Biol.* **14**, 287–294.

[267] Leoni G, Tramontano A (2016). A structural view of microRNA-target recognition. *Nucleic Acids Res.* **44**, e82.

[268] Seok H, Ham J, Jang ES, Chi SW (2016). MicroRNA target recognition: Insights from transcriptome-wide non-canonical interactions. *Mol. Cells*. **39**, 375–381.

[269] Baek D, Villén J, Shin C, Camargo FD, Gygi SP, Bartel DP (2008). The impact of microRNAs on protein output. *Nature*. **455**, 64–71.

[270] Addo-Quaye C, Eshoo TW, Bartel DP, Axtell MJ (2008). Endogenous siRNA and miRNA targets identified by sequencing of the *Arabidopsis* degradome. *Curr. Biol.* **18**, 758–762.

[271] Arava Y (2003). Isolation of polysomal RNA for microarray analysis. *Methods Mol. Biol.* **224**, 79–87.

[272] Davies E, Abe S (1995). Methods for isolation and analysis of polyribosomes. *Methods Cell Biol.* **50**, 209–222.

[273] Panda A, Martindale J, Gorospe M (2017). Polysome fractionation to analyze mRNA distribution profiles. *Bio Protoc.* **7**, e2126.

[274] Ule J, Jensen KB, Ruggiu M, Mele A, Ule A, Darnell RB (2003). CLIP identifies Nova-regulated RNA networks in the brain. *Science.* **302**, 1212–1215.

[275] Chi SW, Zang JB, Mele A, Darnell RB (2009). Argonaute HITS-CLIP decodes microRNA-mRNA interaction maps. *Nature*. **460**, 479–486.

[276] Stark A, Brennecke J, Russell RB, Cohen SM (2003). Identification of *Drosophila* microRNA targets. *PLoS Biol.* **1**, E60.

[277] Lagos-Quintana M, Rauhut R, Yalcin A, Meyer J, Lendeckel W, Tuschl T (2002). Identification of tissue-specific microRNAs from mouse. *Curr. Biol.* **12**, 735–739.

[278] Chang J, Nicolas E, Marks D, Sander C, Lerro A, Buendia MA, Xu C, Mason WS, Moloshok T, Bort R, Zaret KS, Taylor JM (2004). miR-122, a mammalian liver-specific microRNA, is processed from *hcr* mRNA and may downregulate the high affinity cationic amino acid transporter CAT-1. *RNA Biol.* **1**, 106–113.

[279] Girard M, Jacquemin E, Munnich A, Lyonnet S, Henrion-Caude A (2008). miR-122, a paradigm for the role of microRNAs in the liver. *J. Hepatol.* **48**, 648–656.

[280] Gatfield D, Le Martelot G, Vejnar CE, Gerlach D, Schaad O, Fleury-Olela F, Ruskeepää AL, Oresic M, Esau CC, Zdobnov EM, Schibler U (2009). Integration of microRNA miR-122 in hepatic circadian gene expression. *Genes Dev.* **23**, 1313–1326.

[281] Simerzin A, Zorde-Khvalevsky E, Rivkin M, Adar R, Zucman-Rossi J, Couchy G, Roskams T, Govaere O, Oren M, Giladi H, Galun E (2016). The liver-specific microRNA-122*, the complementary strand of microRNA-122, acts as a tumor suppressor by modulating the p53/ mouse double minute 2 homolog circuitry. *Hepatology*. **64**, 1623–1636.

[282] Xu H, He JH, Xiao ZD, Zhang QQ, Chen YQ, Zhou H, Qu LH (2010). Liver-enriched transcription factors regulate microRNA-122 that targets CUTL1 during liver development. *Hepatology*. **52**, 1431–1442.

[283] Chien CH, Sun YM, Chang WC, Chiang-Hsieh PY, Lee TY, Tsai WC, Horng JT, Tsou AP, Huang HD (2011). Identifying transcriptional start sites of human microRNAs based on high-throughput sequencing data. *Nucleic Acids Res.* **39**, 9345–9356.

[284] Laudadio I, Manfroid I, Achouri Y, Schmidt D, Wilson MD, Cordi S, Thorrez L, Knoops L, Jacquemin P, Schuit F, Pierreux CE, Odom DT, Peers B, Lemaigre FP (2012). A feedback loop between the liver-enriched transcription factor network and miR-122 controls hepatocyte differentiation. *Gastroenterology*. **142**, 119–129.

[285] Jung CJ, Iyengar S, Blahnik KR, Ajuha TP, Jiang JX, Farnham PJ, Zern M (2011). Epigenetic modulation of miR-122 facilitates human embryonic stem cell self-renewal and hepatocellular carcinoma proliferation. *PLoS One*. **6**, e27740.

[286] Song K, Han C, Zhang J, Lu D, Dash S, Feitelson M, Lim K, Wu T (2013). Epigenetic regulation of miR-122 by PPARγ and hepatitis B virus X protein in hepatocellular carcinoma cells. *Hepatology*. **58**, 1681–1692.

[287] Li Y, Ren Q, Zhu L, Li Y, Li J, Zhang Y, Zheng G, Han T, Sun S, Feng F (2018). Involvement of methylation of microRNA-122, -125b and -106b in regulation of Cyclin G1, CAT-1 and STAT3 target genes in isoniazid-induced liver injury. *BMC Pharmacol. Toxicol.* **19**, 11.

[288] Bai J, Yu J, Wang J, Xue B, He N, Tian Y, Yang L, Wang Y, Wang Y, Tang Q (2019). DNA methylation of miR-122 aggravates oxidative stress in colitis targeting SELENBP1 partially by p65NF-κB signaling. *Oxid. Med. Cell. Longev.* **2019**, 5294105.

[289] Vanden Heuvel GB, Bodmer R, Mcconnell KR, Nagami GT, Igarashi P (1996). Expression of a *cut*-related homeobox gene in developing and polycystic mouse kidney. *Kidney Int.* **50**, 453–461.

[290] Nepveu A (2001). Role of the multifunctional CDP/ Cut/ Cux homeodomain transcription factor in regulating differentiation, cell growth and development. *Gene*. **270**, 1–15.

[291] Krützfeldt J, Rajewsky N, Braich R, Rajeev KG, Tuschl T, Manoharan M, Stoffel M (2005). Silencing of microRNAs *in vivo* with `antagomirs´. *Nature*. **438**, 685–689.

[292] Esau C, Davis S, Murray SF, Yu XX, Pandey SK, Pear M, Watts L, Booten SL, Graham M, McKay R, Subramaniam A, Propp S, Lollo B a, Freier S, Bennett CF, Bhanot S, Monia BP (2006). miR-122 regulation of lipid metabolism revealed by *in vivo* antisense targeting. *Cell Metab.* **3**, 87–98.

[293] Hu J, Xu Y, Hao J, Wang S, Li C, Meng S (2012). miR-122 in hepatic function and liver diseases. *Protein Cell*. **3**, 364–371.

[294] Hsu SH, Wang B, Kota J, Yu J, Costinean S, Kutay H, Yu L, Bai S, La Perle K, Chivukula RR, Mao H, Wei M, Clark KR, Mendell JR, Caligiuri MA, Jacob ST, Mendell JT, Ghoshal K (2012). Essential metabolic, anti-inflammatory, and anti-tumorigenic functions of miR-122 in liver. *J. Clin. Invest.* **122**, 2871–2883.

[295] Tsai WC, Hsu S Da, Hsu CS, Lai TC, Chen SJ, Shen R, Huang Y, Chen HC, Lee CH, Tsai TF, Hsu MT, Wu JC, Huang HD, Shiao MS, Hsiao M, Tsou AP (2012). MicroRNA-122 plays a critical role in liver homeostasis and hepatocarcinogenesis. *J. Clin. Invest.* **122**, 2884–2897.

[296] Lin CJ, Gong HY, Tseng HC, Wang WL, Wu JL (2008). miR-122 targets an anti-apoptotic gene, *Bcl-w*, in human hepatocellular carcinoma cell lines. *Biochem. Biophys. Res. Commun.* **375**, 315–320.

[297] Gramantieri L, Ferracin M, Fornari F, Veronese A, Sabbioni S, Liu CG, Calin GA, Giovannini C, Ferrazzi E, Grazi GL, Croce CM, Bolondi L, Negrini M (2007). Cyclin G1 is a target of miR-122a, a microRNA frequently down-regulated in human hepatocellular carcinoma. *Cancer Res.* **67**, 6092–6099.

[298] Bai S, Nasser MW, Wang B, Hsu SH, Datta J, Kutay H, Yadav A, Nuovo G, Kumar P, Ghoshal K (2009). MicroRNA-122 inhibits tumorigenic properties of hepatocellular carcinoma cells and sensitizes these cells to sorafenib. *J. Biol. Chem.* **284**, 32015–32027.

[299] Fornari F, Gramantieri L, Giovannini C, Veronese A, Ferracin M, Sabbioni S, Calin GA, Grazi GL, Croce CM, Tavolari S, Chieco P, Negrini M, Bolondi L (2009). miR-122/ cyclin G1 interaction modulates p53 activity and affects doxorubicin sensitivity of human hepatocarcinoma cells. *Cancer Res.* **69**, 5761–5767.

[300] Okamoto K, Li H, Jensen MR, Zhang T, Taya Y, Thorgeirsson SS, Prives C (2002). Cyclin G recruits PP2A to dephosphorylate Mdm2. *Mol. Cell*. **9**, 761–771.

[301] Tsai WC, Hsu PW, Lai TC, Chau GY, Lin CW, Chen CM, Lin C Der, Liao YL, Wang JL, Chau YP, Hsu MT, Hsiao M, Huang HD, Tsou AP (2009). MicroRNA-122, a tumor suppressor microRNA that regulates intrahepatic metastasis of hepatocellular carcinoma. *Hepatology*. **49**, 1571–1582.

[302] Li X-N, Yang H, Yang T (2020). miR-122 inhibits hepatocarcinoma cell progression by targeting LMNB2. *Oncol. Res.* **28**, 41–49.

[303] Xu J, Zhu X, Wu L, Yang R, Yang Z, Wang Q, Wu F (2012). MicroRNA-122 suppresses cell proliferation and induces cell apoptosis in hepatocellular carcinoma by directly targeting Wnt/ β-catenin pathway. *Liver Int.* **32**, 752–760.

[304] Wang N, Wang Q, Shen D, Sun X, Cao X, Wu D (2016). Downregulation of microRNA-122 promotes proliferation, migration, and invasion of human hepatocellular carcinoma cells by activating epithelial–mesenchymal transition. *Onco. Targets. Ther.* **9**, 2035–2047.

[305] Ahsani Z, Mohammadi-Yeganeh S, Kia V, Karimkhanloo H, Zarghami N, Paryan M (2017). *WNT1* gene from WNT signaling pathway is a direct target of miR-122 in hepatocellular carcinoma. *Appl. Biochem. Biotechnol.* **181**, 884–897.

[306] Jin Y, Wang J, Han J, Luo D, Sun Z (2017). miR-122 inhibits epithelial-mesenchymal transition in hepatocellular carcinoma by targeting Snail1 and Snail2 and suppressing WNT/ β-cadherin signaling pathway. *Exp. Cell Res.* **360**, 210–217.

[307] Castoldi M, Spasic MV, Altamura S, Elmén J, Lindow M, Kiss J, Stolte J, Sparla R, D´Alessandro LA, Klingmüller U, Fleming RE, Longerich T, Gröne HJ, Benes V, Kauppinen S, Hentze MW, Muckenthaler MU (2011). The liver-specific microRNA miR-122 controls systemic iron homeostasis in mice. *J. Clin. Invest.* **121**, 1386–1396.

[308] Castoldi M, Muckenthaler MU (2012). Regulation of iron homeostasis by microRNAs. *Cell. Mol. Life Sci.* **69**, 3945–3952.

[309] Weinberg ED (1996). Iron withholding: A defense against viral infections. *Biometals*. **9**, 393–399.

[310] Johnson EE, Wessling-Resnick M (2012). Iron metabolism and the innate immune response to infection. *Microbes Infect.* **14**, 207–216.

[311] Satishchandran A, Ambade A, Rao S, Hsueh YC, Iracheta-Vellve A, Tornai D, Lowe P, Gyongyosi B, Li J, Catalano D, Zhong L, Kodys K, Xie J, Bala S, Gao G, Szabo G (2018). MicroRNA-122, regulated by GRLH2, protects livers of mice and patients from ethanol-induced liver disease. *Gastroenterology*. **154**, 238-252.e7.

[312] Cheung O, Puneet P, Eicken C, Contos MJ, Mirshahi F, Maher JW, Kellum JM, Min H, Luketic VA, Sanyal AJ (2008). Nonalcoholic steatohepatitis is associated with altered hepatic microRNA expression. *Hepatology*. **48**, 1810–1820.

[313] Takaki Y, Saito Y, Takasugi A, Toshimitsu K, Yamada S, Muramatsu T, Kimura M, Sugiyama K, Suzuki H, Arai E, Ojima H, Kanai Y, Saito H (2014). Silencing of microRNA-122 is an early event during hepatocarcinogenesis from non-alcoholic steatohepatitis. *Cancer Sci.* **105**, 1254–1260.

[314] Padgett KA, Lan RY, Leung PC, Lleo A, Dawson K, Pfeiff J, Mao TK, Coppel RL, Ansari AA, Gershwin ME (2009). Primary biliary cirrhosis is associated with altered hepatic microRNA expression. *J. Autoimmun.* **32**, 246–253.

[315] Wang S, Qiu L, Yan X, Jin W, Wang Y, Chen L, Wu E, Ye X, Gao GF, Wang F, Chen Y, Duan Z, Meng S (2012). Loss of microRNA-122 expression in patients with hepatitis B enhances hepatitis B virus replication through cyclin G_1-modulated p53 activity. *Hepatology*. **55**, 730–741.

[316] Halász T, Horváth G, Pár G, Werling K, Kiss A, Schaff Z, Lendvai G (2015). miR-122 negatively correlates with liver fibrosis as detected by histology and fibroscan. *World J. Gastroenterol.* **21**, 7814–7823.

[317] Kutay H, Bai S, Datta J, Motiwala T, Pogribny I, Jacob ST, Ghoshal K, Frankel W, Jacob ST, Ghoshal K (2006). Downregulation of miR-122 in the rodent and human hepatocellular carcinomas. *J. Cell Biol.* **99**, 671–678.

[318] Coulouarn C, Factor VM, Andersen JB, Durkin ME, Thorgeirsson SS (2009). Loss of miR-122 expression in liver cancer correlates with suppression of the hepatic phenotype and gain of metastatic properties. *Oncogene*. **28**, 3526–3536.

[319] Burchard J, Zhang C, Liu AM, Poon RTP, Lee NPY, Wong KF, Sham PC, Lam BY, Ferguson MD, Tokiwa G, Smith R, Leeson B, Beard R, Lamb JR, Lim L, Mao M, Dai H, Luk JM (2010). MicroRNA-122 as a regulator of mitochondrial metabolic gene network in hepatocellular carcinoma. *Mol. Syst. Biol.* **6**, 402.

[320] Ji F, Yang B, Peng X, Ding H, You H, Tien P (2011). Circulating microRNAs in hepatitis B virus-infected patients. *J. Viral Hepat.* **18**, e242–e251.

[321] Zhou X, Fang S, Wang M, Xiong A, Zheng C, Wang J, Yin C (2019). Diagnostic value of circulating miRNA-122 for hepatitis B virus and/ or hepatitis C virus-associated chronic viral hepatitis. *Biosci. Rep.* **39**, BSR20190900.

[322] Cermelli S, Ruggieri A, Marrero JA, Ioannou GN, Beretta L (2011). Circulating microRNAs in patients with chronic hepatitis C and non-alcoholic fatty liver disease. *PLoS One*. **6**, e23937.

[323] Dubin PH, Yuan H, Devine RK, Hynan LS, Jain MK, Lee WM, the Acute Liver Failure Study Group (2014). Micro-RNA-122 levels in acute liver failure and chronic hepatitis C. *J. Med. Virol.* **86**, 1507–1514.

[324] Tan Y, Ge G, Pan T, Wen D, Gan J (2014). A pilot study of serum microRNAs panel as potential biomarkers for diagnosis of nonalcoholic fatty liver disease. *PLoS One*. **9**, e105192.

[325] Jampoka K, Muangpaisarn P, Khongnomnan K, Treeprasertsuk S, Tangkijvanich P, Payungporn S (2018). Serum miR-29a and miR-122 as potential biomarkers for non-alcoholic fatty liver disease (NAFLD). *MicroRNA*. **7**, 215–222.

[326] Pirola CJ, Gianotti TF, Castaño GO, Mallardi P, San Martino J, Mora Gonzalez Lopez Ledesma M, Flichman D, Mirshahi F, Sanyal AJ, Sookoian S (2015). Circulating microRNA signature in non-alcoholic fatty liver disease: From serum non-coding RNAs to liver histology and disease pathogenesis. *Gut*. **64**, 800–812.

[327] Wang K, Zhang S, Marzolf B, Troisch P, Brightman A, Hu Z, Hood LE, Galas DJ (2009). Circulating microRNAs, potential biomarkers for drug-induced liver injury. *Proc. Natl. Acad. Sci. U. S. A.* **106**, 4402–4407.

[328] Starkey Lewis PJ, Dear J, Platt V, Simpson KJ, Craig DGN, Antoine DJ, French NS, Dhaun N, Webb DJ, Costello EM, Neoptolemos JP, Moggs J, Goldring CE, Park BK (2011). Circulating microRNAs as potential markers of human drug-induced liver injury. *Hepatology*. **54**, 1767–1776.

[329] Bala S, Petrasek J, Mundkur S, Catalano D, Levin I, Ward J, Alao H, Kodys K, Szabo G (2012). Circulating microRNAs in exosomes indicate hepatocyte injury and inflammation in alcoholic, drug-induced, and inflammatory liver diseases. *Hepatology*. **56**, 1946–1957.

[330] Wu Q, Liu HO, Liu YD, Liu WS, Pan D, Zhang WJ, Yang L, Fu Q, Xu JJ, Gu JX (2015). Decreased expression of hepatocyte nuclear factor 4α (Hnf4α)/ microRNA-122 (miR-122) axis in hepatitis B virus-associated hepatocellular carcinoma enhances potential oncogenic GALNT10 protein activity. *J. Biol. Chem.* **290**, 1170–1185.

[331] Xu Q, Zhang M, Tu J, Pang L, Cai W, Liu X (2015). MicroRNA-122 affects cell aggressiveness and apoptosis by targeting PKM2 in human hepatocellular carcinoma. *Oncol. Rep.* **34**, 2054–2064.

[332] Zhang Y, Li Y, Jiang W, Li Q, Lan Y (2019). The clinical significance of microRNA-122 in predicting the prognosis of patients with hepatocellular carcinoma. *Medicine (Baltimore).* **98**, e14810.

[333] Sarasin-Filipowicz M, Krol J, Markiewicz I, Heim MH, Filipowicz W (2009). Decreased levels of microRNA miR-122 in individuals with hepatitis C responding poorly to interferon therapy. *Nat. Med.* **15**, 31–33.

[334] Thomas M, Deiters A (2013). MicroRNA miR-122 as a therapeutic target for oligonucleotides and small molecules. *Curr. Med. Chem.* **20**, 3629–3640.

[335] Qiu Z, Dai Y (2014). Roadmap of miR-122-related clinical application from bench to bedside. *Expert Opin. Investig. Drugs*. **23**, 347–355.

[336] Fujiyama A, Miyanohara A, Nozaki C, Yoneyama T, Ohtomo N, Matsubara K (1983). Cloning and structural analyses of hepatitis B virus DNAs, subtype *adr*. *Nucleic Acids Res.* **11**, 4604–4610.

[337] Kao JH, Chen PJ, Chen DS (2010). Recent advances in the research of hepatitis B virus-related hepatocellular carcinoma. Epidemiologic and molecular biological aspects. *Adv. Cancer Res.* **108**, 21–72.

[338] Chen Y, Shen A, Rider PJ, Yu Y, Wu K, Mu Y, Hao Q, Liu Y, Gong H, Zhu Y, Liu F, Wu J (2011). A liver-specific microRNA binds to a highly conserved RNA sequence of hepatitis B virus and negatively regulates viral gene expression and replication. *FASEB J.* **25**, 4511–4521.

[339] Fan CG, Wang CM, Tian C, Wang Y, Li L, Sun WS, Li RF, Liu YG (2011). miR-122 inhibits viral replication and cell proliferation in hepatitis B virus-related hepatocellular carcinoma and targets NDRG3. *Oncol. Rep.* **26**, 1281–1286.

[340] Shan Y, Zheng J, Lambrecht RW, Bonkovsky HL (2007). Reciprocal effects of micro-RNA-122 on expression of heme oxygenase-1 and hepatitis C virus genes in human hepatocytes. *Gastroenterology*. **133**, 1166–1174.

[341] Protzer U, Seyfried S, Quasdorff M, Sass G, Svorcova M, Webb D, Bohne F, Hösel M, Schirmacher P, Tiegs G (2007). Antiviral activity and hepatoprotection by heme oxygenase-1 in hepatitis B virus infection. *Gastroenterology*. **133**, 1156–1165.

[342] Lehmann E, El-Tantawy WH, Ocker M, Bartenschlager R, Lohmann V, Hashemolhosseini S, Tiegs G, Sass G (2010). The heme oxygenase 1 product biliverdin interferes with hepatitis C virus replication by increasing antiviral interferon response. *Hepatology*. **51**, 398–404.

[343] Koeberlein B, Hausen A zur, Bektas N, Zentgraf H, Chin R, Toan NL, Kandolf R, Torresi J, Bock CT (2010). Hepatitis B virus overexpresses suppressor of cytokine signaling-3 (SOCS3) thereby contributing to severity of inflammation in the liver. *Virus Res.* **148**, 51–59.

[344] Gao D, Zhai A, Qian J, Li A, Li Y, Song W, Zhao H, Yu X, Wu J, Zhang Q, Kao W, Wei L, Zhang F, Zhong Z (2015). Down-regulation of suppressor of cytokine signaling 3 by miR-122 enhances interferon-mediated suppression of hepatitis B virus. *Antiviral Res.* **118**, 20–28.

[345] Bode JG, Ludwig S, Ehrhardt C, Albrecht U, Erhardt A, Schaper F, Heinrich PC, Häussinger D (2003). IFN-α antagonistic activity of HCV core protein involves induction of suppressor of cytokine signaling-3. *FASEB J.* **17**, 488–490.

[346] Li C, Wang Y, Wang S, Wu B, Hao J, Fan H, Ju Y, Ding Y, Chen L, Chu X, Liu W, Ye X, Meng S (2013). Hepatitis B virus mRNA-mediated miR-122 inhibition upregulates PTTG1-binding protein, which promotes hepatocellular carcinoma tumor growth and cell invasion. *J. Virol.* **87**, 2193–2205.

[347] Choi YH, Kim H Il, Seong JK, Yu DY, Cho H, Lee MO, Lee JM, Ahn YH, Kim SJ, Park JH (2004). Hepatitis B virus X protein modulates peroxisome proliferator-activated receptor γ through protein-protein interaction. *FEBS Lett.* **557**, 73–80.

[348] Peng F, Xiao X, Jiang Y, Luo K, Tian Y, Peng M, Zhang M, Xu Y, Gong G (2014). HBx down-regulated Gld2 plays a critical role in HBV-related dysregulation of miR-122. *PLoS One*. **9**, e92998.

[349] Jopling CL, Yi M, Lancaster AM, Lemon SM, Sarnow P (2005). Modulation of hepatitis C virus RNA abundance by a liver-specific miRNA. *Science.* **309**, 1577–1581.

[350] Wu X, Wu S, Tong L, Luan T, Lin L, Lu S, Zhao W, Ma Q, Liu H, Zhong Z (2009). miR-122 affects the viability and apoptosis of hepatocellular carcinoma cells. *Scand. J. Gastroenterol.* **44**, 1332–1339.

[351] Jopling CL, Norman KL, Sarnow P (2006). Positive and negative modulation of viral and cellular mRNAs by liver-specific microRNA miR-122. *Cold Spring Harb. Symp. Quant. Biol.* **71**, 369–376.

[352] Chang J, Guo JT, Jiang D, Guo H, Taylor JM, Block TM (2008). Liver-specific microRNA miR-122 enhances the replication of hepatitis C virus in nonhepatic cells. *J. Virol.* **82**, 8215–8223.

[353] Jopling CL, Schütz S, Sarnow P (2008). Position-dependent function for a tandem microRNA miR-122-binding site located in the hepatitis C virus RNA genome. *Cell Host Microbe*. **4**, 77–85.

[354] Shimakami T, Yamane D, Jangra RK, Kempf BJ, Spaniel C, Barton DJ, Lemon SM (2012). Stabilization of hepatitis C virus RNA by an Ago2-miR-122 complex. *Proc. Natl. Acad. Sci. U. S. A.* **109**, 941–946.

[355] Li Y, Masaki T, Yamane D, McGivern DR, Lemon SM (2013). Competing and noncompeting activities of miR-122 and the 5' exonuclease Xrn1 in regulation of hepatitis C virus replication. *Proc. Natl. Acad. Sci. U. S. A.* **110**, 1881–1886.

[356] Thibault PA, Huys A, Amador-Cañizares Y, Gailius JE, Pinel DE, Wilson JA (2015). Regulation of hepatitis C virus genome replication by Xrn1 and microRNA-122 binding to individual sites in the 5' untranslated region. *J. Virol.* **89**, 6294–6311.

[357] Sedano CD, Sarnow P (2014). Hepatitis C virus subverts liver-specific miR-122 to protect the viral genome from exoribonuclease Xrn2. *Cell Host Microbe*. **16**, 257–264.

[358] Henke JI, Goergen D, Zheng J, Song Y, Schüttler CG, Fehr C, Jünemann C, Niepmann M (2008). MicroRNA-122 stimulates translation of hepatitis C virus RNA. *EMBO J.* **27**, 3300–3310.

[359] Jangra RK, Yi M, Lemon SM (2010). Regulation of hepatitis C virus translation and infectious virus production by the microRNA miR-122. *J. Virol.* **84**, 6615–6625.

[360] Díaz-Toledano R, Ariza-Mateos A, Birk A, Martínez-Garcí B, Gómez J (2009). *In vitro* characterization of a miR-122-sensitive double-helical switch element in the 5' region of hepatitis C virus RNA. *Nucleic Acids Res.* **37**, 5498–5510.

[361] Schult P, Roth H, Adams RL, Mas C, Imbert L, Orlik C, Ruggieri A, Pyle AM, Lohmann V (2018). MicroRNA-122 amplifies hepatitis C virus translation by shaping the structure of the internal ribosomal entry site. *Nat. Commun.* **9**, 2613.

[362] Chahal J, Gebert LFR, Gan HH, Camacho E, Gunsalus KC, MacRae IJ, Sagan SM (2019). miR-122 and Ago interactions with the HCV genome alter the structure of the viral 5' terminus. *Nucleic Acids Res.* **47**, 5307–5324.

[363] Lanford RE, Hildebrandt-Eriksen ES, Petri A, Persson R, Lindow M, Munk ME, Kauppinen S, Rum H, Ørum H (2009). Therapeutic silencing of microRNA-122 in primates with chronic hepatitis C virus infection. *Science.* **327**, 198–201.

[364] Gebert LFR, Rebhan MA, Crivelli SE, Denzler R, Stoffel M, Hall J (2014). Miravirsen (SPC3649) can inhibit the biogenesis of miR-122. *Nucleic Acids Res.* **42**, 609–621.

[365] Janssen HL, Reesink HW, Lawitz EJ, Zeuzem S, Rodriguez-Torres M, Patel K, Van Der Meer AJ, Patick AK, Chen A, Zhou Y, Persson R, King BD, Kauppinen S, Levin AA, Hodges MR (2013). Treatment of HCV infection by targeting microRNA. *N. Engl. J. Med.* **368**, 1685–1694.

[366] Jopling CL (2012). Liver-specific microRNA-122 - Biogenesis and function. *RNA Biol.* **9**, 137–142.

[367] Schinazi R, Halfon P, Marcellin P, Asselah T (2014). HCV direct-acting antiviral agents: The best interferon-free combinations. *Liver Int.* **34**, 69–78.

[368] Afdhal N, Zeuzem S, Kwo P, Chojkier M, Gitlin N, Puoti M, Romero-Gomez M, Zarski JP, Agarwal K, Buggisch P, Foster GR, Bräu N, Buti M, Jacobson IM, Subramanian GM, Ding X, Mo H, Yang JC, Pang PS, Symonds WT, McHutchison JG, Muir AJ, Mangia A, Marcellin P, ION-1 Investigators (2014). Ledipasvir and sofosbuvir for untreated HCV genotype 1 infection. *N. Engl. J. Med.* **370**, 1889–1898.

[369] Sulkowski MS, Gardiner DF, Rodriguez-Torres M, Reddy KR, Hassanein T, Jacobson I, Lawitz E, Lok AS, Hinestrosa F, Thuluvath PJ, Schwartz H, Nelson DR, Everson GT, Eley T, Wind-Rotolo M, Huang SP, Gao M, Hernandez D, McPhee F, Sherman D, Hindes R, Symonds W, Pasquinelli C, Grasela DM, AI444040 Study Group (2014). Daclatasvir plus sofosbuvir for previously treated or untreated chronic HCV infection. *N. Engl. J. Med.* **370**, 211–221.

[370] Bandiera S, Pfeffer S, Baumert TF, Zeisel MB (2015). miR-122 – A key factor and therapeutic target in liver disease. *J. Hepatol.* **62**, 448–457.

[371] Tang A, Hallouch O, Chernyak V, Kamaya A, Sirlin CB (2018). Epidemiology of hepatocellular carcinoma: Target population for surveillance and diagnosis. *Abdom. Radiol.* **43**, 13–25.

[372] Braicu C, Burz C, Berindan-Neagoe I, Balcescu O, Graur F, Cristea V, Irimie A (2009). Hepatocellular carcinoma: Tumorigenesis and prediction markers. *Gastroenterol. Res.* **2**, 191–199.

[373] Gramantieri L, Fornari F, Callegari E, Sabbioni S, Lanza G, Croce CM, Bolondi L, Negrini M (2008). MicroRNA involvement in hepatocellular carcinoma. *J. Cell. Mol. Med.* **12**, 2189–2204.

[374] Warburg O, Posener K, Negelein E (1924). The metabolism of cancer cells. *Biochem. Z.* **152**, 319–344.

[375] Warburg O, Wind F, Negelein E (1927). The metabolism of tumors in the body. *J. Gen. Physiol.* **8**, 519–530.

[376] Ladeiro Y, Couchy G, Balabaud C, Bioulac-Sage P, Pelletier L, Rebouissou S, Zucman-Rossi J (2008). MicroRNA profiling in hepatocellular tumors is associated with clinical features and oncogene/ tumor suppressor gene mutations. *Hepatology*. **47**, 1955–1963.

[377] Budhu A, Jia HL, Forgues M, Liu CG, Goldstein D, Lam A, Zanetti KA, Ye QH, Qin LX, Croce CM, Tang ZY, Wang XW (2008). Identification of metastasis-related microRNAs in hepatocellular carcinoma. *Hepatology*. **47**, 897–907.

[378] Varnholt H, Drebber U, Schulze F, Wedemeyer I, Schirmacher P, Dienes HP, Odenthal M (2008). MicroRNA gene expression profile of hepatitis C virus-associated hepatocellular carcinoma. *Hepatology*. **47**, 1223–1232.

[379] Ura S, Honda M, Yamashita T, Ueda T, Takatori H, Nishino R, Sunakozaka H, Sakai Y, Horimoto K, Kaneko S (2009). Differential microRNA expression between hepatitis B and hepatitis C leading disease progression to hepatocellular carcinoma. *Hepatology*. **49**, 1098–1112.

[380] Spaniel C, Honda M, Selitsky SR, Yamane D, Shimakami T, Kaneko S, Lanford RE, Lemon SM (2013). MicroRNA-122 abundance in hepatocellular carcinoma and non-tumor liver tissue from Japanese patients with persistent HCV *versus* HBV infection. *PLoS One*. **8**, e76867.

[381] Bei C, Liu S, Yu X, Qiu M, Tang B, Liao W, He S, Yu H (2018). Single nucleotide polymorphisms in miR-122 are associated with the risk of hepatocellular carcinoma in a southern Chinese population. *Biomed Res. Int.* **2018**, 1540201.

[382] Wang B, Hsu SH, Wang X, Kutay H, Bid HK, Yu J, Ganju RK, Jacob ST, Yuneva M, Ghoshal K (2014). Reciprocal regulation of microRNA-122 and c-Myc in hepatocellular cancer: Role of E2F1 and transcription factor dimerization partner 2. *Hepatology*. **59**, 555–566.

[383] Liu AM, Xu Z, Shek FH, Wong KF, Lee NP, Poon RT, Chen J, Luk JM (2014). miR-122 targets pyruvate kinase M2 and affects metabolism of hepatocellular carcinoma. *PLoS One*. **9**, e86872.

[384] Pan C, Wang X, Shi K, Zheng Y, Li J, Chen Y, Jin L, Pan Z (2016). miR-122 reverses the doxorubicin-resistance in hepatocellular carcinoma cells through regulating the tumor metabolism. *PLoS One*. **11**, e0152090.

[385] Xu Y, Huang J, Ma L, Shan J, Shen J, Yang Z, Liu L, Luo Y, Yao C, Qian C (2016). MicroRNA-122 confers sorafenib resistance to hepatocellular carcinoma cells by targeting IGF-1R to regulate RAS/ RAF/ ERK signaling pathways. *Cancer Lett.* **371**, 171–181.

[386] Yahya SMM, Fathy SA, El-Khayat ZA, El-Toukhy SE, Hamed AR, Hegazy MGA, Nabih HK (2018). Possible role of microRNA-122 in modulating multidrug resistance of hepatocellular carcinoma. *Indian J. Clin. Biochem.* **33**, 21–30.

[387] Xu Y, Xia F, Ma L, Shan J, Shen J, Yang Z, Liu J, Cui Y, Bian X, Bie P, Qian C (2011). MicroRNA-122 sensitizes HCC cancer cells to adriamycin and vincristine through modulating expression of MDR and inducing cell cycle arrest. *Cancer Lett.* **310**, 160–169.

[388] Benes V, Collier P, Kordes C, Stolte J, Rausch T, Muckentaler MU, Häussinger D, Castoldi M (2015). Identification of cytokine-induced modulation of microRNA expression and secretion as measured by a novel microRNA specific qPCR assay. *Sci. Rep.* **5**, 11590.

[389] Livak KJ, Schmittgen TD (2001). Analysis of relative gene expression data using real-time quantitative PCR and the $2^{-\Delta\Delta CT}$ method. *Methods*. **25**, 402–408.

[390] Hellemans J, Mortier G, De Paepe A, Speleman F, Vandesompele J (2007). qBase relative quantification framework and software for management and automated analysis of real-time quantitative PCR data. *Genome Biol.* **8**, R19.

[391] Freeman WH (2004). Life: The science of biology, 7th Edition, Oxford University Press, ISBN: 0-7167-9856-5, Fig. 12.13.

[392] Emig D, Salomonis N, Baumbach J, Lengauer T, Conklin BR, Albrecht M (2010). AltAnalyze and DomainGraph: Analyzing and visualizing exon expression data. *Nucleic Acids Res.* **38**, W755–W762.

[393] Darpolor MM, Basu SS, Worth A, Nelson DS, Clarke-Katzenberg RH, Glickson JD, Kaplan DE, Blair IA (2014). The aspartate metabolism pathway is differentiable in human hepatocellular carcinoma: Transcriptomics and ^{13}C-isotope based metabolomics. *NMR Biomed.* **27**, 381–389.

[394] Eden E, Navon R, Steinfeld I, Lipson D, Yakhini Z (2009). *GOrilla*: A tool for discovery and visualization of enriched GO terms in ranked gene lists. *BMC Bioinformatics*. **10**, 48.

[395] Ye C, Tao R, Cao Q, Zhu D, Wang Y, Wang J, Lu J, Chen E, Li L (2016). Whole-genome DNA methylation and hydroxymethylation profiling for HBV-related hepatocellular carcinoma. *Int. J. Oncol.* **49**, 589–602.

[396] Park YM, Choi JY, Bae SH, Byun BH, Ahn BM, Kim BS, Shin DY (2000). Microsatellite instability and mutations of *E2F-4* in hepatocellular carcinoma from Korea. *Hepatol. Res.* **17**, 102–111.

[397] Huang YL, Ning G, Chen LB, Lian YF, Gu YR, Wang JL, Chen DM, Wei H, Huang YH (2019). Promising diagnostic and prognostic value of E2Fs in human hepatocellular carcinoma. *Cancer Manag. Res.* **11**, 1725–1740.

[398] Speletas M, Argentou N, Germanidis G, Vasiliadis T, Mantzoukis K, Patsiaoura K, Nikolaidis P, Karanikas V, Ritis K, Germenis AE (2011). Foxp3 expression in liver correlates with the degree but not the cause of inflammation. *Mediators Inflamm.* **2011**, 827565.

[399] Germanidis G, Argentou N, Hytiroglou P, Vassiliadis T, Patsiaoura K, Germenis AE, Speletas M (2013). Liver FOXP3 and PD1/ PDL1 expression is down-regulated in chronic HBV hepatitis on maintained remission related to the degree of inflammation. *Front. Immunol.* **4**, 207.

[400] Wang WH, Jiang CL, Yan W, Zhang YH, Yang JT, Zhang C, Yan B, Zhang W, Han W, Wang JZ, Zhang YQ (2010). FOXP3 expression and clinical characteristics of hepatocellular carcinoma. *World J. Gastroenterol.* **16**, 5502–5509.

[401] Jeannot E, Mellottee L, Bioulac-Sage P, Balabaud C, Scoazec JY, Van Nhieu JT, Bacq Y, Michalak S, Buob D, Laurent-Puig P, Rusyn I, Zucman-Rossi J (2010). Spectrum of *HNF1A* somatic mutations in hepatocellular adenoma differs from that in patients with MODY3 and suggests genotoxic damage. *Diabetes*. **59**, 1836–1844.

[402] Willson JSB, Godwin TD, Wiggins GA, Guilford PJ, McCall JL (2013). Primary hepatocellular neoplasms in a MODY3 family with a novel *HNF1A* germline mutation. *J. Hepatol.* **59**, 904–907.

[403] Cho SJ, Ferrell LD, Gill RM (2016). Expression of liver fatty acid binding protein in hepatocellular carcinoma. *Hum. Pathol.* **50**, 135–139.

[404] Wang W, Hayashi Y, Ninomiya T, Ohta K, Nakabayashi H, Tamaoki T, Itoh H (1998). Expression of HNF-1α and HNF-1β in various histological differentiations of hepatocellular carcinoma. *J. Pathol.* **184**, 272–278.

[405] The Cancer Genome Atlas Research Network (2017). Comprehensive and integrative genomic characterization of hepatocellular carcinoma. *Cell*. **169**, 1327–1341.

[406] Patitucci C, Couchy G, Bagattin A, Cañeque T, De Reyniès A, Scoazec JY, Rodriguez R, Pontoglio M, Zucman-Rossi J, Pende M, Panasyuk G (2017). Hepatocyte nuclear factor 1α suppresses steatosis-associated liver cancer by inhibiting PPARγ transcription. *J. Clin. Invest.* **127**, 1873–1888.

[407] Ni Q, Ding K, Wang KQ, He J, Yin C, Shi J, Zhang X, Xie WF, Shi YQ (2017). Deletion of *HNF1α* in hepatocytes results in fatty liver-related hepatocellular carcinoma in mice. *FEBS Lett.* **591**, 1947–1957.

[408] Alunni-Fabbroni M, Rönsch K, Huber T, Cyran CC, Seidensticker M, Mayerle J, Pech M, Basu B, Verslype C, Benckert J, Malfertheiner P, Ricke J (2019). Circulating DNA as prognostic biomarker in patients with advanced hepatocellular carcinoma: A translational exploratory study from the SORAMIC trial. *J. Transl. Med.* **17**, 328.

[409] Vallianou I, Dafou D, Vassilaki N, Mavromara P, Hadzopoulou-Cladaras M (2016). Hepatitis C virus suppresses hepatocyte nuclear factor 4 alpha, a key regulator of hepatocellular carcinoma. *Int. J. Biochem. Cell Biol.* **78**, 315–326.

[410] Shim J, Lee H, Han S, Kang H, Yu E, Lee S (2013). Hepatocyte nuclear factor 1β is a novel prognostic marker independent of the Milan criteria in transplantable hepatocellular carcinoma: A retrospective analysis based on tissue microarrays. *Liver Transplant.* **19**, 336–345.

[411] Yu DD, Jing YY, Guo SW, Ye F, Lu W, Li Q, Dong YL, Gao L, Yang YT, Yang Y, Wu MC, Wei LX (2015). Overexpression of hepatocyte nuclear factor-1β predicting poor prognosis is associated with biliary phenotype in patients with hepatocellular carcinoma. *Sci. Rep.* **5**, 13319.

[412] Zhu JN, Jiang L, Jiang JH, Yang X, Li XY, Zeng JX, Shi RY, Shi Y, Pan XR, Han ZP, Wei LX (2017). Hepatocyte nuclear factor-1β enhances the stemness of hepatocellular carcinoma cells through activation of the Notch pathway. *Sci. Rep.* **7**, 4793.

[413] Kotalova R, Dusatkova P, Cinek O, Dusatkova L, Dedic T, Seeman T, Lebl J, Pruhova S (2015). Hepatic phenotypes of *HNF1B* gene mutations: A case of neonatal cholestasis requiring portoenterostomy and literature review. *World J. Gastroenterol.* **21**, 2550–2557.

[414] De Leusse C, Maues De Paula A, Aschero A, Parache C, Hery G, Cailliez M, Missirian C, Fabre A (2019). Hepatocarcinoma and cholestasis associated to germline hemizygous deletion of gene *HNF1B*. *J. Pediatr. Gastroenterol. Nutr.* **68**, e85.

[415] Kettunen JLT, Parviainen H, Miettinen PJ, Färkkilä M, Tamminen M, Salonen P, Lantto E, Tuomi T (2017). Biliary anomalies in patients with HNF1B diabetes. *J. Clin. Endocrinol. Metab.* **102**, 2075–2082.

[416] Lei X, Xu JF, Chang RM, Fang F, Zuo CH, Yang LY (2016). JARID2 promotes invasion and metastasis of hepatocellular carcinoma by facilitating epithelial-mesenchymal transition through PTEN/ AKT signaling. *Oncotarget*. **7**, 40266–40284.

[417] Sun C, Sun L, Jiang K, Gao DM, Kang XN, Wang C, Zhang S, Huang S, Qin X, Li Y, Liu YK (2013). NANOG promotes liver cancer cell invasion by inducing epithelial-mesenchymal transition through NODAL/ SMAD3 signaling pathway. *Int. J. Biochem. Cell Biol.* **45**, 1099–1108.

[418] Liang C, Zhang K, Ge H, Li W, Li G, Wu J (2018). Prognostic and clinicopathological value of Nanog in hepatocellular carcinoma: A meta-analysis. *Clin. Chim. Acta*. **477**, 24–31.

[419] Gawlik-Rzemieniewska N, Bednarek I (2016). The role of NANOG transcriptional factor in the development of malignant phenotype of cancer cells. *Cancer Biol. Ther.* **17**, 1–10.

[420] Zhou JJ, Chen RF, Deng XG, Zhou Y, Ye X, Yu M, Tang J, He XY, Cheng D, Zeng B, Zhou QB, Li ZH (2014). Hepatitis C virus core protein regulates NANOG expression via the stat3 pathway. *FEBS Lett.* **588**, 566–573.

[421] Ching RHH, Sze KMF, Lau EYT, Chiu YT, Lee JMF, Ng IOL, Lee TKW (2017). C-terminal truncated hepatitis B virus X protein regulates tumorigenicity, self-renewal and drug resistance via STAT3/ Nanog signaling pathway. *Oncotarget*. **8**, 23507–23516.

[422] Xu Z, Chen L, Leung L, Yen TSB, Lee C, Chan JY (2005). Liver-specific inactivation of the *Nrf1* gene in adult mouse leads to nonalcoholic steatohepatitis and hepatic neoplasia. *Proc. Natl. Acad. Sci. U. S. A.* **102**, 4120–4125.

[423] Parola M, Novo E (2005). Nrf1 gene expression in the liver: A single gene linking oxidative stress to NAFLD, NASH and hepatic tumours. *J. Hepatol.* **43**, 1096–1097.

[424] Zhang T, Zhao X, Steer CJ, Yan G, Song G (2018). A negative feedback loop between microRNA-378 and *Nrf1* promotes the development of hepatosteatosis in mice treated with a high fat diet. *Metabolism.* **85**, 183–191.

[425] Yin L, Wang Y, Guo X, Xu C, Yu G (2018). Comparison of gene expression in liver regeneration and hepatocellular carcinoma formation. *Cancer Manag. Res.* **10**, 5691–5708.

[426] Wang J, Liu F, Ao P, Li X, Zheng H, Wu D, Zhang N, She J, Yuan J, Wu X (2016). Correlation of PDK1 expression with clinicopathologic features and prognosis of hepatocellular carcinoma. *Onco. Targets. Ther.* **9**, 5597–5602.

[427] Xia H, Dai X, Yu H, Zhou S, Fan Z, Wei G, Tang Q, Gong Q, Bi F (2018). EGFR-PI3K-PDK1 pathway regulates YAP signaling in hepatocellular carcinoma: The mechanism and its implications in targeted therapy. *Cell Death Dis.* **9**, 269.

[428] Li C, Lin C, Cong X, Jiang Y (2018). PDK1-WNK1 signaling is affected by HBx and involved in the viability and metastasis of hepatic cells. *Oncol. Lett.* **15**, 5940–5946.

[429] Kim MG, Moon JS, Kim EJ, Lee SH, Oh JW (2012). Destabilization of PDK1 by Hsp90 inactivation suppresses hepatitis C virus replication through inhibition of PRK2-mediated viral RNA polymerase phosphorylation. *Biochem. Biophys. Res. Commun.* **421**, 112–118.

[430] Jung GS, Jeon JH, Choi YK, Jang SY, Park SY, Kim SW, Byun JK, Kim MK, Lee S, Shin EC, Lee IK, Kang YN, Park KG (2016). Pyruvate dehydrogenase kinase regulates hepatitis C virus replication. *Sci. Rep.* **6**, 30846.

[431] Yu Y, Li S, Zhang H, Zhang X, Guo D, Zhang J (2018). NRSF/ REST levels are decreased in cholangiocellular carcinoma but not hepatocellular carcinoma compared with normal liver tissues: A tissue microarray study. *Oncol. Lett.* **15**, 6592–6598.

[432] Park MY, Kim KR, Park HS, Park BH, Choi HN, Jang KY, Chung MJ, Kang MJ, Lee DG, Moon WS (2007). Expression of the serum response factor in hepatocellular carcinoma: Implications for epithelial-mesenchymal transition. *Int. J. Oncol.* **31**, 1306–1315.

[433] Kwon CY, Kim KR, Choi HN, Chung MJ, Noh SJ, Kim DG, Kang MJ, Lee DG, Moon WS (2010). The role of serum response factor in hepatocellular carcinoma: Implications for disease progression. *Int. J. Oncol.* **37**, 837–844.

[434] Kim K, Bae J, Choi H, Park H, Jang K, Chung M, Moon W (2011). The role of serum response factor in hepatocellular carcinoma: An association with matrix metalloproteinase. *Oncol. Rep.* **26**, 1567–1572.

[435] Bae JS, Noh SJ, Kim KM, Jang KY, Chung MJ, Kim DG, Moon WS (2014). Serum response factor induces epithelial to mesenchymal transition with resistance to sorafenib in hepatocellular carcinoma. *Int. J. Oncol.* **44**, 129–136.

[436] Ohrnberger S, Thavamani A, Braeuning A, Lipka DB, Kirilov M, Geffers R, Authenrieth SE, Römer M, Zell A, Bonin M, Schwarz M, Schütz G, Schirmacher P, Plass C, Longerich T, Nordheim A (2015). Dysregulated serum response factor triggers formation of hepatocellular carcinoma. *Hepatology*. **61**, 979–989.

[437] Zeng C, Wang YL, Xie C, Sang Y, Li TJ, Zhang M, Wang R, Zhang Q, Zheng L, Zhuang SM (2015). Identification of a novel TGF-β-miR-122-fibronectin 1/ serum response factor signaling cascade and its implication in hepatic fibrogenesis. *Oncotarget*. **6**, 12224–12233.

[438] Kong M, Hong W, Shao Y, Lv F, Fan Z, Li P, Xu Y, Guo J (2019). Ablation of serum response factor in hepatic stellate cells attenuates liver fibrosis. *J. Mol. Med.* **97**, 1521–1533.

[439] Lin KH, Shieh HY, Chen SL, Hsu HC (1999). Expression of mutant thyroid hormone nuclear receptors in human hepatocellular carcinoma cells. *Mol. Carcinog.* **26**, 53–61.

[440] Chan IH, Privalsky ML (2006). Thyroid hormone receptors mutated in liver cancer function as distorted antimorphs. *Oncogene*. **25**, 3576–3588.

[441] Wang T, Xia L, Ma S, Qi X, Li Q, Xia Y, Tang X, Cui D, Wang Z, Chi J, Li P, Feng YX, Xia Q, Zhai B (2016). Hepatocellular carcinoma: Thyroid hormone promotes tumorigenicity through inducing cancer stem-like cell self-renewal. *Sci. Rep.* **6**, 25183.

[442] Manka P, Coombes JD, Boosman R, Gauthier K, Papa S, Syn WK (2018). Thyroid hormone in the regulation of hepatocellular carcinoma and its microenvironment. *Cancer Lett.* **419**, 175–186.

[443] Lu Y, Ma Z, Zhang Z, Xiong X, Wang X, Zhang H, Shi G, Xia X, Ning G, Li X (2014). Yin Yang 1 promotes hepatic steatosis through repression of farnesoid X receptor in obese mice. *Gut*. **63**, 170–178.

[444] Her GM, Pai WY, Lai CY, Hsieh YW, Pang HW (2013). Ubiquitous transcription factor YY1 promotes zebrafish liver steatosis and lipotoxicity by inhibiting CHOP-10 expression. *Biochim. Biophys. Acta*. **1831**, 1037–1051.

[445] Wu GY, Rui C, Chen JQ, Sho E, Zhan SS, Yuan XW, Ding YT (2017). MicroRNA-122 inhibits lipid droplet formation and hepatic triglyceride accumulation via Yin Yang 1. *Cell. Physiol. Biochem.* **44**, 1651–1664.

[446] Yuan X, Chen J, Cheng Q, Zhao Y, Zhang P, Shao X, Bi Y, Shi X, Ding Y, Sun X, Xue B (2018). Hepatic expression of Yin Yang 1 (YY1) is associated with the non-alcoholic fatty liver disease (NAFLD) progression in patients undergoing bariatric surgery. *BMC Gastroenterol.* **18**, 147.

[447] Notarbartolo M, Giannitrapani L, Vivona N, Poma P, Labbozzetta M, Florena AM, Porcasi R, Muggeo VM, Sandonato L, Cervello M, Montalto G, D'Alessandro N (2011). Frequent alteration of the Yin Yang 1/ Raf-1 Kinase inhibitory protein ratio in hepatocellular carcinoma. *Omi. A J. Integr. Biol.* **15**, 267–272.

[448] Zhang S, Jiang T, Feng L, Sun J, Lu H, Wang Q, Pan M, Huang D, Wang X, Wang L, Jin H (2012). Yin Yang-1 suppresses differentiation of hepatocellular carcinoma cells through the downregulation of CCAAT/ enhancer-binding protein alpha. *J. Mol. Med.* **90**, 1069–1077.

[449] Tsang DP, Wu WK, Kang W, Lee YY, Wu F, Yu Z, Xiong L, Chan AW, Tong JH, Yang W, Li MS, Lau SS, Li X, Lee SD, Yang Y, Lai PB, Yu DY, Xu G, Lo KW, Chan MT, Wang H, Lee TL, Yu J, Wong N, Yip KY, To KF, Cheng AS (2016). Yin Yang 1-mediated epigenetic silencing of tumour-suppressive microRNAs activates nuclear factor-κB in hepatocellular carcinoma. *J. Pathol.* **238**, 651–664.

[450] Li Y, Kasim V, Yan X, Li L, Meliala ITS, Huang C, Li Z, Lei K, Song G, Zheng X, Wu S (2019). Yin Yang 1 facilitates hepatocellular carcinoma cell lipid metabolism and tumor progression by inhibiting PGC-1β–induced fatty acid oxidation. *Theranostics*. **9**, 7599–7615.

[451] Hayashi Y, Kitamura Y, Nakanishi M, Koike K (2000). The binding site of transcription factor YY1 is required for intramolecular recombination between terminally repeated sequences of linear replicative hepatitis B virus DNA. *J. Virol.* **74**, 9471–9478.

[452] Zhang L, Cai X, Chen K, Wang Z, Wang L, Ren M, Huang A, Tang H (2011). Hepatitis B virus protein up-regulated HLJ1 expression via the transcription factor YY1 in human hepatocarcinoma cells. *Virus Res.* **157**, 76–81.

[453] Shan X, Ren M, Chen K, Huang A, Tang H (2015). Regulation of the microRNA processor DGCR8 by hepatitis B virus proteins via the transcription factor YY1. *Arch. Virol.* **160**, 795–803.

[454] Waidmann O, Köberle V, Brunner F, Zeuzem S, Piiper A, Kronenberger B (2012). Serum microRNA-122 predicts survival in patients with liver cirrhosis. *PLoS One*. **7**, e45652.

[455] Hironaka K, Factor VM, Calvisi DF, Conner EA, Thorgeirsson SS (2003). Dysregulation of DNA repair pathways in a transforming growth factor α/ c-myc transgenic mouse model of accelerated hepatocarcinogenesis. *Lab. Investig.* **83**, 643–654.

[456] Nowacka-Zawisza M, Bryś M, Romanowicz-Makowska H, Kulig A, Małgorzata Krajewska W (2006). Loss of heterozygosity and microsatellite instability at RAD52 and RAD54 loci in breast cancer. *Polish J. Pathol.* **57**, 83–89.

[457] Qadeer ZA, Harcharik S, Valle-Garcia D, Chen C, Birge MB, Vardabasso C, Duarte LF, Bernstein E (2014). Decreased expression of the chromatin remodeler ATRX associates with melanoma progression. *J. Invest. Dermatol.* **134**, 1768–1772.

[458] Wood LD, Heaphy CM, Daniel HD, Naini BV, Lassman CR, Arroyo MR, Kamel IR, Cosgrove DP, Boitnott JK, Meeker AK, Torbenson MS (2013). Chromophobe hepatocellular carcinoma with abrupt anaplasia: A proposal for a new subtype of hepatocellular carcinoma with unique morphological and molecular features. *Mod. Pathol.* **26**, 1586–1593.

[459] Weisbrod AB, Zhang L, Jain M, Barak S, Quezado MM, Kebebew E (2013). Altered *PTEN*, *ATRX*, *CHGA*, *CHGB*, and *TP53* expression are associated with aggressive VHL-associated pancreatic neuroendocrine tumors. *Horm. Cancer*. **4**, 165–175.

[460] Haines K, Sarabia S, Alvarez K, Tomlinson G, Vasudevan S, Heczey A, Roy A, Finegold M, Parsons D, Plon S, López-Terrada D (2019). Characterization of pediatric hepatocellular carcinoma reveals genomic heterogeneity and diverse signaling pathway activation. *Pediatr. Blood Cancer*. **66**, e27745.

[461] Aveic S, Pigazzi M, Basso G (2011). BAG1: The guardian of anti-apoptotic proteins in acute myeloid leukemia. *PLoS One*. **6**, e26097.

[462] Papadakis ES, Reeves T, Robson NH, Maishman T, Packham G, Cutress RI (2017). BAG-1 as a biomarker in early breast cancer prognosis: A systematic review with meta-analyses. *Br. J. Cancer*. **116**, 1585–1594.

[463] D'Arcangelo D, Giampietri C, Muscio M, Scatozza F, Facchiano F, Facchiano A (2018). *WIPI1*, *BAG1*, and *PEX3* autophagy-related genes are relevant melanoma markers. *Oxid. Med. Cell. Longev.* **2018**, 1471682.

[464] Ni W, Chen B, Zhou G, Lu C, Xiao M, Guan C, Zhang Y, He S, Shen A, Ni R (2013). Overexpressed nuclear BAG-1 in human hepatocellular carcinoma is associated with poor prognosis and resistance to doxorubicin. *J. Cell. Biochem.* **114**, 2120–2130.

[465] Garcia EJ, Lawson D, Cotsonis G, Cohen C (2002). Hepatocellular carcinoma and markers of apoptosis (bcl-2, bax, bcl-x): Prognostic significance. *Appl. Immunohistochem. Mol. Morphol.* **10**, 210–217.

[466] Guo XZ, Shao XD, Liu MP, Xu JH, Ren LN, Zhao JJ, Li HY, Wang D (2002). Effect of bax, bcl-2 and bcl-xL on regulating apoptosis in tissues of normal liver and hepatocellular carcinoma. *World J. Gastroenterol.* **8**, 1059–1062.

[467] Wang C, Yao B, Xu M, Zheng X (2016). RIP1 upregulation promoted tumor progression by activating AKT/ Bcl-2/ BAX signaling and predicted poor postsurgical prognosis in HCC. *Tumor Biol.* **37**, 15305–15313.

[468] Wang Y, Ausman LM, Russell RM, Greenberg AS, Wang XD (2008). Increased apoptosis in high-fat diet–induced nonalcoholic steatohepatitis in rats is associated with c-Jun NH2-terminal kinase activation and elevated proapoptotic Bax. *J. Nutr.* **138**, 1866–1871.

[469] Li CP, Li JH, He SY, Li P, Zhong XL (2014). Roles of Fas/ Fasl, Bcl-2/ Bax, and Caspase-8 in rat nonalcoholic fatty liver disease pathogenesis. *Genet. Mol. Res.* **13**, 3991–3999.

[470] Chung YL, Sheu ML, Yen SH (2003). Hepatitis C virus NS5A as a potential viral Bcl-2 homologue interacts with Bax and inhibits apoptosis in hepatocellular carcinoma. *Int. J. Cancer*. **107**, 65–73.

[471] Deng L, Adachi T, Kitayama K, Bungyoku Y, Kitazawa S, Ishido S, Shoji I, Hotta H (2008). Hepatitis C virus infection induces apoptosis through a Bax-triggered, mitochondrion-mediated, caspase 3-dependent pathway. *J. Virol.* **82**, 10375–10385.

[472] Wang J, Liu G, Liu M, Xiang L, Xiao Y, Zhu H, Wu X, Peng Y, Zhang W, Jiang P, Li A, Nan Q, Chen Y, Chen C, Cheng T, Liu S, Wang J (2018). The FOXK1-CCDC43 axis promotes the invasion and metastasis of colorectal cancer cells. *Cell. Physiol. Biochem.* **51**, 2547–2563.

[473] Lee TK, Cheung VC, Lu P, Lau EY, Ma S, Tang KH, Tong M, Lo J, Ng IO (2014). Blockade of CD47-mediated cathepsin S/ protease-activated receptor 2 signaling provides a therapeutic target for hepatocellular carcinoma. *Hepatology*. **60**, 179–191.

[474] Lo J, Lau EY, Ching RH, Cheng BY, Ma MK, Ng IO, Lee TK (2015). Nuclear factor kB-mediated CD47 up-regulation promotes sorafenib resistance and its blockade synergizes the effect of sorafenib in hepatocellular carcinoma in mice. *Hepatology*. **62**, 534–545.

[475] Roberts DD, Kaur S, Soto-Pantoja DR (2015). Therapeutic targeting of the thrombospondin-1 receptor CD47 to treat liver cancer. *J. Cell Commun. Signal.* **9**, 101–102.

[476] Xiaoa Z, Chung H, Banan B, Manning PT, Ott KC, Lin S, Capoccia BJ, Subramanian V, Hiebsch RR, Upadhya GA, Mohanakumar T, Frazier WA, Lin Y, Chapman WC (2015). Antibody mediated therapy targeting CD47 inhibits tumor progression of hepatocellular carcinoma. *Cancer Lett.* **360**, 302–309.

[477] Liu Q, Yu S, Jiang GC, Zhou ZL, Liu BC, Bu L, Yang F, Qiao F, Wang J (2013). Change of CMTM7 expression, a potential tumor suppressor, is associated with poor clinical outcome in human non-small cell lung cancer. *Chin. Med. J. (Engl).* **126**, 3006–3012.

[478] Li H, Li J, Su Y, Fan Y, Guo X, Li L, Su X, Rong R, Ying J, Mo X, Liu K, Zhang Z, Yang F, Jiang G, Wang J, Zhang Y, Ma D, Tao Q, Han W (2014). A novel 3p22.3 gene *CMTM7* represses oncogenic EGFR signaling and inhibits cancer cell growth. *Oncogene*. **33**, 3109–3118.

[479] Liu B, Su Y, Li T, Yuan W, Mo X, Li H, He Q, Ma D, Han W (2015). CMTM7 knockdown increases tumorigenicity of human non-small cell lung cancer cells and EGFR-AKT signaling by reducing Rab5 activation. *Oncotarget*. **6**, 41092–41107.

[480] Jin Y, Qin X, Jia G (2018). SOX10-dependent CMTM7 expression inhibits cell proliferation and tumor growth in gastric carcinoma. *Biochem. Biophys. Res. Commun.* **507**, 91–99.

[481] Huang ZM, Li PL, Yang P, Hou XD, Yang YL, Xu X, Xu F (2019). Overexpression of CMTM7 inhibits cell growth and migration in liver cancer. *Kaohsiung J. Med. Sci.* **35**, 332–340.

[482] Lv Q, Hua F, Hu ZW (2012). DEDD, a novel tumor repressor, reverses epithelial-mesenchymal transition by activating selective autophagy. *Autophagy*. **8**, 1675–1676.

[483] Lv Q, Hua F, Hu Z (2014). Use of the tumor repressor DEDD as a prognostic marker of cancer metastasis. *Methods Mol. Biol.* **1165**, 197–222.

[484] Xue JF, Hua F, Lv Q, Lin H, Wang ZY, Yan J, Liu JW, Lv XX, Yang HZ, Hu ZW (2010). DEDD negatively regulates transforming growth factor-β1 signaling by interacting with Smad3. *FEBS Lett.* **584**, 3028–3034.

[485] Wang L, Cao XX, Chen Q, Zhu TF, Zhu HG, Zheng L (2009). DIXDC1 targets p21 and cyclin D1 via PI3K pathway activation to promote colon cancer cell proliferation. *Cancer Sci.* **100**, 1801–1808.

[486] Xu Z, Liu D, Fan C, Luan L, Zhang X, Wang E (2014). DIXDC1 increases the invasion and migration ability of non-small-cell lung cancer cells via the PI3K-AKT/ AP-1 pathway. *Mol. Carcinog.* **53**, 917–925.

[487] Tan C, Qiao F, Wei P, Chi Y, Wang W, Ni S, Wang Q, Chen T, Sheng W, Du X, Wang L (2016). DIXDC1 activates the Wnt signaling pathway and promotes gastric cancer cell invasion and metastasis. *Mol. Carcinog.* **55**, 397–408.

[488] Li X, Xiao Y, Fan S, Xiao M, Wang X, Zhu X, Chen X, Li C, Zong G, Zhou G, Wan C (2016). Overexpression of DIXDC1 correlates with enhanced cell growth and poor prognosis in human pancreatic ductal adenocarcinoma. *Hum. Pathol.* **57**, 182–192.

[489] Zhou S, Shen J, Lin S, Liu X, Xu M, Shi L, Wang X, Cai X (2016). Downregulated expression of DIXDC1 in hepatocellular carcinoma and its correlation with prognosis. *Tumor Biol.* **37**, 13607–13616.

[490] Kim BY, Lee JG, Park S, Ahn JY, Ju YJ, Chung JH, Han CJ, Jeong SH, Yeom Y Il, Kim S, Lee YS, Kim CM, Eom EM, Lee DH, Choi KY, Cho MH, Suh KS, Choi DW, Lee KH (2004). Feature genes of hepatitis B virus-positive hepatocellular carcinoma, established by its molecular discrimination approach using prediction analysis of microarray. *Biochim. Biophys. Acta*. **1739**, 50–61.

[491] Han CP, Yu YH, Wang AG, Tian Y, Zhang HT, Zheng ZM, Liu YS (2018). Desmoglein-2 overexpression predicts poor prognosis in hepatocellular carcinoma patients. *Eur. Rev. Med. Pharmacol. Sci.* **22**, 5481–5489.

[492] Fang WK, Gu W, Liao L Di, Chen B, Wu ZZ, Wu JY, Shen J, Xu LY, Li EM (2014). Prognostic significance of desmoglein 2 and desmoglein 3 in esophageal squamous cell carcinoma. *Asian Pacific J. Cancer Prev.* **15**, 871–876.

[493] Barber AG, Castillo-Martin M, Bonal DM, Rybicki BA, Christiano AM, Cordon-Cardo C (2014). Characterization of desmoglein expression in the normal prostatic gland. Desmoglein 2 is an independent prognostic factor for aggressive prostate cancer. *PLoS One*. **9**, e98786.

[494] Saaber F, Chen Y, Cui T, Yang L, Mireskandari M, Petersen I (2015). Expression of desmogleins 1–3 and their clinical impacts on human lung cancer. *Pathol. Res. Pract.* **211**, 208–213.

[495] Tang W, Lázaro CA, Campbell JS, Parks WT, Katze MG, Fausto N (2007). Responses of nontransformed human hepatocytes to conditional expression of full-length hepatitis C virus open reading frame. *Am. J. Pathol.* **171**, 1831–1846.

[496] Berger KL, Cooper JD, Heaton NS, Yoon R, Oakland TE, Jordan TX, Mateu G, Grakoui A, Randall G (2009). Roles for endocytic trafficking and phosphatidylinositol 4-kinase III alpha in hepatitis C virus replication. *Proc. Natl. Acad. Sci. U. S. A.* **106**, 7577–7582.

[497] Lai CK, Jeng KS, Machida K, Lai MM (2010). Hepatitis C virus egress and release depend on endosomal trafficking of core protein. *J. Virol.* **84**, 11590–11598.

[498] Kaufmann R, Rahn S, Pollrich K, Hertel J, Dittmar Y, Hommann M, Henklein P, Biskup C, Westermann M, Hollenberg MD, Settmacher U (2007). Thrombin-mediated hepatocellular carcinoma cell migration: Cooperative action via proteinase-activated receptors 1 and 4. *J. Cell. Physiol.* **211**, 699–707.

[499] Jan YJ, Ko BS, Liu TA, Wu YM, Liang SM, Chen SC, Wang J, Liou JY (2013). Expression of partitioning defective 3 (Par-3) for predicting extrahepatic metastasis and survival with hepatocellular carcinoma. *Int. J. Mol. Sci.* **14**, 1684–1697.

[500] Wang F, Anderson PW, Salem N, Kuang Y, Tennant BC, Lee Z (2007). Gene expression studies of hepatitis virus-induced woodchuck hepatocellular carcinoma in correlation with human results. *Int. J. Oncol.* **30**, 33–44.

[501] Colman H, Le Berre-Scoul C, Hernandez C, Pierredon S, Bihouee A, Houlgatte R, Vagner S, Rosenberg AR, Feray C (2013). Genome-wide analysis of host mRNA translation during hepatitis C virus infection. *J. Virol.* **87**, 6668–6677.

[502] Colucci S, Pagani A, Pettinato M, Artuso I, Nai A, Camaschella C, Silvestri L (2017). The immunophilin FKBP12 inhibits hepcidin expression by binding the BMP type I receptor ALK2 in hepatocytes. *Blood*. **130**, 2111–2120.

[503] Chen YG, Liu F, Massagué J (1997). Mechanism of TGFβ receptor inhibition by FKBP12. *EMBO J.* **16**, 3866–3876.

[504] Wei SC, Fattet L, Tsai JH, Guo Y, Pai VH, Majeski HE, Chen AC, Sah RL, Taylor SS, Engler AJ, Yang J (2015). Matrix stiffness drives epithelial-mesenchymal transition and tumour metastasis through a TWIST1-G3BP2 mechanotransduction pathway. *Nat. Cell Biol.* **17**, 678–688.

[505] Gupta N, Badeaux M, Liu Y, Naxerova K, Sgroi D, Munn LL, Jain RK, Garkavtsev I (2017). Stress granule-associated protein G3BP2 regulates breast tumor initiation. *Proc. Natl. Acad. Sci. U. S. A.* **114**, 1033–1038.

[506] Takayama KI, Suzuki T, Tanaka T, Fujimura T, Takahashi S, Urano T, Ikeda K, Inoue S (2018). TRIM25 enhances cell growth and cell survival by modulating p53 signals via interaction with G3BP2 in prostate cancer. *Oncogene*. **37**, 2165–2180.

[507] Schwerk J, Jarret AP, Joslyn RC, Savan R (2015). Landscape of post-transcriptional gene regulation during hepatitis C virus infection. *Curr. Opin. Virol.* **12**, 74–84.

[508] Huang J, Yang J, Lei Y, Gao H, Wei T, Luo L, Zhang F, Chen H, Zeng Q, Guo L (2016). An ANCCA/ PRO2000-miR-520a-E2F2 regulatory loop as a driving force for the development of hepatocellular carcinoma. *Oncogenesis*. **5**, e229.

[509] Alcedo KP, Guerrero A, Basrur V, Fu D, Richardson ML, McLane JS, Tsou C, Nesvizhskii AI, Welling TH, Lebrilla CB, Otey CA, Kim HJ, Omary MB, Snider NT (2019). Tumor-selective altered glycosylation and functional attenuation of CD73 in human hepatocellular carcinoma. *Hepatol. Commun.* **3**, 1400–1414.

[510] Chang SH, Hong SH, Jiang HL, Minai-Tehrani A, Yu KN, Lee JH, Kim JE, Shin JY, Kang B, Park S, Han K, Chae C, Cho MH (2012). GOLGA2/ GM130, cis-golgi matrix protein, is a novel target of anticancer gene therapy. *Mol. Ther.* **20**, 2052–2063.

[511] Zhao J, Yang C, Guo S, Wu Y (2015). GM130 regulates epithelial-to-mesenchymal transition and invasion of gastric cancer cells via Snail. *Int. J. Clin. Exp. Pathol.* **8**, 10784–10791.

[512] Minocha S, Villeneuve D, Praz V, Moret C, Lopes M, Pinatel D, Rib L, Guex N, Herr W (2019). Rapid recapitulation of nonalcoholic steatohepatitis upon loss of host cell factor 1 function in mouse hepatocytes. *Mol. Cell. Biol.* **39**, e00405–e00418.

[513] Tyagi S, Chabes AL, Wysocka J, Herr W (2007). E2F activation of S phase promoters via association with HCF-1 and the MLL family of histone H3K4 methyltransferases. *Mol. Cell*. **27**, 107–119.

[514] Ye Y, Huang A, Huang C, Liu J, Wang B, Lin K, Chen Q, Zeng Y, Chen H, Tao X, Wei G, Wu Y (2013). Comparative mitochondrial proteomic analysis of hepatocellular carcinoma from patients. *Proteomics - Clin. Appl.* **7**, 403–415.

[515] Qi LN, Li LQ, Chen YY, Chen ZH, Bai T, Xiang BD, Qin X, Xiao KY, Peng MH, Liu ZM, Liu TW, Qin X, Li S, Han ZG, Mo ZN, Santella RM, Winkler CA, O'Brien SJ, Peng T (2013). Genome-wide and differential proteomic analysis of hepatitis B virus and aflatoxin B1 related hepatocellular carcinoma in Guangxi, China. *PLoS One*. **8**, e83465.

[516] Chu S, Wen Q, Qing Z, Luo J, Wang W, Chen L, Feng J, Xu L, Zang H, Fan S (2017). High expression of heat shock protein 10 correlates negatively with estrogen/ progesterone receptor status and predicts poor prognosis in invasive ductal breast carcinoma. *Hum. Pathol.* **61**, 173–180.

[517] Jia H, Halilou AI, Hu L, Cai W, Liu J, Huang B (2011). Heat shock protein 10 (Hsp10) in immune-related diseases: One coin, two sides. *Int. J. Biochem. Mol. Biol.* **2**, 47–57.

[518] Xie H, Bae H, Noh J, Eun J, Kim J, Jung K, Ryu J, Ahn Y, Kim S, Lee S, Yoo N, Lee J, Park W, Nam S (2009). Mutational analysis of *JAK1* gene in human hepatocellular carcinoma. *Neoplasma*. **56**, 136–140.

[519] Arbuthnot P, Capovilla A, Kew M (2000). Putative role of hepatitis B virus X protein in hepatocarcinogenesis: Effects on apoptosis, DNA repair, mitogen-activated protein kinase and JAK/ STAT pathways. *J. Gastroenterol. Hepatol.* **15**, 357–368.

[520] Yang S, Luo C, Gu Q, Xu Q, Wang G, Sun H, Qian Z, Tan Y, Qin Y, Shen Y, Xu X, Chen SH, Chan CC, Wang H, Mao M, Fang DD (2016). Activating JAK1 mutation may predict the sensitivity of JAK-STAT inhibition in hepatocellular carcinoma. *Oncotarget*. **7**, 5461–5469.

[521] Lee YH, Yun Y (1998). HBx protein of hepatitis B virus activates Jak1-STAT signaling. *J. Biol. Chem.* **273**, 25510–25515.

[522] Wang ZC, Gao Q, Shi JY, Yang LX, Zhou J, Wang XY, Shi YH, Ke AW, Shi GM, Ding ZB, Dai Z, Qiu SJ, Fan J (2013). Genetic polymorphism of the kinesin-like protein *KIF1B* gene and the risk of hepatocellular carcinoma. *PLoS One*. **8**, e62571.

[523] Yang SZ, Wang JT, Yu WW, Liu Q, Wu YF, Chen SG (2015). Downregulation of *KIF1B* mRNA in hepatocellular carcinoma tissues correlates with poor prognosis. *World J. Gastroenterol.* **21**, 8418–8424.

[524] Chen JH, Wang YY, Lv WB, Gan Y, Chang W, Tian NN, Huang XH, Liu L, Yu XF, Chen SD (2016). Effects of interactions between environmental factors and *KIF1B* genetic variants on the risk of hepatocellular carcinoma in a Chinese cohort. *World J. Gastroenterol.* **22**, 4183–4190.

[525] Zhang H, Zhai Y, Hu Z, Wu C, Qian J, Jia W, Ma F, Huang W, Yu L, Yue W, Wang Z, Li P, Zhang Y, Liang R, Wei Z, Cui Y, Xie W, Cai M, Yu X, Yuan Y, Xia X, Zhang X, Yang H, Qiu W, Yang J, Gong F, Chen M, Shen H, Lin D, Zeng YX, He F, Zhou G (2010). Genome-wide association study identifies 1p36.22 as a new susceptibility locus for hepatocellular carcinoma in chronic hepatitis B virus carriers. *Nat. Genet.* **42**, 755–758.

[526] Yu Y, Feng YM (2010). The role of kinesin family proteins in tumorigenesis and progression. *Cancer*. **116**, 5150–5160.

[527] Liu Z, Rebowe RE, Wang Z, Li Y, Wang Z, DePaolo JS, Guo J, Qian C, Liu W (2014). KIF3a promotes proliferation and invasion via Wnt signaling in advanced prostate cancer. *Mol. Cancer Res.* **12**, 491–503.

[528] Chen J, Li S, Zhou S, Cao S, Lou Y, Shen H, Yin J, Li G (2017). Kinesin superfamily protein expression and its association with progression and prognosis in hepatocellular carcinoma. *J. Cancer Res. Ther.* **13**, 651–659.

[529] Ma J, Cao X (2006). Regulation of Stat3 nuclear import by importin α5 and importin α7 via two different functional sequence elements. *Cell. Signal.* **18**, 1117–1126.

[530] Sun Z, Wu T, Zhao F, Lau A, Birch CM, Zhang DD (2011). KPNA6 (Importin α-7)-mediated nuclear import of Keap1 represses the Nrf2-dependent antioxidant response. *Mol. Cell. Biol.* **31**, 1800–1811.

[531] Kann M, Schmitz A, Rabe B (2007). Intracellular transport of hepatitis B virus. *World J. Gastroenterol.* **13**, 39–47.

[532] Boyault S, Rickman DS, De Reyniès A, Balabaud C, Rebouissou S, Jeannot E, Hérault A, Saric J, Belghiti J, Franco D, Bioulac-Sage P, Laurent-Puig P, Zucman-Rossi J (2007). Transcriptome classification of HCC is related to gene alterations and to new therapeutic targets. *Hepatology*. **45**, 42–52.

[533] Yang L, Hu B, Zhang Y, Qiang S, Cai J, Huang W, Gong C, Zhang T, Zhang S Sen, Xu P, Wu X, Liu J (2015). Suppression of the nuclear transporter-KPNβ1 expression inhibits tumor proliferation in hepatocellular carcinoma. *Med. Oncol.* **32**, 128.

[534] Germain MA, Chatel-Chaix L, Gagné B, Bonneil É, Thibault P, Pradezynski F, de Chassey B, Meyniel-Schicklin L, Lotteau V, Baril M, Lamarre D (2014). Elucidating novel hepatitis C virus–host interactions using combined mass spectrometry and functional genomics approaches. *Mol. Cell. Proteomics*. **13**, 184–203.

[535] Gagné B, Tremblay N, Park AY, Baril M, Lamarre D (2017). Importin β1 targeting by hepatitis C virus NS3/4A protein restricts IRF3 and NF-κB signaling of IFNB1 antiviral response. *Traffic.* **18**, 362–377.

[536] Nishitsuji H, Ujino S, Shimizu Y, Harada K, Zhang J, Sugiyama M, Mizokami M, Shimotohno K (2015). Novel reporter system to monitor early stages of the hepatitis B virus life cycle. *Cancer Sci.* **106**, 1616–1624.

[537] Chang X, Liu F, Wang X, Lin A, Zhao H, Su B (2011). The kinases MEKK2 and MEKK3 regulate transforming growth factor-β-mediated helper T cell differentiation. *Immunity*. **34**, 201–202.

[538] Martinez GJ (2017). MINK1: The missing link between ROS and its inhibition of Th17 cells. *J. Exp. Med.* **214**, 1205–1206.

[539] Fu G, Xu Q, Qiu Y, Jin X, Xu T, Dong S, Wang J, Ke Y, Hu H, Cao X, Wang D, Cantor H, Gao X, Lu L (2017). Suppression of Th17 cell differentiation by misshapen/ NIK-related kinase MINK1. *J. Exp. Med.* **214**, 1453–1469.

[540] Daulat AM, Luu O, Sing A, Zhang L, Wrana JL, McNeill H, Winklbauer R, Angers S (2012). Mink1 regulates β-catenin-independent Wnt signaling via Prickle phosphorylation. *Mol. Cell. Biol.* **32**, 173–185.

[541] Mikryukov A, Moss T (2012). Agonistic and antagonistic roles for TNIK and MINK in non-canonical and canonical Wnt signalling. *PLoS One*. **7**, e43330.

[542] Nakamura M, Takii Y, Ito M, Komori A, Yokoyama T, Shimizu-Yoshida Y, Koyabu M, Matsuyama M, Mori T, Kamihira T, Daikoku M, Migita K, Yatsuhashi H, Nozaki N, Shimoda S, Ishibashi H (2006). Increased expression of nuclear envelope gp210 antigen in small bile ducts in primary biliary cirrhosis. *J. Autoimmun.* **26**, 138–145.

[543] Nakamura M, Kondo H, Mori T, Komori A, Matsuyama M, Ito M, Takii Y, Koyabu M, Yokoyama T, Migita K, Daikoku M, Abiru S, Yatsuhashi H, Takezaki E, Masaki N, Sugi K, Honda K, Adachi H, Nishi H, Watanabe Y, Nakamura Y, Shimada M, Komatsu T, Saito A, Saoshiro T, Harada H, Sodeyama T, Hayashi S, Masumoto A, Sando T, Yamamoto T, Sakai H, Kobayashi M, Muro T, Koga M, Shums Z, Norman GL, Ishibashi H (2007). Anti-gp210 and anti-centromere antibodies are different risk factors for the progression of primary biliary cirrhosis. *Hepatology*. **45**, 118–127.

[544] Czaja AJ (2010). Autoantibodies as prognostic markers in autoimmune liver disease. *Dig. Dis. Sci.* **55**, 2144–2161.

[545] Yamagiwa S, Kamimura H, Takamura M, Aoyagi Y (2014). Autoantibodies in primary biliary cirrhosis: Recent progress in research on the pathogenetic and clinical significance. *World J. Gastroenterol.* **20**, 2606–2612.

[546] Li J, Ghazwani M, Zhang Y, Lu J, Li J, Fan J, Gandhi CR, Li S (2013). miR-122 regulates collagen production via targeting hepatic stellate cells and suppressing P4HA1 expression. *J. Hepatol.* **58**, 522–528.

[547] Kanno M, Hasegawa M, Ishida A, Isono K, Taniguchi M (1995). *Mel-18*, a Polycomb group-related mammalian gene, encodes a transcriptional negative regulator with tumor suppressive activity. *EMBO J.* **14**, 5672–5678.

[548] Guo WJ, Zeng MS, Yadav A, Song LB, Guo BH, Band V, Dimri GP (2007). Mel-18 acts as a tumor suppressor by repressing Bmi-1 expression and down-regulating Akt activity in breast cancer cells. *Cancer Res.* **67**, 5083–5089.

[549] Wang W, Yuasa T, Tsuchiya N, Ma Z, Maita S, Narita S, Kumazawa T, Inoue T, Tsuruta H, Horikawa Y, Saito M, Hu W, Ogawa O, Habuchi T (2009). The novel tumor-suppressor Mel-18 in prostate cancer: Its functional polymorphism, expression and clinical significance. *Int. J. Cancer*. **125**, 2836–2843.

[550] Park JH, Lee JY, Shin DH, Jang KS, Kim HJ, Kong G (2011). Loss of Mel-18 induces tumor angiogenesis through enhancing the activity and expression of HIF-1α mediated by the PTEN/ PI3K/ Akt pathway. *Oncogene*. **30**, 4578–4589.

[551] Chen Q, Yan CQ, Liu FJ, Tong J, Miao SL, Chen JP (2008). Overexpression of the PDCD2-like gene results in Inhibited TNF-α production in activated Daudi cells. *Hum. Immunol.* **69**, 259–265.

[552] Barboza N, Minakhina S, Medina DJ, Balsara B, Greenwood S, Huzzy L, Rabson AB, Steward R, Schaar DG (2013). PDCD2 functions in cancer cell proliferation and predicts relapsed leukemia. *Cancer Biol. Ther.* **14**, 546–555.

[553] Yang Y, Jin Y, Du W (2015). Programmed cell death 2 functions as a tumor suppressor in osteosarcoma. *Int. J. Clin. Exp. Pathol.* **8**, 10894–10900.

[554] Liu H, Wang M, Liang N, Guan L (2019). PDCD2 sensitizes HepG2 cells to sorafenib by suppressing epithelial-mesenchymal transition. *Mol. Med. Rep.* **19**, 2173–2179.

[555] Zhang S, Li J, Jiang Y, Xu Y, Qin C (2009). Programmed cell death 4 (PDCD4) suppresses metastastic potential of human hepatocellular carcinoma cells. *J. Exp. Clin. Cancer Res.* **28**, 71.

[556] Matsuhashi S, Hamajima H, Xia JH, Zhang H, Mizuta T, Anzai K, Ozaki I (2014). Control of a tumor suppressor PDCD4: Degradation mechanisms of the protein in hepatocellular carcinoma cells. *Cell. Signal.* **26**, 603–610.

[557] Kamel RR, Amr KS, Afify M, Elhosary YA, Hegazy AE, Fahim HH, Ezzat WM (2016). Relation between microRNAs and apoptosis in hepatocellular carcinoma. *Maced. J. Med. Sci.* **4**, 31–37.

[558] Zhang Z, Zha Y, Hu W, Huang Z, Gao Z, Zang Y, Chen J, Dong L, Zhang J (2013). The autoregulatory feedback loop of microRNA-21/ programmed cell death protein 4/ activation protein-1 (miR-21/ PDCD4/ AP-1) as a driving force for hepatic fibrosis development. *J. Biol. Chem.* **288**, 37082–37093.

[559] Damania P, Sen B, Dar SB, Kumar S, Kumari A, Gupta E, Sarin SK, Venugopal SK (2014). Hepatitis B virus induces cell proliferation via HBx-induced microRNA-21 in hepatocellular carcinoma by targeting programmed cell death protein 4 (PDCD4) and phosphatase and tensin homologue (PTEN). *PLoS One*. **9**, e91745.

[560] Antonacopoulou AG, Grivas PD, Skarlas L, Kalofonos M, Scopa CD, Kalofonos HP (2008). POLR2F, ATP6V0A1 and PRNP expression in colorectal cancer: New molecules with prognostic significance? *Anticancer Res.* **28**, 1221–1227.

[561] Jia Z, Ai X, Sun F, Zang T, Guan Y, Gao F (2015). Identification of new hub genes associated with bladder carcinoma via bioinformatics analysis. *Tumori J.* **101**, 117–122.

[562] Roset R, Inagaki A, Hohl M, Brenet F, Lafrance-Vanasse J, Lange J, Scandura JM, Tainer JA, Keeney S, Petrini JHJ (2014). The Rad50 hook domain regulates DNA damage signaling and tumorigenesis. *Genes Dev.* **28**, 451–462.

[563] Lin Z, Xu SH, Wang HQ, Cai YJ, Ying L, Song M, Wang YQ, Du SJ, Shi KQ, Zhou MT (2016). Prognostic value of DNA repair based stratification of hepatocellular carcinoma. *Sci. Rep.* **6**, 25999.

[564] Machida K, McNamara G, Cheng KT, Huang J, Wang CH, Comai L, Ou JH, Lai MM (2010). Hepatitis C virus inhibits DNA damage repair through reactive oxygen and nitrogen species and by interfering with the ATM-NBS1/ Mre11/ Rad50 DNA repair pathway in monocytes and hepatocytes. *J. Immunol.* **185**, 6985–6998.

[565] Katoh M (2001). Molecular cloning and characterization of *RNF26* on human chromosome 11q23 region, encoding a novel ring finger protein with leucine zipper. *Biochem. Biophys. Res. Commun.* **282**, 1038–1044.

[566] Qin Y, Zhou MT, Hu MM, Hu YH, Zhang J, Guo L, Zhong B, Shu HB (2014). RNF26 temporally regulates virus-triggered type I interferon induction by two distinct mechanisms. *PLoS Pathog.* **10**, e1004358.

[567] Stefanska B, Cheishvili D, Suderman M, Arakelian A, Huang J, Hallett M, Han ZG, Al-Mahtab M, Akbar SM, Khan WA, Raqib R, Tanvir I, Khan HA, Rabbani SA, Szyf M (2014). Genome-wide study of hypomethylated and induced genes in patients with liver cancer unravels novel anticancer targets. *Clin. Cancer Res.* **20**, 3118–3132.

[568] Wong CC, Wong CM, Tung EK, Man K, Ng IO (2009). Rho-kinase 2 is frequently overexpressed in hepatocellular carcinoma and involved in tumor invasion. *Hepatology*. **49**, 1583–1594.

[569] Liu T, Yu X, Li G, Yuan R, Wang Q, Tang P, Wu L, Liu X, Peng X, Shao J (2012). Rock2 regulates Cdc25A through ubiquitin proteasome system in hepatocellular carcinoma cells. *Exp. Cell Res.* **318**, 1994–2003.

[570] Zheng F, Liao YJ, Cai MY, Liu YH, Liu TH, Chen SP, Bian XW, Guan XY, Lin MC, Zeng YX, Kung HF, Xie D (2012). The putative tumour suppressor microRNA-124 modulates hepatocellular carcinoma cell aggressiveness by repressing ROCK2 and EZH2. *Gut*. **61**, 278–289.

[571] Huang D, Du X, Yuan R, Chen L, Liu T, Wen C, Huang M, Li M, Hao L, Shao J (2014). Rock2 promotes the invasion and metastasis of hepatocellular carcinoma by modifying MMP2 ubiquitination and degradation. *Biochem. Biophys. Res. Commun.* **453**, 49–56.

[572] Peng F, Jiang J, Yu Y, Tian R, Guo X, Li X, Shen M, Xu M, Zhu F, Shi C, Hu J, Wang M, Qin R (2013). Direct targeting of SUZ12/ ROCK2 by miR-200b/c inhibits cholangiocarcinoma tumourigenesis and metastasis. *Br. J. Cancer*. **109**, 3092–3104.

[573] Kavsak P, Rasmussen RK, Causing CG, Bonni S, Zhu H, Thomsen GH, Wrana JL (2000). Smad7 binds to Smurf2 to form an E3 ubiquitin ligase that targets the TGFβ receptor for degradation. *Mol. Cell*. **6**, 1365–1375.

[574] Liu N, Jiao T, Huang Y, Liu W, Li Z, Ye X (2015). Hepatitis B virus regulates apoptosis and tumorigenesis through the microRNA-15a-Smad7-transforming growth factor beta pathway. *J. Virol.* **89**, 2739–2749.

[575] Wang J, Zhao J, Chu ES, Mok MT, Go MY, Man K, Heuchel R, Lan HY, Chang Z, Sung JJ, Yu J (2013). Inhibitory role of Smad7 in hepatocarcinogenesis in mice and *in vitro*. *J. Pathol.* **230**, 441–452.

[576] Feng T, Dzieran J, Gu X, Marhenke S, Vogel A, Machida K, Weiss TS, Ruemmele P, Kollmar O, Hoffmann P, Grässer F, Allgayer H, Fabian J, Weng HL, Teufel A, Maass T, Meyer C, Lehmann U, Zhu C, Mertens PR, Gao CF, Dooley S, Meindl-Beinker NM (2015). Smad7 regulates compensatory hepatocyte proliferation in damaged mouse liver and positively relates to better clinical outcome in human hepatocellular carcinoma. *Clin. Sci.* **128**, 761–774.

[577] Kan H, Guo W, Huang Y, Liu D (2015). MicroRNA-520g induces epithelial-mesenchymal transition and promotes metastasis of hepatocellular carcinoma by targeting SMAD7. *FEBS Lett.* **589**, 102–109.

[578] Argentou N, Germanidis G, Hytiroglou P, Apostolou E, Vassiliadis T, Patsiaoura K, Sideras P, Germenis AE, Speletas M (2016). TGF-β signaling is activated in patients with chronic HBV infection and repressed by SMAD7 overexpression after successful antiviral treatment. *Inflamm. Res.* **65**, 355–365.

[579] Li H, Yang X, Yang G, Hong Z, Zhou L, Yin P, Xiao Y, Chen L, Chung RT, Zhang L (2014). Hepatitis C virus NS5A hijacks ARFGAP1 to maintain a phosphatidylinositol 4-phosphate-enriched microenvironment. *J. Virol.* **88**, 5956–5966.

[580] Xu Z, Zhai L, Yi T, Gao H, Fan F, Li Y, Wang Y, Li N, Xing X, Su N, Wu F, Chang L, Chen X, Dai E, Zhao C, Yang X, Cui C, Xu P (2016). Hepatitis B virus X induces inflammation and cancer in mice liver through dysregulation of cytoskeletal remodeling and lipid metabolism. *Oncotarget*. **7**, 70559–70574.

[581] Balistreri G, Horvath P, Schweingruber C, Zünd D, McInerney G, Merits A, Mühlemann O, Azzalin C, Helenius A (2014). The host nonsense-mediated mRNA decay pathway restricts mammalian RNA virus replication. *Cell Host Microbe*. **16**, 403–411.

[582] Ma XN, Liu XY, Yang YF, Xiao FJ, Li QF, Yan J, Zhang QW, Wang LS, Li XY, Wang H (2011). Regulation of human hepatocellular carcinoma cells by Spred2 and correlative studies on its mechanism. *Biochem. Biophys. Res. Commun.* **410**, 803–808.

[583] Momeny M, Khorramizadeh MR, Ghaffari SH, Yousefi M, Yekaninejad MS, Esmaeili R, Jahanshiri Z, Nooridaloii MR (2008). Effects of silibinin on cell growth and invasive properties of a human hepatocellular carcinoma cell line, HepG-2, through inhibition of extracellular signal-regulated kinase 1/ 2 phosphorylation. *Eur. J. Pharmacol.* **591**, 13–20.

[584] Villar V, Kocić J, Santibanez JF (2010). Spred2 inhibits TGF-β1-induced urokinase type plasminogen activator expression, cell motility and epithelial mesenchymal transition. *Int. J. Cancer*. **127**, 77–85.

[585] Wakabayashi H, Ito T, Fushimi S, Nakashima Y, Itakura J, Qiuying L, Win MM, Cuiming S, Chen C, Sato M, Mino M, Ogino T, Makino H, Yoshimura A, Matsukawa A (2012). Spred-2 deficiency exacerbates acetaminophen-induced hepatotoxicity in mice. *Clin. Immunol.* **144**, 272–282.

[586] Yang X, Fujisawa M, Yoshimura T, Ohara T, Sato M, Mino M, San TH, Gao T, Kunkel SL, Matsukawa A (2018). Spred2 deficiency exacerbates *D*-galactosamine/ lipopolysaccharide-induced acute liver injury in mice via increased production of TNFα. *Sci. Rep.* **8**, 188.

[587] Gao B, Wang H, Lafdil F, Feng D (2012). STAT proteins - Key regulators of anti-viral responses, inflammation, and tumorigenesis in the liver. *J. Hepatol.* **57**, 430–441.

[588] Lim YP, Hsu YA, Tsai KH, Tsai FJ, Peng CY, Liao WL, Hung DZ, Tien N, Lin CY, Wan L (2013). The impact of polymorphisms in STAT6 on treatment outcome in HCV infected Taiwanese Chinese. *BMC Immunol.* **14**, 21.

[589] Qing T, Yamin Z, Guijie W, Yan J, Zhongyang S (2017). STAT6 silencing induces hepatocellular carcinoma-derived cell apoptosis and growth inhibition by decreasing the RANKL expression. *Biomed. Pharmacother.* **92**, 1–6.

[590] Ngo HT, Pham LV, Kim JW, Lim YS, Hwang SB (2013). Modulation of mitogen-activated protein kinase-activated protein kinase 3 by hepatitis C virus core protein. *J. Virol.* **87**, 5718–5731.

[591] Lai KK, Kweon SM, Chi F, Hwang E, Kabe Y, Higashiyama R, Qin L, Yan R, Wu RP, Fujii N, French S, Xu J, Wang JY, Murali R, Mishra L, Lee JS, Ntambi JM, Tsukamoto H (2017). Stearoyl-CoA desaturase promotes liver fibrosis and tumor development in mice via Wnt signaling and stabilization of low density lipoprotein receptor-related proteins 5 and 6. *Gastroenterology*. **152**, 1477–1491.

[592] Levin A, Neufeldt CJ, Pang D, Wilson K, Loewen-Dobler D, Joyce MA, Wozniak RW, Tyrrell DL (2014). Functional characterization of nuclear localization and export signals in hepatitis C virus proteins and their role in the membranous web. *PLoS One*. **9**, e114629.

[593] Zhao J, Chen J, Lu B, Dong L, Wang H, Bi C, Wu G, Guo H, Wu M, Guo Y (2008). TIP30 induces apoptosis under oxidative stress through stabilization of p53 messenger RNA in human hepatocellular carcinoma. *Cancer Res.* **68**, 4133–4141.

[594] Zhu M, Yin F, Fan X, Jing W, Chen R, Liu L, Zhang L, Liu Y, Liang Y, Bu F, Tong X, Zheng H, Zhao J, Guo Y (2015). Decreased TIP30 promotes Snail-mediated epithelial-mesenchymal transition and tumor-initiating properties in hepatocellular carcinoma. *Oncogene*. **34**, 1420–1431.

[595] Zhang Z, Xu L, Sun C (2018). Comprehensive characterization of cancer genes in hepatocellular carcinoma genomes. *Oncol. Lett.* **15**, 1503–1510.

[596] Imai H, Chan EK, Kiyosawa K, Fu XD, Tan EM (1993). Novel nuclear autoantigen with splicing factor motifs identified with antibody from hepatocellular carcinoma. *J. Clin. Invest.* **92**, 2419–2426.

[597] Li J, Cheng D, Zhu M, Yu H, Pan Z, Liu L, Geng Q, Pan H, Yan M, Yao M (2019). OTUB2 stabilizes U2AF2 to promote the Warburg effect and tumorigenesis via the AKT/ mTOR signaling pathway in non-small cell lung cancer. *Theranostics*. **9**, 179–195.

[598] McGarvey TW, Nguyen T, Puthiyaveettil R, Tomaszewski JE, Malkowicz SB (2003). *TERE1*, a novel gene affecting growth regulation in prostate carcinoma. *Prostate*. **54**, 144–155.

[599] Fredericks WJ, McGarvey T, Wang H, Lal P, Puthiyaveettil R, Tomaszewski J, Sepulveda J, Labelle E, Weiss JS, Nickerson ML, Kruth HS, Brandt W, Wessjohann LA, Malkowicz SB (2011). The bladder tumor suppressor protein TERE1 (UBIAD1) modulates cell cholesterol: Implications for tumor progression. *DNA Cell Biol.* **30**, 851–864.

[600] Fredericks WJ, Sepulveda J, Lai P, Tomaszewski JE, Lin M-F, McGarvey T, Rauscher FJ, Malkowicz SB (2013). The tumor suppressor TERE1 (UBIAD1) prenyltransferase regulates the elevated cholesterol phenotype in castration resistant prostate cancer by controlling a program of ligand dependent SXR target genes. *Oncotarget*. **4**, 1075–1092.

[601] Schumacher MM, Jun DJ, Jo Y, Seemann J, DeBose-Boyd RA (2016). Geranylgeranyl-regulated transport of the prenyltransferase UBIAD1 between membranes of the ER and Golgi. *J. Lipid Res.* **57**, 1286–1299.

[602] Woo HG, Park ES, Lee JS, Lee YH, Ishikawa T, Kim YJ, Thorgeirsson SS (2009). Identification of potential driver genes in human liver carcinoma by genome-wide screening. *Cancer Res.* **69**, 4059–4066.

[603] Park ER, Kim SB, Lee JS, Kim YH, Lee DH, Cho EH, Park SH, Han CJ, Kim BY, Choi DW, Yoo YD, Yu A, Lee JW, Jang JJ, Park YN, Suh KS, Lee KH (2017). The mitochondrial hinge protein, UQCRH, is a novel prognostic factor for hepatocellular carcinoma. *Cancer Med.* **6**, 749–760.

[604] Moniz S, Jordan P (2010). Emerging roles for WNK kinases in cancer. *Cell. Mol. Life Sci.* **67**, 1265–1276.

[605] Lee BH, Chen W, Stippec S, Cobb MH (2007). Biological cross-talk between WNK1 and the transforming growth factor β-Smad signaling pathway. *J. Biol. Chem.* **282**, 17985–17996.

[606] Nara H, Onoda T, Rahman M, Araki A, Juliana FM, Tanaka N, Asao H (2010). Regulation of interleukin-21 receptor expression and its signal transduction by WSB-2. *Biochem. Biophys. Res. Commun.* **392**, 171–177.

[607] Mutlu P, Ural AU, Gündüz U (2012). Differential oncogene-related gene expressions in myeloma cells resistant to prednisone and vincristine. *Biomed. Pharmacother.* **66**, 506–511.

[608] Li XG, Song JD, Wang YQ (2001). Differential expression of a novel colorectal cancer differentiation-related gene in colorectal cancer. *World J. Gastroenterol.* **7**, 551–554.

[609] Xu Y, Liu AJ, Gao YX, Hu MG, Zhao GD, Zhao ZM, Liu R (2014). Expression of Ku86 and presence of Ku86 antibody as biomarkers of hepatitis B virus related hepatocellular carcinoma. *Dig. Dis. Sci.* **59**, 614–622.

[610] Li R, Yang Y, An Y, Zhou Y, Liu Y, Yu Q, Lu D, Wang H, Jin L, Zhou W, Qian J, Shugart YY (2011). Genetic polymorphisms in DNA double-strand break repair genes *XRCC5*, *XRCC6* and susceptibility to hepatocellular carcinoma. *Carcinogenesis*. **32**, 530–536.

[611] Wei S, Xiong M, Zhan DQ, Liang BY, Wang YY, Gutmann DH, Huang ZY, Chen XP (2012). Ku80 functions as a tumor suppressor in hepatocellular carcinoma by inducing S-phase arrest through a p53-dependent pathway. *Carcinogenesis*. **33**, 538–547.

[612] Liu ZH, Wang N, Wang FQ, Dong Q, Ding J (2019). High expression of XRCC5 is associated with metastasis through Wnt signaling pathway and predicts poor prognosis in patients with hepatocellular carcinoma. *Eur. Rev. Med. Pharmacol. Sci.* **23**, 7835–7847.

[613] Schwanhäusser B, Busse D, Li N, Dittmar G, Schuchhardt J, Wolf J, Chen W, Selbach M (2011). Global quantification of mammalian gene expression control. *Nature*. **473**, 337–342.

[614] Jeffery J, Sinha D, Srihari S, Kalimutho M, Khanna KK (2016). Beyond cytokinesis: The emerging roles of CEP55 in tumorigenesis. *Oncogene*. **35**, 683–690.

[615] Zhang S, Wang XM, Yin ZY, Zhao WX, Zhou JY, Zhao BX, Liu PG (2013). Chloride intracellular channel 1 is overexpression in hepatic tumor and correlates with a poor prognosis. *Acta Pathol. Microbiol. Immunol. Scand.* **121**, 1047–1053.

[616] Wei X, Li J, Xie H, Wang H, Wang J, Zhang X, Zhuang R, Lu D, Ling Q, Zhou L, Xu X, Zheng S (2015). Chloride intracellular channel 1 participates in migration and invasion of hepatocellular carcinoma by targeting maspin. *J. Gastroenterol. Hepatol.* **30**, 208–216.

[617] Hirasawa Y, Arai M, Imazeki F, Tada M, Mikata R, Fukai K, Miyazaki M, Ochiai T, Saisho H, Yokosuka O (2006). Methylation status of genes upregulated by demethylating agent 5-aza-2'-deoxycytidine in hepatocellular carcinoma. *Oncology*. **71**, 77–85.

[618] Niehof M, Borlak J (2008). *EPS15R, TASP1*, and *PRPF3* are novel disease candidate genes targeted by HNF4α splice variants in hepatocellular carcinomas. *Gastroenterology*. **134**, 1191–1202.

[619] Inoue M, Takahashi Y, Fujii T, Kitagawa M, Fukusato T (2014). Significance of downregulation of liver fatty acid-binding protein in hepatocellular carcinoma. *World J. Gastroenterol.* **20**, 17541–17551.

[620] Wang B, Tao X, Huang CZ, Liu JF, Ye YB, Huang AM (2014). Decreased expression of liver-type fatty acid-binding protein is associated with poor prognosis in hepatocellular carcinoma. *Hepatogastroenterology.* **61**, 1321–1326.

[621] Gkretsi V, Bogdanos DP (2015). Experimental evidence of Migfilin as a new therapeutic target of hepatocellular carcinoma metastasis. *Exp. Cell Res.* **334**, 219–227.

[622] Hu H, Ding X, Yang Y, Zhang H, Li H, Tong S, An X, Zhong Q, Liu X, Ma L, Liu Q, Liu B, Lu Z, Zhang D, Hu P, Ren H (2014). Changes in glucose-6-phosphate dehydrogenase expression results in altered behavior of HBV-associated liver cancer cells. *Am. J. Physiol. Liver Physiol.* **307**, G611–G622.

[623] Hong X, Song R, Song H, Zheng T, Wang J, Liang Y, Qi S, Lu Z, Song X, Jiang H, Liu L, Zhang Z (2014). PTEN antagonises Tcl1/ hnRNPK-mediated G6PD pre-mRNA splicing which contributes to hepatocarcinogenesis. *Gut*. **63**, 1635–1647.

[624] Sun Y, Wang Y, Yin Y, Chen X, Sun Z (2014). GSTM3 reverses the resistance of hepatoma cells to radiation by regulating the expression of cell cycle/ apoptosis-related molecules. *Oncol. Lett.* **8**, 1435–1440.

[625] White DL, Li D, Nurgalieva Z, El-Serag HB (2008). Genetic variants of *glutathione* S-*transferase* as possible risk factors for hepatocellular carcinoma: A HuGE systematic review and meta-analysis. *Am. J. Epidemiol.* **167**, 377–389.

[626] Brind AM, Hurlstone A, Edrisinghe D, Gilmore I, Fisher N, Pirmohamed M, Fryer AA (2004). The role of polymorphisms of glutathione S-transferases GSTM1, M3, P1, T1 and A1 in susceptibility to alcoholic liver disease. *Alcohol Alcohol.* **39**, 478–483.

[627] Chen F, Zhu HH, Zhou LF, Wu SS, Wang J, Chen Z (2010). IQGAP1 is overexpressed in hepatocellular carcinoma and promotes cell proliferation by Akt activation. *Exp. Mol. Med.* **42**, 477–483.

[628] Xia F Da, Wang ZL, Chen HX, Huang Y, Li JD, Wang ZM, Li XY (2014). Differential expression of IQGAP1/2 in hepatocellular carcinoma and its relationship with clinical outcomes. *Asian Pacific J. Cancer Prev.* **15**, 4951–4956.

[629] Liu C, Zhou N, Li J, Kong J, Guan X, Wang X (2017). Eg5 overexpression is predictive of poor prognosis in hepatocellular carcinoma patients. *Dis. Markers*. **2017**, 2176460.

[630] Chen J, Rajasekaran M, Xia H, Zhang X, Kong SN, Sekar K, Seshachalam VP, Deivasigamani A, Goh BK, Ooi LL, Hong W, Hui KM (2016). The microtubule-associated protein PRC1 promotes early recurrence of hepatocellular carcinoma in association with the Wnt/ β-catenin signalling pathway. *Gut*. **65**, 1522–1534.

[631] Doan CC, Doan NT, Nguyen QH, Nguyen MH, Do MS, Le VD (2015). Downregulation of kinesin spindle protein inhibits proliferation, induces apoptosis and increases chemosensitivity in hepatocellular carcinoma cells. *Iran. Biomed. J.* **19**, 1–16.

[632] Wang HW, Hsieh TH, Huang SY, Chau GY, Tung CY, Su CW, Wu JC (2013). Forfeited hepatogenesis program and increased embryonic stem cell traits in young hepatocellular carcinoma (HCC) comparing to elderly HCC. *BMC Genomics*. **14**, 736.

[633] Wang SC, Yang JF, Wang CL, Huang CF, Lin YY, Chen YY, Lo CT, Lee PY, Wu KT, Lin CI, Hsieh MH, Chuang HY, Ho CK, Yu ML, Dai CY (2016). Distinct subpopulations of hepatitis C virus infectious cells with different levels of intracellular hepatitis C virus core protein. *Kaohsiung J. Med. Sci.* **32**, 487–493.

[634] Li K, Ding S, Chen K, Qin D, Qu J, Wang S, Sheng Y, Zou C, Chen L, Tang H (2013). Hepatitis B virus X protein up-regulates AKR1C1 expression through nuclear factor-Y in human hepatocarcinoma cells. *Hepat. Mon.* **13**, e8792.

[635] Chen Z, Lu X, Wang Z, Jin G, Wang Q, Chen D, Chen T, Li J, Fan J, Cong W, Gao Q, He X (2015). Co-expression of PKM2 and TRIM35 predicts survival and recurrence in hepatocellular carcinoma. *Oncotarget*. **6**, 2538–2548.

[636] Liu WR, Tian MX, Yang LX, Lin YL, Jin L, Ding ZB, Shen YH, Peng YF, Gao DM, Zhou J, Qiu SJ, Dai Z, He R, Fan J, Shi YH (2015). PKM2 promotes metastasis by recruiting myeloid-derived suppressor cells and indicates poor prognosis for hepatocellular carcinoma. *Oncotarget*. **6**, 846–861.

[637] Dong T, Yan Y, Chai H, Chen S, Xiong X, Sun D, Yu Y, Deng L, Cheng F (2015). Pyruvate kinase M2 affects liver cancer cell behavior through up-regulation of HIF-1α and Bcl-xL in culture. *Biomed. Pharmacother.* **69**, 277–284.

[638] Sun HW, Yu XJ, Wu WC, Chen J, Shi M, Zheng L, Xu J (2016). GLUT1 and ASCT2 as predictors for prognosis of hepatocellular carcinoma. *PLoS One*. **11**, e0168907.

[639] Namikawa M, Kakizaki S, Kaira K, Tojima H, Yamazaki Y, Horiguchi N, Sato K, Oriuchi N, Tominaga H, Sunose Y, Nagamori S, Kanai Y, Oyama T, Takeyoshi I, Yamada M (2015). Expression of amino acid transporters (LAT1, ASCT2 and xCT) as clinical significance in hepatocellular carcinoma. *Hepatol. Res.* **45**, 1014–1022.

[640] Zhang J, Sun M, Li R, Liu S, Mao J, Huang Y, Wang B, Hou L, Ibrahim MM, Tang J (2013). Ech1 is a potent suppressor of lymphatic metastasis in hepatocarcinoma. *Biomed. Pharmacother.* **67**, 557–560.

[641] Tamai S, Masuda H, Ishii Y, Suzuki S, Kanai Y, Endou H (2001). Expression of *L*-type amino acid transporter 1 in a rat model of liver metastasis: Positive correlation with tumor size. *Cancer Detect. Prev.* **25**, 439–445.

[642] Kondoh N, Imazeki N, Arai M, Hada A, Hatsuse K, Matsuo H, Matsubara O, Ohkura S, Yamamoto M (2007). Activation of a system A amino acid transporter, ATA1/ SLC38A1, in human hepatocellular carcinoma and preneoplastic liver tissues. *Int. J. Oncol.* **31**, 81–87.

[643] Wang L, Huang J, Jiang M, Chen Q, Jiang Z, Feng H (2014). CAMK1 phosphoinositide signal-mediated protein sorting and transport network in human hepatocellular carcinoma (HCC) by biocomputation. *Cell Biochem. Biophys.* **70**, 1011–1016.

[644] Besharat S, Katoonizadeh A, Moossavi S, Darvishi Z, Roshandel, Gholamreza Poustchi H, Mohamadkhani A (2016). The possible impact of sortilin in reducing HBsAg expression in chronic hepatitis B. *J. Med. Virol.* **88**, 647–652.

[645] Moylan CA, Pang H, Dellinger A, Suzuki A, Garrett ME, Guy CD, Murphy SK, Ashley-Koch AE, Choi SS, Michelotti GA, Hampton DD, Chen Y, Tillmann HL, Hauser MA, Abdelmalek MF, Diehl AM (2014). Hepatic gene expression profiles differentiate presymptomatic patients with mild *versus* severe nonalcoholic fatty liver disease. *Hepatology*. **59**, 471–482.

[646] Zhang SY, Lin BD, Li BR (2015). Evaluation of the diagnostic value of alpha-*L*-fucosidase, alpha-fetoprotein and thymidine kinase 1 with ROC and logistic regression for hepatocellular carcinoma. *FEBS Open Bio*. **5**, 240–244.

[647] Yeh HW, Lee SS, Chang CY, Hu CM, Jou YS (2017). Pyrimidine metabolic rate limiting enzymes in poorly differentiated hepatocellular carcinoma are signature genes of cancer stemness and associated with poor prognosis. *Oncotarget*. **8**, 77734–77751.

[648] Baba H, Teramoto K, Kawamura T, Mori A, Imamura M, Arii S (2003). Dihydropyrimidine dehydrogenase and thymidylate synthase activities in hepatocellular carcinomas and in diseased livers. *Cancer Chemother. Pharmacol.* **52**, 469–476.

[649] Sunaga M, Tomonaga T, Yoshikawa M, Ebara M, Shimada H, Saisho H, Nomura F (2007). Gene expression of 5-fluorouracil metabolic enzymes in hepatocellular carcinoma and non-tumor tissue. *J. Chemother.* **19**, 709–715.

[650] Nii A, Shimada M, Ikegami T, Harino Y, Imura S, Morine Y, Kanemura H, Arakawa Y, Sugimoto K (2009). Significance of dihydropyrimidine dehydrogenase and thymidylate synthase mRNA expressions in hepatocellular carcinoma. *Hepatol. Res.* **39**, 274–281.

[651] Wood T (1986). Physiological functions of the pentose phosphate pathway. *Cell Biochem. Funct.* **4**, 241–247.

[652] Kletzien RF, Harris PK, Foellmi LA (1994). Glucose-6-phosphate dehydrogenase: A `housekeeping´ enzyme subject to tissue-specific regulation by hormones, nutrients, and oxidant stress. *FASEB J.* **8**, 174–181.

[653] Rao KN, Elm MS, Kelly RH, Chandar N, Brady EP, Rao B, Shinozuka H, Eagon PK (1997). Hepatic hyperplasia and cancer in rats: Metabolic alterations associated with cell growth. *Gastroenterology*. **113**, 238–248.

[654] Kowalik MA, Columbano A, Perra A (2017). Emerging role of the pentose phosphate pathway in hepatocellular carcinoma. *Front. Oncol.* **7**, 87.

[655] Liu B, Fang M, He Z, Cui D, Jia S, Lin X, Xu X, Zhou T, Liu W (2015). Hepatitis B virus stimulates G6PD expression through HBx-mediated Nrf2 activation. *Cell Death Dis.* **6**, e1980.

[656] But DY, Lai CL, Yuen MF (2008). Natural history of hepatitis-related hepatocellular carcinoma. *World J. Gastroenterol.* **14**, 1652–1656.

[657] Thakral S, Ghoshal K (2015). miR-122 is a unique molecule with great potential in diagnosis, prognosis of liver disease, and therapy both as miRNA mimic and antimir. *Curr. Gene Ther.* **15**, 142–150.

[658] Nakao K, Miyaaki H, Ichikawa T (2014). Antitumor function of microRNA-122 against hepatocellular carcinoma. *J. Gastroenterol.* **49**, 589–593.

[659] Hamad IA, Fei Y, Kalea AZ, Yin D, Smith AJ, Palmen J, Humphries SE, Talmud PJ, Walker AP (2015). Demonstration of the presence of the `deleted´ *MIR122* gene in HepG2 cells. *PLoS One*. **10**, e0122471.

[660] Tilg H, Kaser A, Moschen AR (2006). How to modulate inflammatory cytokines in liver diseases. *Liver Int.* **26**, 1029–1039.

[661] Inman GJ, Nicolás FJ, Callahan JF, Harling JD, Gaster LM, Reith AD, Laping NJ, Hill CS (2002). SB-431542 is a potent and specific inhibitor of transforming growth factor-β superfamily type I activin receptor-like kinase (ALK) receptors ALK4, ALK5, and ALK7. *Mol. Pharmacol.* **62**, 65–74.

[662] Ben-Moshe S, Shapira Y, Moor AE, Manco R, Veg T, Bahar Halpern K, Itzkovitz S (2019). Spatial sorting enables comprehensive characterization of liver zonation. *Nat. Metab.* **1**, 899–911.

[663] Burns DM, D'Ambrogio A, Nottrott S, Richter JD (2011). CPEB and two poly(A) polymerases control miR-122 stability and p53 mRNA translation. *Nature*. **473**, 105–108.

[664] Verma V, Chakravarti A, Kar P (2008). Cytokine levels of TGF-β, IL-10, and sTNFαRII in type C chronic liver disease. *Dig. Dis. Sci.* **53**, 2233–2237.

[665] Xu H, Xu SJ, Xie SJ, Zhang Y, Yang JH, Zhang WQ, Zheng MN, Zhou H, Qu LH (2019). MicroRNA-122 supports robust innate immunity in hepatocytes by targeting the RTKs/ STAT3 signaling pathway. *Elife*. **8**, e41159.

[666] Ho HH, Ivashkiv LB (2006). Role of STAT3 in type I interferon responses: Negative regulation of STAT1-dependent inflammatory gene activation. *J. Biol. Chem.* **281**, 14111–14118.

[667] Nakamura M, Kanda T, Sasaki R, Haga Y, Jiang X, Wu S, Nakamoto S, Yokosuka O (2015). MicroRNA-122 inhibits the production of inflammatory cytokines by targeting the PKR activator PACT in human hepatic stellate cells. *PLoS One*. **10**, e0144295.

[668] Hong MH, Chou YC, Wu YC, Tsai KN, Hu CP, Jeng KS, Chen ML, Chang C (2012). Transforming growth factor-β1 suppresses hepatitis B virus replication by the reduction of hepatocyte nuclear factor-4α expression. *PLoS One*. **7**, e30360.

[669] Yin S, Fan Y, Zhang H, Zhao Z, Hao Y, Li J, Sun C, Yang J, Yang Z, Yang X, Lu J, Xi JJ (2016). Differential TGFβ pathway targeting by miR-122 in humans and mice affects liver cancer metastasis. *Nat. Commun.* **7**, 11012.

[670] de Gramont A, Faivre S, Raymond E (2016). Novel TGF-β inhibitors ready for prime time in onco-immunology. *Oncoimmunology*. **6**, e1257453.

[671] Khorramdelazad H, Hassanshahi G, Nasiri Ahmadabadi B, Kazemi Arababadi M (2012). High serum levels of TGF-β in Iranians with chronic HBV infection. *Hepat. Mon.* **12**, e7581.

[672] Yu X, Guo R, Ming D, Deng Y, Su M, Lin C, Li J, Lin Z, Su Z (2015). The transforming growth factor β1/ interleukin-31 pathway is upregulated in patients with hepatitis B virus-related acute-on-chronic liver failure and is associated with disease severity and survival. *Clin. Vaccine Immunol.* **22**, 484–492.

[673] Karimi-Googheri M, Daneshvar H, Nosratabadi R, Zare-Bidaki M, Hassanshahi G, Ebrahim M, Arababadi MK, Kennedy D (2014). Important roles played by TGF-β in hepatitis B infection. *J. Med. Virol.* **86**, 102–108.

[674] Yang P, Markowitz GJ, Wang XF (2014). The hepatitis B virus-associated tumor microenvironment in hepatocellular carcinoma. *Natl. Sci. Rev.* **1**, 396–412.

[675] Gori M, Arciello M, Balsano C (2014). MicroRNAs in nonalcoholic fatty liver disease : Novel biomarkers and prognostic tools during the transition from steatosis to hepatocarcinoma. *Biomed Res. Int.* **2014**, 741465.

[676] Yang L, Roh YS, Song J, Zhang B, Liu C, Loomba R, Seki E (2014). TGF-β signaling in hepatocytes participates in steatohepatitis through regulation of cell death and lipid metabolism. *Hepatology*. **59**, 483–495.

[677] Pohlers D, Brenmoehl J, Löffler I, Müller CK, Leipner C, Schultze-Mosgau S, Stallmach A, Kinne RW, Wolf G (2009). TGF-β and fibrosis in different organs — Molecular pathway imprints. *Biochim. Biophys. Acta*. **1792**, 746–756.

[678] Fabregat I, Caballero-Díaz D (2018). Transforming growth factor-β-induced cell plasticity in liver fibrosis and hepatocarcinogenesis. *Front. Oncol.* **8**, 357.

[679] Giannelli G, Villa E, Lahn M (2014). Transforming growth factor-β as a therapeutic target in hepatocellular carcinoma. *Cancer Res.* **74**, 1890–1894.

[680] El-Tayeh SF, Hussein TD, El-Houseini ME, Amer MA, El-Sherbini M, Elshemey WM (2012). Serological biomarkers of hepatocellular carcinoma in Egyptian patients. *Dis. Markers*. **32**, 225–263.

[681] Neuman M, Angulo P, Malkiewicz I, Jorgensen R, Shear N, Dickson ER, Haber J, Katz G, Lindor K (2002). Tumor necrosis factor-α and transforming growth factor-β reflect severity of liver damage in primary biliary cirrhosis. *J. Gastroenterol. Hepatol.* **17**, 196–202.

[682] Rivkin M, Simerzin A, Zorde-Khvalevsky E, Chai C, Yuval JB, Rosenberg N, Harari-Steinfeld R, Schneider R, Amir G, Condiotti R, Heikenwalder M, Weber A, Schramm C, Wege H, Kluwe J, Galun E, Giladi H (2016). Inflammation-induced expression and secretion of microRNA-122 leads to reduced blood levels of kidney-derived erythropoietin and anemia. *Gastroenterology*. **151**, 999–1010.

[683] Li C, Deng M, Hu J, Li X, Chen L, Ju Y, Hao J, Meng S (2016). Chronic inflammation contributes to the development of hepatocellular carcinoma by decreasing miR-122 levels. *Oncotarget*. **7**, 17021–17034.

[684] Arndt S, Wacker E, Dorn C, Koch A, Saugspier M, Thasler WE, Hartmann A, Bosserhoff AK, Hellerbrand C (2015). Enhanced expression of BMP6 inhibits hepatic fibrosis in non-alcoholic fatty liver disease. *Gut*. **64**, 973–981.

[685] Sampath P, Pritchard DK, Pabon L, Reinecke H, Schwartz SM, Morris DR, Murry CE (2008). A hierarchical network controls protein translation during murine embryonic stem cell self-renewal and differentiation. *Cell Stem Cell*. **2**, 448–460.

[686] Molotski N, Soen Y (2012). Differential association of microRNAs with polysomes reflects distinct strengths of interactions with their mRNA targets. *RNA*. **18**, 1612–1623.

[687] Adjibade P, Grenier St-Sauveur V, Droit A, Khandjian EW, Toren P, Mazroui R (2016). Analysis of the translatome in solid tumors using polyribosome profiling/ RNA-Seq. *J. Biol. Methods*. **3**, e59.

[688] Kong M, Chen X, Lv F, Ren H, Fan Z, Qin H, Yu L, Shi X, Xu Y (2019). Serum response factor (SRF) promotes ROS generation and hepatic stellate cell activation by epigenetically stimulating NCF1/ 2 transcription. *Redox Biol.* **26**, 101302.

[689] Yang ZX, Shen W, Sun H (2010). Effects of nuclear receptor FXR on the regulation of liver lipid metabolism in patients with non-alcoholic fatty liver disease. *Hepatol. Int.* **4**, 741–748.

[690] He J, Zhao K, Zheng L, Xu Z, Gong W, Chen S, Shen X, Huang G, Gao M, Zeng Y, Zhang Y, He F (2015). Upregulation of microRNA-122 by farnesoid X receptor suppresses the growth of hepatocellular carcinoma cells. *Mol. Cancer*. **14**, 163.

[691] Jornayvaz FR, Shulman GI (2010). Regulation of mitochondrial biogenesis. *Essays Biochem.* **47**, 69–84.

[692] Biswas M, Chan JY (2010). Role of Nrf1 in antioxidant response element-mediated gene expression and beyond. *Toxicol. Appl. Pharmacol.* **244**, 16–20.

[693] Bult CJ, Blake JA, Smith CL, Kadin JA, Richardson JE, Mouse Genome Database Group (2019). Mouse Genome Database (MGD) 2019. *Nucleic Acids Res.* **47**, D801–D806.

[694] Wen J, Friedman JR (2012). miR-122 regulates hepatic lipid metabolism and tumor suppression. *J. Clin. Invest.* **122**, 2773–2776.

[695] Castoldi M, Kordes C, Sawitza I, Häussinger D (2016). Isolation and characterization of vesicular and non-vesicular microRNAs circulating in sera of partially hepatectomized rats. *Sci. Rep.* **6**, 31869.

[696] Xu J, Wu C, Che X, Wang L, Yu D, Zhang T, Huang L, Li H, Tan W, Wang C, Lin D (2011). Circulating microRNAs, miR-21, miR-122, and miR-223, in patients with hepatocellular carcinoma or chronic hepatitis. *Mol. Carcinog.* **50**, 136–142.

[697] Howell LS, Ireland L, Park BK, Goldring CE (2018). miR-122 and other microRNAs as potential circulating biomarkers of drug-induced liver injury. *Expert Rev. Mol. Diagn.* **18**, 47–54.

[698] Sherley JL, Kelly TJ (1988). Regulation of human thymidine kinase during the cell cycle. *J. Biol. Chem.* **263**, 8350–8358.

[699] Huang S, Lin J, Guo N, Zhang M, Yun X, Liu S, Zhou J, He E, Skog S (2011). Elevated serum thymidine kinase 1 predicts risk of pre/ early cancerous progression. *Asian Pacific J. Cancer Prev.* **12**, 497–505.

[700] Alegre MM, Weyant MJ, Bennett DT, Yu JA, Ramsden MK, Elnaggar A, Robison RA, O'Neill KL (2014). Serum detection of thymidine kinase 1 as a means of early detection of lung cancer. *Anticancer Res.* **34**, 2145–2151.

[701] Coda L, Salcini AE, Confalonieri S, Pelicci G, Sorkina T, Sorkin A, Pelicci PG, Di Fiore PP (1998). Eps15R is a tyrosine kinase substrate with characteristics of a docking protein possibly involved in coated pits-mediated internalization. *J. Biol. Chem.* **273**, 3003–3012.

[702] Sigismund S, Avanzato D, Lanzetti L (2018). Emerging functions of the EGFR in cancer. *Mol. Oncol.* **12**, 3–20.

[703] Zhang J, Li M, Song M, Chen W, Mao J, Song L, Wei Y, Huang Y, Tang J (2015). Clic1 plays a role in mouse hepatocarcinoma via modulating Annexin A7 and Gelsolin *in vitro* and *in vivo*. *Biomed. Pharmacother.* **69**, 416–419.

[704] Lu J, Dong Q, Zhang B, Wang X, Ye B, Zhang F, Song X, Gao G, Mu J, Wang Z, Ma F, Gu J (2015). Chloride intracellular channel 1 (CLIC1) is activated and functions as an oncogene in pancreatic cancer. *Med. Oncol.* **32**, 616.

[705] Kekuda R, Prasad PD, Fei YJ, Torres-Zamorano V, Sinha S, Yang-Feng TL, Leibach FH, Ganapathy V (1996). Cloning of the sodium-dependent, broad-scope, neutral amino acid transporter B^o from a human placental choriocarcinoma cell line. *J. Biol. Chem.* **271**, 18657–18661.

[706] Scalise M, Pochini L, Console L, Losso MA, Indiveri C (2018). The Human SLC1A5 (ASCT2) amino acid transporter: From function to structure and role in cell biology. *Front. Cell Dev. Biol.* **6**, 96.

[707] Häussinger D, Schliess F (2007). Glutamine metabolism and signaling in the liver. *Front. Biosci.* **12**, 371–391.

[708] Häussinger D, Graf D, Weiergräber OH (2001). Glutamine and cell signaling in liver. *J. Nutr.* **131**, 2509S-2514S.

[709] Häussinger D, Schliess F, Dombrowski F, Vom Dahl S (1999). Involvement of $p38^{MAPK}$ in the regulation of proteolysis by liver cell hydration. *Gastroenterology*. **116**, 921–935.

[710] Dore MP, Vidili G, Marras G, Assy S, Pes GM (2018). Inverse association between glucose-6-phosphate dehydrogenase deficiency and hepatocellular carcinoma. *Asian Pacific J. cancer Prev.* **19**, 1069–1073.

[711] Dong J, Xiao D, Zhao Z, Ren P, Li C, Hu Y, Shi J, Su H, Wang L, Liu H, Li B, Gao P, Qing G (2017). Epigenetic silencing of microRNA-137 enhances ASCT2 expression and tumor glutamine metabolism. *Oncogenesis*. **6**, e356.

[712] Sengupta D, Cassel T, Teng K, Aljuhani M, Chowdhary VK, Hu P, Zhang X, Fan TW-M, Ghoshal K (2020). Regulation of hepatic glutamine metabolism by miR-122. *Mol. Metab.* **34**, 174–186.

[713] Barajas JM, Reyes R, Guerrero MJ, Jacob ST, Motiwala T, Ghoshal K (2018). The role of miR-122 in the dysregulation of glucose-6-phosphate dehydrogenase (G6PD) expression in hepatocellular cancer. *Sci. Rep.* **8**, 9105.

[714] Arvey A, Larsson E, Sander C, Leslie CS, Marks DS (2010). Target mRNA abundance dilutes microRNA and siRNA activity. *Mol. Syst. Biol.* **6**, 363.

[715] Werfel S, Leierseder S, Ruprecht B, Kuster B, Engelhardt S (2017). Preferential microRNA targeting revealed by *in vivo* competitive binding and differential Argonaute immunoprecipitation. *Nucleic Acids Res.* **45**, 10218–10228.

[716] Edmunds WJ, Medley GF, Nokes DJ, Hall AJ, Whittle HC (1993). The influence of age on the development of the hepatitis B carrier state. *Proc. R. Soc. B Biol. Sci.* **253**, 197–201.

[717] Tinkle CL, Haas-Kogan D (2012). Hepatocellular carcinoma: Natural history, current management, and emerging tools. *Biol. Targets Ther.* **6**, 207–219.

[718] Yoo Y Do, Ueda H, Park K, Flanders KC, Lee YI, Jay G, Kim SJ (1996). Regulation of transforming growth factor-beta 1 expression by the hepatitis B virus (HBV) X transactivator. Role in HBV pathogenesis. *J. Clin. Invest.* **97**, 388–395.

[719] Murata M, Matsuzaki K, Yoshida K, Sekimoto G, Tahashi Y, Mori S, Uemura Y, Sakaida N, Fujisawa J, Seki T, Kobayashi K, Yokote K, Koike K, Okazaki K (2009). Hepatitis B virus X protein shifts human hepatic transforming growth factor (TGF)-β signaling from tumor suppression to oncogenesis in early chronic hepatitis B. *Hepatology*. **49**, 1203–1217.

[720] Liu Y, Xu Y, Ma H, Wang B, Xu L, Zhang H, Song X, Gao L, Liang X, Ma C (2016). Hepatitis B virus X protein amplifies TGF-β promotion on HCC motility through down-regulating PPM1a. *Oncotarget*. **7**, 33125–33135.

[721] Hu T, Zhang C, Tang Q, Su Y, Li B, Chen L, Zhang Z, Cai T, Zhu Y (2013). Variant G6PD levels promote tumor cell proliferation or apoptosis via the STAT3/5 pathway in the human melanoma xenograft mouse model. *BMC Cancer*. **13**, 251.

6. Acknowledgments

I would particularly like to thank Prof. Dr. Häussinger for the possibility to conduct my PhD thesis in his clinic and for his continuous and constructive scientific input throughout my time as a graduate student in his research group. During this time, I was given the chance to contribute to various research projects and therefore to develop as a scientific member of the Experimental Hepatology.

I would also like to express my graditude to Prof. Dr. Westhoff for his time and his interest in my research topic and for reviewing my PhD thesis.

A special thanks goes to Dr. Mirco Castoldi, who supervised me during the first years of my PhD and who substantially contributed to the progress of this work. Moreover, he was very encouraging when I was needing it the most.

Furthermore, I would like to thank Dr. Claus Kordes and Dr. Maria Reich for proof-reading my work and for their constructive criticism.

I would also like to thank my colleagues and friends at the Experimental Hepatology. It has been a pleasure to work with very talented researchers in such a friendly environment.

Last but not least, I would like to thank my family and friends for their kind support, for being understanding and patient with me. In particular, I want to thank my father who taught me how to live through difficult times and who raised me to become a strong-minded and ambitious person. I would not be writing this thesis, if it was not for him.

Na koniec chciałabym podziękować mojej rodzinie i przyjaciołom za wsparcie, wyrozumiałość i cierpliwość. W szczególności chciałabym podziękować mojemu ojcu, który nauczył mnie życia pomimo różnych przeciwności i który wychował mnie na osobę silną i ambitną. Nie napisałabym tej pracy, gdyby nie on!

7. Appendix

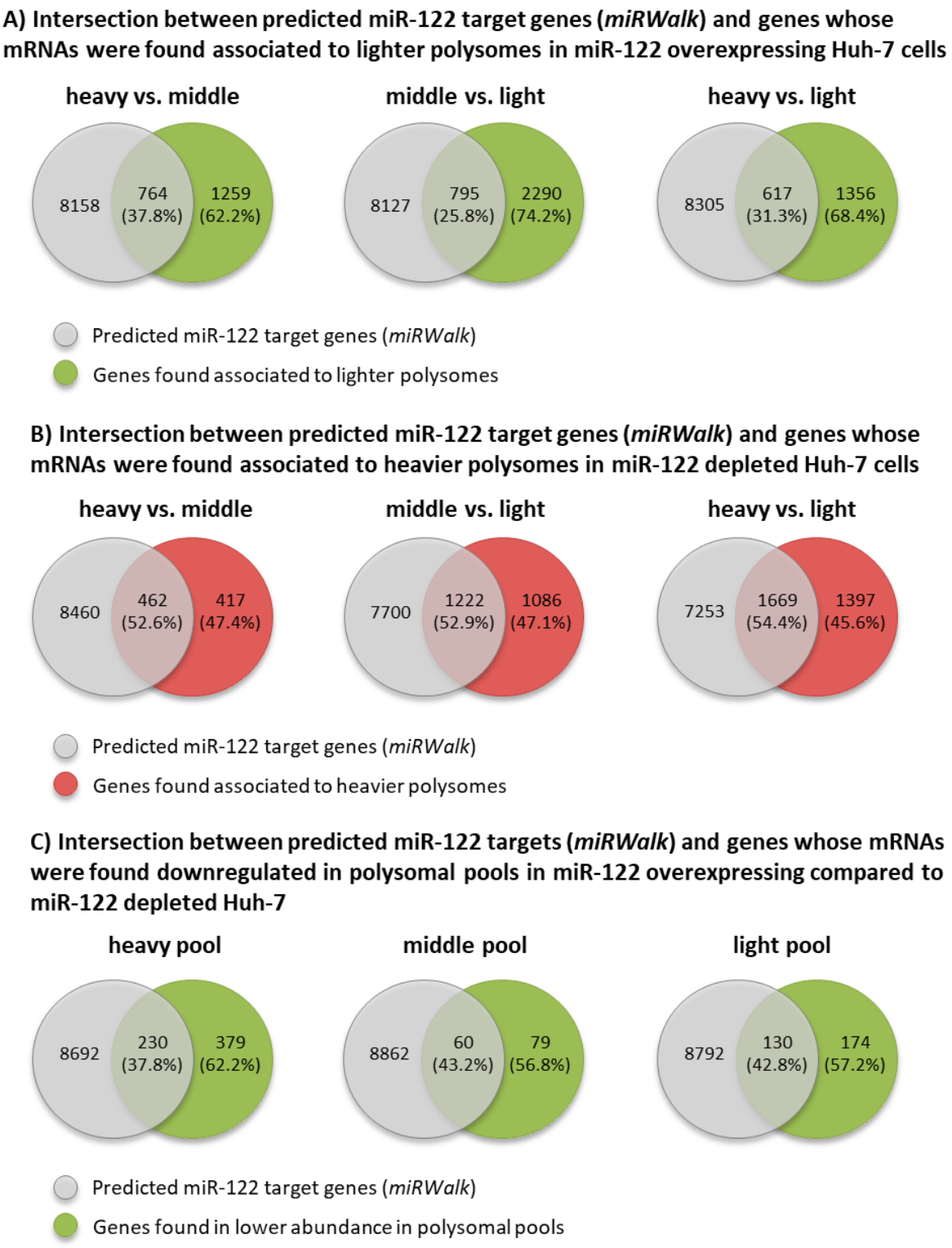

Figure 7.1 Intersection between predicted miRNA target genes and genes regulated on polysomes upon miR-122 overexpession or inhibition. Venn diagrams illustrate the number of genes whose transcripts were found significantly regulated in polysomes isolated from Huh-7 cells treated with miR-122 mimic or miR-122 inhibitor. **A)** Genes associated with lighter polysomes in miR-122 overexpressing cells. **B)** Genes associated with heavier polysomes in miR-122 inhibitor transfected cells. **C)** Genes with lower abundance in polysomal pools when comparing miR-122 mimic to miR-122 inhibitor transfected cells.

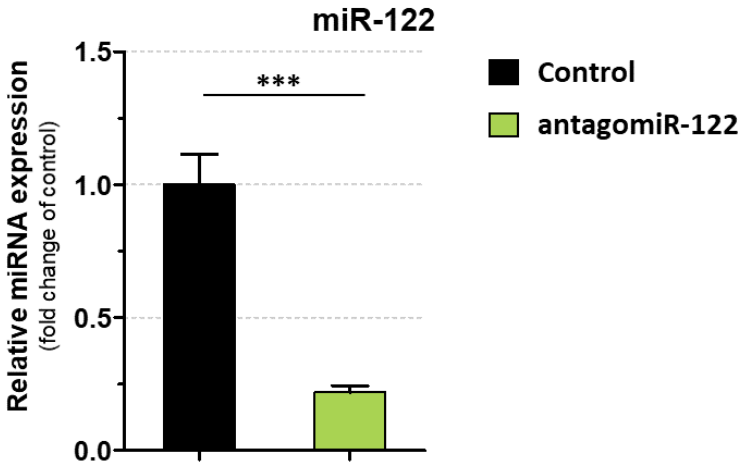

Figure 7.2 Quantitative analysis of cellular miR-122 levels in antagomiR-122 transfected Huh-7 cells. Huh-7 cells were transfected with antagomiR-122 for 48 h. Control cells were mock-transfected in absence of miR-122 inhibitor. Following RNA isolation, miRNAs were quantified by miQPCR. Levels of miR-122 were normalized to miR-192 for each sample and are displayed as fold change (± standard error of the mean [SEM]) relative to control of 4 independent experiments. Asterisks indicate significant differences to control (student´s t-test with significance level *** $p < 0.001$).

Binding partners	Heteroduplex	p-value	Folding Energy
miR-122-5p human *BAG1* 3´UTR; Position 1654	3´-GUUUGUGGU - - AACAGUGUGAGGU-5´ 5´-CGGGUCCCAGCCCACCGCACCCCA-3´	p = 0.03	-13.9 kcal/mol
miR-122-5p human *BAG1* 3´UTR; Position 2322	3´-GUUUGUGGUAACAGUGUGAGGU-5´ 5´-UGAACAGC - UCCUCACCUUCCU-3´	p = 0.07	-12.1 kcal/mol
miR-122-5p human *BAG1* 3´UTR; Position 2491	3´-GUUUGUGGUAACAGUGUGAGGU-5´ 5´-UUCACAGCAUUUACAUAGUCCA-3´	p = 0.23	-14.3 kcal/mol
miR-122-5p human *BAX* 3´UTR; Position 117	3´-GUUUGUGGUAAC - AGUGUGAGGU-5´ 5´-CAA - GUUCAUUGAUGACCCUCUG-3´	p = 0.06	-10.2 kcal/mol
miR-122-5p human *BAX* 3´UTR; Position 305	3´-GUUUGUGGUAA - CAGUGUGAGGU-5´ 5´-AAUGC - CCGUUCAUCUCAGUCCC-3´	p = 0.05	-11.6 kcal/mol
miR-122-5p human *BAX* 3´UTR; Position 320	3´-GUUUGUGGUAAC - AGUGUGAGGU-5´ 5´-CAG - - UCCCCUGCCCGCAAUCCU-3´	p = 0.05	-8.4 kcal/mol
miR-122-5p human *BAX* 3´UTR; Position 499	3´-GUUUGUGGUAAC - AGUGUGAGGU-5´ 5´-CAG - - UCCCCUGCCCGCAAUCCU-3´	p = 0.10	-12.7 kcal/mol
miR-122-5p human *CCDC43* 3´UTR; Position 146	3´-GUUUGUGGUAACAGUGUGAGGU-5´ 5´-CGAUAACC - UUGGCCUACUCUA-3´	p = 0.09	-11.0 kcal/mol
miR-122-5p human *CCDC43* 3´UTR; Position 1087	3´-GUUUGUGGUAACAGUGUGAGGU-5´ 5´-UUUCUACUUCUGUCACAAACCA-3´	p = 0.04	-16.0 kcal/mol
miR-122-5p human *CCDC43* 3´UTR; Position 1479	3´-GU - UUGUGG - UAACAGUGUGAGGU-5´ 5´-CAUGUUACCUCUUCAUACACUCCU-3´	p = 0.27	-14.4 kcal/mol
miR-122-5p human *CD47* 3´UTR; Position 605	3´-GUUUGUGGUAACAGUGUGAGGU-5´ 5´-GGGUUGCCAUUCCCACAUUCCC-3´	p = 0.09	-17.6 kcal/mol
miR-122-5p human *CD47* 3´UTR; Position 838	3´-GUUUGUGGUAACAGUGUGAGGU-5´ 5´-AGAGCACUGUGUUCACACUUUU-3´	p = 0.06	-19.3 kcal/mol
miR-122-5p human *CD47* 3´UTR; Position 1598	3´-GUUUGUGGUAACAGUGUGAGGU-5´ 5´-CAAAU - UGAUUGUCAUAUUUCA-3´	p = 0.10	-17.9 kcal/mol
miR-122-5p human *CD47* 3´UTR; Position 1769	3´-GUUUGUG - GUAACAGUGUGAGGU-5´ 5´-UAUACACACAU - - GUAUAUUCUU-3´	p = 0.01	-12.1 kcal/mol
miR-122-5p human *CD47* 3´UTR; Position 2920	3´-GUUUGUGGUAACAGUGUGAGGU-5´ 5´-GAAACUCCA - GGUC - CAUUCUG-3´	p = 0.28	-14.8 kcal/mol
miR-122-5p human *CD47* 3´UTR; Position 4014	3´-GUU - UGUGGUAACAGUGUGAGGU-5´ 5´-CAGCAGACCACAAGCACAUUUCU-3´	p = 0.03	-13.4 kcal/mol
miR-122-5p human *CMTM7* 3´UTR; Position 208	3´-GUUUGUGGUAACAGUGUGAGGU-5´ 5´-AGAACAUC - - CCUCCCAUUCUG-3´	p = 0.06	-11.5 kcal/mol
miR-122-5p human *CMTM7* 3´UTR; Position 342	3´-GUUUGUGG - UAACAGUGUGAGGU-5´ 5´-UAAAUCCCUUCUACUUCACUCCU-3´	p = 0.28	-12.1 kcal/mol
miR-122-5p human *CMTM7* 3´UTR; Position 815	3´-GUUUGUGGU - AACAGUGUGAGGU-5´ 5´-GCAAUACCAAUCUUCUCAUUUUG-3´	p = 0.03	-10.3 kcal/mol

Figure 7.3 Binding site analysis of miR-122 target gene candidates identified by polysomal profiling. *RNA22* identified several miR-122 MREs in the 3´UTRs of human miR-122 target candidates. Blue lines indicate predicted base pairing between miRNA and target sequence, dashed blue lines indicate weaker hydrogen bonds between the nucleobases. The seed sequence of miR-122 is illustrated in grey boxes and nucleic acids are displayed with red font.

Figure 7.3 continued

Binding partners	Heteroduplex	p-value	Folding Energy
miR-122-5p human *DIXDC1* 3´UTR; Position 126	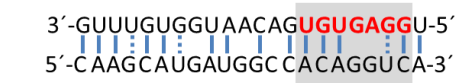	p=0.01	-14.2 kcal/mol
miR-122-5p human *DIXDC1* 3´UTR; Position 203		p<0.01	-10.3 kcal/mol
miR-122-5p human *DIXDC1* 3´UTR; Position 397	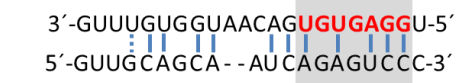	p=0.01	-10.0 kcal/mol
miR-122-5p human *DIXDC1* 3´UTR; Position 506	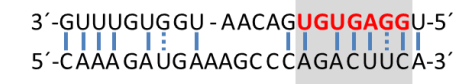	p=0.13	-9.6 kcal/mol
miR-122-5p human *DIXDC1* 3´UTR; Position 634	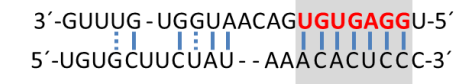	p=0.30	-11.9 kcal/mol
miR-122-5p human *DIXDC1* 3´UTR; Position 2672	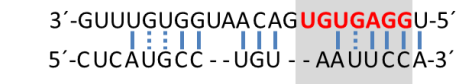	p<0.01	-10.7 kcal/mol
miR-122-5p human *DIXDC1* 3´UTR; Position 2801	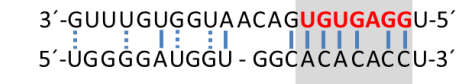	p<0.01	-11.3 kcal/mol
miR-122-5p human *DIXDC1* 3´UTR; Position 3245	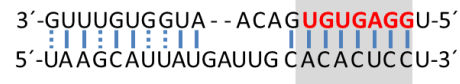	p=0.21	-21.1 kcal/mol
miR-122-5p human *DIXDC1* 3´UTR; Position 3378	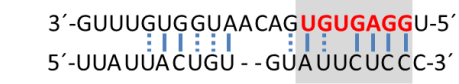	p<0.01	-9.0 kcal/mol
miR-122-5p human *DSG2* 3´UTR; Position 463	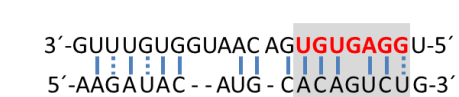	p=0.03	-12.1 kcal/mol
miR-122-5p human *DSG2* 3´UTR; Position 577	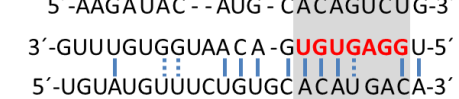	p=0.03	-9.4 kcal/mol
miR-122-5p human *DSG2* 3´UTR; Position 908	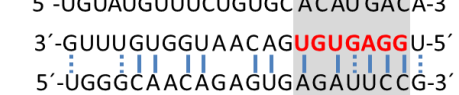	p=0.04	-13.4 kcal/mol
miR-122-5p human *F2RL2* 3´UTR; Position 76	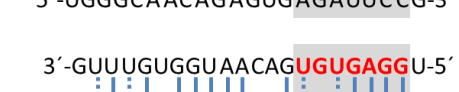	p=0.04	-15.7 kcal/mol
miR-122-5p human *F2RL2* 3´UTR; Position 770	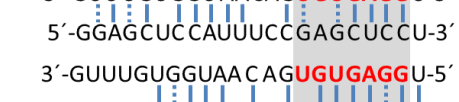	p=0.03	-11.1 kcal/mol
miR-122-5p human *F2RL2* 3´UTR; Position 842	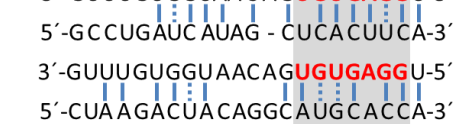	p<0.01	-10.3 kcal/mol
miR-122-5p human *F2RL2* 3´UTR; Position 1038	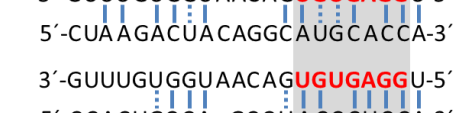	p=0.03	-12.4 kcal/mol
miR-122-5p human *F2RL2* 3´UTR; Position 1184	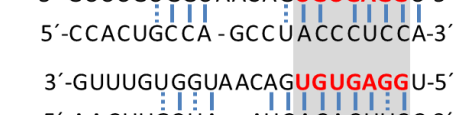	p=0.02	-12.8 kcal/mol
miR-122-5p human *G3BP2* 3´UTR; Position 629	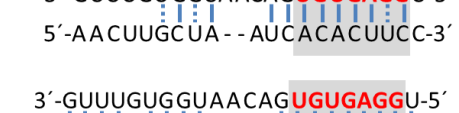	p=0.24	-12.4 kcal/mol
miR-122-5p human *G3BP2* 3´UTR; Position 1667	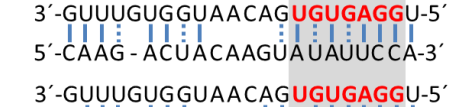	p=0.10	-9.6 kcal/mol
miR-122-5p human *G3BP2* 3´UTR; Position 2240	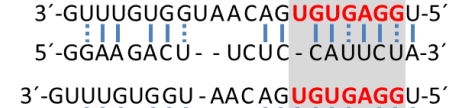	p=0.06	-9.9 kcal/mol

Figure 7.3 continued

Binding partners	Heteroduplex	p-value	Folding Energy
miR-122-5p human *HCFC1* 3´UTR; Position 82		p<0.01	-15.5 kcal/mol
miR-122-5p human *HCFC1* 3´UTR; Position 473		p=0.06	-12.7 kcal/mol
miR-122-5p human *HCFC1* 3´UTR; Position 1370	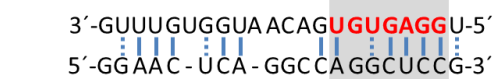	p=0.14	-13.1 kcal/mol
miR-122-5p human *HCFC1* 3´UTR; Position 1625		p=0.32	-12.2 kcal/mol
miR-122-5p human *KIF1B* 3´UTR; Position 117		p=0.15	-12.3 kcal/mol
miR-122-5p human *KIF1B* 3´UTR; Position 289	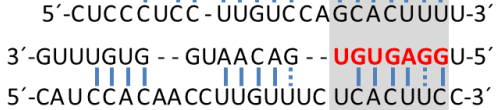	p=0.13	-13.6 kcal/mol
miR-122-5p human *KIF1B* 3´UTR; Position 2355	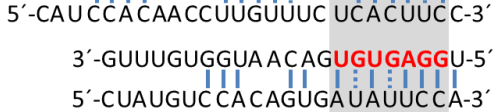	p=0.31	-13.8 kcal/mol
miR-122-5p human *KIF3A* 3´UTR; Position 923	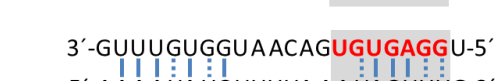	p=0.02	-8.9 kcal/mol
miR-122-5p human *KIF3A* 3´UTR; Position 1301	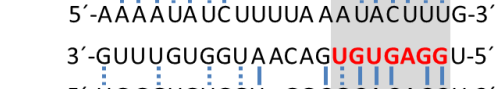	p=0.01	-11.2 kcal/mol
miR-122-5p human *KPNA6* 3´UTR; Position 2053		p=0.08	-14.4 kcal/mol
miR-122-5p human *KPNA6* 3´UTR; Position 2319	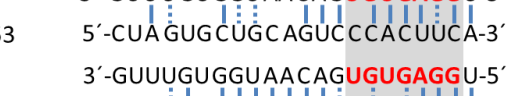	p=0.21	-14.9 kcal/mol
miR-122-5p human *KPNA6* 3´UTR; Position 3628	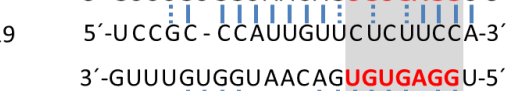	p=0.04	-12.5 kcal/mol
miR-122-5p human *KPNB1* 3´UTR; Position 1439	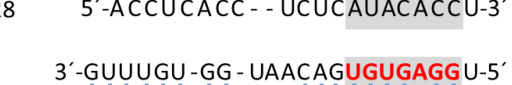	p=0.07	-18.2 kcal/mol
miR-122-5p human *KPNB1* 3´UTR; Position 1711	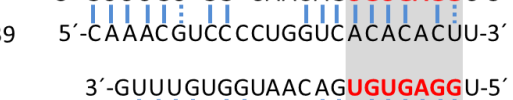	p=0.02	-9.6 kcal/mol
miR-122-5p human *KPNB1* 3´UTR; Position 2043	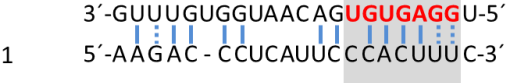	p=0.16	-14.0 kcal/mol
miR-122-5p human *KPNB1* 3´UTR; Position 3051		p=0.18	-10.1 kcal/mol
miR-122-5p human *NUP210* 3´UTR; Position 652		p=0.18	-13.0 kcal/mol
miR-122-5p human *NUP210* 3´UTR; Position 806		p=0.21	-14.1 kcal/mol
miR-122-5p human *NUP210* 3´UTR; Position 895		p=0.05	-13.1 kcal/mol

Figure 7.3 continued

Binding partners	Heteroduplex	p-value	Folding Energy
miR-122-5p human *MINK1* 3´UTR; Position 23	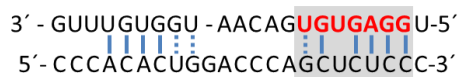	p = 0.09	-12.0 kcal/mol
miR-122-5p human *MINK1* 3´UTR; Position 90		p = 0.06	-14.9 kcal/mol
miR-122-5p human *MINK1* 3´UTR; Position 467		p = 0.06	-13.8 kcal/mol
miR-122-5p human *MINK1* 3´UTR; Position 542	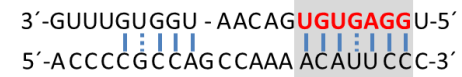	p = 0.02	-14.9 kcal/mol
miR-122-5p human *P4HA1* 3´UTR; Position 143		p = 0.38	-6.9 kcal/mol
miR-122-5p human *P4HA1* 3´UTR; Position 177		p = 0.02	-11.0 kcal/mol
miR-122-5p human *P4HA1* 3´UTR; Position 301		p = 0.36	-8.8 kcal/mol
miR-122-5p human *PCGF2* 3´UTR; Position 27	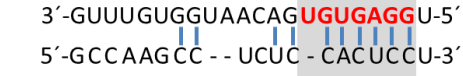	p = 0.03	-10.2 kcal/mol
miR-122-5p human *PCGF2* 3´UTR; Position 67	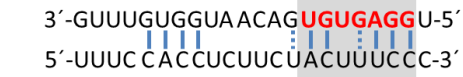	p = 0.02	-9.4 kcal/mol
miR-122-5p human *PDCD2* 3´UTR; Position 962		p = 0.35	-9.9 kcal/mol
miR-122-5p human *PDCD2* 3´UTR; Position 1996	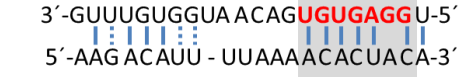	p < 0.01	-9.9 kcal/mol
miR-122-5p human *PDCD4* 3´UTR; Position 962	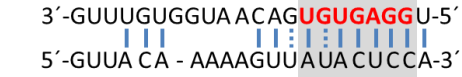	p = 0.01	-15.7 kcal/mol
miR-122-5p human *PDCD4* 3´UTR; Position 1840	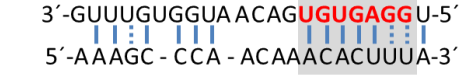	p = 0.05	-12.0 kcal/mol
miR-122-5p human *RNF26* 3´UTR; Position 17	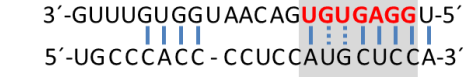	p = 0.07	-15.7 kcal/mol
miR-122-5p human *RNF26* 3´UTR; Position 356	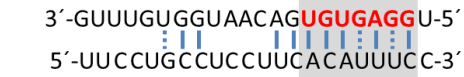	p = 0.01	-12.5 kcal/mol
miR-122-5p human *RNF26* 3´UTR; Position 767	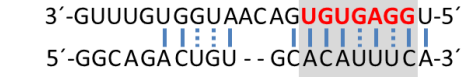	p = 0.19	-12.4 kcal/mol

Figure 7.3 continued

Binding partners	Heteroduplex	p-value	Folding Energy
miR-122-5p human *SPRED2* 3´UTR; Position 72	3´-GUUUGUGGUAAC AG**UGUGAGG**U-5´ 5´-CCCCCGCUCCCUUC - CACUCCA-3´	p = 0.03	-13.8 kcal/mol
miR-122-5p human *SPRED2* 3´UTR; Position 205	3´-GUUUGU - GGUAACAG**UGUGAGG**U-5´ 5´-GCCACAUCCAUACACACACGCUC-3´	p < 0.01	-12.2 kcal/mol
miR-122-5p human *SPRED2* 3´UTR; Position 1542	3´-GUUUGUGGU - AAC - AG - **UGUGAGG**U-5´ 5´-AAGACAUGGCCUGCUCCCACUC CC-3´	p < 0.01	-13.0 kcal/mol
miR-122-5p human *SPRED2* 3´UTR; Position 2237	3´-GUUUGUGGU - AACAG**UGUGAGG**U-5´ 5´-ACGUCUCUAAUUGCCACACUGCA-3´	p = 0.11	-12.5 kcal/mol
miR-122-5p human *TBC1D22B* 3´UTR; Position 781	3´-GUUUGUGGUA - - ACAG**UGUGAGG**U-5´ 5´-CCUUUUCCAUGAUG ACCCACUC CA-3´	p < 0.01	-13.1 kcal/mol
miR-122-5p human *TNPO1* 3´UTR; Position 4	3´-GUUUGUGGUAAC AG**UGUGAGG**U-5´ 5´-AAUACACUUAAGCUGCAGUCCC-3´	p = 0.06	-12.4 kcal/mol
miR-122-5p human *TNPO1* 3´UTR; Position 667	3´-GUUUGUGGU - AACAG**UGUGAGG**U-5´ 5´-GAAAUGCCAAAUGAGUCACUCCU-3´	p = 0.10	-15.2 kcal/mol
miR-122-5p human *TNPO1* 3´UTR; Position 2968	3´-GUUUGUGGU AACAG**UGUGAGG**U-5´ 5´-AGUUUGUCUUUGUUACAUUCCA-3´	p = 0.21	-17.6 kcal/mol
miR-122-5p human *TNPO1* 3´UTR; Position 3284	3´-GUUUGUGGU AACAG**UGUGAGG**U-5´ 5´-CAG - UUCCAU - GUUACAGUCCA-3´	p = 0.05	-18.3 kcal/mol
miR-122-5p human *TNPO1* 3´UTR; Position 4833	3´-GUUUGUGG - UAACAG**UGUGAGG**U-5´ 5´-UUUUCACCUCUUGU - ACAUUUUA-3´	p = 0.02	-12.3 kcal/mol

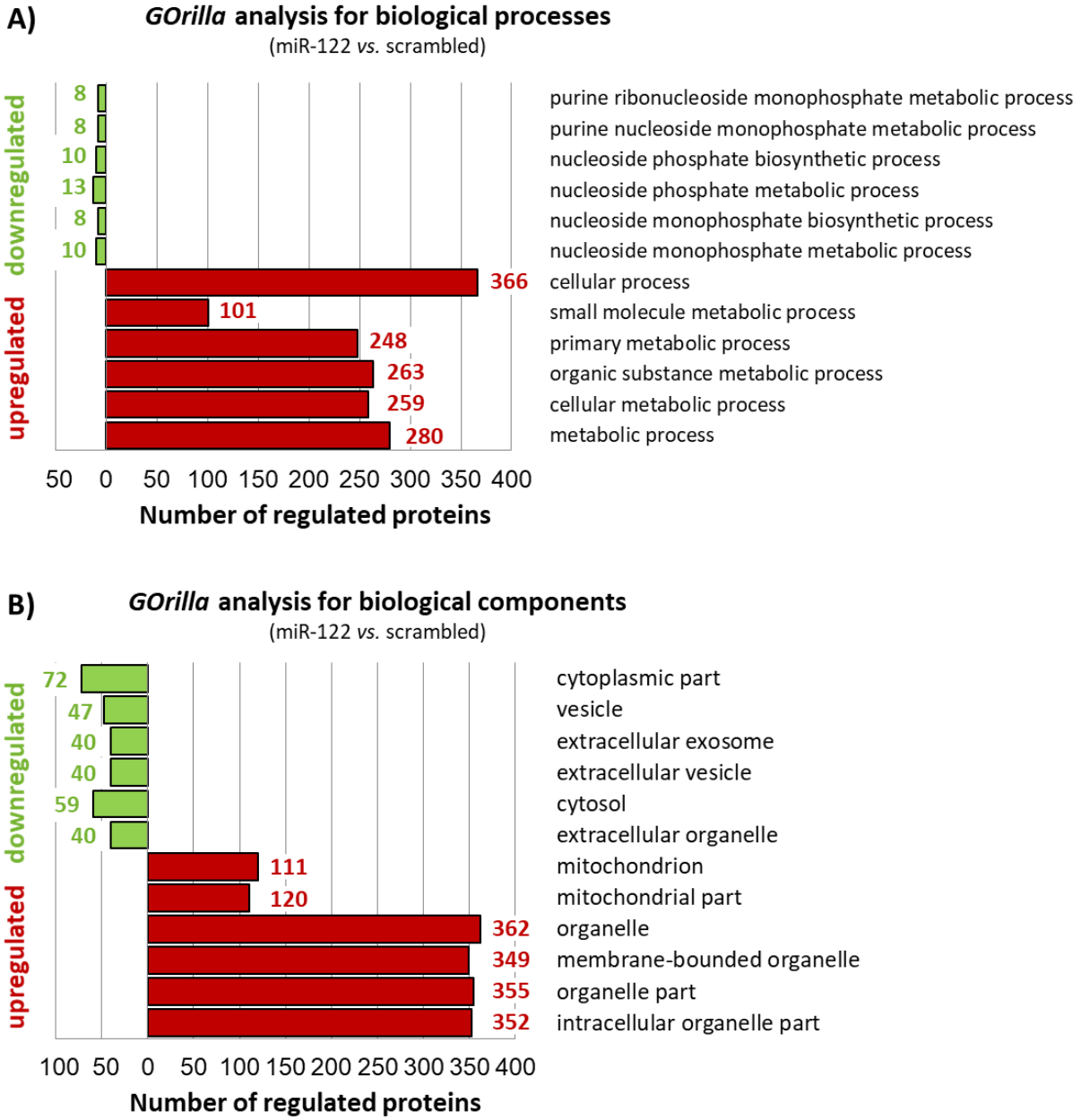

Figure 7.4 Gene Ontology analysis of significantly regulated proteins in miR-122 overexpressing (mimic) *versus* scrambled control cells. *GOrilla* GO enrichment tool was utilized to investigate the six most significantly depleted **(green)** and enriched **(red)** GO terms. Numbers of proteins associated with a given term are illustrated in green (downregulated term) and red (upregulated term). **A)** GO analysis with respect to biological processes. **B)** GO analysis with an emphasis on cellular components.

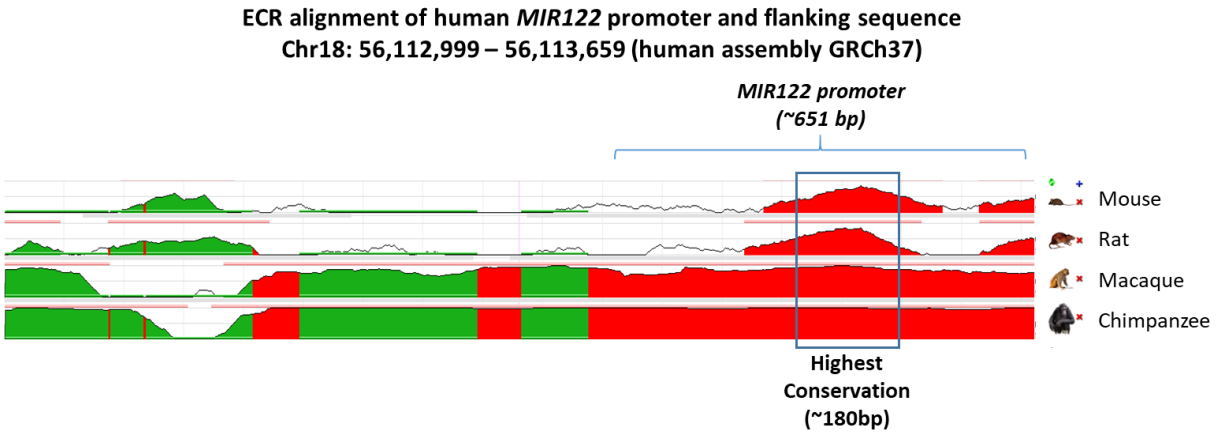

Figure 7.5 Sequence conservation of human *MIR122* promoter constructs and flanking sequence. The *MIR122* promoter was identified by Li *et al.* [*119*]**.** *Evolutionary Conservation of Genomes (ECR) Browser* was used to align the human *MIR122* promoter and flanking sequence to the mouse (assembly mm10), rat (assembly rn4), macaque (assembly rheMac2), and chimpanzee (assembly panTro3) genome. The section illustrated above shows the human genomic location 56,112,999 – 56,113,659 on chromosome 18 (release GRCh37/ hg19).

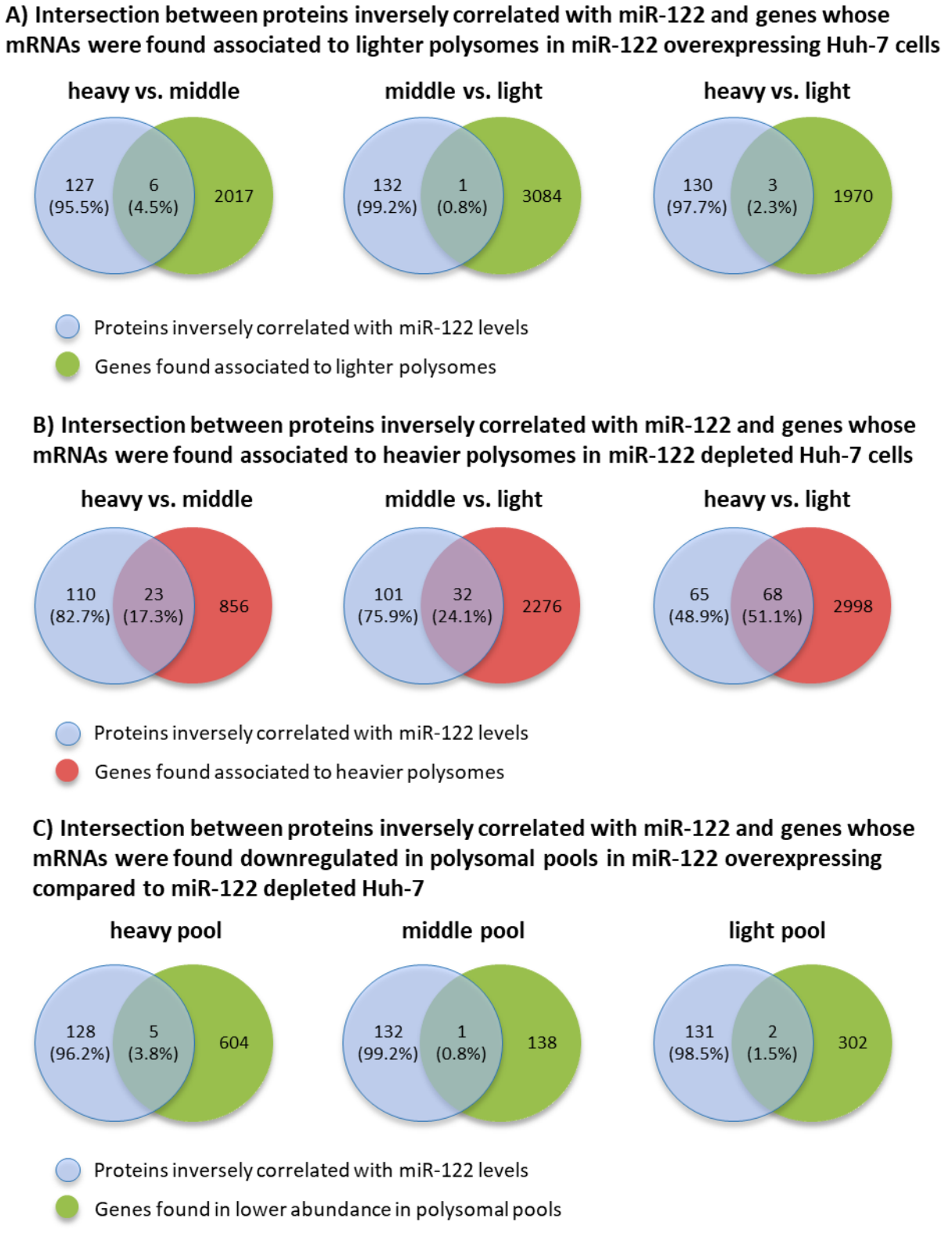

Figure 7.6 Intersection between proteins inversely correlated with miRNA levels and genes regulated on polysomes upon miR-122 overexpression or inhibition in Huh-7 cells. Venn diagrams illustrate the number of genes whose transcripts were found significantly regulated in polysomes isolated from Huh-7 cells treated with miR-122 mimic or miR-122 inhibitor (microarray) and the 133 proteins identified as inversely correlated with miR-122 levels (proteomics). **A)** Genes associated with lighter polysomes in miR-122 overexpressing cells. **B)** Genes associated with heavier polysomes in miR-122 inhibitor transfected cells. **C)** Genes with lower abundance in polysomal pools when comparing miR-122 mimic to miR-122 inhibitor transfected cells.

Eidesstattliche Erklärung

Ich versichere an Eides Statt, dass die Dissertation von mir selbständig und ohne unzulässige fremde Hilfe unter Beachtung der „Grundsätze zur Sicherung guter wissenschaftlicher Praxis an der Heinrich-Heine-Universität Düsseldorf“ erstellt worden ist. Die Dissertation wurde in der vorgelegten oder in ähnlicher Form noch bei keiner anderen Institution eingereicht. Ich habe bisher keine erfolglosen Promotionsversuche unternommen.

Ort, Datum	Martha Magdalene Paluschinski